

6-2014

Retrofitting of Shear-Deficient Reinforced Concrete T-Girders with Composite-Based Systems

Alaa Ahmad Ata Maali

Follow this and additional works at: https://scholarworks.uaeu.ac.ae/all_theses

Part of the [Civil Engineering Commons](#)

Recommended Citation

Ata Maali, Alaa Ahmad, "Retrofitting of Shear-Deficient Reinforced Concrete T-Girders with Composite-Based Systems" (2014).
Theses. 519.

https://scholarworks.uaeu.ac.ae/all_theses/519

This Thesis is brought to you for free and open access by the Electronic Theses and Dissertations at Scholarworks@UAEU. It has been accepted for inclusion in Theses by an authorized administrator of Scholarworks@UAEU. For more information, please contact fadl.musa@uaeu.ac.ae.



United Arab Emirates University

College of Engineering

Department of Civil and Environmental Engineering

RETROFITTING OF SHEAR-DEFICIENT REINFORCED
CONCRETE T-GIRDERS WITH COMPOSITE-BASED
SYSTEMS

Alaa Ahmad Ata Maali

This thesis is submitted in partial fulfillment of the requirements
for the degree of Master of Science in Civil Engineering

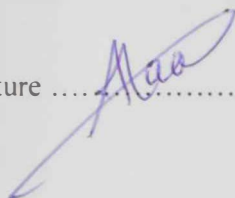
Under the direction of Dr. Tamer El Maaddawy

June 2014

DECLARATION OF ORIGINAL WORK

I, Alaa Ahmad Ata Maali, the undersigned, a graduate student at the United Arab Emirates University (UAEU) and the author of the thesis titled "Retrofitting of Shear-deficient Reinforced Concrete T-girders with Composite-based Systems", hereby solemnly declare that this thesis is an original work done and prepared by me under the guidance of Dr. Tamer El Maaddawy, in the College of Engineering at UAEU. This work has not been previously formed as the basis for the award of any degree, diploma or similar title at this or any other university. The materials borrowed from other sources and included in my thesis have been properly cited and acknowledged.

Student's Signature



Date 11/6/2014

Copyright © 2014 by Alaa Ahmad Ata Maali
All Rights Reserved

Approved by

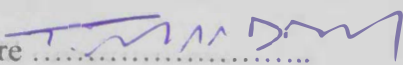
Thesis Examination Committee:

1) Advisor (Committee Chair): Tamer El Maaddawy

Title: Associate Professor

Department of Civil and Environmental Engineering

College of Engineering, United Arab Emirates University

Signature 

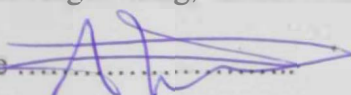
Date: 4 June 2014

2) Member: Ahmed El Refai

Title: Assistant Professor

Department of Civil and Environmental Engineering

College of Engineering, United Arab Emirates University

Signature 

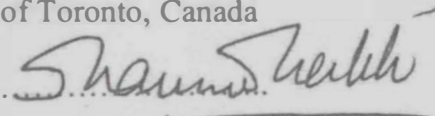
Date: 4 June 2014

3) Member (External Examiner): Shamim A. Sheikh

Title: Professor

Department of Civil Engineering,


University of Toronto, Canada

Signature 

Date: 4 June 2014

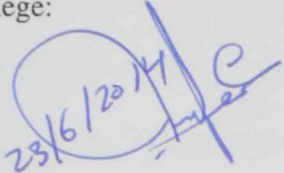
Accepted by

Master's Program Coordinator:

Signature: 

Date: 11/6/2014

Dean of the College:

Signature: 

Date: 23/6/2014

Copy of

ABSTRACT

This research examines the viability of using different composite-based systems to upgrade the shear resistance of shear-deficient reinforced concrete T-girders. The research comprised experimental testing and analytical investigation. Test parameters included the retrofitting system; externally-bonded carbon fiber-reinforced polymer (EB-CFRP) laminates with or without a mechanical end anchorage (MA) and embedded through depth glass fiber-reinforced (ETD-GFRP) rebars; amount of internal stirrups; no stirrups, limited amount of stirrups with spacing $s_1 = 0.6d$, higher amount of stirrups with spacing $s_2 = 0.375d$; and initial shear damage prior to retrofitting; no damage, pre-cracking, and pre-failure.

The shear strength gain for the non-damaged specimens decreased as the amount of stirrups increased. The EB-CFRP system without MA increased the shear resistance by 17, 19, and 13%, for the specimens without stirrups, with stirrups spacing s_1 and s_2 , respectively. The inclusion of the MA in the EB-CFRP system increased the former shear strength gains to 64, 36, and 32%, respectively. The shear strength gains provided by the ETD-GFRP system were comparable to those provided by the EB-CFRP with MA.

The presence of shear damage prior to retrofitting significantly reduced the strengthening effectiveness. For the pre-cracked specimens with the lower amount of stirrups, only 11, 27, 11% shear strength gains were recorded after retrofitting with the EB-CFRP solely, EB-CFRP with MA, and ETD-GFRP systems, respectively. The EB-CFRP system without MA was not successful in restoring the shear resistance of the pre-failed specimens. The EB-CFRP with MA and ETD-GFRP systems fully restored the shear resistance of the pre-failed

specimens. The shear resistance of the pre-failed specimens retrofitted by the EB-CFRP with MA was 1.1 to 1.4 times the original shear resistance compared to 1 to 1.1 times for the pre-failed specimens retrofitted with the ETD-GFRP system.

In the analytical investigation, the accuracy of five different international guidelines/standards and two recent analytical models published in the literature to predict the contribution of the EB-CFRP system to the shear resistance have been assessed. The validity of a recent analytical approach published in the literature to predict the contribution of the ETD-GFRP system to the shear capacity has been demonstrated.

Keywords: concrete, composites, shear, retrofitting, anchorage.

ACKNOWLEDGEMENTS

First of all, I would like to thank Allah for giving me the faith, luck and strength to successfully complete my work. My deepest thanks go to my family and fiancé who has supported me with all facilities, strength and encouragement to complete this work. I would like to express my deepest thanks for every single person helped me during this unforgettable period of my life. At the first place, I would like to deliver my endless respect and appreciation to my thesis supervisor Dr. Tamer El Maaddawy for his unlimited support, being friendly with enormous guidance, being on time, providing me with precious knowledge and advices during the whole project stages. My acknowledgments are extended to all faculty members of the Department of Civil and Environmental Engineering at the United Arab Emirates University for their continuous support and encouragement. I would like also to express my intense gratitude to the structural engineering laboratory specialist Eng. Tarek Salah who didn't keep any effort in helping me with the experimental testing through the whole project. My deepest thanks are extended to the concrete laboratory specialist Mr. Faisal Abdul-Wahab who assisted me during casting, repair and strengthening of the concrete beams. Also, I would like to thank Mr. Abdelrahman Alsallamin, Mr. Jwan Al Khalil and Mr. Amer Ayyad for their help throughout testing and fabrication of test specimens

DEDICATION

To my beloved family, fiancé and friends

TABLE OF CONTENTS

DECLARATION OF ORIGINAL WORK	i
COPYRIGHT PAGE.....	ii
SIGNATURE PAGE.....	iii
ABSTRACT	v
ACKNOWLEDGEMENTS	vii
DEDICATION	viii
TABLE OF CONTENTS	ix
LIST OF TABLES	xvi
LIST OF FIGURES.....	xviii
LIST OF NOMENCLATURE	xxviii
Chapter 1: INTRODUCTION.....	1
1.1 Background.....	1
1.2 Shear strength in concrete members.....	1
1.3 Types of destruction in concrete members.....	3
1.3.1 Deterioration	3
1.3.2 Concrete damage.....	4
1.3.3 Concrete member defects.....	4
1.4 Types of fiber reinforced polymers (FRPs).....	5
1.5 Applications of fiber reinforced polymers (FRPs)	6
1.6 Properties of fiber reinforced polymers (FRPs).....	9

1.7 Advantages and disadvantages of fiber reinforced polymers	10
1.8 Arrangement of work	11
Chapter 2: LITERATURE REVIEW	13
2.1 Introduction.....	13
2.2 Studies on shear strengthening using EB-FRP system without end anchorage	13
2.3 Studies on shear strengthening using EB-CFRP with end anchorage	36
2.4 Studies on shear strengthening using ETD-FRP system	53
2.5 Research Objectives.....	56
2.5.1 Research needs	56
2.5.2 Scope of the current study	57
Chapter 3: EXPERIMENTAL PROGRAM.....	58
3.1 Introduction.....	58
3.2 Test Program.....	59
3.2.1 Test Matrix	59
3.3 Test specimens.....	61
3.4 Material properties.....	63
3.4.1 Concrete	63
3.4.2 Steel reinforcement	65
3.4.3 Fiber reinforced polymers (FRP)	66
3.5 Fabrication of test specimens.....	66
3.6 Strengthening/retrofitting systems.....	68

3.6.1 The EB-CFRP system	69
3.6.2 The EB-CFRP system with mechanical end anchorage (MA)	71
3.6.3 The ETD-GFRP system	73
3.7 Test set-up and instrumentation	75
3.7.1 Loading history	76
3.7.2 Strain measurements	77
3.7.3 Displacement and load measurements	80
Chapter 4: EXPERIMENTAL RESULTS	81
4.1 Introduction.....	81
4.2 Test results	81
4.2.1 Group [A]	81
4.2.1.1 Failure mode	81
4.2.1.2 Shear capacity.....	84
4.2.1.3 Deflection response	84
4.2.1.4 Diagonal tensile displacement response	86
4.2.1.5 Flexural steel strain response	87
4.2.1.6 FRP strain response	88
4.2.2 Group B	90
4.2.2.1 Specimens without initial shear damage	90
4.2.2.1.1 Failure mode	90
4.2.2.1.2 Shear capacity	94
4.2.2.1.3 Deflection response	94

4.2.2.1.4	Diagonal tensile displacement response	96
4.2.2.1.5	Flexural steel strain response	97
4.2.2.1.7	FRP strain response	99
4.2.2.2	Specimens with damage state D1	101
4.2.2.2.1	Failure mode	101
4.2.2.2.2	Shear capacity	106
4.2.2.2.3	Deflection response	106
4.2.2.2.4	Diagonal tensile displacement response	108
4.2.2.2.5	Flexural steel strain response	109
4.2.2.2.6	Stirrups strain response	110
4.2.2.2.7	FRP strain response	111
4.2.2.3	Specimens with the damage state D2	113
4.2.2.3.1	Failure mode	113
4.2.2.3.2	Shear capacity	118
4.2.2.3.3	Deflection response	119
4.2.2.3.4	Diagonal tensile displacement response	122
4.2.2.3.5	Flexural steel strain response	125
4.2.2.3.6	Stirrups strain response	127
4.2.2.3.7	FRP strain response	132
4.2.3	Group C	133
4.2.3.1	Specimens without initial shear damage	133
4.2.3.1.1	Failure mode	133

4.2.3.1.2	Shear capacity	136
4.2.3.1.3	Deflection response	136
4.2.3.1.4	Diagonal tensile displacement response	138
4.2.3.1.5	Flexural steel strain response	139
4.2.3.1.6	Stirrups strain response	140
4.2.3.1.7	FRP strain response	142
4.2.3.2	Specimens with damage state (D2)	143
4.2.3.2.1	Failure mode	143
4.2.3.2.2	Shear capacity	148
4.2.3.2.3	Deflection response	149
4.2.3.2.4	Diagonal tensile displacement response	153
4.2.3.2.5	Flexural steel strain response	156
4.2.3.2.6	Stirrups strain response	159
4.2.3.2.7	FRP strain response	163
4.3	Analysis of test results and discussion.....	165
4.3.1	Performance evaluation of the non-damaged specimens	165
4.3.1.1	Effect of strengthening system	165
4.3.1.2	Effect of amount of internal stirrups	166
4.3.2	Performance evaluation of the pre-damaged specimens.....	167
4.3.2.1	Effect of initial shear damage.....	167
4.3.2.1.1	Specimens with the lower amount of stirrups.....	167
4.3.2.1.2	Specimens with the higher amount of stirrups	169

4.4 Efficiency of the strengthening/retrofitting systems.....	170
Chapter 5: ANALYTICAL INVESTIGATION.....	172
5.1 Introduction.....	172
5.2 Shear resistance of the EB-CFRP system	172
5.2.1 International guidelines/ standards for EB-CFRP resistance	172
5.2.1.1 ACI 440.2R (2008).....	173
5.2.1.2 <i>fib</i> TG 9.3 (2001).....	174
5.2.1.3 CNR-DT200 (2004)	175
5.2.1.4 HB 305 (2008).....	176
5.3.1.5 JSCE (2001)	177
5.3.2 Recent analytical models for EB-CFRP shear resistance	178
5.3.2.1 Mofidi and Chaallal (2011) analytical model.....	178
5.3.2.2 Chen et al. (2013) analytical model.....	179
5.3 Shear resistance of the ETD-GFRP system	181
5.3.1 Mofidi et al. (2012) analytical model.....	181
5.4 Maximum shear resistance	182
5.5. Comparative analysis for specimen's strengthened with EB-CFRP system	185
5.5.1. Accuracy of international guidelines/standards	185
5.5.1.1 Non-damaged specimens.....	188
5.5.1.2 Pre-cracked specimens	190
5.5.1.3 Pre-failed specimens.....	190
5.5.2 Accuracy of recent analytical models published in the literature	194

5.5.2.1 Non-damaged specimens.....	196
5.5.2.2 Pre-cracked specimens	196
5.5.2.3 Pre-failed specimens.....	197
5.6 Comparative analysis for specimens strengthened with ETD-GFRP system.....	197
5.6.1 Accuracy of Mofidi et al. (2012) analytical model	197
5.6.1.1 Non-damaged specimens.....	197
5.6.1.2 Pre-cracked specimens	198
5.6.1.3 Pre-failed specimens.....	198
Chapter 6: CONCLUSIONS AND RECOMMENDATIONS	201
6.1 General.....	201
6.2. Conclusions.....	201
6.2.1. Conclusions of the experimental work.....	201
6.2.2. Conclusions of the analytical investigation	202
6.3. Recommendations for practical applications.....	205
6.4. Recommendations for future studies	207
REFERENCES	208
APPENDIX A: STRAIN RESPONSE OF FRP.....	216
APPENDIX B: STRAIN RESPONSE OF STIRRUPS	224

LIST OF TABLES

Table 3.1: Test matrix of the experimental program	58
Table 3.3: Compressive and splitting tests results for the tested cylinders	64
Table 3.2: Concrete mix properties by weight	64
Table 3.4: Properties of the flexural steel reinforcement	65
Table 3.5: Properties of the shear steel reinforcement	65
Table 3.6: Mechanical properties of materials used in shear strengthening (data obtained from manufacturer).....	66
Table 4.1: Test results of group [A].	84
Table 4.2: Test results for the non-damaged specimens of group [B].	94
Table 4.3: Test results for specimens of group [B] with damage state D1	106
Table 4.4: Test results for specimens of group [B] with damage state D2	118
Table 4.5 : Test results for the non-damaged specimens of group [C].	136
Table 4.6: Test results for specimens of group [C] with the damage state D2 ...	148
Table 4.7: Efficiency of the strengthening systems	171
Table 5.1: The values of $V_{fd,max}$ based on the guidelines/standards.....	184
Table 5.2: The values of $V_{fn,max}$ based on the guidelines/standards.....	185
Table 5.3: Guidelines/predictions or EB-CFRP shear resistance	186
Table 5.4: Comparison between the experimental values and guidelines/standards predictions (EB-CFRP system)	187
Table 5.5: Predictions of analytical models for nominal EB-CFRP shear resistance	194
Table 5.6: Comparison between experimental values and predictions of analytical models (EB-CFRP).....	194

Table 5.7: Analytical and experimental values of ETD-GFRP shear resistance. 200

LIST OF FIGURES

Figure 1.1: The contribution of concrete and steel reinforcement in shear resistance (Nogueira et al. 2013)	2
Figure 1.2: Components and products of FRP composites (ISIS Canada 2006)	5
Figure 1.3: Shear strengthening of bridge girders using externally bonded FRP composites (ISIS Canada 2006)	7
Figure 1.4: Stress strain diagram for different types of fibers and steel reinforcement (ISIS Canada 2006).....	10
Figure 2.1: Peeling off of the CFRP reinforcement	17
Figure 2.2: Debonding and rupture failure modes of the strengthened beams (Leung et al. 2007)	19
Figure 2.3: Debonding of CFRP sheets failure mode in the strengthened specimens (Mofidi and Chaallal 2011)	26
Figure 2.4: CFRP sheets delamination at the opening corners (El-Maaddawy and El-Ariss 2012)	27
Figure 2.5: Detachment of the CFRP sheets failure mode at beam sides (El-Maaddawy and Chekfeh 2013).....	32
Figure 2.6: Typical CFRP debonding failure modes for the tested beams (Hussein et al. 2013).....	34
Figure 2.7: CFRP delamination failure mode (Mofidi and Chaallal 2014).....	35
Figure 2.8: Details of the U-Anchor at the corner of flange-web (Khalifa et al. 2000).....	37
Figure 2.9: Anchorage details of strengthening specimen beams (Tanarslan and Ertutar 2008).....	38

Figure 2.10: Strap configurations for test specimens (Hoult and Lees 2009)	40
Figure 2.11: CFRP strap layout and beam cross-section (Hoult and Lees 2009) .	40
Figure 2.12: Anchorage systems used in PC and RC specimens (Ortega et al. 2009).....	42
Figure 2.13: Configurations of various anchorage systems (Belarabi et al. 2010)	43
Figure 2.14: Details of mechanical anchorage system (Belarabi et al. 2010)	44
Figure 2.15: Implemented strengthening schemes (Deifalla and Ghobarah 2010)	45
Figure 2.16: Isometric view-Details of CFRP anchors (Kim et al. 2011).....	46
Figure 2.17: Various end anchorage systems (Mofidi et al. 2012)	48
Figure 2.18: Strengthening configurations for the tested beams (Kuotas and Triantafillou 2012)	49
Figure 2.19: EB-CFRP retrofitting regime with mechanical end anchorage (El-Maaddawy and Chekfeh 2012).....	50
Figure 2.20: Externally bonded GFRP sheets/strips configurations (Panigrahi et al. 2014).....	52
Figure 2.21: Strengthened specimens with ETS-CFRP rods (Chaallal et al. 2012)	54
Figure 2.22: Diagonal tension shear mode of failure for the strengthened specimen (Mofidi et al. 2012)	55
Figure 3.1: Test of the right shear span	62
Figure 3.2: Test of the left shear span	62
Figure 3.3: Details of reinforcement for beams of group [A]	62
Figure 3.4: Details of reinforcement for beams of group [B]	63
Figure 3.5: Details of reinforcement for beams of group [C]	63
Figure 3.6: Compressive and splitting tests for the tested concrete cylinders	64

Figure 3.7: Fabrication of formworks and steel cages	67
Figure 3.8: Installation of steel cages in the forms before casting	68
Figure 3.9: Concrete after casting	68
Figure 3.10: Crack sealing and surface preparation of the pre-failed specimens..	69
Figure 3.11: Positions and dimensions of the EB-CFRP sheets (dimensions are in mm)	70
Figure 3.12: Materials used in the EB-CFRP system.....	70
Figure 3.13: Strengthening procedures of the EB-CFRP system without MA	71
Figure 3.14: Positions and dimensions of the CFRP sheets and the MA system (dimensions are in mm).....	72
Figure 3.15: Materials used in the MA system	72
Figure 3.16: Strengthening procedures of the EB-CFRP system with MA	73
Figure 3.17: Layout of the ETD-GFRP system.....	74
Figure 3.18: Materials used in the ETD-GFRP system.....	74
Figure 3.19: Strengthening procedures of the ETD-GFRP system	75
Figure 3.20: Test setup and instrumentations.....	76
Figure 3.21: A test in progress	76
Figure 3.22: Positions of the strain gauges for specimens of group [A] (All dimensions are in mm)	78
Figure 3.23: Positions of the strain gauges for specimens of group [B] (All dimensions are in mm).....	78
Figure 3.24: Positions of the strain gauges for specimens of group [C] (All dimensions are in mm).....	78
Figure 3.25: Positions of the strain gauges bonded to the EB-CFRP sheets (Specimens with the EB-CFRP system).....	79

Figure 3.26: Positions of the strain gauges bonded to the EB-CFRP sheets (Specimens with the EB-CFRP+MA system)	79
Figure 3.27: Positions of the strain gauges bonded to the GFRP bars (Specimens with the ETD-GFRP system)	79
Figure 3.28: Location of concrete clip gauge on the beam surface	80
Figure 3.29: Data loggers	80
Figure 4.1: Failure mode of specimen ND-NS-NR	82
Figure 4.2: Failure mode of specimen ND-NS-EB	83
Figure 4.3: Failure mode of specimen ND-NS-EB+MA	83
Figure 4.4: Failure mode of specimen ND-NS-ETD	83
Figure 4.5: Load-deflection curves for specimens of group [A]	85
Figure 4.6: Load-diagonal tensile displacement curves for specimens of group [A].	86
Figure 4.7: Load-flexural strain relationships for specimens of group [A]	88
Figure 4.8: Load-FRP strain relationships for specimens of group [A]	89
Figure 4.9: Failure mode of specimen ND-SI-NR	91
Figure 4.10: Failure mode of specimen ND-SI-EB	91
Figure 4.11: Failure mode of specimen ND-SI-EB+MA	92
Figure 4.12: Failure mode of specimen ND-SI-ETD	93
Figure 4.13: Load-deflection curves for the non-damaged specimens of group [B]	95
Figure 4.14: Load-diagonal tensile displacement curves for the non-damaged specimens of group [B].	97
Figure 4.15: Load-flexural strain relationship for the non-damaged specimens of group [B]	98

Figure 4.16: Load-stirrups strain curves for the non-damaged specimens of group [B].....	98
Figure 4.17: Load-FRP strain relationships for the non-damaged specimens of group [B]	100
Figure 4.18: Failure mode of specimen D1-S1-NR	102
Figure 4.19: Failure mode of specimen D1-S1-EB	103
Figure 4.20: Failure mode of specimen D1-S1-EB+MA	104
Figure 4.21: Failure mode of specimen D1-S1-ETD	105
Figure 4.22: Load-deflection curves for specimens of group [B] with damage state D1	107
Figure 4.23: Load – diagonal tensile displacement response for specimens of group [B] with damage state D1.....	109
Figure 4.24: Load-flexural strain relationship for specimens group [B] with damage state D1	110
Figure 4.25: Load- stirrups strains curves for specimens of group [B] with damage state D1.....	111
Figure 4.26: Load-FRP strains relationships for specimens of group [B] with damage state D1.....	112
Figure 4.27: Failure mode of specimen D2-S1-NR	114
Figure 4.28: Failure mode of specimen D2-S1-EB	115
Figure 4.29: Failure mode of specimen D2-S1-EB+MA	116
Figure 4.30: Failure mode of specimen D2-S1-ETD	117
Figure 4.31: Load-deflection curves of specimen D2-S1-NR.....	119
Figure 4.32: Load-deflection curves of specimen D2-S1-EB	120
Figure 4.33: Load-deflection curves of specimen D2-S1-EB+MA	120

Figure 4.34: Load-deflection curves of specimen D2-S1-ETD	121
Figure 4.35: Load-diagonal tensile displacement curves for specimen D2-S1-EB	122
Figure 4.36: Load-diagonal tensile displacement curves for specimen D2-S1- EB+MA	123
Figure 4.37: Load-diagonal tensile displacement curves for specimen D2-S1-ETD	123
Figure 4.38: Load-flexural strain relationships for specimen D2-S1-NR	125
Figure 4.39: Load-flexural strain relationships for specimen D2-S1-EB	126
Figure 4.40: Load-flexural strain relationships for specimen D2-S1-EB+MA ...	126
Figure 4.41: Load-stirrups strain response for specimen D2-S1-NR	128
Figure 4.42: Load-stirrups strain response for specimen D2-S1-EB	128
Figure 4.43: Load-stirrups strain response for specimen D2-S1-EB+MA.....	129
Figure 4.44: Load-stirrups strain response for specimen D2-S1-ETD.....	129
Figure 4.45: Load-FRP strains relationship for specimens of group [B] with damage state D2.	132
Figure 4.46: Failure mode for specimen ND-S2-NR	134
Figure 4.47: Failure mode of specimen ND-S2-EB	134
Figure 4.48: Failure mode of specimen ND-S2-EB+MA	134
Figure 4.49: Failure mode of specimen ND-S2-ETD	135
Figure 4.50: Load-deflection curves for the non-damaged specimens of group [C]	137
Figure 4.51: Load- diagonal tensile displacement curves for the non damage specimens of group [C]	139

Figure 4.52: Load-flexural strain relationships for the non-damaged specimens of group [C]	140
Figure 4.53: Load- stirrups strain response for the non- damaged specimens of group [C]	141
Figure 4.54: Load-FRP strain relationships for the non- damaged specimens of group [C]	142
Figure 4.55: Failure mode of specimen D2-S2-NR	144
Figure 4.56: Failure mode of specimen D2-S2-EB	145
Figure 4.57: Failure mode of specimen D2-S2-EB+MA	146
Figure 4.58: Failure mode of specimen D2-S2-ETD	147
Figure 4.59: Load-deflection curves of specimen D2-S2-EB	151
Figure 4.60: Load-deflection curves of specimen D2-S2-NR.....	151
Figure 4.61: Load-deflection curves of specimen D2-S2-ETD	152
Figure 4.62: Load-deflection curves of specimen D2-S2-EB+MA	152
Figure 4.63: Load-diagonal tensile displacement for specimen D2-S2-NR	153
Figure 4.64: Load-diagonal tensile displacement for specimen D2-S2-EB.....	153
Figure 4.65: Load-diagonal tensile displacement for specimen D2-S2-EB+MA	154
Figure 4.66: Load-diagonal tensile displacement for specimen D2-S2-ETD	154
Figure 4.67: Load-flexural strain relationship for specimen D2-S2-NR.....	157
Figure 4.68: Load-flexural strain relationship for specimen D2-S2-EB	157
Figure 4.69: Load-flexural strain relationship for specimen D2-S2-EB+MA	158
Figure 4.70: Load-flexural strain relationship for specimen D2-S2-ETD	158
Figure 4.71: Stirrup's strain response of specimen D2-S2-NR.....	160
Figure 4.72: Stirrup's strain response of specimen D2-S2-EB	160
Figure 4.73: Stirrup's strain response of specimen D2-S2-EB+MA.....	161

Figure 4.74: Stirrup's strain response of specimen D2-S2-ETD.....	161
Figure 4.75: Load-FRP strain relationships for specimens of group [C] with damage state D2	164
Figure 4.76: Interaction between strengthening system, amount of internal steel stirrups and shear strength gain	165
Figure 4.77: Effect of initial shear damage on shear strength gain of the specimens with the lower amount of stirrups.....	168
Figure 4.78: Effect of shear damage D2 on shear strength gain of the specimens with the higher amount of stirrups	169
Figure 5.1: Comparison between experimental results of the non-damaged specimens and predictions of international guidelines/standards for EB-CRP system; (a) V_{fn} vs. $V_{f,exp}$, (b) V_{fd} vs. $V_{f,exp}$	189
Figure 5.2: Comparison between experimental results of the pre-cracked specimens and predictions of international guidelines/standards for EB-CFRP system; (a) V_{fn} vs. $V_{f,exp}$, (b) V_{fd} vs. $V_{f,exp}$	192
Figure 5.3: Comparison between experimental results of the pre-failed specimens and predictions of international guidelines/standards for EB-CFRP system; (a) V_{fn} vs. $V_{f,exp}$, (b) V_{fd} vs. $V_{f,exp}$	193
Figure 5.4: Analytical models predictions of V_{fn} vs. $V_{f,exp}$ for EB-CFRP system; (a) non damaged, (b) pre-cracked, (c) pre-failed specimens	195
Figure A. 1: Load vs. CFRP strain for ND-NS-EB.....	216
Figure A.2: Load vs. CFRP strain for ND-NS-EB+MA.....	216
Figure A.3: Load vs. GFRP strain for ND-NS-ETD.....	217
Figure A.4: Load vs. FRP strain for ND-S1-EB.....	217

Figure A.5: Load vs. FRP strain for ND-S1-EB+MA.....	218
Figure A.6: Load vs. FRP strain for ND-S1-ETD.....	218
Figure A.7: Load vs. FRP strain for D1-S1-EB.....	219
Figure A.8: Load vs. FRP strain for D1-S1-EB+MA.....	219
Figure A.9: Load vs. FRP strain for D1-S1-ETD.....	220
Figure A.10: Load vs. FRP strain for D2-S1-EB.....	220
Figure A.11: Load vs. FRP strain for D2-S1-EB+MA.....	221
Figure A.12: Load vs. FRP strain for D2-S1-ETD.....	221
Figure A.13: Load vs. GFRP strain for ND-S2-ETD.....	222
Figure A.14: Load vs. CFRP strain for D2-S2-EB.....	222
Figure A.15: Load vs. CFRP strain for D2-S2-EB+MA.....	223
Figure A.16: Load vs. GFRP strain for D2-S2-ETD.....	223
Figure B.1: Load vs. stirrup strain for ND-S1-NR.....	224
Figure B.2: Load vs. stirrup strain for ND-S1-EB.....	225
Figure B.3: Load vs. stirrup strain for ND-S1-EB+MA.....	225
Figure B.4: Load vs. stirrup strain for ND-S1-ETD.....	226
Figure B.5: Load vs. stirrup strain for D1-S1-NR.....	226
Figure B.6: Load vs. stirrup strain for D1-S1-EB.....	227
Figure B.7: Load vs. stirrup strain for D1-S1-EB+MA.....	227
Figure B.8: Load vs. stirrup strain for D1-S1-ETD.....	228
Figure B.9: Load vs. stirrup strain for D2-S1-NR.....	228
Figure B.10: Load vs. stirrup strain for D2-S1-EB before retrofitting.....	229
Figure B.11: Load vs. stirrup strain for D2-S1-EB after retrofitting.....	229
Figure B.12: Load vs. stirrup strain for D2-S1-EB+MA before retrofitting.....	230

Figure B.13: Load vs. stirrup strain for D2-S1-EB+MA after retrofitting..	230
Figure B.14: Load vs. stirrup strain for D2-S1-ETD before retrofitting....	231
Figure B.15: Load vs. stirrup strain for D2-S1-ETD after retrofitting.....	231
Figure B.16: Load vs. stirrup strain for ND-S2-NR.....	232
Figure B.17: Load vs. stirrup strain for ND-S2-NR.....	232
Figure B.18: Load vs. stirrup strain for ND-S2-EB+MA.....	233
Figure B.19: Load vs. stirrup strain for ND-S2-ETD.....	233
Figure B.20: Load vs. stirrup strain for D2-S2-NR.....	234
Figure B.21: Load vs. stirrup strain for D2-S2-EB before retrofitting.....	234
Figure B.22: Load vs. stirrup strain for D2-S2-EB after retrofitting.....	235
Figure B.23: Load vs. stirrup strain for D2-S2-EB+MA before retrofitting...	235
Figure B.24: Load vs. stirrup strain for D2-S2-EB+MA after retrofitting....	236
Figure B.25: Load vs. stirrup strain for D2-S2-ETD before retrofitting.....	236
Figure B.26: Load vs. stirrup strain for D2-S2-ETD after retrofitting.....	237

LIST OF NOMENCLATURE

- a = shear span
- A_f = cross sectional area of FRP
- A_s = area of tensile steel reinforcement
- A_v = cross section area of transverse steel reinforcement
- b_f = width of beam flange
- b_w = Width of beam web
- d = effective depth of tensile steel reinforcement
- d_f = effective depth of FRP from the extreme compression fiber to the centroid of tension reinforcement (also might be written as d_{frp})
- D_f = stress distribution factor
- D_{frp} = stress/strain distribution factor
- E_f = tensile modulus of FRP (also might be written as E_{frp})
- f_c = concrete compressive strength
- f'_{cd} = compressive design concrete strength
- f_{ct} = concrete tensile strength
- f_{ctm} = concrete tensile strength
- f_{cu} = cube compressive strength of concrete

- f_{dd} = ultimate design strength of FRP
- f_{fd} = design value for the ultimate FRP stress
- f_{fe} = effective stress in FRP
- f_{fed} = design value for the FRP effective stress
- f_{fu} = ultimate tensile strength of FRP
- f_{fud} = design tensile strength of FRP
- $f(s_m)$ = stress in FRP rods corresponding to maximum bond stress
- f_v = transverse steel reinforcement yield stress
- G_{fk} = bonded joint specific fracture energy
- h = beam depth
- h_{df} = vertical distance from the crack tip to the point of the intersection
between the debonding front and the critical shear crack
- h_{fe} = effective bond length of EB-CFRP shear reinforcement
- h_w = beam stem depth
- K = shear reinforcing factor
- K_{max} = maximum value of shear interaction factor
- k_f = factor related to width of the bonded plate and width of the concrete
member.

- k_L = effective anchorage length coefficient
- L_e = effective anchorage length
- L_{eff} = effective length of FRP rod
- L_{max} = maximum available bond length
- L_v = vertical bonded length of FRP
- N = total number of FRP shear reinforcement in the shear span
- r_w = corner radius of the section to be wrapped
- s = spacing between transverse reinforcement
- s_f = center to center spacing between FRP shear reinforcement in longitudinal direction
- s_f' = center to center spacing between FRP shear reinforcement in orthogonal direction
- s_m = slip at maximum bond stress
- t_f = thickness of FRP composite
- V_c = contribution of concrete in shear resistance
- V_{cd} = design shear resistance of concrete
- $V_{d,max}$ = maximum design shear strength of the concrete member
- V_f = contribution of FRP in shear resistance
- V_{fd} = calculated FRP design shear resistance

$V_{fd,max}$ = maximum FRP design shear resistance

$V_{f,exp}$ = experimental FRP shear resistance

$V_{fn,max}$ = maximum FRP nominal shear resistance

V'_n = nominal shear strength of concrete

$V'_{n,max}$ = maximum nominal shear resistance

V'_s = contribution of transverse reinforcement in shear resistance

V'_{sd} = design shear resistance of stirrups

w/c = water to cement ratio

$w_{e,p}$ = crack end width when the FRP shear contribution reaches its peak value

w_f = width of CFRP sheet

w_{fe} = effective FRP width

z = the lever arm length

α = angle of inclination of FRP shear reinforcement

α' = curve fitting parameter

ρ = longitudinal tensile reinforcement ratio

ρ_f = FRP shear reinforcement ratio

ρ_s = transverse steel ratio

ε_{fe} = effective strain in FRP

ϵ_{frp} = the effective strain in the FRP rod

ϵ_{fu} = ultimate strain of FRP

β_L = coefficient to compensate for insufficient FRP anchorage length

β_w = FRP- width-to-spacing-ratio coefficient

β_c = concrete cracking coefficient based on transverse steel and FRP rigidity

values

κ_1 = concrete-strength modification factor

κ_2 = wrapping-scheme modification factor

κ = FRP design reduction factor

κ_b = covering/scale coefficient

κ_v = bond-reduction coefficient

γ_b = member strength reduction factor

γ_c = compressive strength material factor

γ_m = member factor

γ_f = safety factor accounts to mode of failure of FRP

γ_{fd} = partial safety factor depending on the application quality

γ_{Rd} = partial factor for resistance model

τ_{eff} = average bond shear stress at failure

τ_m = maximum bond stress

δ_f = interfacial slip at the shear crack at which the FRP is fully debonded

$\sigma_{db,max}$ = maximum achievable debonding stress in FRP strips intersected by the critical shear crack

$\sigma_{f,max}$ = maximum design stress in FRP

A = normalized maximum bond length

ϕ = shear design factor of concrete

ϕ_s = stirrups bar diameter

Ψ = FRP strength reduction factor

θ = angle of inclination of shear cracks

CHAPTER 1: INTRODUCTION

1.1 Background

The main purpose of strengthening reinforced concrete (RC) structures is to enhance their capacity in order to safely resist the anticipated applied loads. The trend is going toward adopting more conservative safety factors and higher live loads which will lead to unsafe old structures if not strengthened. These conservative safety factors could also account for the presence of damage due to frequent overloading conditions or under extreme events such as earthquakes. Strengthening is considered as an efficient, economical and environmental friendly solution relative to the demolishing option.

Reinforced concrete beams are generally designed to fail in a ductile manner. Therefore, providing sufficient transverse shear reinforcement would guarantee the incident of a ductile flexural failure. Consequently, shear strengthening is typically needed to eliminate the brittle shear mode of failure.

The internal transverse shear reinforcement is usually spaced at large spacings, e.g half the beam depth. Failure of one stirrup thus would result in a serious hazardous and unsafe situation. Also, an error in design or in steel detailing might be another reason of failure. The exposure of stirrups to adverse environmental conditions could result in extreme hazardous failure conditions.

1.2 Shear strength in concrete members

The design of a reinforced concrete member typically starts by flexural design using code equations and provisions. The outcomes of the flexural design are the dimensions of the cross section of the member and longitudinal reinforcement.

The shear design typically follows the flexural design. Shear failure is characterized as a sudden and brittle failure. Therefore, it is required to meet the condition that shear strength exceeds the flexural strength at every section along the entire length of the beam.

The nominal shear strength (V_n) of a concrete beam is obtained using the following equation:

$$V_n = V_c + V_s \quad (1.1)$$

Where, V_c is the concrete contribution to the shear capacity and V_s is the contribution of the shear reinforcement (stirrups) and bent-up bars to the shear capacity. The contribution of concrete, V_c , includes shear resistance of un-cracked concrete, the dowel action of the longitudinal tensile reinforcement and the aggregates interlock as shown in Figure 1.1.

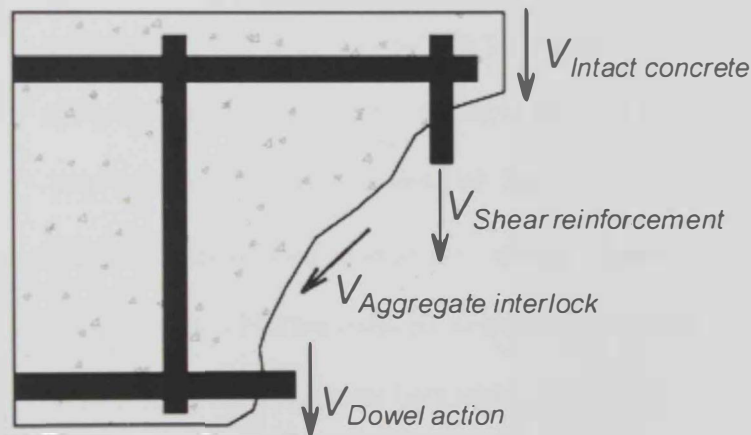


Figure 1.1: The contribution of concrete and steel reinforcement in shear resistance (Nogueira et al. 2013)

Reinforced concrete beams strengthened using FRP have an additional term to be added to equation 1.1, which is the contribution of FRP to the shear capacity, V_f .

1.3 Types of destruction in concrete members.

Reinforced concrete members are continuously exposed to various sources of damage, defects and deterioration that causes weakness or damage of the exposed member. These sources may highly cause unexpected risks to these members in terms of safety and serviceability.

1.3.1 Deterioration

Deterioration is considered as one type of unsatisfactory conditions in concrete structures. Deterioration results from aging and continuous exposure to harsh environments. Causes of deterioration include:

- *Wet-dry cycles*; which causes variation in the internal humidity of the concrete member in addition to other effects such as expansion and shrinkage that weaken the concrete members.
- *Chloride-induced corrosion*; which was found to be the most common deterioration mechanism that results by the penetration of chloride ions into concrete structures causing pitting corrosion of steel reinforcement (Angst and Ueli 2011).
- *Carbonation-induced corrosion*; which occurs in slower rate compared to chloride-induced corrosion. It causes uniform steel corrosion to reinforcement bars which accelerates the formation of Deterioration cracks on the concrete member surface (Ivan et al. 2005).
- *Alkali silica reaction (ASR)*; which is a reaction in the concrete between the hydroxyl ions in the alkaline cement pore solution in concrete and reactive forms of silica in aggregates generating a gel.

This gel expands by taking up water causing pressure that results in a typical map of cracks in concrete structures.

- *Sulfate attack*: which occurs due to penetration of sulfate ions into concrete which interacts with Hydrated Calcium Aluminates in the cement matrix resulting in Gypsum and Ettringite. These products expand causing pressure disrupting the cement matrix and loss of mortar from concrete surface (surface scaling) and concrete disintegration.

1.3.2 Concrete damage

Damage of concrete is another source that weakens concrete structures which typically results from unexpected accidents or unplanned problems. Causes of damage include:

- Overloading of concrete structures ahead of their capacities.
- Sudden collision accidents (e.g truck collides with beam or girder).
- Seismic load effects such as earthquakes.
- Foundation settlement
- Fire
- Chemical spills

1.3.3 Concrete member defects

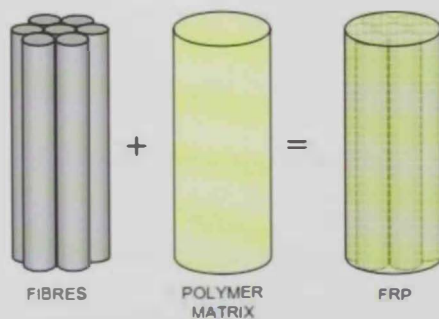
Defects in concrete members are another source that weakens the concrete structures. Defects mainly deal with problems that occur

during construction. Causes of defects include:

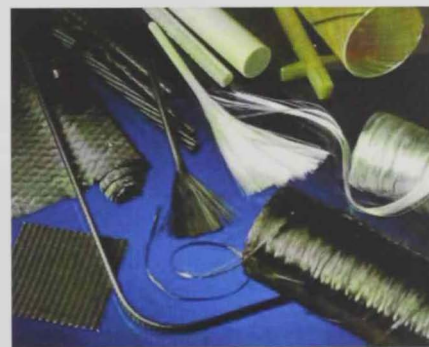
- Errors in design, either in the mix or in using improper code equations.
- Improper detailing of reinforcement.
- Movement of formwork during and or after casting.
- Use of improper materials
- Inadequate concrete cover.

1.4 Types of fiber reinforced polymers (FRPs)

Fiber reinforced polymers (FRPs) are composite materials that are made of two main components: fibers and matrix. The FRP composites are made by embedding a continuous high strength fibers in a resin matrix which then binds fibers together and also could be used to create bonds between the concrete and FRP as shown in Figure 1.2(a). Various fiber types commonly used include carbon, glass and aramid. Fibers could also be used to produce different products flexible fabrics, circular and rectangular composite strips/plates as shown in Figure 1.2(b).



(a) Components of FRP composite



(b) Various FRP products

Figure 1.2: Components and products of FRP composites (ISIS Canada 2006)

The common kinds of matrices are the epoxy, Vinyl Ester, and phenol formaldehyde resins. The matrix is used to bind the fibers together, split the disperse fibers within the composite used in, help in transmitting forces between fibers and protect the fibers from abrasion or any expected environmental degradation (ISIS Canada 2006). The author has used both flexible carbon fiber fabrics and GFRP bars in strengthening/retrofitting of the tested RC beams.

1.5 Applications of fiber reinforced polymers (FRPs)

Fiber reinforced polymer (FRP) is widely used in strengthening and repair applications of RC structures. The availability of FRP composites in many types such as sheets, plates, rods and strips facilitates its wide-spread usage. The FRP sheets are made using the wet lay-up process. In this process, the fibers are placed on concrete after the surface is coated using a liquid resin. Subsequently, another layer of the liquid resin is sprayed over the fiber followed by rolling in order to achieve completely wet fiber without air bubbles.

Commonly, FRP sheets are extensively used as externally bonded to concrete surface and are applied either continuously or as separated sheets. Generally, FRP sheets can be used as confining reinforcements or in shear and flexural strengthening applications.

Fiber reinforced polymers as confining reinforcement are frequently used in strengthening of RC columns. Fiber reinforced polymers are wrapped circumferentially and perpendicular to the longitudinal axis of the column which was found to enhance its strength and ductility. Applying FRP by this manner will

generate confining stresses that results when a compressive axial load is applied perpendicular to the columns' cross section causing a lateral expansion.

In flexural strengthening, FRP sheets are externally bonded along the tension side of the RC beam to act as additional tensile reinforcement. This by its role provides additional strength in bending. The fibers are always oriented along the direction of interest. Therefore, in flexural strengthening, the fibers are aligned in the longitudinal axis of the RC beam.

For shear strengthening, FRP sheets are applied on a scheme that is similar to the way of applying the transverse reinforcement. In other words, FRP sheets are applied either in U-wraps or full wrapping where the fibers are applied upright to the longitudinal axis of the RC beam. The U-wrapping pattern is commonly used in RC beams that have T-shaped cross section as shown in Figure 1.3.

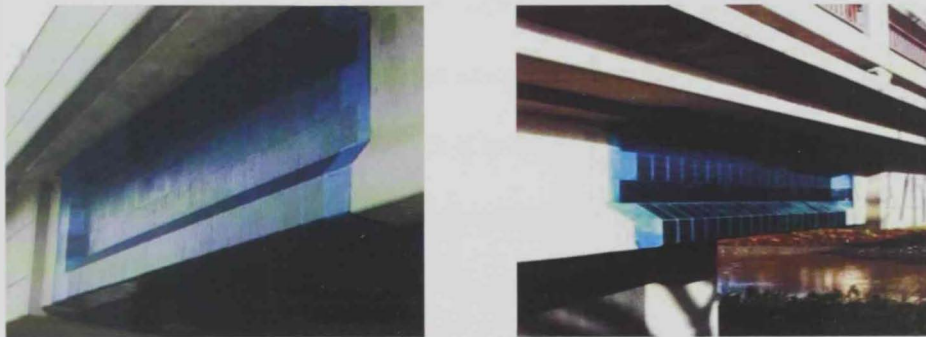


Figure 1.3: Shear strengthening of bridge girders using externally bonded FRP composites (ISIS Canada 2006)

The FRP bars and strips are produced by a pultrusion process. In this process, the continuous fibers are wetted by un-cured resin and pulled through a die in order to form the required cross section. Once the bar passes through the die, additional process are used to impart a deformation pattern to the bar surface to achieve better bonding when used as reinforcement in concrete. After that, the

resin is allowed to crosslink (Castro and Carino 1998). The FRP rods or strips can be installed in the longitudinal direction of the RC beam to provide additional strength to tensile reinforcement. They can also be installed in the transverse direction to enhance the shear strength. Historically, the first use of fiber reinforced polymers (FRP) in structural applications was in the mid 50's as reported by Rizkalla et.al. (2003). The FRP composites were used at that time in different applications ranged from semi-permanent structures to restoration of old buildings. In early 80's, the applications of composite products were established in Asia and Europe.

In cases if adequate bond lengths of the FRP laminates are not available due to certain RC beam geometry, end mechanical anchorage systems should be used in order to achieve the full design capacity of the FRP sheets used in strengthening (Eshwar et al. 2008). Commonly, the main role of FRP anchorage system is to prevent or postpone the debonding failure mode of the externally bonded FRP when separated from the concrete surface due to low tensile strength of concrete or inadequate bond length (Ceroni et al. 2008). Many researchers have developed anchorage methods that are expected to be effective when used side by side with the FRP U-jacketing shear strengthening system (Kalfat et al. 2013). A common case that requires end anchorage is a T-girder in a typical RC bridge or floor. The presence of the flange in T-shaped girders makes shear strengthening by fully wrapped externally bonded FRP impractical (El-Maaddawy and Chekfeh 2012). Moreover; anchorage systems provide the critical locations of a structural member with a load transfer mechanism. The FRP strengthening systems with mechanical end anchorages are expected to fail in global anchorage failure or due

to FRP rupture since sudden and brittle local stresses are imposed by the anchorage itself (Grelle and Sneed 2013).

The current work emphasis on shear strengthening of RC beams using externally bonded FRP sheets, GFRP bars embedded through the beam depth, and FRP plates that were used as a part of mechanical end anchorage system.

1.6 Properties of fiber reinforced polymers (FRPs)

It is important to recognize the difference between the properties of steel and FRP. The FRP composites have higher strength than steel as well as they do not yield.

The strain of FRP at failure is significantly less than that of the steel. The FRP composites do not have the same properties. Hence, there are different factors that play a major role in making this variation among FRP composites. The type of fiber and matrix, the used amount of each and the way of applying the fibers as orientation and the length of the applied FRP are some factors that differ from each supplier or manufacturer which result in different FRP composite properties. This variation is important since strengthening or repair cases differ in their requirements.

Carbon fiber reinforced polymers (CFRP) are commonly used in structural repair or strengthening applications. They have low density, high resistance to expected environmental effect, high modulus of elasticity and high strength. (ISIS Canada 2006)

Glass fiber reinforced polymers (GFRP) are cheaper than the CFRP. They are commonly used in wide range of strengthening applications of RC members. The GFRP are known by their low thermal conductivity, high strength, moderate elastic modulus and density. (ISIS Canada 2006)

Aramid fiber reinforced polymers (AFRP) are sensitive to degradation by ultraviolet radiations as well as moisture. The AFRPs are known by their low density, moderate elastic modulus high strength, and low compressive and shear strengths. Figure 1.4 compares the stress-strain relationship of different types of FRP composites with that of steel reinforcement. (ISIS Canada 2006)

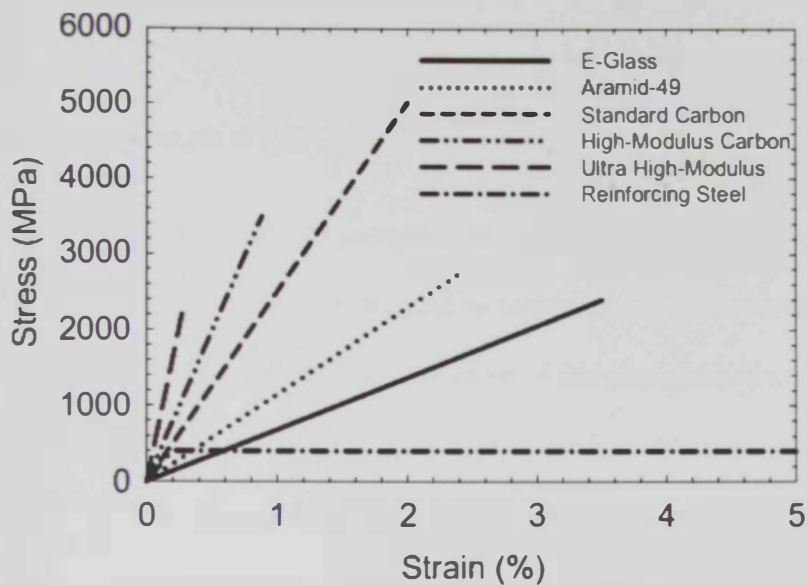


Figure 1.4: Stress strain diagram for different types of fibers and steel reinforcement (ISIS Canada 2006)

1.7 Advantages and disadvantages of fiber reinforced polymers

The FRP have showed promising results when being used in different structural engineering applications. Many advantages have been observed for FRP materials which made them favorable to be used in strengthening or repair applications compared to the traditional materials such as steel and concrete. The advantages and disadvantages of FRP composites are discussed herein.

Typical advantages of FRP composites include (ISIS Canada 2006)

- Durability in different environments
- High strength to weight ratios.

- Electromagnetic neutrality
- Corrosion resistant.
- Easy to apply
- Ability to modify the mechanical properties of the FRP material by tailoring the direction of the fibers in addition to the suitable choice of the fibers.

Typical disadvantages of FRP materials include:

- High initial cost compared to traditional material and strengthening system. However, it could be cost effective in long term considering the entire life cycle of the strengthened or repaired member.
- Low fire resistance. Therefore, the position of applying FRP materials is important as well as the surrounding environment.
- Volatile to high temperature.
- Some FRP materials such as glass fibers have low modulus of elasticity with some durability doubts especially in alkaline environments.
- Critical to fail by debonding.

1.8 Arrangement of work

The current research work was initiated to study the performance of shear deficient RC beams strengthened with two different composite based systems namely; externally bonded carbon fiber reinforced polymer (EB-CFRP) sheets and embedded through depth glass fiber reinforced polymer (ETD-GFRP) rebars. It comprises experimental testing and analytical investigation.

A literature review on shear strengthening of RC beams with composite-based systems is presented in Chapter (2). The chapter includes research needs and objectives of the current study.

Chapter (3) provides thorough information on the experimental test program, specimens' geometry, cross sectional dimensions and procedure of specimens' fabrication. The materials properties and strengthening methodologies are presented. A complete description of the test set-up, used instruments, way of controlling the experiments, loading conditions and schemes are all presented in details in this chapter.

Chapter (4) presents the experimental test results and interpretations. The obtained results include the various observed failure modes and records of shear capacity of test specimens. The deflection response, load versus diagonal tensile displacement across cracks, stirrups strain response and FRP strain response are presented and discussed. The chapter includes discussions and analysis of test results.

In Chapter (5) different analytical approaches recommended by international guidelines and standards or published in the literature are presented and reviewed. A comparative analysis between the experimental and analytical results is given in the same chapter.

Chapter (6) summarizes the general conclusions of the completed work followed by recommendations for future studies on shear strengthening of RC beams with composites.

CHAPTER 2: LITERATURE REVIEW

2.1 Introduction

Many experimental studies have been conducted on shear strengthening of RC structures using different composite-based systems. These studies have shown promising results on the effectiveness of FRP composites to improve the shear resistance of RC members. This chapter includes a review on the available literature related to shear strengthening of reinforced concrete beams with composites. The review focuses on two main shear strengthening systems namely; external-bonded (EB) FRP sheets, and embedded through depth (ETD) FRP bars.

2.2 Studies on shear strengthening using EB-FRP system without end anchorage

Research studies performed during the last decade on shear strengthening with the EB-FRP composite system are provided and discussed hereafter.

Carolin and Täljsten (2005) investigated the viability of using externally bonded CFRP composites to increase the shear capacity of RC beams. A total of 23 beams with a rectangular cross section were constructed and tested. Test specimen had a length of either 3500 or 4500 mm. The cross section was either 160 x 500 mm or 180 x 400 mm. Test parameters included the presence of internal steel stirrups, damage state (non damaged or pre-cracked), fiber direction (0, 45 and 90°) and amount (one, two and three layers), and the strengthening scheme. The concrete compressive strength was 55 MPa, on average. The stirrups steel yield strength was 515 MPa. The shear span to depth ratio was $a/h = 2.5$. The strengthening regime consisted of carbon fiber fabrics applied as two-side bonding only or fully wrapped around the entire beam cross section. After repair,

some specimens were subjected to fatigue loading, and all beams were finally tested to failure. The composite used for side bonding and wrapping had tensile modulus of 234 GPa and tensile strength of 4500 MPa. The identified failure modes were fiber rupture along the shear crack, fiber rupture at the corner, and combinations thereof. Test results indicated that beams with stirrups do not have the same lack of shear reinforcement, and the strengthening effect cannot be as large as for beams without stirrups. Also, a damaged beam can be strengthened and repaired to a level comparable to a strengthened beam that was not damaged before strengthening. Specimen repaired with side bonding of two layers of the CFRP sheets at 45° around their cross sections showed an enhancement of approximately two and a half fold in their ultimate shear capacity. It was also concluded that there was no significant difference between the 45° and 90° fiber directions while the 0° fiber direction turned to have insignificant contribution to the shear capacity. The use of higher FRP amount gave higher strengthening effect. The use of full wrapping enhanced the shear capacity by 11 to 23% compared to specimens strengthened with side bonding.

Zhang et al. (2005) studied shear strengthening of RC beams using CFRP laminates. A total of 11 beams with a rectangular cross section were constructed and tested. Test specimens had a length of either 1220 or 183 mm. The cross section had a width of 152.4 mm and depth of 228.6 mm. Test parameters included the CFRP type and orientation. The concrete compressive strength was 42 MPa, on average. No internal shear reinforcement was used in any of the beams. The shear span to depth ratio was $a/h = 2.3$. The strengthening regime consisted of continuous long unidirectional pultruded CFRP strips oriented parallel to beam length, short unidirectional CFRP strips placed at 90° and

45°/135° along the shear span, and CFRP woven composite fabric sheets externally bonded to concrete. The composite CFRP strips and sheets had a tensile modulus of 165 and 73.1 GPa, tensile strength of 2800 and 906 MPa, and ultimate elongation of 1.9 and 1.33%, correspondingly. The specimens strengthened with CFRP strips failed due to concrete debonding underneath the epoxy, while failure of the specimens strengthened with CFRP sheets was due to fabric rupture. Test results indicated that 45° CFRP strips orientation is recommended which resulted in 80% increase in shear capacity compared to 90° CFRP strips orientation which resulted in 60% increase in shear capacity. It was concluded that CFRP strips were more effective in increasing the shear capacity compared to the continuous CFRP sheets which showed the least shear contribution among the other CFRP shear strengthened beams with 16% increase in shear capacity.

Bousselham and Chaallal (2006) examined the performance of RC beams retrofitted in shear with externally bonded carbon fiber-reinforced polymer (EB-CFRP). A total of 22 tests were performed on 11 full scale beams with a T-shaped cross section were constructed and tested. Test specimens had a length of 4520 mm. The T-section had a flange width and thickness of 508 and 102 mm, respectively, a depth of 406 mm, and a web width of 152 mm. Test parameters included the number of CFRP layers (*0L*, *0.5L*, *1L* and *2L*), stirrups spacing (no stirrups, $s = d/2$ and $s = d/4$), and shear length to beam's effective depth ratio ($a/d = 1.5$ and $a/d = 3$). The concrete compressive strength was 25 MPa. The stirrups steel yield stress was 650 MPa. The strengthening regime consisted of a continuous U-shaped CFRP sheet laterally applied to beam's web sides. The composites had a tensile modulus of 231 GPa, a tensile strength of 3650 MPa, and ultimate elongation of 1.4%. It was noticed that the shear failure occurred by

crushing of concrete struts. Test results indicated that the increase in shear capacity due to CFRP was higher for deep beams with $a/d = 1.5$ (between 9.9% to 62.2%) compared to slender specimens with $a/d = 3$ (between 1.7% to 49.8%). It was also concluded that the addition of stirrups has decreased the gain in shear capacity. The shear strength gain was not proportional to the CFRP thickness. Neither the crack angle nor the crack pattern was changed by the use of CFRP; however, they were affected by the presence of stirrups. It is worth to say that stirrups yielded in most cases knowing that their strains were considerably higher in specimens with no CFRP.

Pellegrino and Modena (2006) conducted a study on shear strengthening of RC concrete beams using externally bonded U-wrapped CFRP sheets. A total of 12 tests were conducted. The beam had a rectangular section with a width of 150 mm and a depth of 300 mm. Test parameters included the load scheme (simply supported or continuous), distribution of the internal steel stirrups ($s = 170$ mm or $s = 200$ mm), and the number of CFRP layers. The cylinder concrete compressive strength was 41.4 MPa. The stirrups steel yield stress was 534 MPa. The shear span to effective depth ratio was $a/d = 3$. The strengthening regime consisted of continuous/simply supported beams externally bonded with U-shaped CFRP sheets with one or two layers. The strengthened specimens failed due to peeling off of the CFRP-reinforcement as shown in Figure 2.1. Test results showed that the increment of shear strength for the continuous beams were between 28.6 to 35.8%, while it was between 2 to 24.8% for the simply supported specimens. It was concluded that a general reduction of efficiency of the strengthened technique with U-wrapped CFRP sheets is observed when stirrups

spacing decreases. Small increments of strength were observed from one to two layers of the CFRP-strengthened beams.

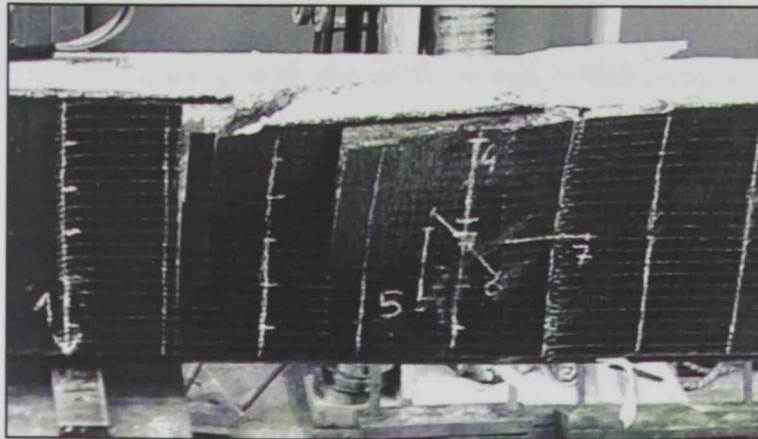


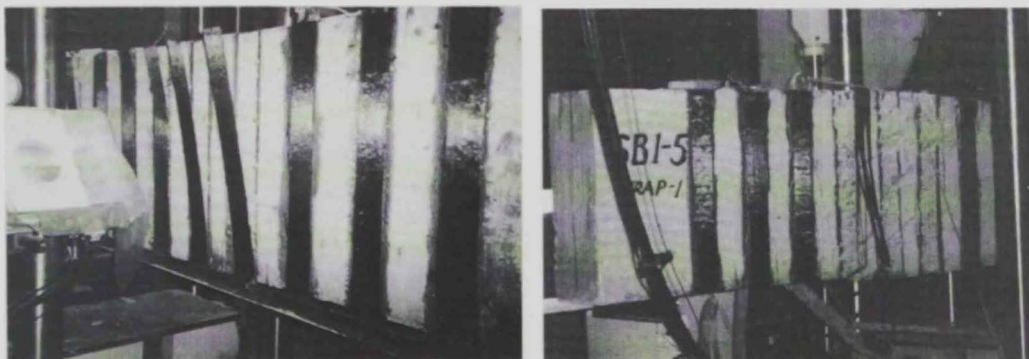
Figure 2.1: Peeling off of the CFRP reinforcement
(Pellegrino and Modena 2006)

Kesse and Lees (2007) studied the behavior of RC beams strengthened with prestressed CFRP shear straps. A total of 12 cantilever beams with a rectangular cross section were constructed and tested. Test specimens had a length of 1200 mm. The rectangular section had a width of 105 mm and a depth of 280 mm. Test parameters included the strap spacing, strap stiffness, initial strap prestress level, and the presence of pre-cracks. The concrete compressive strength was 32 MPa. The stirrups steel yield stress was around 400 MPa. The shear span to effective depth ratio was $a/d = 3$. The strengthening regime consisted of layers of CFRP tape wrapped around the beam to form a strap acting as a discrete unbonded vertical prestressing tendon. The pre-cracking was achieved by loading the specimen up to 70% of the un-retrofitted ultimate load capacity before being unloaded and strengthened with one strap of five layers or two straps of 10-layers. The composites had a tensile modulus of 130 GPa and ultimate strain of 11000 $\mu\epsilon$. Specimens strengthened with a single strap failed in shear mode of failure, while several specimens strengthened with two straps failed in flexure mode of

failure. Test results indicated that all strengthened beams had a shear capacity at least 50% higher than that of an equivalent unstrengthened beam. The spacing of the straps did not solely influence the capacity and mode of failure, but also the interaction of the spacing with the stiffness and initial prestress force. The existence of shear cracks seemed to influence the stiffness of the beam, but did not have a significant influence on the ultimate shear capacity. The prestressing force was found to provide an advantage over a passive strengthening system since it would help in closing any existing cracks. The stiffness of the strap played a main role once the crack crossed the straps, where a rapid growth of cracks was expected in the case of straps with inadequate stiffness. The mode of failure for a strengthened specimen with CFRP straps changed from shear to flexure mode of failure with an ultimate load capacity of 90% higher than that of an equivalent unstrengthened specimen when a suitable strap spacing, initial prestress, and stiffness were selected.

Leung et al. (2007) examined the effect of section size on the failure of concrete beams with a similar span to effective depth ratio when retrofitted in shear using CFRP strips. A total of 15 beams with a rectangular cross section were constructed and tested. Test specimens had various depths of 180, 360, and 720 mm and lengths of 950, 1900, and 3800 mm, correspondingly. Test parameters included the beam size, the CFRP strip spacing, width, thickness and the strengthening scheme. The concrete compressive strength was 27.4 MPa. The shear span to effective depth ratio was in the range of 2.73 to 2.95. The strengthening regime consisted of U-shaped or fully wrapped CFRP strips spaced at 60, 120 and 240 mm. The CFRP composite sheets had a tensile modulus of 235, GPa a tensile strength of 4200 MPa, and ultimate elongation of 1.8%. The beams

strengthened with the U-wraps failed by debonding of the CFRP sheets as shown in Figure 2.2(a), while the fully-wrapped beams failed by rupture of the CFRP sheets as shown in Figure 2.2(b). Test results indicated that beams strengthened with U-shaped CFRP sheets showed approximately 60% increase in shear capacity for the small beam, while the large and midsize beams showed only 4-7% increase in shear capacity. However, a similar range of 57 to 67% increase in shear capacity was observed for the beams strengthened by fully wrapped CFRP sheets regardless of the member size. The larger the spacing between the CFRP sheets, the less the contribution of the CFRP strips to shear resistance. It was concluded that for the fully-wrapped CFRP sheets regime, the variation of the CFRP strip width, spacing and thickness with the members of different sizes showed similar effectiveness of strengthening as long as the increase in the width, spacing and thickness of the CFRP is proportional to the increase of the cross section dimensions.



(a) Debonding of the CFRP sheets

(b) Rupture of the CFRP sheets

Figure 2.2: Debonding and rupture failure modes of the strengthened beams
(Leung et al. 2007)

Bousselham and Chaallal (2008) extended their earlier study (Bousselham and Chaallal 2006) on shear behavior of RC beams strengthened in shear with externally bonded CFRP. A total of six new tests were performed on three full

size T-beams . Test specimens had a length of either 3000 (ED1 series) or 4520 mm (ED2 series). The ED1 and ED2 series had flange widths of 508 and 270 mm, and flange thicknesses of 102 and 55 mm, respectively. Test specimens of ED1 and ED2 series had depths of 406 and 220 mm with widths of 152 and 95 mm, respectively. Test parameters included the number of CFRP layers (0L, 0.5L, 1L, and 2L), stirrups spacing, and the size of the specimen. Specimens of the ED1 series had either no stirrups or stirrups of $\phi 8$ spaced at $s = d/2$ or $s = d/4$ (where $d = 350$ mm), while, ED2 series specimens had either no stirrups or stirrups of $\phi 4.8$ spaced at $s = 100$ mm (where $d = 175$ mm). The concrete compressive strength was 25 MPa, on average. The stirrups steel yield stress for $\phi 4.8$ and $\phi 8$ were 660 and 600 MPa, respectively. The shear span to effective depth ratio was $a/d = 3$. The strengthening regime consisted of U-shaped CFRP sheets which were continuously applied over the test zone around the web. The composites had a tensile modulus of 231 MPa, a tensile strength of 3650 MPa and ultimate elongation of 1.4% as provided by the manufacturer. The shear failure occurred by crushing of concrete struts and yielding of stirrups in most cases as generally assumed by the design guidelines. Test results indicated that the gain in shear capacity due to CFRP was higher for ED2 series (between 3% to 90%) compared to ED1 series (between 2% to 50%). Increasing the transverse steel ratio lowers the contribution of the CFRP to the shear resistance. It was concluded that the shear capacity gain due to the CFRP is greater for beams with smaller size (ED1 series) than for those of bigger size (ED2 series). The maximum strain in CFRP within the same section of the tested beams was smaller for the thicker CFRP fabrics. For instance, the maximum strain attained for a fabric of two layers was

about 11% of the ultimate strain value, while the maximum strain for the fabric with half layer was 38% of the ultimate strain.

Alrousan and Issa (2009) studied the size effect of RC beams on the contribution of CFRP composites to the shear resistance. A total of 16 beams with a rectangular cross section were constructed and tested. Test specimens had a length of 1524 mm. The cross section had various depths of 225, 300, 375, and 450 mm. The concrete compressive strength was 60 MPa. The stirrups yield strength was 410 MPa. The shear span to effective depth ratio was in the range of 1.2 to 2.7. The strengthening regime consisted of one layer of 90° CFRP sheets U-wrapped around the beam section. The CFRP composite had a tensile modulus of 230 GPa and a tensile strength of 3800 MPa. The specimens failed due to detachment of the CFRP sheets from the concrete surface. Test results indicated the use of CFRP sheets increased the shear capacity by 15-19% over that of the control specimens. Providing larger bonding lengths could be an effective solution in preventing the detachment of the CFRP sheets. It was also concluded that the shear strength increased with an increase in the effective depth. Also, the shear crack developed at slower rate as the effective depth increased.

Grande et al. (2009) examined the effect of transverse steel on the response of RC beams strengthened in shear by CFRP sheets. A total of 15 RC beams with a rectangular cross section were constructed and tested. Test specimens had a length of 2800 mm. The rectangular cross section was 250 mm wide and 450 mm deep. Test parameters included stirrups spacing ($s = 200$ mm, $s = 300$ mm, $s = 400$ mm) and the strengthening regime. The concrete compressive strength was 21 MPa. The stirrups steel yield strength was 476 MPa. The shear span to effective depth ratio was $a/d = 3$. Three strengthening regimes were

applied namely: complete wrapping with CFRP sheets around the cross section, improved U-jacketing with CFRP sheets surrounding only three sides of the section with additional strip placed along the upper part of the beam to enhance the anchorage of the CFRP sheets, and side bonding of CFRP sheets applied only at lateral faces of the beam section. The CFRP composites had a tensile modulus of 392 GPa a tensile strength of 2600 MPa, and ultimate tensile strain of about 0.6%. Strengthened specimens with complete wrapping failed in tensile fracture of the composite sheet since CFRP sheets cannot delaminate, while side bonded specimens failed by upper and lower FRP edge debonding. The beams strengthened with improved U-jacketing failed by rupture of the CFRP. Test results indicated that the complete wrapping showed comparatively the best response and the U-jacketing appeared better than the side bonding. The complete wrapping resulted in an increase in the ultimate shear force of the beam in the range of 140 to 208%. The U-jacketing and the side bonding resulted in an increase in the ultimate shear force of the beam in the range 130 to 186% and 112 to 150%, respectively. The CFRP shear resisting action was generally smaller in the beams having closer stirrups with exception of the fully-wrapped specimens with 300 mm stirrups spacing. The stirrups yielded only in the specimens with 400 and 300 mm stirrups spacing; however, they didn't yield in the specimens with 200 mm stirrups spacing.

Teng et al. (2009) studied the behavior of RC beams strengthened with bonded or unbonded CFRP wraps in shear. A total of nine beams with a length of 1500 mm and a rectangular cross section of 150 and 300 mm were constructed and tested. Test parameters included the existence of steel stirrups in the shear span, the diameter of the stirrups (6 mm or 8 mm), and the bonding/unbonding of

the CFRP strips. The concrete cube compressive strength was 47.2 MPa. The stirrups steel yield stress of $\phi 6$ and $\phi 8$ were 271 and 342.2 MPa, correspondingly. The shear span to depth ratio was approximately $a/h = 2.8$. The strengthening regime consisted of either complete wrapping of CFRP strips within the shear span or CFRP wraps bonded only to the compression and tension faces and the corners and unbonded on the sides. The CFRP composites had a tensile modulus of 266 GPa, a tensile strength of 3970 MPa, and rupture strain of 15000 $\mu\epsilon$. All specimens failed in shear mode of failure. Specimens strengthened with complete wrapping failed due to CFRP rupture, while specimens with unbounded CFRP failed in compression failure near the loading point. Test results indicated that the unbonded FRP wraps had slightly higher shear strength contribution with an increase in the shear resistance in the range of 38 to 94% compared to that of the bonded CFRP wraps which showed enhancement in shear resistance in the range of 49 to 65%. The existence of the steel stirrups had a significant effect on the distribution of CFRP strain along the critical shear crack. The larger the diameter of the steel stirrup, the less the enhancement in the shear capacity. It was also concluded that the specimens strengthened with fully wrapped CFRP wraps expressed more ductility compared to the specimens with the unbonded sides which was useful in giving warnings prior to the impending failure.

Godat et al. (2010) examined the size effect for reinforced concrete beams strengthened in shear using CFRP sheets. A total of seven beams with a rectangular cross section were constructed and tested. Test specimens had lengths of 900, 1800 and 2700 mm, with web widths of 100, 200, and 300 mm, and total depths of 200, 400, and 600 mm, correspondingly. Test parameters included the beam size, strengthening scheme, and CFRP regime/amount. The concrete

compressive strength was approximately 51 MPa on average. No steel stirrups were provided in the shear span. The shear span to effective depth ratio was $a/d = 1.51$. The strengthening regime consisted of CFRP sheets that were applied vertically in U-wraps or a completely wrapped pattern around the beam section along the shear span. The specimens strengthened with U-wraps failed in shear due to debonding of the CFRP sheets, while the fully wrapped specimens failed due to CFRP rupture. Test results indicated that the contribution of the CFRP to shear resistance was higher for smaller size specimens. The small beam size specimens showed a 28% increase in the ultimate capacity, while the medium and large size specimens showed 14 and 24% increase in shear capacity. The section size had no effect on shear strength gain of the fully wrapped specimens where an improvement of 37% in the shear capacity was recorded. It was also concluded that if the dimensions of the beams as well as the amount of CFRP increased proportionally, the contribution of the CFRP would be higher in the smaller specimens.

Nikopour and Nehdi (2011) conducted a study on shear repair of RC beams using epoxy injection and hybrid external FRP laminates. A total of six RC beams with a rectangular cross section were constructed and tested. Test specimens had a span of 1320 mm. The rectangular section was 150 mm wide and 250 mm deep. Test parameters included the repairing method (epoxy injection only, or with external strengthening using unidirectional carbon fiber), FRP type (carbon, glass, and aramid), and FRP wrapping scheme (hybrid composite of Carbon-Glass "CG", hybrid composite of Carbon-Aramid "CA", vertical unidirectional carbon fiber fabric "C", and +45/-45 glass fibers "GG"). The concrete compressive strength was 25.1 MPa on average. The stirrups steel yield

stress was 465 MPa. The shear span to effective depth ratio $a/d = 2.5$. The composites of C, CG, CA, GG had a tensile modulus of 87.3, 95.8, 72.4, and 19.3 GPa, respectively. Most of the specimens failed by formation of cracks inclined at 45° followed by debonding of the FRP laminates. The results indicated that the highest improvement in ultimate capacity was found by using the hybrid of CA, where a 35% enhancement was recorded. It was also concluded that the use of hybrid applications of FRP sheets showed better performance in enhancing the ultimate shear capacity of retrofitted RC beams compared with specimens retrofitted by unidirectional carbon fibers. Crack injection with low viscosity epoxy supplied the performance of the repaired specimens with better stiffness. The specimens repaired with thicker and stronger FRP sheets were less likely to fail by rupture of the FRP sheet.

Mofidi and Chaallal (2011) investigated the effect of strip-width-to-strip-spacing ratio in shear strengthening of RC beams with externally bonded CFRP composites. A total of seven full size beams with a T-shaped cross section were constructed and tested. Test specimens had a length of 4520 mm. The T-section had a flange width and thickness of 508 and 102 mm, respectively, a total depth of 406 mm and a web width of 152 mm. Test parameters included the strengthening regime, CFRP rigidity, strip location with respect to stirrups location. The concrete compressive strength was 29 MPa. The stirrups were 8 mm in diameter and spaced at $s = d/2$ where $d = 350$ mm. The stirrups steel yield stress was 540 MPa. The shear span to effective depth ratio was $a/d = 3$. The strengthening regime consisted of U-shaped intermittent CFRP strips or U-shaped continuous CFRP sheets covering the entire shear span. The composites had a tensile modulus of 230 GPa, a tensile strength of 3450 MPa, and ultimate strain of 1.5%.

The specimens strengthened using CFRP sheets failed by crushing in concrete struts followed by CFRP debonding as shown in Figure 2.3. It is worth to say that local CFRP fracture was noticed, however, due to stress concentrations at the web corners. Test results indicated that specimens strengthened with U-shaped strips had 66% gain in shear capacity owing to CFRP compared to 31% for the specimens strengthened using continuous CFRP sheets. It was also concluded that the addition of stirrups has resulted in remarkable decrease in the shear strength gain caused by CFRP. The installation of CFRP strips in the same places of stirrups along the longitudinal direction showed more flexible behavior compared to specimens with CFRP strips installed at mid-positions between stirrups. The wider the CFRP strips, the higher the contribution of CFRP to shear resistance for the same CFRP strip-width-to-strip-spacing ratio.

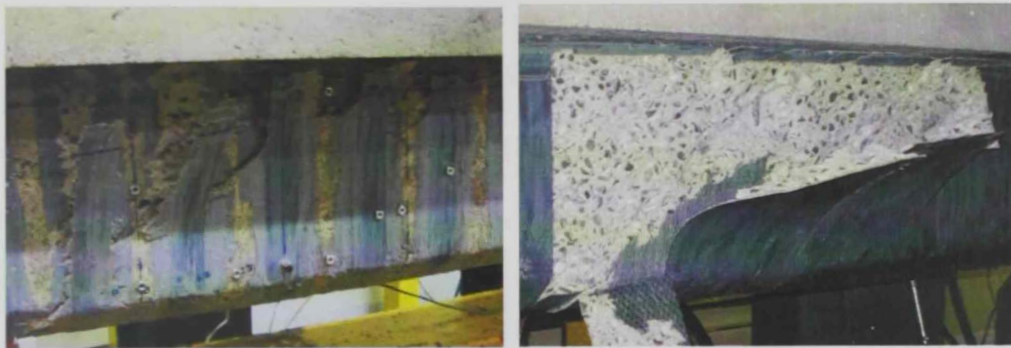


Figure 2.3: Debonding of CFRP sheets failure mode in the strengthened specimens (Mofidi and Chaallal 2011)

EI-Maaddawy and EI-Ariss (2012) examined the behavior of concrete beams with short shear span and web openings strengthened in shear with CFRP composites. A total of 16 beams with a rectangular cross section were constructed and tested. Test specimens had a length of 2600 mm. The rectangular section was 85 mm wide and 400 mm deep. Test parameters included the width of the opening (200, 350, 500 mm), the depth of the opening (120, 160, and 200 mm), and the

strengthening regime around the opening using CFRP. The concrete compressive strength was 20 MPa. The shear span to depth ratio was $avh = 2$. Two strengthening regimes were used around the openings. Regime 1 consisted of horizontal strengthening using one layer of CFRP fibers placed parallel to the longitudinal axis of the beam and vertical strengthening using one layer of CFRP placed perpendicular to the longitudinal direction of the beam. Regime 2 was almost similar to Regime 1; however, two layers of CFRP were applied in the vertical strengthening. The carbon fabric had a tensile modulus of 230 GPa, a tensile strength of 3450 MPa and ultimate elongation of 1.5 %. All strengthened specimens failed in shear by debonding of the CFRP sheets at the opening corners as shown in Figure 2.4. Test results indicated that the existence of web openings in concrete beams without providing stirrups resulted in huge reduction in shear capacity. The CFRP shear strengthening around the opening restored 90% to 100% of the shear capacity of the solid reference beam without the opening. Increasing the opening depth and width reduced the gain in shear capacity caused by CFRP. It was also concluded that increasing the amount of vertical sheets around the opening enhanced the shear capacity, but the additional improvement was not proportional to the added amount of CFRP.

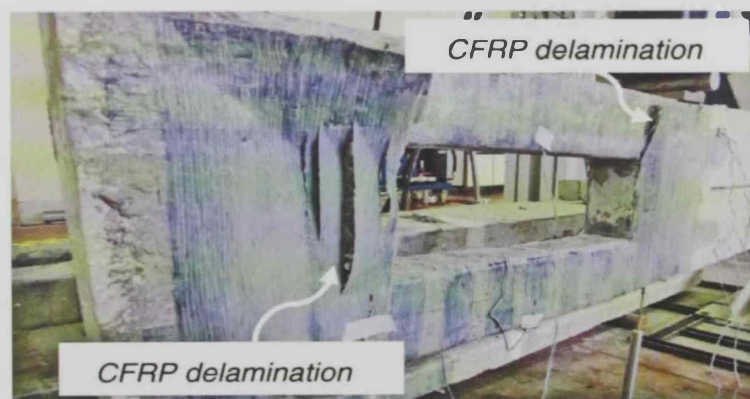


Figure 2.4: CFRP sheets delamination at the opening corners (El-Maaddawy and El-Ariss 2012)

Dirar et al. (2012) investigated the structural behavior of pre-cracked reinforced concrete T-beams repaired in shear using bonded carbon fiber-reinforced polymer sheets. A total of seven beams with a T-shaped cross section were constructed and tested. Test specimens had a length of 3800 mm. The T-section had a flange width and thickness of 250 and 105 mm, respectively, and a total depth of either 270 or 350 mm with a thickness of 105 mm for the web. Test parameters included the influence of loading history, beam depth and percentage of longitudinal steel reinforcement on the structural behavior. The concrete cube compressive strength was 25 MPa. The stirrups steel yield strength was 580 MPa. The shear span to effective depth ratio was $a/d = 3.8$. Three loading schemes were applied for testing. Control specimens were loaded up to failure. Other specimens were loaded up to 70% of the unstrengthened shear force capacity, then unloaded to 40% of the unstrengthened capacity prior to installation of the strengthening system. After strengthening, the specimens were either loaded at the same position up to failure, or the loading position was shifted prior to loading up to failure. The strengthening regime consisted of continuous U-shaped CFRP sheets applied along the shear span. The composites had a tensile modulus of 238 GPa, a tensile strength of 4300 MPa, and ultimate strain of 1.8%. Generally, all specimens failed in shear due to an inclined crack that extended from the flange to the load pad except a one specimen that failed in flexure. Test results indicated that the strengthened specimens had higher capacities compared to the control specimens with an enhancement of 9.7 to 26.2%. It was also concluded that the applied loading patterns had no significant effect on the peak load at failure. Also, the increase of beam depth caused better contribution of CFRP sheets, while

decreasing the longitudinal reinforcement ratio from 4.5 to 3.3% changed the mode of failure to ductile flexural failure.

Higgins et al. (2012) examined shear strengthening of reinforced concrete girders with CFRP. A total of eight full scale beams with a T-shaped cross section were constructed and tested. Test specimens had a length of 6278 mm. The T-section had a flange width and thickness of 914 and 152 mm, respectively, and a total depth of 1219 mm with a thickness of 356 mm for the web. The specimens were initially loaded to induce diagonal cracking with maximum diagonal crack sizes ranged from 0.635 to 1.27 mm. Test parameters included flexural cutoff details, stirrups spacing and repair configuration. The concrete compressive strength was 24 MPa. The stirrups steel yield strength was 350 MPa. The shear span to effective depth ratio was in range of $a/d = 2.8$ to $a/d = 3.27$. The strengthening regime consisted of CFRP strips applied on the surface of the specimen within the shear span. Two types of composites (Type A and B) that differs in their thickness with a tensile modulus of 22.7 GPa, a tensile strength of 3800, and rupture strain of 1.67% were used in strengthening. Most of the specimens failed in shear compression failure mode. The failure was controlled by debonding of the CFRP strips termination close to the deck-stem interface. Test results indicated that CFRP strengthening provided a significant increase in the ultimate strength capacity compared to the non strengthened specimens. The CFRP enhanced the shear capacity by 80% across the majority of the specimens. It was also concluded that the strengthened specimens showed a stiffer behavior in terms of displacement and diagonal deformation compared to cracked beams without CFRP strengthening. The addition of transverse CFRP strips enhanced the contribution of the longitudinal strips to the beam at cutoff locations. Also, thicker

CFRP material exhibited reduced amounts of debonding and cracking and achieved higher bond stress compared to similar but thinner CFRP strips. The addition of longitudinal CFRP strips did not increase the shear capacity due to debonding and bending of fibers at the poorly constrained diagonal cracks. The repair scheme for shear using discrete CFRP strips provided a considerable increase in shear strength capacity compared to unrepaired members.

Panda et al. (2012) examined the effect of transverse steel reinforcement on the shear performance and modes of failure of RC beams strengthened in the shear zone with GFRP sheets. A total of 18 beams with a T-shaped cross section were constructed and tested. Test specimens had a length of 2500 mm. The T-section had a flange width and thickness of 250 and 60 mm, respectively, and a total depth of 260 mm with a thickness of 100 mm for the web. Test parameters included the amount of transverse reinforcement (without stirrups, $s=200$ mm and $s=300$), and the configuration of the GFRP sheets. The concrete compressive strength was 49.3 MPa after 28 days. The reinforcing steel yield stress was 252 MPa. The shear span to effective depth ratio was 3.26. The strengthening regime of GFRP sheets consisted of side bonding, U-jacketing and U-jacketing with extended anchorage length bonded to the bottom face of the flange. One layer of GFRP had an elastic modulus and ultimate tensile strength of 13.18 GPa and 160 MPa, respectively. The mode of failure was GFRP rupture along the main shear crack when adequate transverse reinforcement was provided, while a combination of GFRP rupture and debonding was noticed when shear reinforcements was not provided in the shear zone. Test results indicated that specimens without stirrups expressed a gain in load shear capacity in range of 30-40%, while specimens with stirrups spaced at 200 and 300 mm expressed a gain of 15-22.5% and 26.24-

36.17%. respectively knowing that the U-jacketing with extended anchorage length was the most efficient strengthening scheme. It was also concluded that at a given shear force, the stirrups were more strained in control specimens compared to the strengthened ones. The use of U-jacket with extended anchorage length has showed additional reduction in stirrups strain when compared to the other strengthening schemes.

EI-Maaddawy and Chekfeh (2013) conducted a study on shear strengthening of RC T-beams with corroded stirrups using composites. A total of 12 beams with a T-shaped cross section were constructed and tested. Test specimens had a length of 3200 mm. The T-section had a flange width and thickness of 300 and 50 mm, respectively, a total depth of 240 mm and a web width of 120 mm. Test parameters included the level of corrosion damage in the stirrups, 8% and 15% cross-sectional loss, and amount of CFRP, one and two layers. The concrete compressive strength was 32 MPa. The stirrups had a diameter of 5.5 mm with a yield stress of 344 MPa. The shear span to effective depth ratio was $a/d = 3$. The strengthening regime consisted of externally bonded U-shaped CFRP sheets. The carbon fiber fabrics had a tensile modulus of 230 GPa, a tensile strength of 3450 MPa, and ultimate elongation of 1.5%. The strengthened beams failed by debonding of the CFRP sheets accompanied by separation of both side concrete covers at the stirrups' level as shown in Figure 2.5. For the beams with a corrosion damage of 8% cross-sectional loss in the stirrups, only one layer of CFRP was sufficient to restore the original shear capacity but for the beams with stirrups corrosion of 15%, two layers of CFRP were necessary to restore the original shear capacity. The gain in shear capacity increased with increasing the number of CFRP layers. The ACI 440.2R-08 (2008)

analytical approach gave satisfactory prediction for the contribution of the CFRP to the shear capacity of the beams with the lower stirrups corrosion of 8%. Nevertheless, for the beams with the higher stirrups corrosion of 15%, the ACI 440.2R-08 (2008) analytical model tended to overestimate the contribution of the CFRP to the shear capacity. This was more significant for the heavily corroded specimens strengthened with the lower amount of CFRP.



Figure 2.5: Detachment of the CFRP sheets failure mode at beam sides (El-Maaddawy and Chekfeh 2013)

Haddad et al. (2013) studied the repair of shear-deficient and sulfate – damaged reinforced concrete beams using FRP composites. A total of 14 prototype beams with a rectangular cross section were constructed and tested. Test specimens had a length of 1000 mm. The cross section had a depth and width of 150 and 100 mm, respectively. Test parameters included the existence of damage by sulfate cyclic action, type of FRP composite (CFRP or GFRP), and CFRP/GFRP strengthening configuration. The concrete compressive strengths were 38 and 28 MPa for control and damaged specimens, respectively. No stirrups were provided in the shear span. The shear span to depth ratio was $a/h = 2$. The strengthening regime consisted of CFRP strips and GFRP/CFRP sheets at different configuration (45° or 90°). The CFRP and GFRP composites had an

elastic modulus, ultimate tensile strength and ultimate strain capacity of the unidirectional fibers of 238 and 72.5 GPa, 4300 and 2276 MPa, and 0.015 and 0.04, respectively. Test results indicated that RC beams exposed to sulfate cyclic treatment caused a reduction in concrete compressive strength of approximately 26% and the shear strength was reduced by 24%. The use of CFRP sheets was the most efficient technique for the sulfate-damaged specimens followed by GFRP/CFRP strips at 45° and 90°, respectively. The percentage increase in load capacity after strengthening for the sulfate-deteriorated beams was in the range of 9 to 36% as compared to a range of 13 to 66% for the corresponding intact ones. It was also concluded that the FRP composites increased crack resistance, and postponed the initiating of shear and flexural cracks which enhanced the ultimate shear cracking load, toughness and stiffness.

Hussein et al. (2013) proposed an innovative technique for repair of RC beams pre-damaged in shear. The study assessed the usage of a temporary compressive force by being applied parallel to beam depth to close the initiated shear cracks in the shear zone before CFRP strengthening. A total of seven beams with a rectangular cross section were constructed and tested. Test specimens had a length of 2000 mm. The rectangular section had a depth and width of 300 and 150 mm, respectively. Test parameters included the method of closing cracks prior to strengthening and the technique of strengthening. The concrete compressive strength was 30 MPa. The stirrups were 6 mm in diameter, spaced at 200 mm and had a yield strength of 245 MPa. The shear span to effective depth ratio was $a/d = 2.5$. The strengthening regime consisted of three externally bonded U-shaped CFRP sheets spaced at 100 mm in the shear span. The specimens were preloaded up to either 85% or 95% of the control beam capacity where cracks initiated,

released for repair, and then reloaded up to failure. Prior to strengthening, the cracks were either closed by epoxy injection, or by a pre-stressing force applied till the developed cracks became invisible. The CFRP composite had an elastic modulus and ultimate tensile strength of 230 GPa and 3500 MPa, respectively. After loading the specimens subsequent to strengthening, the dominating failure mode was debonding of the CFRP sheets at peak load as shown in Figure 2.6. Test results indicated that an increase in the ultimate load in range of 49-57% was obtained by the repaired beams. It was also concluded that appropriate crack repair methods can reduce the effect of existing shear cracks and enhance the capacity to around 57%. Also, a successful preparation of the CFRP-concrete contact surface prior to strengthening was found to be a main key factor for a successful shear strengthening.



Figure 2.6: Typical CFRP debonding failure modes for the tested beams (Hussein et al. 2013)

Mofidi and Chaallal (2014) investigated the effect of steel stirrups on shear resistance gain in RC beams strengthened with externally bonded CFRP composites. A total of five beams with a T-shaped cross section were constructed and tested. Test specimens had a length of 4520 mm. The T-section had a flange width and thickness of 508 and 102 mm, respectively, a total depth of 406 mm with and a web width of 152 mm. Test parameters included the spacing of the CFRP strips, the existence of steel stirrups, the spacing between the steel stirrups

and the use of CFRP sheets versus CFRP strips. The concrete compressive strength was 27 MPa, on average. The stirrups steel yield stress was 650 MPa. The shear span to effective depth ratio was $a/d = 3$. The strengthening regime consisted of CFRP strip and sheets applied along the shear span. The CFRP strips were spaced at 87.5, 125 and 175 mm along the test region. The steel stirrups were spaced at $s = d/2$ and $s = 3d/4$ where $d = 350$ mm. The composite material had a tensile modulus of 230 GPa, an ultimate tensile strength of 3450 MPa and an ultimate strain of 1.5%. All specimens failed in a shear. The non-strengthened specimens failed by diagonal tension shear mode of failure. Some specimens strengthened with CFRP failed by either local fracture while the majority failed by CFRP debonding preceded by diagonal tension mode of failure as shown in Figure 2.7. Test results indicated that the gains due to CFRP in specimens strengthened with CFRP sheets and strips were in the range of 8 to 48% and 6 to 85%, respectively. The existence of steel stirrups resulted in a remarkable decrease in the shear strength gain. However, the presence of CFRP did not significantly reduce the stirrups strain. The authors concluded that the contribution of steel stirrups to shear resistance was not influenced by the addition of CFRP strengthening system.

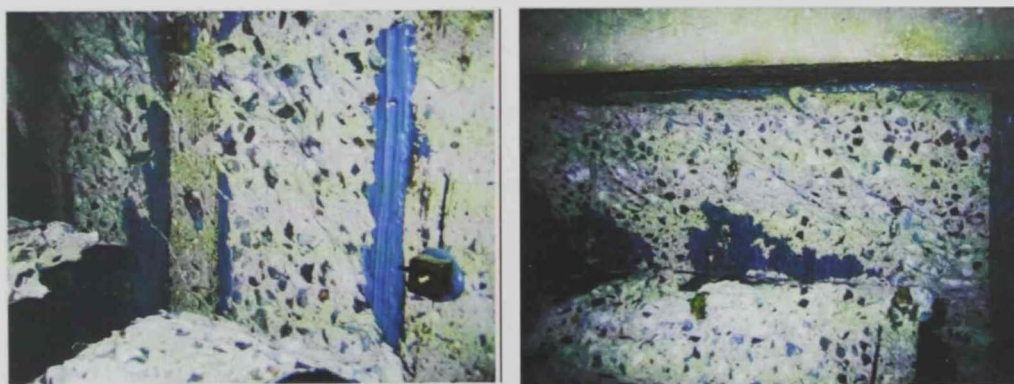


Figure 2.7: CFRP delamination failure mode (Mofidi and Chaallal 2014)

2.3 Studies on shear strengthening using EB-CFRP with end anchorage

The latest report by the ACI committee 440 (ACI 440.2R-08) emphasized the importance of studying the systems that are designed to mechanically anchor externally bonded FRP composites in addition to performing physical testing verifications (Grelle and Sneed 2013). The importance of using mechanical end anchorage system appears in the challenge to improve the FRP strength at positions where the development length is not sufficient which probably leads to debonding mode of failure (ACI 440.2R-08). Research studies performed in the area of shear strengthening using externally bonded FRP sheets with end anchorages are summarized hereafter.

Khalifa and Nanni (2000) studied the shear behavior of RC T-beams strengthened with CFRP composites with end anchorage. A total of six beams with a T-shaped cross section were constructed and tested. Test specimens had a length of 3050 mm. The T-section had a flange width and thickness of 380 and 100 mm, respectively, and a total depth of 405 mm with a thickness of 150 mm for the web. Test parameters included the amount and distribution of the CFRP, the bonded surface (two sides of U-wraps), fiber direction combination and the use of end anchorage. The concrete compressive strength was 35 MPa. The reinforcing steel had a yielding point of 350 MPa. The shear span to effective depth ratio was $a/d = 3$. The strengthening regime consisted of CFRP strips or continuous sheets bonded either as U-wrap or two side bonded with 90° - 0° fiber direction combination or 90° direction and with or without end anchorage. The anchorage system was attained by creating a groove along the contact line between the flange and web followed by installing a GFRP rod to anchor the attached CFRP sheet/strip as shown in Figure 2.8. The CFRP sheets (fiber only)

had and an elastic modulus and ultimate tensile strength of 228 GPa and 3790 MPa, respectively. The control specimen failed in shear compression, while the other specimens failed in CFRP debonding except for the specimen strengthened with continuous U-wraps with end anchor which failed in flexure mode of failure. Test results indicated that an increase in shear strength of 35% for strips bonded to two sides to 145% for continuous U-wrapped specimen with end anchorage was achieved among the tested specimens. It was concluded that performance of externally bonded CFRP can be enhanced if a suitable anchoring is proposed, as well as using of U-wrap CFRP sheets leads to higher shear contribution compared to side bonding.

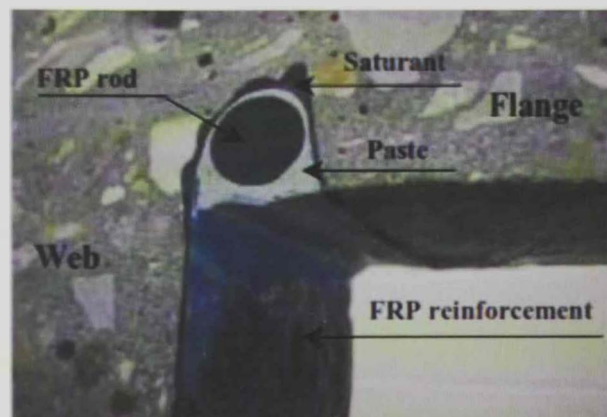


Figure 2.8: Details of the U-Anchor at the corner of flange-web (Khalifa et al. 2000)

Tanarslan and Ertutar (2008) studied the effect of using CFRP strips to improve the shear capacity of RC beams. A total of seven beams with a T-shaped cross section were constructed and tested. The T-section had a flange width and thickness of 360 and 75 mm, respectively, and a total depth of 360 mm with a thickness of 120 mm for the web. Test parameters included arrangement of CFRP strips and the anchorage system. The concrete compressive strength was 30 MPa.

The reinforcing steel stirrup yield strength was 275 MPa. The shear span to effective depth ratio was $a/d = 4.7$. The strengthening regime consisted of L-shaped, U-jacketed, side-bonded and U-jacket CFRP strips extended along the bottom surface of flange. The CFRP had an elastic modulus and an ultimate tensile strength of 231 GPa and 4100 MPa, respectively. The specimens failed due to detachment of CFRP strips, rupture of CFRP strips or concrete cover separation over the longitudinal reinforcement. The anchorage systems consisted of steel plates or angles, which were anchored to CFRP strips and concrete surface by steel bolts in both lateral and bottom surface of the flange as shown in Figure 2.9. Test results indicated that the used strengthening schemes have increased the ultimate load carrying capacity by 51% to 127%. The use of U-jacket CFRP strips extended along the bottom surface of the flange with end anchorage was found to have the highest efficiency. It was also concluded that the use of bottom anchorage (close to bottom corners of the web) prevented premature debonding, while the top anchorage prevented peeling of the CFRP strips from concrete. The use of side bonded or U-jacketing without anchorage caused collapse with brittle shear mode of failure due to detachment of the CFRP strips.

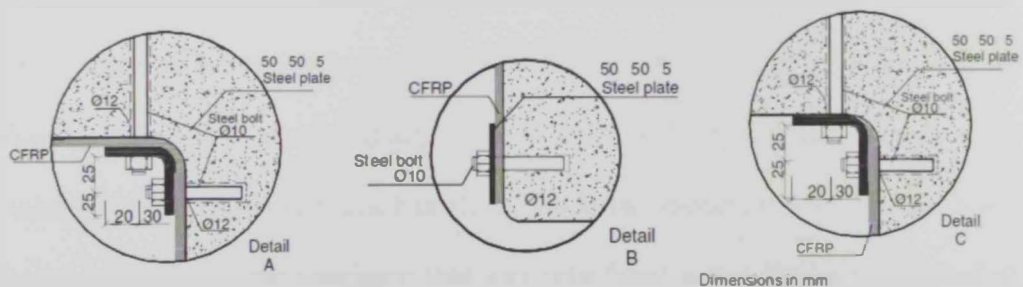


Figure 2.9: Anchorage details of strengthening specimen beams (Tanarslan and Ertutar 2008)

Hoult and Lees (2009) examined the effectiveness of CFRP strap configurations for the shear strengthening of RC beams. A total of seven specimens with a T-shaped cross section were constructed and tested. The T-section had a flange width and thickness of 250 and 105 mm, respectively, and a total depth of 280 mm with a thickness of 105 mm for the web. Test parameters included the penetration depth of CFRP straps into the compression flange, CFRP strap spacing, concrete strength, presence of holes in the compression flange and loading pads size. The concrete compressive strengths were in range of 19.8 to 50 MPa. The reinforcing steel yield strength was 578 MPa. The shear span to depth ratio was $a/h = 2.7$. The strengthening regime consisted of ten loops of CFRP straps inserted into holes through the beam's flange with various angles at where these holes were left open with metallic support inserts filled with grouted concrete as shown in Figure 2.10. The CFRP straps were spaced either at 200 or 250 mm. The CFRP straps were prestressed to 25% of the ultimate strap capacity. The CFRP straps were supported on metal pads that were placed on the top and bottom of the beam. The end anchorage system consisted of drilled holes through the beams flanges then fixed at beam's top and bottom as shown in Figure 2.11. Typically, the specimens failed in shear mode of failure, knowing that none of the CFRP straps failed during testing. The CFRP straps consisted of ten loops with an ultimate stress and rupture strain of 1544 MPa and 0.0127, respectively. The majority of the specimens failed in shear, while the specimen with grouted holes inclined at 30° and the specimen that was retrofitted with CFRP straps installed using support pads on top and bottom of the beam failed in flexure. Test results indicated that the used anchorage enhanced the ultimate shear capacity by 3.6-

67.8%. It was also concluded that CFRP straps improved the beam stiffness in the post-cracking stage.

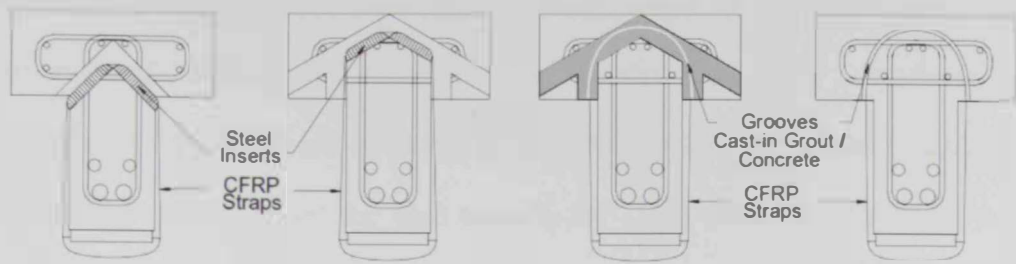


Figure 2.10: Strap configurations for test specimens
(Hoult and Lees 2009)

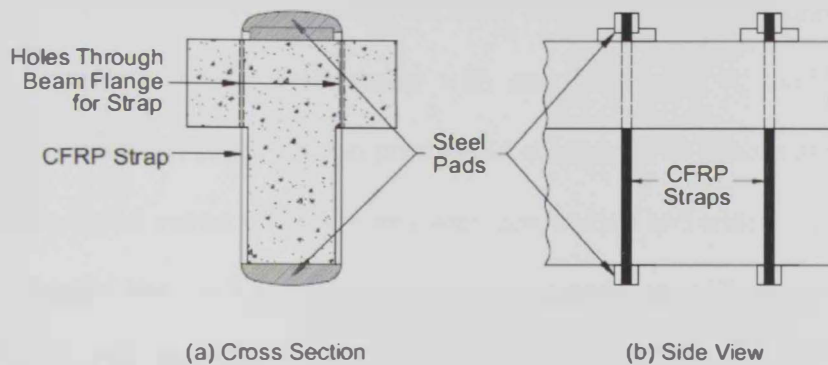


Figure 2.11: CFRP strap layout and beam cross-section
(Hoult and Lees 2009)

Gamino et al. (2009) studied the application of CFRP in shear strengthening of RC beams. A total of five RC beams with a T-shaped cross section were constructed and tested. Test specimens had a length of 1500 mm. The T-section had a flange width and thickness of 400 and 80 mm, respectively and a total depth of 300 mm with a web width of 80 mm. Test parameters included the CFRP strips spacing (150 or 175 mm) and the use of anchorage system. No information was provided regarding the anchorage mechanism. The concrete compressive strength was 60 MPa on average. The stirrups were of 5 mm spaced at 290 mm with a steel yield strength was 530 MPa. Various types of

CFRP materials with different spacing were used in strengthening of the specimens. The strengthening regime consisted of CFRP strips with and without anchorage. The control specimens failed in shear rupture while the anchored and non-anchored CFRP strips failed in fiber rupture and CFRP detachment, respectively. Test results indicated that the use of end anchorage system enhanced the ductility and increased the load capacity by 13 to 52%. The CFRP strips spaced at 150 mm had better contribution to shear resistance compared to the CFRP strips spaced at 175 mm.

Ortega et al. (2009) examined the shear strengthening of concrete girders using externally bonded CFRP sheets with end anchorage. A total of eight specimens divided as four I-section prestressed concrete (PC) girders and four T-section reinforced concrete (RC) beams were constructed and tested. The PC and RC specimens had a 9.5 mm steel stirrups spaced at 457 and 305 mm, respectively. The strengthening regime consisted of CFRP sheets applied at 90° with respect to the longitudinal direction of the beam/girder. The anchorage system used in the PC specimens consisted of continuous pultruded CFRP plates bonded to the CFRP sheets and anchored firmly in place with concrete wedge anchors embedded 51 mm through the web (CMA) or with bonding discontinuous pultruded CFRP plates anchored firmly in place with steel bolts through the entire web (DMA) as shown in Figure 2.12. The anchorage system used in the RC specimens consisted of a similar system to DMA but anchor bolts were used instead of thru-bolts in addition to forming a three layer connection at the end of the CFRP sheets (modified anchor bolt system). The failure mode was generally debonding of the CFRP sheets that started at the bottom of the anchorage system and progressively increased until failure. No failure in the anchorage bolts was

observed. Test results indicated that for PC girders, the use of thru-bolt system provided better performance and was more practical compared to anchor bolts. This is because the embedment length of the anchor bolts was insufficient to prevent the early delamination of the strengthening system. It was also concluded that the use of discontinuous individual CFRP anchor plates was better than the use of continuous anchor plate near the top flange that featured a buckling mode of failure. The CFRP shear strengthening with continuous anchorage in the PC specimens enhanced the shear capacity by 15%, while shear strengthening with discontinuous anchorage enhanced the shear capacity by 27%. The use of the modified anchor bolt system enhanced the shear capacity by 24% compared to 19% enhancement in shear capacity using discontinuous anchorage with anchor bolts in the RC specimens.



CMA anchorage



DMA anchorage



Modified anchor bolt system

Figure 2.12: Anchorage systems used in PC and RC specimens
(Ortega et al. 2009)

Belarabi et al. (2010) studied the behavior of full scale RC-beams strengthened in shear with externally bonded FRP sheets. A total of four beams with a T-shaped cross section were constructed and tested. Test specimens had length of 10668 mm. The T-section had a flange width and thickness of 1066.8 and 177.8 mm, respectively, and a total depth of 939.8 mm with a web width of

457.2 mm. Test parameters included the strengthening scheme, the anchorage type, and the shear reinforcement. The concrete compressive strength was 27.6 MPa. The stirrups steel yield stress was 276 MPa. The shear span to effective depth ratio was approximately $a/d = 3.3$. The end anchorage types were addition of horizontal CFRP sheet just below the flange or installation of sandwich panels mechanically anchored with steel bolts as shown in Figure 2.13. Details of the mechanical anchorage are shown in Figure 2.14. The strengthening regime consisted of U-wrapped CFRP sheets. The CFRP sheets had a tensile modulus of 228 GPa a tensile strength of 3792 MPa, and ultimate strain of 1.7%. The control specimens failed when the diagonal cracks reached the flange. The specimens strengthened with CFRP and mechanical anchorage failed due to CFRP debonding, although delayed due to the existence of the end anchorage. Test results indicated that the strengthened specimens reached an increase in shear strength in the range of 23 to 26%. The use of mechanical end anchorage expressed 7 to 48% increase in the shear strength compared to beams without end anchorage. Also, the CFRP shear strengthening was more efficient in specimens with lower amount of stirrups. It was also concluded that the sandwich panel mechanical anchorage was more efficient than providing additional horizontal CFRP strip as end anchorage.

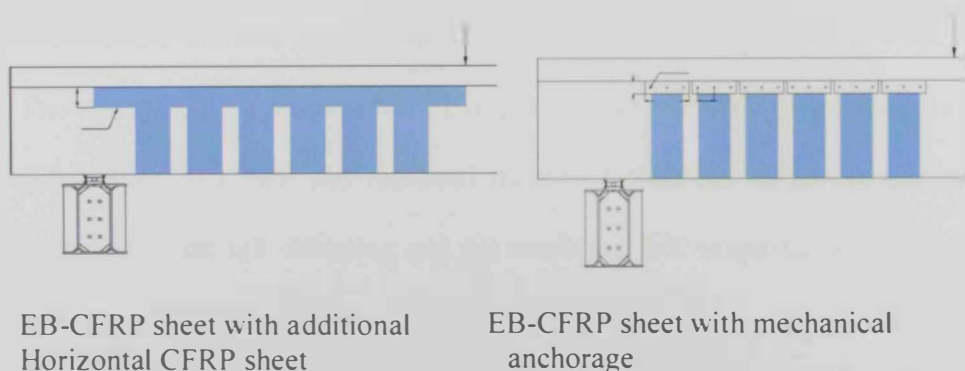


Figure 2.13: Configurations of various anchorage systems (Belarabi et al. 2010)

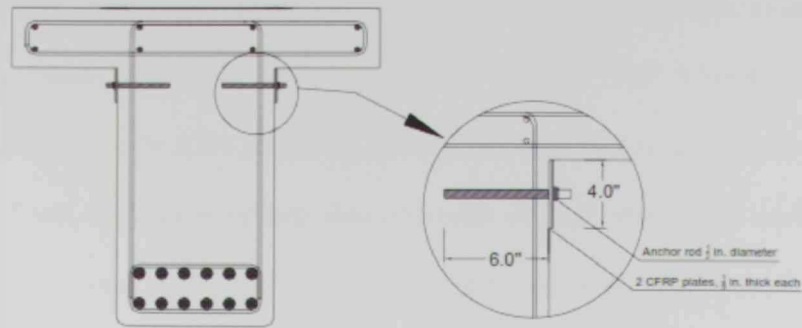


Figure 2.14: Details of mechanical anchorage system (Belarabi et al. 2010)

Deifallah and Ghobarah (2010) studied strengthening of RC beams subjected to combined shear and torsion using CFRP fabrics. A total of six half-scale beams with a T-shaped cross section were constructed and tested. The T-section had a flange width and thickness of 450 and 100 mm, respectively, and a total depth of 350 mm with a thickness of 150 mm for the web. Test parameters included the torque to shear ratio and the anchorage scheme. The concrete compressive strength was 25.6 MPa. The stirrups were 10 mm in diameter, spaced at 170 mm, and had a yield stress of 496 MPa. The torque to shear ratios were 0.5 and 0.1 m. The strengthening regime consisted of bidirectional $\pm 45^\circ$ CFRP sheets that were used in different schemes namely; anchored U-jacket, extended U-jacket, fully wrapped section and combined full wrapping and extended U-jacket as shown in Figure 2.15. The CFRP had an elastic modulus, ultimate tensile strength and ultimate elongation of 63.3 GPa, 609 MPa and 0.96%, respectively. The strengthened specimen with U-jacketing and extended U-jacketing failed by debonding of CFRP and torsional failure of concrete, while the strengthened specimens with full wrapping and the combined full wrapping with extended U-jacketing failed by debonding of CFRP. Test results indicated that the fully wrapped section anchorage system had the highest enhancement of 71% in the

torsional resistance followed by the combined full wrapping and extended U-jacketing, then extended U-jacketing and finally the U-jacketing with improvements of 64%, 63% and 45%, correspondingly. It was also concluded that the use of end anchorage system that consisted of steel angle with anchor bolts can delay the early anchorage failure. The decrease in the torque to shear ratio

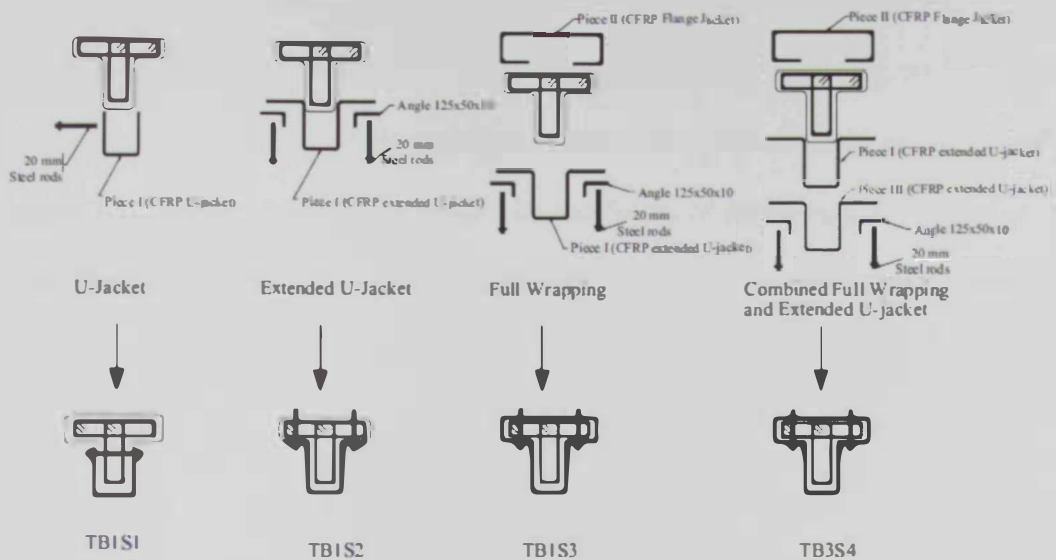


Figure 2.15: Implemented strengthening schemes (Deifalla and Ghobarah 2010)

delayed the concrete cracking.

Kim et al. (2011) investigated the shear strengthening of RC beams using CFRP laminates and spike anchors. Six tests were performed on T-shaped cross section beams. The T-section had a flange width of 711 mm, a total depth of 610 mm, and a web width of 356 mm. Test parameters included the anchorage system, the number of CFRP layers, and the bonding/unbonding of the CFRP laminates to concrete. The concrete compressive stress was 27 MPa. The stirrups steel yield stress was 476 MPa. The shear span to effective depth ratio was $a/d = 3$. The strengthening regime consisted of various schemes. A control specimen was tested without strengthening. One specimen was loaded until yielding in stirrups,

unloaded, repaired with anchored CFRP laminates/strips of one layer, and then retested to failure. Another specimen had no bonding between one layer of CFRP and concrete and anchored with CFRP spike anchors. Another specimen was strengthened with anchored CFRP strips of two layers. The last specimen was strengthened with CFRP laminates without anchors. Figure 2.16 shows an isometric view for the anchorage details. The CFRP composite had ultimate stress of 1062 MPa and ultimate strain of 0.01. The specimens repaired with one layer of anchored CFRP strips and the unbonded anchored specimen failed by rupture of the CFRP strips, while the specimen with two layers of anchored CFRP strips and the un-anchored bonded specimen failed by rupture of the CFRP anchor spikes and detachment of CFRP strips, respectively.

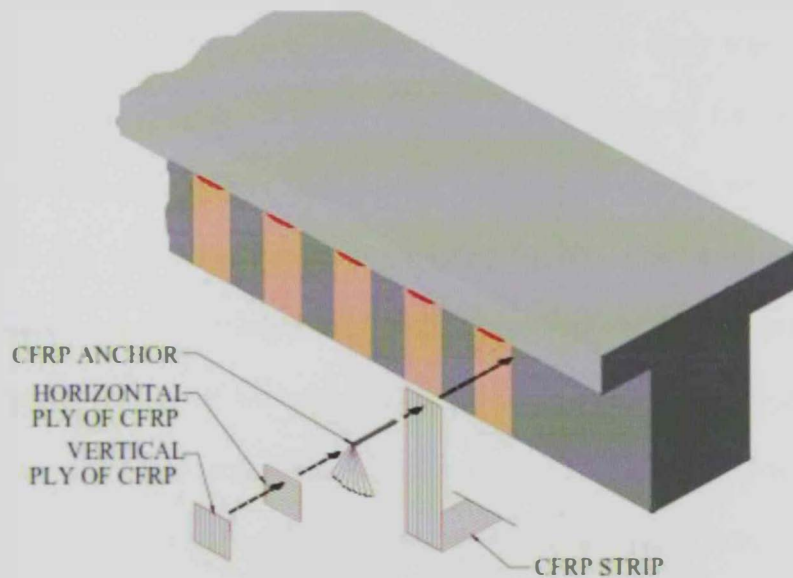


Figure 2.16: Isometric view-Details of CFRP anchors (Kim et al. 2011)

Test results indicated that all specimens repaired or strengthened with anchored CFRP strips showed a close enhancement of 45% regardless the bonding condition and number of CFRP layers. The specimen strengthened with

unanchored CFRP strips showed only 4% enhancement in shear resistance. In the presence of spike anchors, the initial damage state had no effect on the performance of the repaired specimen. The CFRP anchor spikes prevented the pre-mature delamination of the CFRP laminates and accordingly increased the shear strength gain. It was also concluded that the contribution of the CFRP to the shear resistance was independent on the amount of the CFRP material used.

Mofidi et al. (2012) investigated the performance of different end-anchorage systems for RC beams strengthened in shear with EB-CFRP system. A total of five specimens with a T-shaped cross section were constructed and tested. Test specimens had a length of 4520 mm. The T-section had a flange width and thickness of 508 and 102 mm, respectively, and a total depth of 406 mm with a thickness of 152 mm for the web. The main objective of the study was to evaluate the effectiveness of four different end-anchorage systems for RC beams strengthened using EB-CFRP. The concrete compressive strength was 33.7 MPa. The reinforcing steel yield strength was 650 MPa. The shear span to effective depth ratio $a/d = 3$. The strengthening regime consisted of CFRP U-jacket with a surface bonded flat CFRP laminate end anchorage (SBFA), CFRP U-jacket with an embedded flat CFRP laminate as end anchorage (EFLA), CFRP U-jackets with a mechanical anchorage consisted of a double aluminum plate fixed to concrete with a threaded stainless steel threaded rods inserted in pre-drilled horizontal holes through the web (DAMA), and CFRP U-jackets with an embedded rounded CFRP bar as end anchorage (ERBA) as shown in Figure 2.17. The dry fiber sheet and the composite CFRP laminate, respectively had elastic moduli, ultimate strengths and rupture strains of 231,165 GPa, 3650, 3100 MPa, and 1.4,1.69 %, respectively. The use of EB-CFRP system with SBFA or ERBA end anchorage

systems resulted in up to 41% increase in shear resistance. The most efficient end anchorage systems were EFLA and DAMA which resulted in strength gains of 48 and 43%, correspondingly. It was also concluded that all specimens failed in shear mode of failure except specimens strengthened with CFRP integrated with EFLA and DAMA end anchorage systems which failed in flexure.



SBFA anchorage system



DAMA anchorage system



ERBA anchorage system



EFLA anchorage system

Figure 2.17: Various end anchorage systems (Mofidi et al. 2012)

Koutas and Triantafillou (2012) examined the effectiveness of using FRP spike anchors to improve the shear resistance of RC beams strengthened in shear with CFRP composites. A total of six beams with a T-shaped cross section were constructed and tested. Test specimens had an effective span of 1750 mm. The T-section had a flange width and thickness of 300 and 80 mm, respectively, and a total depth of 300 mm with a thickness of 140 mm for the web. Test parameters included the orientation of the anchors, spacing/number of anchors in the shear

span, and the role of glass fibers against carbon in the anchors. The concrete compressive strength was 22.6 MPa. The shear span to depth ratio was $a/h = 2$. The strengthening regime consisted of CFRP composite sheets wrapped around the shear-critical span of the specimen's web. The anchorage system consisted of carbon or glass fiber spike anchors placed at each side of the span. The anchors were horizontally embedded through the specimen's web or inclined at an angle of 25° inside the flange as shown in Figure 2.18. Diagonal cracking, debonding of CFRP sheets, anchor pull-out and anchor rupture were the main modes of failure exhibited by the tested specimens. The carbon and glass composites had tensile moduli of 230 and 72.4 GPa, and tensile strengths of 3790 and 3240 MPa, respectively. Test results indicated that the use of externally bonded system integrated with spike end anchors increased the shear resistance by 50% to 116%. The specimen with no anchors experienced an increase of 39% in shear resistance. It was also concluded that anchors of alike geometrical features showed similar effectiveness although they were different in their types. Also, increasing the number of anchors in the shear span resulted in non-proportional increase in the shear resistance as the anchors not above the shear cracks were not active. Also, anchors with same embedment lengths displayed similar effectiveness, despite the variation in the type of fibers.

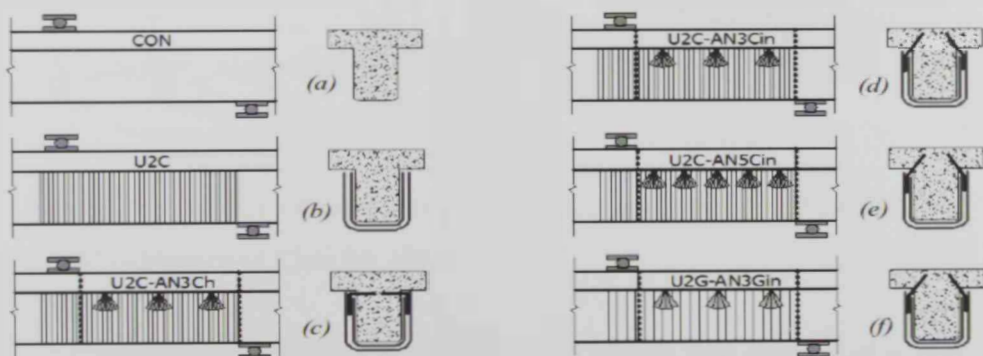


Figure 2.18: Strengthening configurations for the tested beams (Kuotas and Triantafillou 2012)

EI-Maaddawy and Chekfeh (2012) studied the effectiveness of using EB-CFRP system with mechanical end anchorage to repair severely damaged RC beams. A total of 14 tests were conducted on specimens with a T-shaped cross section. Test specimen had a length of 3200 mm. The T-section had a flange width and thickness of 300 and 50 mm, respectively, and a total depth of 240 mm with a thickness of 120 mm for the web. The beams were pre-failed in shear prior to strengthening. Test parameters included the number of EB-CFRP layers and type of end anchorage. The concrete compressive strength was 20 ± 0.4 MPa. The stirrups steel yield strength was 344 MPa. The shear span to effective depth ratio was $a/d = 3$. The strengthening regime consisted of U-shaped CFRP sheets without end anchorage and U-shaped CFRP sheets with mechanical end anchorage using sandwich composite panel (SCP) with either two short galvanized steel powder actuated fasteners (PAFs) or a galvanized steel threaded anchor bolt (TB) inserted through the entire web width as shown in Figure 2.19

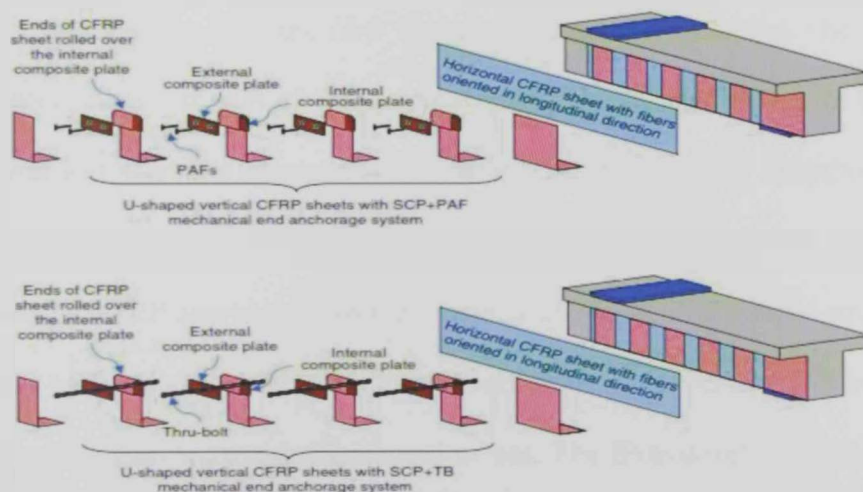


Figure 2.19: EB-CFRP retrofitting regime with mechanical end anchorage (EI-Maaddawy and Chekfeh 2012)

. The cured CFRP composites laminate (fibers and resin) had a tensile modulus of 65.4 GPa, a tensile strength of 894 MPa, and ultimate elongation of

1.33%. Test results indicated that the use of proper end anchorage with EB-CFRP sheets can fully restore and may also upgrade the original shear capacity of the beam. Specimens strengthened with CFRP anchored with SCP+PAF and SCP+TB were able to restore the original shear capacity and upgraded it by 16-17% and 30-45%, respectively. It was also concluded that the use of PAF delayed debonding of the EB-CFRP sheets while the use of TB prevented CFRP debonding and allowed the beam to develop its full shear capacity.

Panigrahi et al. (2014) conducted a study on strengthening of shear deficient RC beams using externally bonded GFRP sheets. The effectiveness of using mechanical end anchorage was examined. A total of 12 beams with a T-shaped cross section were constructed and tested. Test specimens had a length of 1300 mm. The T-section had a flange width and thickness of 350 and 50 mm, respectively, and a total depth of 175 mm with a web width of 150 mm. Test parameters included the amount of GFRP, the GFRP orientation, bonded surface (two lateral sides or U-wrap), fiber direction and number of layers. The concrete compressive strength was 23.7 MPa on average. The steel stirrups were 8 mm in diameter and had yield strength of 523 MPa. The shear span to effective depth ratio was $a/d = 2.38$. The strengthening regime consisted of GFRP strips or continuous GFRP sheets as shown in Figure 2.20. The GFRP sheets/ strips were bonded to the surface either in two lateral sides or as U-wraps. The GFRP continuous sheets were either anchored or not. The fiber direction of the GFRP strips were either 0° or 45° (Inclined, X-shape, and vertical). The end anchorage consisted of steel plates anchored by bolts inserted through pre-drilled holes in the beams' web. The GFRP composite (two and four layers) had a tensile modulus of 6.8 and 7.8 GPa, respectively with ultimate stress of laminates of

172.8 and 209.1 MPa, correspondingly. The specimen strengthened with U-wrapped GFRP sheets with end anchorage failed by rupture of the GFRP sheets, while the specimen strengthened with U-wrapped GFRP sheets without end anchorage failed in detachment of the GFRP sheets.

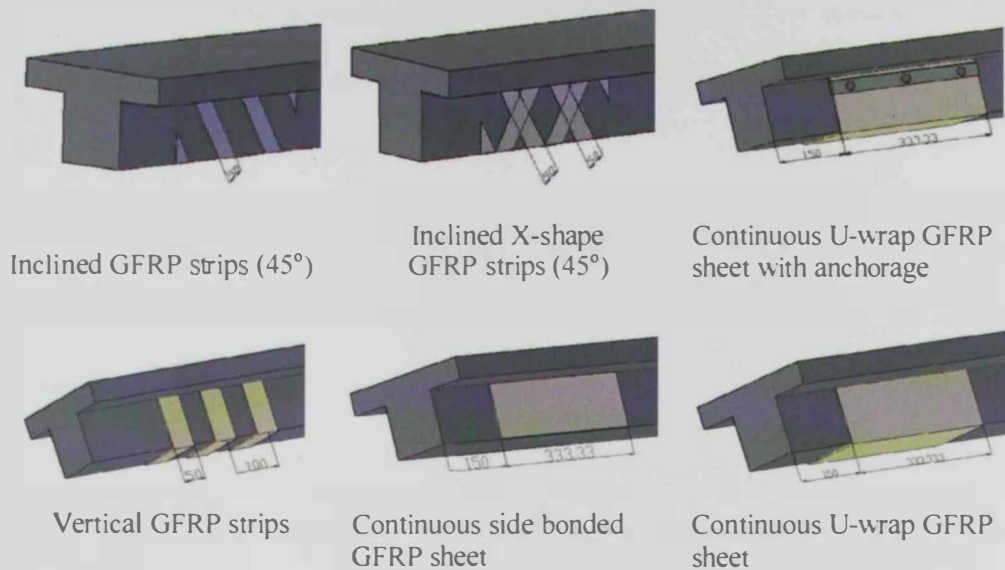


Figure 2.20: Externally bonded GFRP sheets/strips configurations
(Panigrahi et al. 2014)

Test results indicated that the GFRP strips bonded with X-shape had the best performance among the other GFRP strip configurations and reached an ultimate gain in load carrying capacity of 41% compared to the control specimen, while the specimen strengthened with U-wrapped GFRP sheets with end anchorage reached an ultimate gain in load carrying capacity of 65% compared to the control specimen. The specimen strengthened with continuous U-wrapped GFRP sheets without anchorage reached an ultimate gain in load carrying capacity of 42%. It was also concluded that the use of anchorage system prevented the debonding of the GFRP sheet which resulted in better utilization of

the GFRP material. Also, a proportional increase in shear capacity with increasing the amount of GFRP could not be achieved because detachment of GFRP was not prevented.

2.4 Studies on shear strengthening using ETD-FRP system

The use of composite bars embedded through section depth is considered as a quite recent method in shear strengthening of RC beams. Few researchers have investigated the viability of using this technique to improve the shear response of RC beams.

Chaallal et al. (2012) studied the shear performance of RC beams strengthened with embedded through section (ETS) FRP rods. A total of six full-scale beams with a T-shaped cross section were constructed and tested. Test specimens had a length of 4520 mm. The T-section had a flange width and thickness of 508 and 406 mm, respectively and a total depth of 406 mm with a web width of 152 mm. Test parameters included the presence of stirrups and stirrups spacing. The concrete compressive strength was either 25 or 35 MPa. The stirrups were 6 mm in diameter, and spaced at $s = d/2$ or $s = 3d/4$, where $d = 350$ mm. The stirrups steel yield strength was 650 MPa. The shear span to effective depth ratio was $a/d = 3$. The strengthening regime consisted of CFRP rods embedded vertically in pre-drilled holes through the beam's section as shown in Figure 2.21. The composites had a tensile modulus of 140 GPa, an ultimate stress of 1855 MPa, and ultimate elongation of 1.33%. The specimen strengthened with ETS system with no stirrups in the shear span expressed diagonal shear cracking and failed by shear diagonal compression failure, but the existence of the stirrups in the shear span resulted in a flexure mode of failure for the strengthened specimens. Test results indicated that the ETS-CFRP rods increased the shear

resistance by 13% for the specimen with stirrups spaced at $s = d/2$, 45% for the specimen with stirrups spaced at $s = 3d/4$, and 122% for the specimen with no stirrups. This indicated that decreasing the spacing of the transverse steel reduced the shear strength gain attributable to the ETS-CFRP. Also, the use of ETS strengthening technique was very efficient in developing CFRP tensile strength potential prior to the occurrence of the final failure. The authors recommended further researches related to the ETS method to investigate other important features such as the CFRP spacing, cross sectional area, and different types of FRP composite rods.

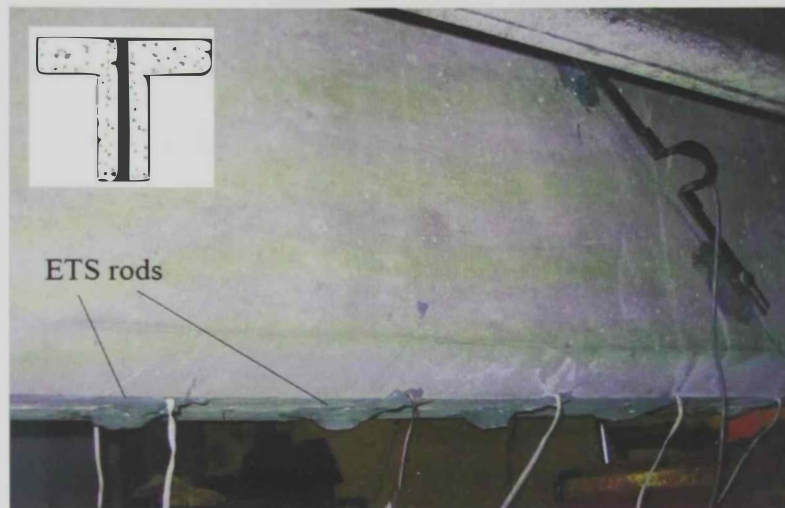


Figure 2.21: Strengthened specimens with ETS-CFRP rods
(Chaallal et al. 2012)

Mofidi et al. (2012) studied strengthening of RC beams in shear using CFRP bars embedded through the beam section (ETS). A total of nine tests were performed on T-shaped RC beams. Test specimens had a length of 4520 mm. The T-section had a flange width and thickness of 508 and 406 mm, respectively and a total depth of 406 mm with a thickness of 152 mm for the web. Test parameters included the effect of surface coating on the CFRP bars, the effect of presence of

stirrups on the CFRP shear contribution, spacing between CFRP bars and the diameter of the CFRP bars. The concrete compressive strength was in the range of 25 to 29.6 MPa. The shear span to effective depth ratio was $a/d = 3$. The strengthening regime consisted of CFRP rods that were either sand coated or plain surfaced, with different spacing ($s_f = 130$ mm and $s_f = 260$ mm) and diameters (9.5 and 12.7 mm). The sand coated and plain-surfaced CFRP rods had a tensile modulus of 148 and 155 GPa, tensile strengths of 1885 and 2800 MPa, and ultimate elongations of 1.27 and 1.8%, respectively. The failure of some specimens occurred by diagonal tension after yielding of the longitudinal steel reinforcement as shown in Figure 2.22. Other specimens experienced flexure mode of failure. Test results indicated that the ETS-FRP method was very effective in enhancing the shear capacity of RC beams to about 35% in the presence of a limited amount of stirrups. It was also concluded that increasing the diameter of the ETS-CFP rods or decreasing the spacing between them improved the contribution of CFRP to shear resistance. Also, rough-surfaced CFRP bars achieved better CFRP-concrete bond behavior compared to that plain surface achieved by CFRP bars.



Figure 2.22: Diagonal tension shear mode of failure for the strengthened specimen (Mofidi et al. 2012)

2.5 Research Objectives

2.5.1 Research needs

The available literature related to the behavior of concrete beams strengthened in shear using externally-bonded (EB) composite laminates and embedded through section depth (ETD) composite rods has been reviewed in this chapter. A significant amount of studies has been conducted to evaluate the effectiveness of using EB composites to improve the shear response of RC beams. These studies have provided interesting findings and conclusions, particularly with regard to failure mode and effect of varying amounts of internal stirrups and external EB composite reinforcement on shear response. The premature debonding of EB composites limited the shear strength gain. In recent years, more attention has been given to develop mechanical end anchorage (MA) systems to delay or prevent the debonding mode of failure, and hence improve the shear strength gain. The viability of using ETD composite rods as alternative innovative strengthening solution has received little attention in the literature. Only two studies were found in the literature on shear strengthening of RC beams with ETD-CFRP rods. The use of GFRP rebars in the ETD system was not investigated. The contribution of the ETD-GFRP rebars to shear resistance is still in question. The majority of previous researchs have focused on the use of composite-based systems for shear strengthening of undamaged RC beams. Practical applications would involve strengthening and retrofitting of already cracked or damaged beams. More research is needed to identify the interaction between the strengthening system, shear damage state prior to retrofitting, amount of internal stirrups, and presence of mechanical end anchorage.

2.5.2 Scope of the current study

In this thesis, two different composite based systems namely; EB-CFRP and ETD-GFRP, have been tested to investigate their performance when used in shear strengthening of pre-cracked or pre-failed RC beams. The particular objectives of this study are to:

- Examine the effectiveness of using two different composite-based systems to upgrade the shear capacity of shear-deficient RC T-beams.
- Investigate the effect of presence of shear cracks or failure prior to retrofitting on the viability of the strengthening solution.
- Investigate the impact of varying the amount of internal stirrups and presence of mechanical end anchorage on shear behavior of RC beams retrofitted with composites.
- Examine the accuracy and validity of available analytical models, international guidelines and standards to predict the contribution of composites to shear resistance of RC T-beams pre-damaged in shear.

CHAPTER 3: EXPERIMENTAL PROGRAM

3.1 Introduction

The experimental program of the current work consisted of 24 tests conducted on 12 T-shaped RC beams. The test specimens were divided into three groups, [A], [B], and [C] based on the amount of the internal steel stirrups. The groups were further divided into subgroups based on the initial shear damage state prior to retrofitting and/or testing as shown in Table 3.1.

Table 3.1: Test matrix of the experimental program

Group	Stirrups spacing	Damage state prior to retrofitting	Retrofitting system	Specimen Designation ^a
[A]	No stirrups	No damage	No retrofitting	ND-NS-NR
			EB-CFRP	ND-NS-EB
			EB-CFRP & MA	ND-NS-EB+MA
			ETD-GFRP	ND-NS-ETD
[B]	S1 (s = 120 mm)	No damage	No retrofitting	ND-S1-NR
			EB-CFRP	ND-S1-EB
			EB-CFRP & MA	ND-S1-EB+MA
			ETD-GFRP	ND-S1-ETD
		D1 (Pre-cracked)	No retrofitting	D1-S1-NR
			EB-CFRP	D1-S1-EB
			EB-CFRP & MA	D1-S1-EB+MA
			ETD-GFRP	D1-S1-ETD
		D2 (Pre-failed)	No retrofitting	D2-S1-NR
			EB-CFRP	D2-S1-EB
			EB-CFRP & MA	D2-S1-EB+MA
			ETD-GFRP	D2-S1-ETD
[C]	S2 (s = 75 mm)	No damage	No retrofitting	ND-S2-NR
			EB-CFRP	ND-S2-EB
			EB-CFRP & MA	ND-S2-EB+MA
			ETD-GFRP	ND-S2-ETD
		D2 (Pre-failed)	No retrofitting	D2-S2-NR
			EB-CFRP	D2-S2-EB
			EB-CFRP & MA	D2-S2-EB+MA
			ETD-GFRP	D2-S2-ETD

^aND = No Damage, NS = No Stirrups, D1 = Shear Damage state D1 (three cycles of loading to first shear cracking then unloading), D2 = Shear Damage state D2 (one cycle of loading up to peak load-unloading). S1 = Spacing of 120 mm between the stirrups. S2 = Spacing of 75 mm between the stirrups. NR = No Retrofitting, ETD = Embedded Through Depth system using GFRP rebars. EB = Externally Bonded system using CFRP. MA = Mechanical Anchorage

Two different composite-based retrofitting systems were examined in the study namely: externally bonded carbon fiber reinforced polymer (EB-CFRP) composite laminates and embedded through depth glass fiber reinforced polymer (ETD-GFRP) composite rebars. Some of the specimens that were retrofitted with the EB-CFRP system had mechanical end anchorage (MA) in an effort to delay and/or prevent delamination of the EB-CFRP sheets. The MA system consisted of sandwich composite panels mechanically-fastened to the ends of the EB laminates by means of galvanized steel threaded anchor bolts. Details of the experimental work, description of test specimens, material properties, fabrication process, retrofitting regimes, test set-up, instrumentations and procedures are presented in this chapter.

3.2 Test Program

3.2.1 Test Matrix

The test matrix of the experimental program is given in Table 3.1. The test specimens were divided into three main groups. The details of each group are summarized below.

Group [A]: This group consisted of four specimens. All specimens had no internal steel stirrups and were not shear-damaged prior to strengthening and/or testing. One specimen was not strengthened. The remaining specimens were strengthened with the EB-CFRP system without MA, EB-CFRP system integrated with MA, and ETD-GFRP system.

Group [B]: This group consisted of 12 specimens. All specimens had internal steel stirrups spaced at 120 mm on center which corresponded to $s = 0.6d$, that is slightly higher than the maximum limit of $s_{max} = 0.5d$ specified by the ACI 318M-

05 (2005) to represent a shear-deficient RC beam with a poor steel detailing. The group was divided into three subgroups based on the initial shear damage state prior to retrofitting and/or testing. Each subgroup consisted of four specimens. In each subgroup, one specimen was not strengthened and three specimens were strengthened/retrofitted with EB-CFRP, EB-CFRP with MA, and ETD-GFRP systems. Specimens of the first subgroup were not damaged prior to strengthening. Specimens of the second and third subgroups were subjected to initial shear damages of D1 and D2, respectively prior to retrofitting/testing. For the shear damage state D1, the specimen was pre-subjected to three cycles of loading-unloading to induce shear cracks. In each cycle, the specimen was loaded up to initiation of shear cracks which took place at about 75 to 80 kN then unloaded. For the shear damage state D2, the specimen was loaded up to its peak load then unloaded. The peak load was considered when a sudden drop in the load took place. The specimens with the damage states D1 and D2 will be called pre-cracked and pre-failed specimens, respectively.

Group [C]: This group consisted of eight specimens with internal steel stirrups spaced at 75 mm on center which corresponded to $s = 0.375d$. The spacing between stirrups adopted in specimens of this group does not exceed the maximum limit of $s_{max} = 0.5d$ specified by the ACI 318M-05 (2005), in an effort to represent a case that could be encountered in practical applications. The specimens were divided into two subgroups, four specimens each. The specimens of the first subgroup were not damaged prior to strengthening/testing. The specimens of the second subgroup were pre-failed prior to retrofitting and/or testing (i.e. pre-subjected to one cycle of loading up to peak load then unloaded).

Similar to other groups, the strengthening/retrofitting systems included EB-CFRP without MA, EB-CFRP with MA, and ETD-GFRP.

3.3 Test specimens

The loading regime adopted in the current study allowed two specimens to be tested on each beam. The right shear span (first test specimen) was first tested keeping the left end zone overhang and unstressed as shown in Figure 3.1. The left shear span (second test specimen) was then tested keeping the right end zone; already tested previously, overhang and as shown in Figure 3.2. Details of reinforcement for beams of groups [A], [B] and [C] are shown in Figures 3.3, 3.4 and 3.5, respectively. Each beam was 4000 mm long, with a T-shaped cross section to better resemble field conditions. The beam cross section had a web width of $b_w = 125$ mm, flange width of $b_f = 250$ mm, total depth of $h = 250$ mm, and effective depth of $d = 200$ mm. The specimens were tested under three point bending with an effective span of 3000 mm and a short shear span of 600 mm rendering a shear span to effective depth ratio of $a/d = 3$. The specimens were designed in a way to ensure that a shear failure would dominate. The tensile steel reinforcement consisted of 4 No. 22 bars ($A_s = 1520.5 \text{ mm}^2$) and the compression steel reinforcement consisted of 4 No.12 bars ($A'_s = 452.4 \text{ mm}^2$). The tensile steel reinforcing bars had a 90° hook at each end to provide sufficient anchorage. Specimens of group [A] had no stirrups in the test region. The internal shear reinforcement in the test region for other specimens consisted of double-leg closed No. 6 plain stirrups ($A_v = 56.5 \text{ mm}^2$) with a clear cover of 15 mm placed at a spacing of $s = 120$ mm for specimens of group [B], and $s = 75$ mm for specimens of group [C]. Double-leg closed stirrups of 8 mm in diameter were

provided as shear reinforcement at $s = 75$ mm through the long shear span in the beams of all groups in order to avoid shear failure outside the test region.

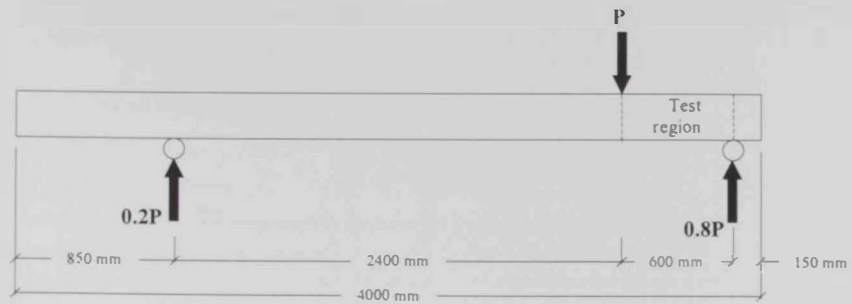


Figure 3.1: Test of the right shear span

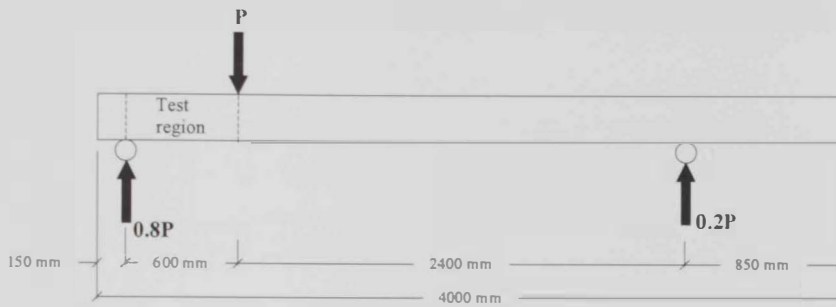


Figure 3.2: Test of the left shear span

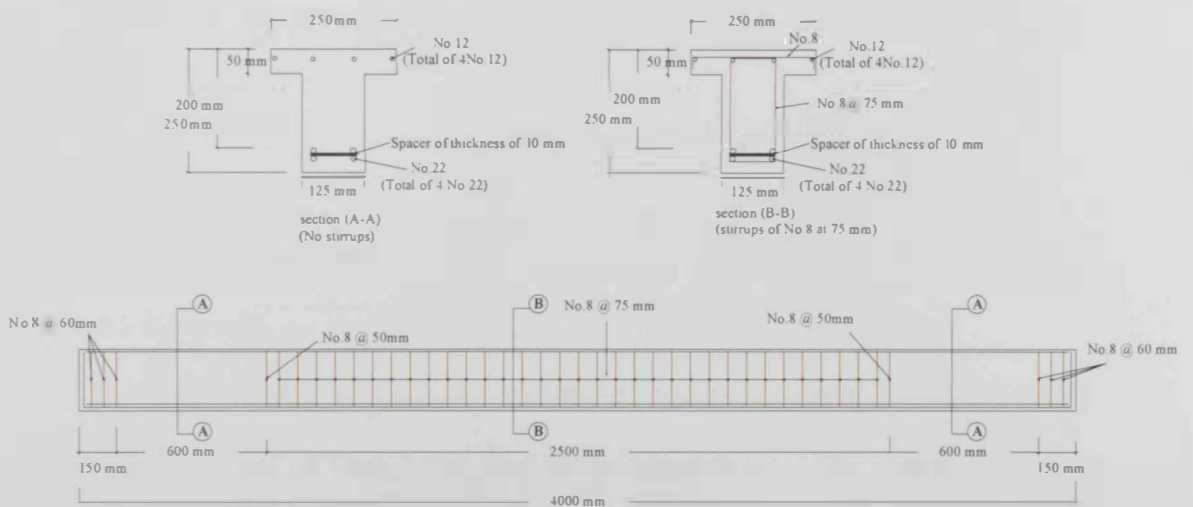


Figure 3.3: Details of reinforcement for beams of group [A]

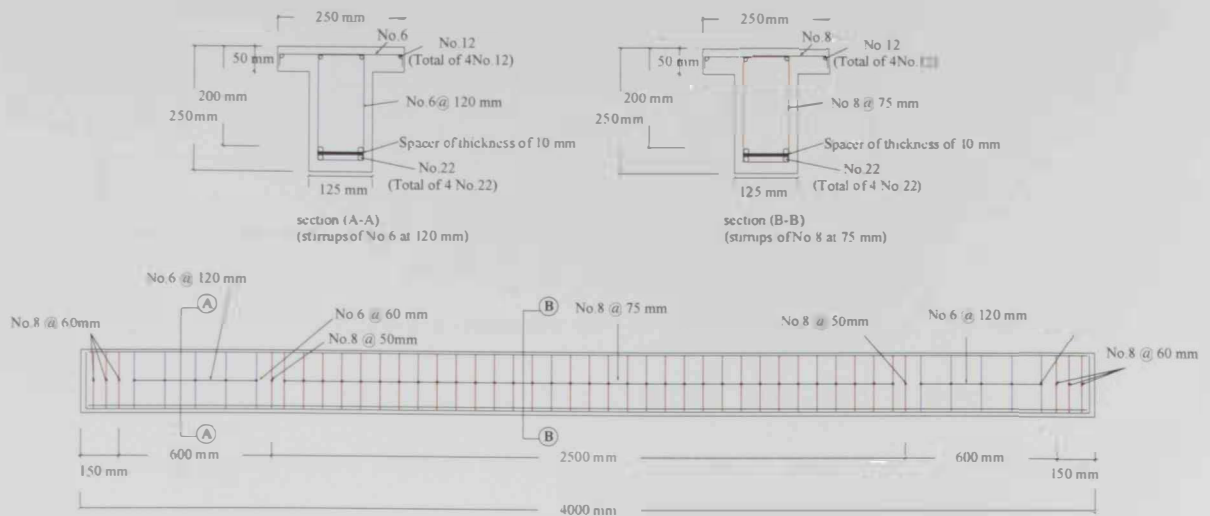


Figure 3.4: Details of reinforcement for beams of group [B]

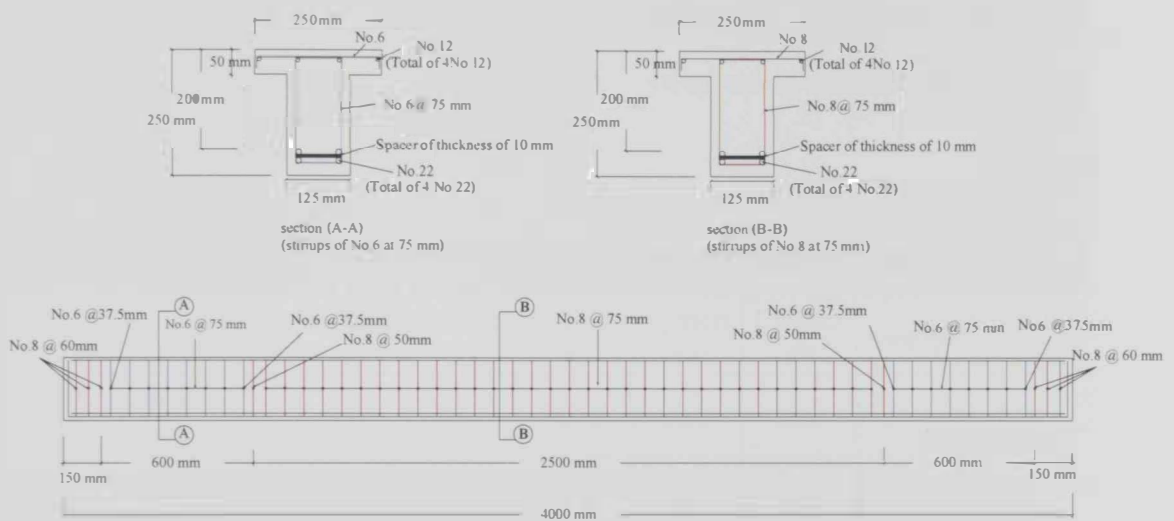


Figure 3.5: Details of reinforcement for beams of group [C]

3.4 Material properties

3.4.1 Concrete

The concrete mix properties by weight are shown in Table 3.2. An ordinary Portland cement of Type I was used in the concrete mix. The coarse aggregates used in the mix were of natural crushed stones with medium and large aggregate sizes of 10 and 20 mm, respectively.

Table 3.2: Concrete mix properties by weight

Concrete mix properties by weight					
Cement	Fine aggregates		Coarse aggregates		Water
	Dune sand	Black sand	Medium	Large	
1	0.64	0.64	1.51	1.51	0.53

Ten cylinders each having a diameter of 150 mm and a length of 300 mm were sampled during concrete casting. Five cylinders were used to determine the concrete compressive strength as shown in Figure 3.6(a). The remaining five cylinders were used to determine the concrete splitting strength as shown in Figure 3.6(b). The compressive and splitting strength results are given in Table 3.3. The average concrete compressive and tensile strengths at the time of structural testing were 30.4 and 3.3 MPa, respectively, with corresponding standard deviations of 3.5 and 0.26 MPa, respectively.

Table 3.3: Compressive and splitting tests results for the tested cylinders

Test	Cylinder #1	Cylinder #2	Cylinder #3	Cylinder #4	Cylinder #5	Average	Standard deviation
Compression (f'_c), MPa	34.5	33.1	28.6	30.0	25.9	30.4	3.50
Splitting (f_{ct}), MPa	3.6	2.9	3.4	3.3	3.1	3.30	0.26



(a) Compressive test



(b) Splitting test

Figure 3.6: Compressive and splitting tests for the tested concrete cylinders

3.4.2 Steel reinforcement

The tensile and compression steel reinforcements were No.22 and No.12 deformed bars, respectively. The stirrups in the test region were No.6 plain bars. Three steel coupons were taken from each bar size and tested to failure under uniaxial tension force to determine the yielding and ultimate strengths. Results of the tensile tests for the flexural and shear steel reinforcements are summarized in Tables 3.4 and 3.5, respectively. The No.22 and No.12 steel bars had average yield strengths of 498 and 502 MPa, respectively, and average ultimate strengths of 593 and 605 MPa, respectively. The No.6 steel bars had average yield and ultimate strengths of 333 and 389 MPa, respectively. The No.8 deformed bars had average yield and ultimate strengths of 588 and 694 MPa, respectively.

Table 3.4: Properties of the flexural steel reinforcement

Nominal bar size (mm)	Sample No.	Nominal area (mm ²)	Yield strength (N/mm ²)	Tensile strength (N/mm ²)
12	Sample #1	113.10	521	626
	Sample #2	113.10	494	596
	Sample #3	113.10	491	594
22	Sample #1	380.10	500	595
	Sample #2	380.10	491	590
	Sample #3	380.10	503	594

Table 3.5: Properties of the shear steel reinforcement

Nominal bar size (mm)	Sample No.	Nominal area (mm ²)	Yield strength (N/mm ²)	Tensile strength (N/mm ²)
6	Sample #1	28.30	323	375
	Sample #2	28.30	331	379
	Sample #3	28.30	344	413
8	Sample #1	50.27	597	699
	Sample #2	50.27	603	703
	Sample #3	50.27	563	680

3.4.3 Fiber reinforced polymers (FRP)

In this study, CFRP composite laminates and GFRP bars were used in the strengthening systems. The CFRP composite laminates consisted of SikaWrap 300C[®] dry fibers (flexible fabric) and Sikadur 330[®] resin. The carbon fiber fabric and epoxy resin used in the EB-CFRP system were manufactured by Sika[®]. The GFRP rods used in the ETD-GFRP system had a nominal diameter of 10 mm. They were manufactured by Pultron composites[®]. The GFRP rebars were inserted into holes pre-drilled through the section depth and held in place using the epoxy adhesive Sikadur 30 LP[®] manufactured by Sika[®]. Mechanical properties of the materials used in shear strengthening are given in Table 3.6.

Table 3.6: Mechanical properties of materials used in shear strengthening (data obtained from manufacturer).

Strengthening system	Material	Tensile modulus (GPa)	Tensile strength (MPa)	Ultimate elongation (%)
EB-CFRP system	Carbon fiber dry fabric ^a	230	3450	1.5
	SikaWrap 300C [®]			
EB-CFRP system	Epoxy resin	-	30	1.5
	Sikadur 330 [®]			
ETD-GFRP system	GFRP rebars	54	900	1.7
	Pultron composites [®]			
ETD-GFRP system	Epoxy adhesive	4.5	25	1
	Sikadur 30 LP [®]			

^a Thickness of a typical one ply of the carbon fiber fabric is 0.17 mm.

3.5 Fabrication of test specimens

Once the design was completed the procedures under taken to fabricate test specimens were as follows:

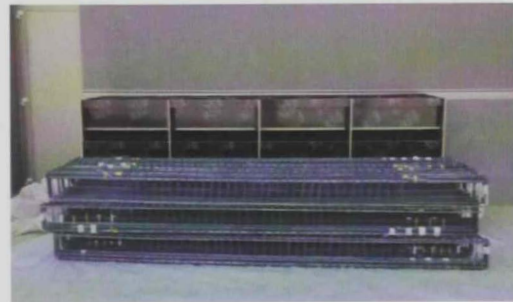
- Preparation of formwork.
- Cutting of steel bars and fabrication of stirrups.
- Preparation of steel cages.

- Installation of strain gauges.
- Casting of concrete.
- Curing of test specimens.
- Inducing of shear damage in the pre-damaged test specimens.
- Shear strengthening with composite-based systems.

Wooden forms were manufactured in the workshop of the United Arab Emirates University using plywood sheets as shown in Figure 3.7(a). The steel reinforcement bars were first cut to desired lengths. The longitudinal tensile steel bars were bent at each end to provide a 90° hook. The stirrups were then fabricated and the entire steel cage was assembled as shown in Figure 3.7(b).



(a) Fabricated formworks



(b) Fabricated steel cages

Figure 3.7: Fabrication of formworks and steel cages

The steel cages were then installed in the forms as shown in Figure 3.8. Cement blocks were prepared and placed in appropriate locations to maintain the concrete cover. The concrete components were placed mixed together in a concrete mixer. The concrete was then placed inside the wooden forms. All specimens were cast in a horizontal position. A hand held vibrator was used during casting to ensure proper consolidation of concrete. The surface was trowel finished after casting as shown in Figure 3.9.



Figure 3.8: Installation of steel cages in the forms before casting



Figure 3.9: Concrete after casting

After casting, the beams were covered by polyethylene sheets for three days. The forms were then stripped and the specimens were kept moist using wet burlaps for two weeks. The specimens were then kept air-cured until installation of the composite system and/or testing.

3.6 Strengthening/retrofitting systems

Two composite-based systems were used for shear strengthening/retrofitting of test specimens. The strengthening/retrofitting regimes and methodology are summarized in the following subsections. For the pre-failed specimens, the pre-existing cracks were chased-out in a V-shape to a depth of approximately 13 mm as shown in Figure 3.10(a), surface-filled with a cementitious grout, and struck off flush with the concrete surface as shown in Figure 3.10(b). Any damaged concrete in the flange were removed, cleaned of dust and loose particles using air blower, and then repaired with the cementations grout.



(a) Chasing-out of pre-existing cracks (b) After sealing of cracks and finishing of concrete surface

Figure 3.10: Crack sealing and surface preparation of the pre-failed specimens

3.6.1 The EB-CFRP system

Layout of the EB-CFRP strengthening system without a mechanical end anchorage is shown in Figure 3.11. The U-shaped CFRP composite sheets, 80 mm width each, were installed in the shear span at a center to center spacing of $s_f = 120$ mm. In the EB-CFRP system, dry carbon fiber fabrics, SikaWrap 300C[®], impregnated in-situ with the epoxy resin Sikadur 330[®] were bonded to the concrete surface. Photos of the dry carbon fiber fabrics and the epoxy resin are shown in Figure 3.12. The dry carbon fiber fabrics were first cut to desired lengths. The concrete surface was ground using a grinder and the bottom corners were rounded to a radius of about 15 mm. An electrical blower was then used to clean the surface from dust or any foreign particles. The locations of the CFRP composite sheets are then marked on the concrete surface. The epoxy resin consisted of two components A and B that were mixed together for about five minutes in a ratio of 4 to 1 by weight, respectively using a low speed drill (400-600 rpm). The epoxy resin was then applied onto the prepared substrate using a trowel. The carbon fiber fabrics, pre-cut to desired dimensions, were placed onto the resin coating and smoothed out with gloved hands. Adequate pressure was

applied until the resin was squeezed out between the fabric's rovings. A final sealer coat of resin was then applied onto the exposed surface. The strengthened specimens were then air-cured for a minimum of two weeks prior to testing. The EB-CFRP strengthening procedures are summarized in Figure 3.13.

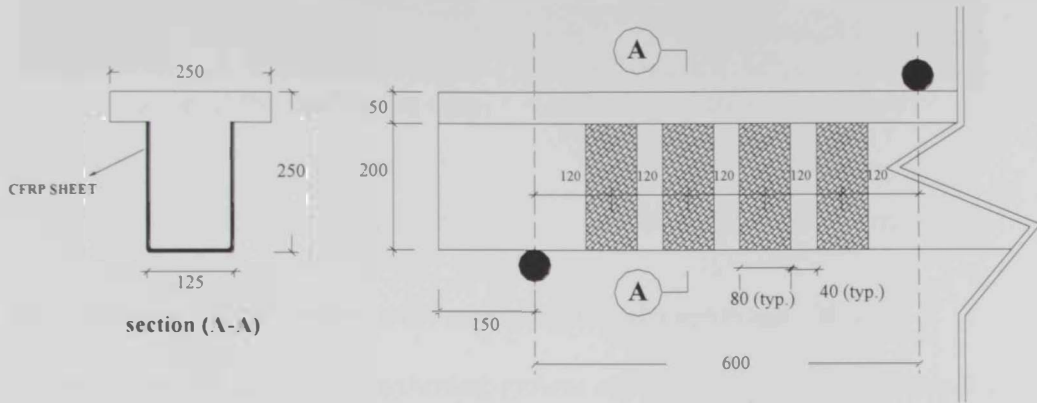
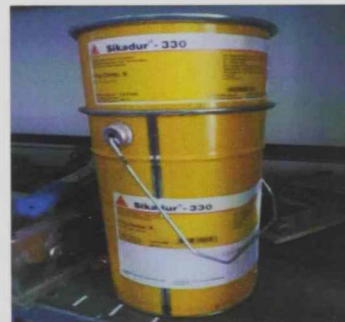


Figure 3.11: Positions and dimensions of the EB-CFRP sheets (dimensions are in mm)



Dry carbon fiber fabrics
SikaWrap 300C[®]



Sikadur 330[®] epoxy resin

Figure 3.12: Materials used in the EB-CFRP system



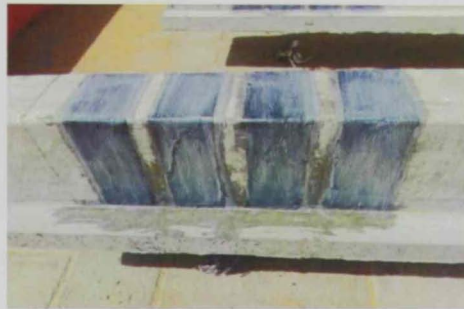
(a) Marked concrete after surface preparation



(b) Bonding of the CFRP sheets to the concrete



(c) Application of the final sealer coat



(d) Curing of the CFRP sheets

Figure 3.13: Strengthening procedures of the EB-CFRP system without MA

3.6.2 The EB-CFRP system with mechanical end anchorage (MA)

Layout of the EB-CFRP strengthening system integrated with the mechanical end anchorage (MA) is shown in Figure 3.14. Pultruded pre-cured FRP composite plates, commercially known as SAFSTRIP[®], were used for the mechanical end anchorage. This type of FRP is a hybrid carbon and glass fiber composite with a vinylester matrix. A typical pre-cured FRP plate has a thickness of 3.2 mm, average tensile modulus of 62.2 GPa, tensile strength of 852 MPa, clamped and unclamped bearing strengths of 351 and 214 MPa, respectively (SAFSTRIP 2008). On the completion of the lay-up process, two 50 x 80 mm SAFSTRIP[®] composite plates were bonded longitudinally on top of each impregnated CFRP sheet, one at each side, directly below the flange. The ends of the impregnated CFRP sheet were rolled over the pre-cured composite plates and then secured tightly by overlapping them with additional pre-cured composite plates, forming a sandwich composite panel (SCP) (Ortega et al.2009; El-Maaddawy and Chekfeh 2012). Each SCP was mechanically fastened to the concrete using a galvanized threaded anchor bolt with a diameter of 8 mm and a length of 55 mm.

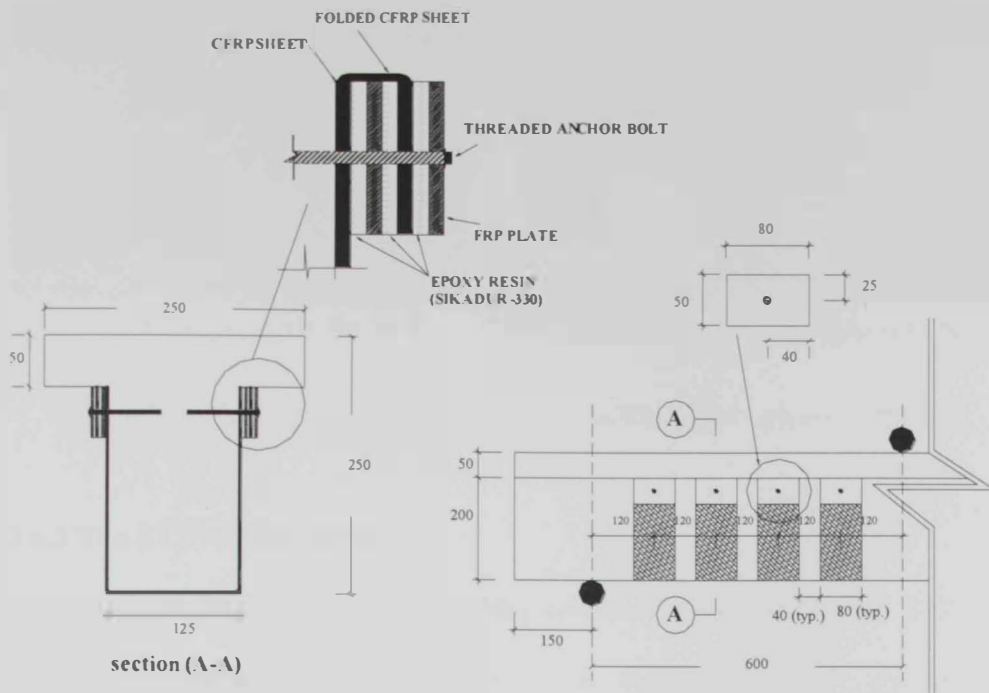


Figure 3.14: Positions and dimensions of the CFRP sheets and the MA system (dimensions are in mm).

The materials used in the MA system are shown in Figure 3.15. The threaded anchor bolts were installed into holes, each having a diameter of 8 mm and a length of 60 mm, predrilled through the SCP and the concrete. Strengthening procedures of the EB-CFRP with the MA are summarized in Figure 3.16.

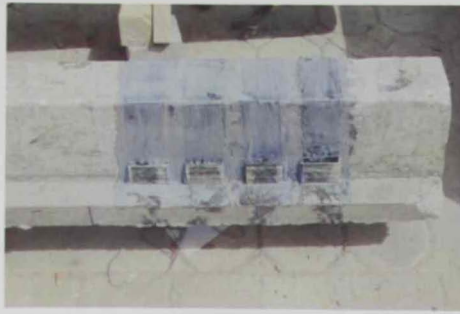


(a) SAFSTRIP



(b) Threaded anchor bolts

Figure 3.15: Materials used in the MA system



(a) EB-CFRP sheets with the SCP

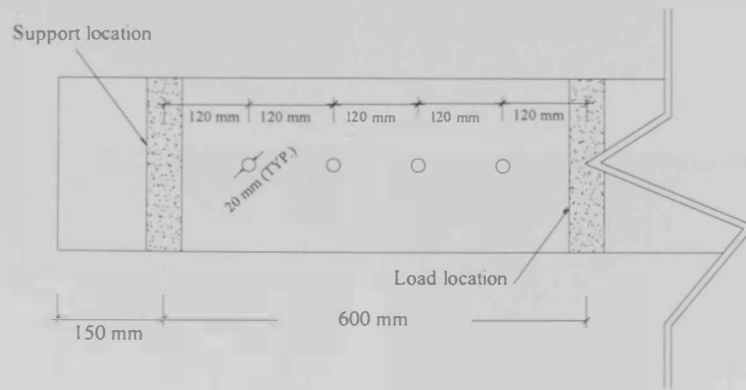


(b) Drilling of holes for the anchor bolts

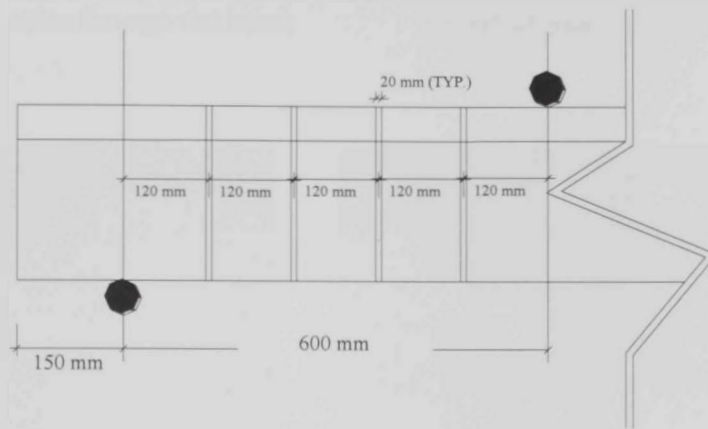
Figure 3.16: Strengthening procedures of the EB-CFRP system with MA

3.6.3 The ETD-GFRP system

Layout of the ETD-GFRP strengthening system is shown in Figure 3.17. The GFRP rebars had a nominal diameter of 10 mm, length of 250 mm, and center to center spacing of $s_f = 120$ mm. The GFRP rebars were installed into holes predrilled through the entire section depth and held in place using the epoxy adhesive Sikadur 30 LP[®]. Photos of sample GFRP rebars and the epoxy adhesive are given in Figure 3.18. The ETD-GFRP strengthening procedures are summarized in Figure 3.19. Holes with a diameter of 20 mm were first drilled through the entire section depth at the desired locations. The holes were then cleaned of dust using an electrical blower. The bottom surface of the beam was sealed using rigid boards. The holes were then filled with the epoxy adhesive Sikadur 30 LP[®]. The epoxy adhesive consisted of two components A and B that were mixed together for about five minutes in a ratio of 3 to 1 by weight, respectively using a low speed drill (400-600 rpm). The GFRP bars were then inserted into the holes. The extra epoxy flooded on the top surface was then cleaned and leveled.

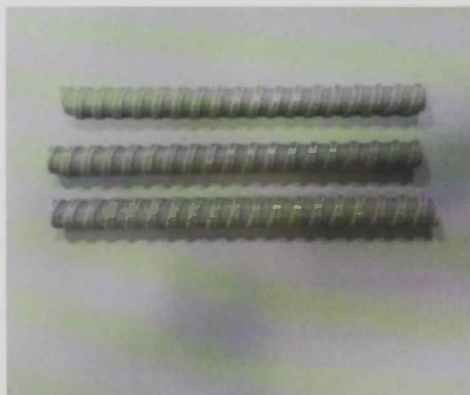


Top view



Elevation

Figure 3.17: Layout of the ETD-GFRP system



GFRP bars



Sikadur 30 LP®

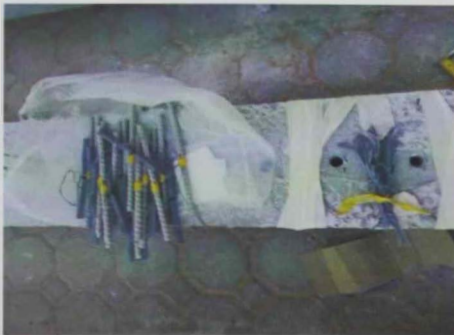
Figure 3.18: Materials used in the ETD-GFRP system



(a) Drilling of holes through the beam depth



(b) Holes after drilling



(c) Preparation of the GFRP bars prior to installation



(d) Removal of extra epoxy and finishing of concrete surface.

Figure 3.19: Strengthening procedures of the ETD-GFRP system

3.7 Test set-up and instrumentation

The specimens were tested under three-point bending with an effective span of 3000 mm and a shear span of $a = 600$ mm, measured from the nearest support to the load point as shown in Figure 3.20. The load was applied incrementally using a hydraulic jack. A test in progress is shown in Figure 3.21.

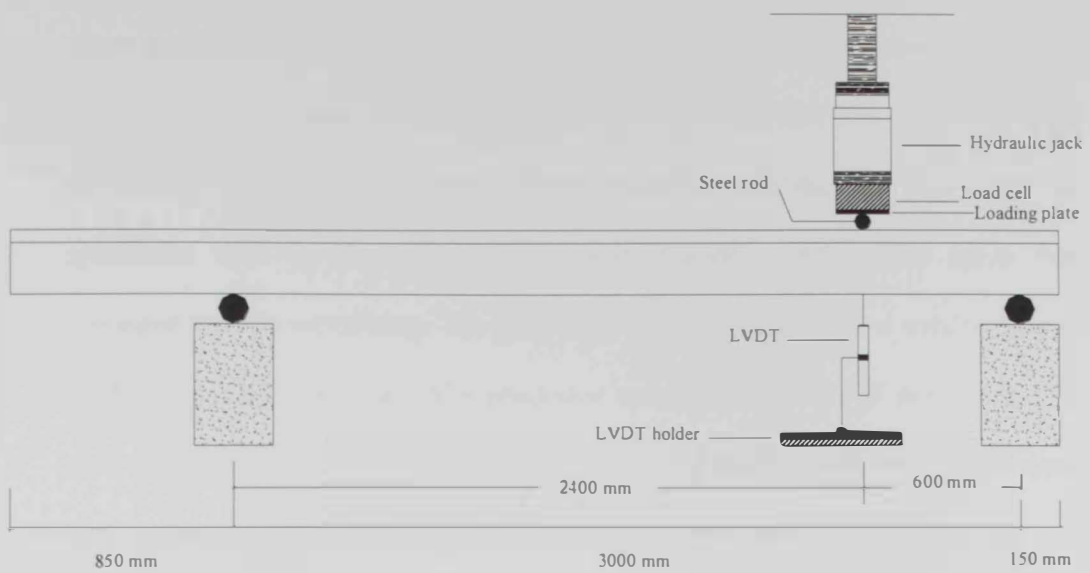


Figure 3.20: Test setup and instrumentations

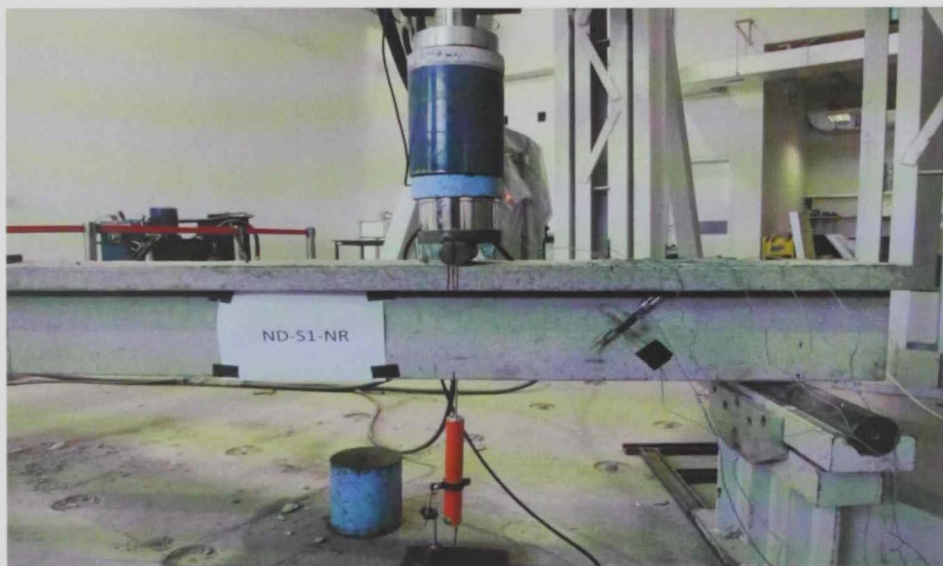


Figure 3.21: A test in progress

3.7.1 Loading history

The specimens with the damage state D1 were pre-subjected to three cycles of loading-unloading to induce shear cracks in the specimen prior to retrofitting. In each cycle, the specimen was loaded up to initiation of shear cracks, which took

place at about 75 to 80 kN then unloaded. The pre-cracked specimen D1-S1-NR with the damage state D1 from group [B] was loaded back to failure without retrofitting to investigate the effect of the pre-cracking on the shear response. The specimens with the damage state D2 were loaded to their peak loads then unloaded prior to retrofitting. The peak load was identified when a sudden drop in the applied load took place. The pre-failed specimens D2-S1-NR and D2-S2-NR with the damage state D2 from groups [B] and [C], respectively were also loaded back to failure without retrofitting to quantify the residual shear capacity after one cycle of loading to peak load then unloading.

3.7.2 Strain measurements

Electrical-resistance strain gauges were used to measure the strains in the internal stirrups, the tensile steel, the EB-CFRP sheets, and the GFRP rebars. A strain gauge was bonded to the tensile steel reinforcement at the section of maximum moment in all test specimens. Strain gauges were bonded to the three and four middle stirrups in the test region in specimens of groups [B] and [C], respectively. The positions of the strain gauges in the internal steel for specimens of groups [A], [B], and [C] are shown in Figures 3.22, 3.23, and 3.24, respectively. The locations of the strain gauges bonded to the composite reinforcement are shown in Figures 3.25, 3.26 and 3.27 for the specimens with the EB-CFRP system without the MA, EB-CFRP system with the MA, and ETD-GFRP system, respectively. The strain gauges have a length of 5 mm, tolerance of ± 0.85 ($\mu\text{m/m}$)/ $^{\circ}\text{C}$, coefficient of thermal expansion of $11.8 \times 10^{-6}/^{\circ}\text{C}$ and current resistance of 120Ω . Characteristics of the strain gauges are provided by the manufacturer.

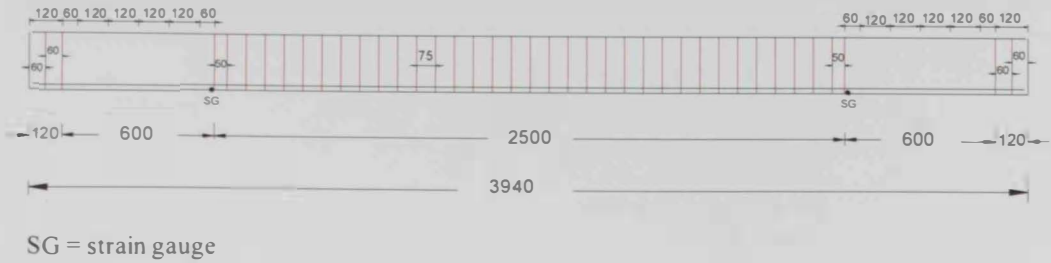


Figure 3.22: Positions of the strain gauges for specimens of group [A]
(All dimensions are in mm)

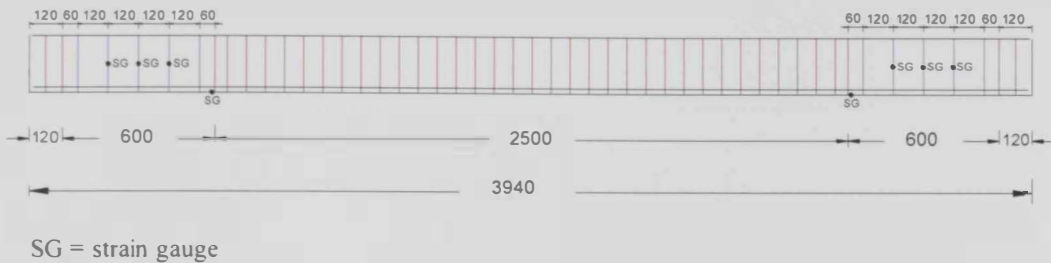


Figure 3.23: Positions of the strain gauges for specimens of group [B]
(All dimensions are in mm)



Figure 3.24: Positions of the strain gauges for specimens of group [C]
(All dimensions are in mm)

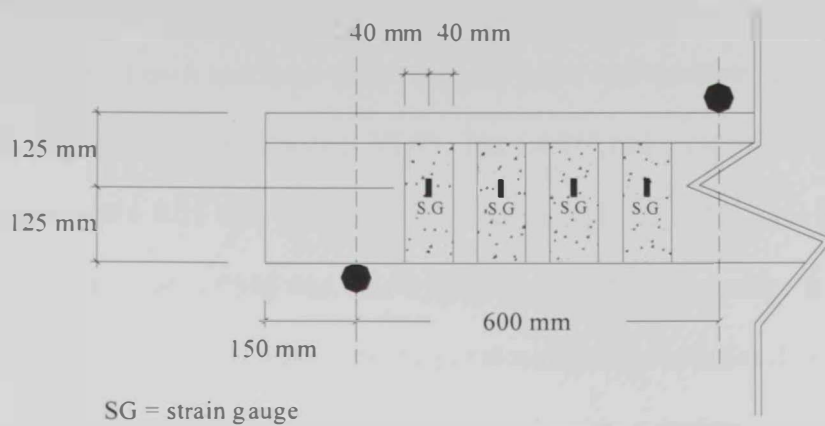


Figure 3.25: Positions of the strain gauges bonded to the EB-CFRP sheets (Specimens with the EB-CFRP system)

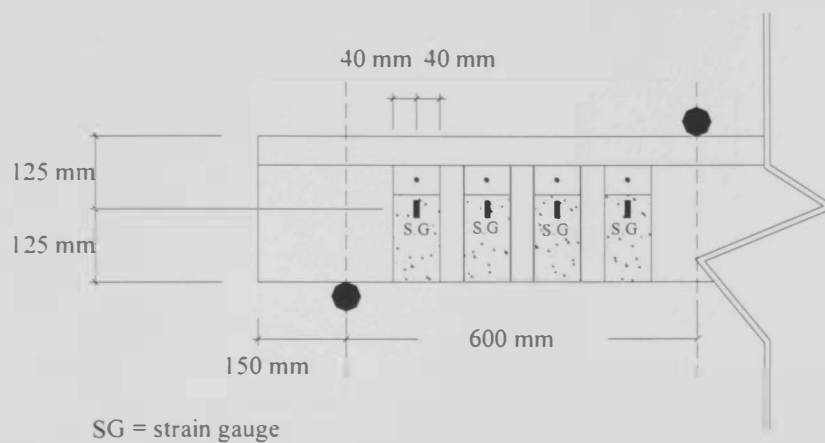


Figure 3.26: Positions of the strain gauges bonded to the EB-CFRP sheets (Specimens with the EB-CFRP+MA system)

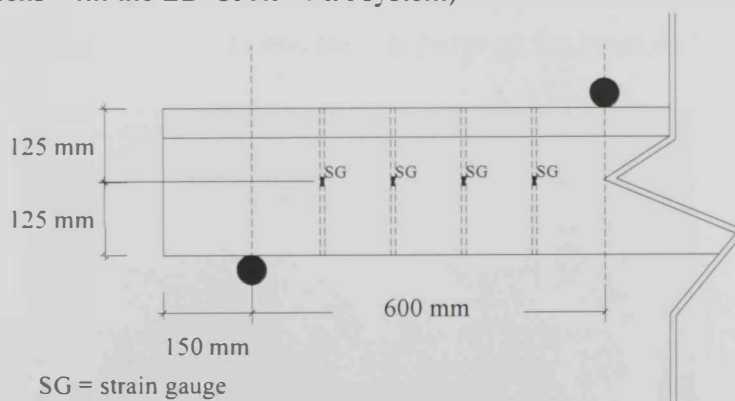


Figure 3.27: Positions of the strain gauges bonded to the GFRP bars (Specimens with the ETD-GFRP system)

3.7.3 Displacement and load measurements

The deflection of each specimen under the load point was measured using a linear variable displacement transducer (LVDT). The LVDT had a capacity of 100 mm and accuracy of ± 0.01 mm. A concrete clip gauge inclined at 45° with a capacity of 5 mm and a length of 100 mm was attached to the concrete surface at the mid-point of the shear span to measure the diagonal tensile displacement during testing as shown in Figure 3.28. The load was applied using a hydraulic jack with a capacity of 200 kN. A load cell with a capacity of 500 kN and accuracy of ± 0.001 kN was used to record the load. The measurements were recorded by means of data loggers as shown in Figure 3.29.

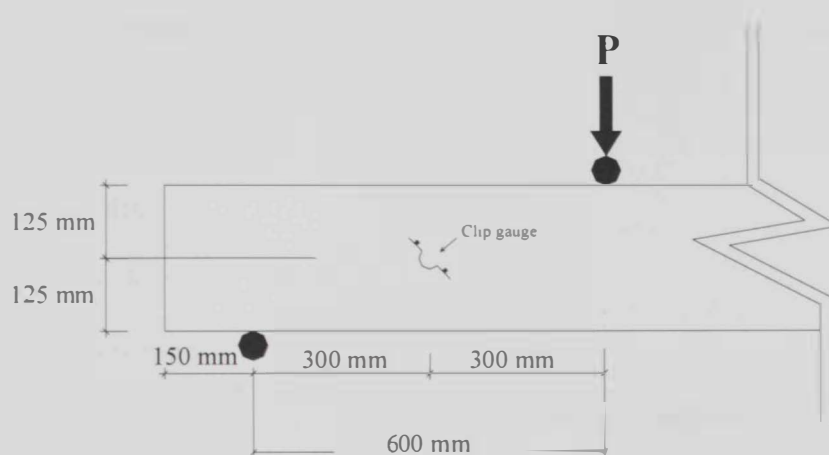


Figure 3.28: Location of concrete clip gauge on the beam surface



Figure 3.29: Data loggers

CHAPTER 4: EXPERIMENTAL RESULTS

4.1 Introduction

This chapter presents the results of the experimental program. The results include the mode of failure, shear capacity, deflection response and diagonal tensile displacement response. The strain responses of the internal steel stirrups, flexural steel, CFRP sheets and GFRP rebars are presented. A discussion of the results is included for all test specimens in terms of shear resistance, stiffness, energy absorption, deflection at peak load and effective strain in the FRP composite reinforcement. The efficiencies of the composite systems adopted in this study for shear strengthening/retrofitting are evaluated at the end of this chapter.

4.2 Test results

4.2.1 Group [A]

4.2.1.1 Failure mode

Photos of test specimens of group [A] before testing, at peak load, and at failure are shown in Figure 4.1 through Figure 4.4. The unstrengthened control specimen ND-NS-NR exhibited one major shear crack initiated at the middle of the shear span at about 70% of the peak load. After crack initiation, the specimen was able to sustain additional load due to the tension stiffening effect (i.e. interlocking and surface roughness). Further increase in the load resulted in formation of additional small cracks adjacent to the major shear crack developed earlier. As the load progressed, the shear cracks started to widen and propagate towards the support and the load points. Finally, the specimen failed in a diagonal tension shear mode of failure as shown in Figure 4.1. The

specimen strengthened with the EB-CFRP system failed by delamination of the EB-CFRP sheets with a thin layer of concrete adhered to them. Debonding of the EB-CFRP system was preceded by formation of diagonal shear cracks in the shear span as shown in Figure 4.2. The specimen strengthened with EB-CFRP integrated with the MA reached its peak load without delamination of the EB-CFRP sheets. Inspection of concrete after failure revealed formation of multiple diagonal shear cracks in the shear span. The specimen failed due to formation of diagonal shear cracks followed by excessive shear deformation and loss of shear integrity as shown in Figure 4.3. In the post peak stage, peeling off of the EB-CFRP sheets along with the MA/pullout of anchor bolts took place. The specimen strengthened with the ETD-GFRP system exhibited a classical shear mode of failure where diagonal cracks developed in the shear span then propagated towards the support and the load points. No rupture of GFRP bars was observed. As the load progressed, the developed cracks widened and increased in length until the specimen failed due to loss of the shear integrity in a diagonal tension mode of failure as shown in Figure 4.4.

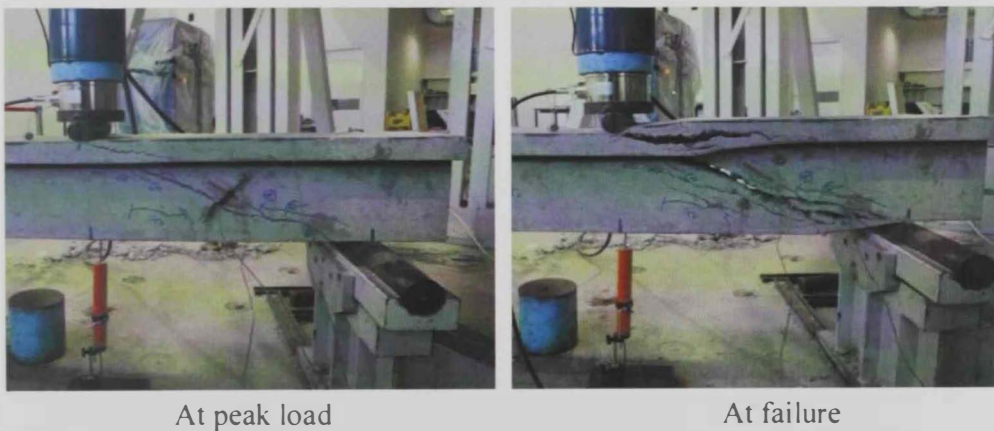
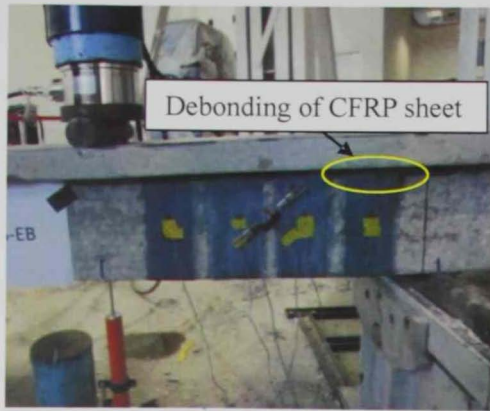


Figure 4.1: Failure mode of specimen ND-NS-NR



At peak load



At failure

Figure 4.2: Failure mode of specimen ND-NS-EB



At peak load



At failure

Figure 4.3: Failure mode of specimen ND-NS-EB+MA



At peak load



At failure

Figure 4.4: Failure mode of specimen ND-NS-ETD

4.2.1.2 Shear capacity

Results of specimens of group [A] are given in Table 4.1. The unstrengthened control specimen ND-NS-NR reached a maximum load of 86 kN which corresponded to a shear resistance of 68.8 kN. The EB-CFRP strengthening system without the MA increased the shear resistance by 17% only. The shear resistance of the specimen ND-NS-EB+MA strengthened with the EB-CFRP system integrated with the MA was 112.8 kN with a CFRP shear resistance of 44 kN. This corresponded to a shear strength gain of 64%. Therefore, the inclusion of the mechanical end anchorage system in the EB-CFRP system was necessary to achieve a significant gain in the shear resistance. The specimen ND-NS-ETD strengthened with the ETD-GFRP system achieved a shear resistance of 107.2 kN. This corresponded to a shear strength gain of 56%. The shear strength gains for specimens ND-NS-EB+MA and ND-NS-ETD were insignificantly different.

Table 4.1: Test results of group [A].

Group	Specimen	Peak load P_{max} (kN)	Shear resistance ^a V_{max} (kN)	FRP shear resistance ^b V_{frp} (kN)	Shear strength gain (%)	Effective FRP strain ϵ_{fe} ($\mu\epsilon$)
[A]	ND-NS-NR	86	68.8	-	-	-
	ND-NS-EB	101	80.8	12.0	17	2592
	ND-NS-EB+MA	141	112.8	44.0	64	8334
	ND-NS-ETD	134	107.2	38.4	56	5510

^a $V_{max} = 0.8P_{max}$

^b With respect to the control unstrengthened specimen ND-NS-NR

4.2.1.3 Deflection response

The load-deflection curves for specimens of group [A] are illustrated in Figure 4.5. All specimens exhibited almost a linear deflection response until initiation of shear cracks at about 60 kN. Following shear cracking, the non-strengthened control specimen ND-NS-NR experienced a sudden increase in deflection. The

specimen could, however, sustain additional load due to the tension stiffening effect until it reached its peak load at a deflection of 6.1 mm. The strengthened specimens exhibited a quasi-linear deflection response in the post-cracking stage. Varying the strengthening system had no effect on the stiffness of the strengthened specimens. Specimen ND-NS-EB reached its peak load at a deflection of 6.4 mm. It experienced several drops/increases in the load in the post-peak stage possibly because of progressive debonding of the CFRP sheets. The specimens strengthened with the EB-CFRP system integrated with the MA and those with the ETD-GFRP system experienced a quasi-linear load-deflection behavior until they reached their peak loads at deflections of 8.8 and 8.0 mm, respectively. After reaching the peak load, specimens ND-NS-EB+MA and ND-NS-ETD exhibited a sudden drop in load followed by a plastic response where the deflection continued to increase without an increase in load.

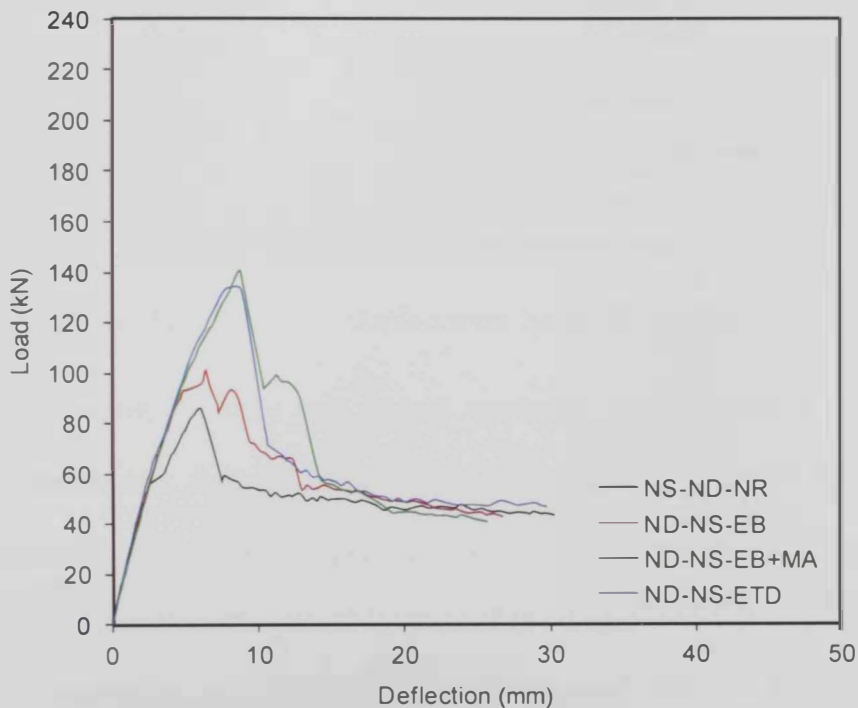


Figure 4.5: Load-deflection curves for specimens of group [A]

The energy absorption (area under the load-deflection response) of all strengthened specimens was higher than that of the control specimen ND-NS-NR. The energy absorption of specimens ND-NS-EB+MA and ND-NS-ETD was almost the same but significantly higher than that of specimen ND-NS-EB.

4.2.1.4 Diagonal tensile displacement response

The load versus the diagonal tensile displacement curves for specimens of group [A] are shown in Figure 4.6.

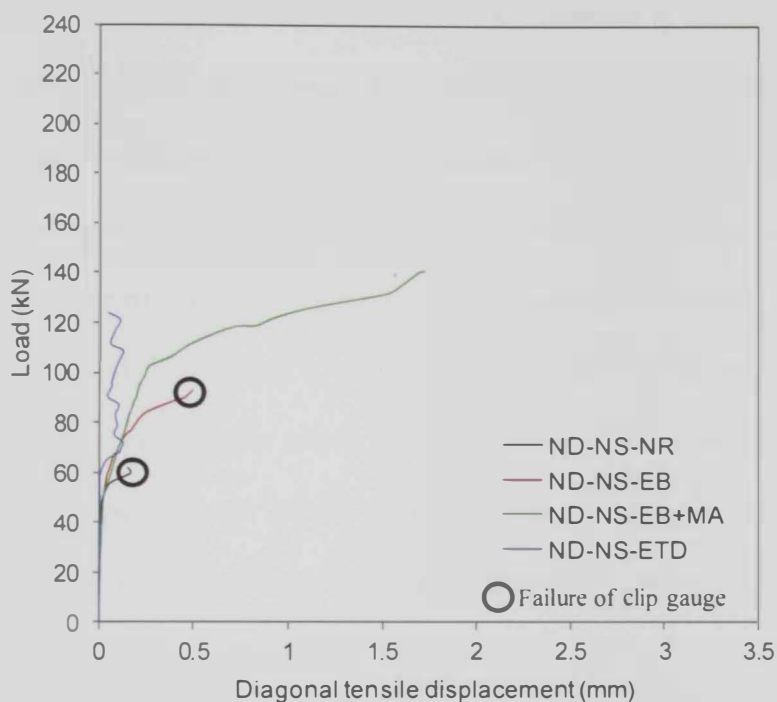


Figure 4.6: Load-diagonal tensile displacement curves for specimens of group [A].

From this figure, it can be seen that all specimens except specimen ND-NS-ETD experienced diagonal shear cracking at approximately 55 kN. The diagonal cracks developed in specimen ND-NS-ETD at approximately 60 kN. After crack initiation, the rate of increase of the diagonal tensile displacement across cracks for the specimens ND-NS-EB and ND-NS-EB+MA was significantly lower than that of the non-strengthened control specimen ND-NS-

NR. The initial rate of increase of the diagonal tensile displacement across cracks for specimen ND-NS-ETD was similar to that of the control specimen ND-NS-NR. Failure of the clip gauge in specimen ND-NS-ETD took place at a load value of approximately 70 kN. Following shear cracking, the diagonal tensile displacement for specimen ND-NS-EB increased almost at a constant rate until it reached a displacement of approximately 0.15 mm at a load value of 78 kN with a corresponding diagonal tensile displacement of about 0.15 mm. Subsequently, the diagonal tensile displacement continued to increase but at a higher rate because of development of new cracks within the clip gauge until the specimen reached its peak load at a diagonal tensile displacement across cracks of 0.5 mm. For specimen ND-NS-EB+MA, the diagonal tensile displacement across cracks increased in the post-cracking stage until it reached a displacement of 0.26 mm at a load value of 100 kN. In the last stage, the diagonal displacement across cracks continued to increase but at a higher rate due to development of new cracks within the clip gauge, until the specimen reached its peak load at a diagonal tensile displacement across cracks of 1.72 mm.

4.2.1.5 Flexural steel strain response

The curves of the load versus the strain in the longitudinal tensile steel reinforcement for specimens of group [A] are shown in Figure 4.7. All specimens exhibited almost a bi-linear strain profile. Figure 4.7 indicates that the specimens experienced flexural cracks at approximately 15 kN. These cracks were invisible during testing. The rate of increase of the steel strain after initiation of the flexural cracks was insignificantly different for all specimens. The longitudinal steel reinforcement in all specimens of group [A] did not

reach the yielding strain prior to the peak load. The longitudinal steel reinforcement in specimen ND-NS-NR has reached a strain of 966 $\mu\epsilon$ at the peak load. However, specimen ND-NS-EB has reached a higher strain of 1098 $\mu\epsilon$ at the peak load. Specimens ND-NS-EB+MA and ND-NS-ETD reached their peak loads at strain values of 1830 and 1670 $\mu\epsilon$, respectively.

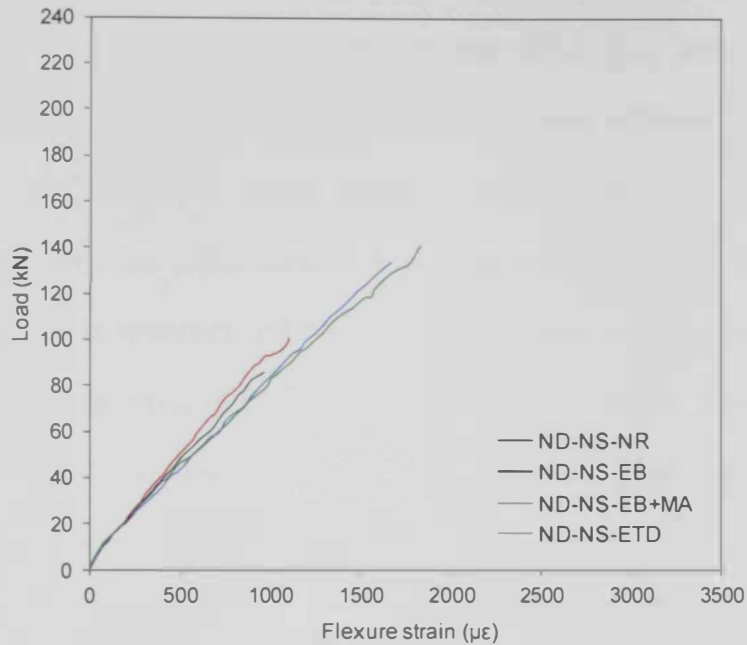


Figure 4.7: Load-flexural strain relationships for specimens of group [A]

4.2.1.6 FRP strain response

The curves of the load versus the FRP strains for the strengthened specimens of group [A] are shown in Figure 4.8. The effective FRP strain values are reported in Table 4.1. The effective FRP strain is considered as the maximum strain value recorded in the FRP reinforcement. It should be noted that the maximum measured FRP strain is not necessarily the maximum absolute FRP strain experienced by the specimen. The FRP reinforcement were not strained in the pre-cracking stage. The FRP reinforcement started to contribute to the shear resistance after crack initiation at approximately 60 kN. Specimen ND-NS-ETD exhibited a sudden increase in the GFRP strain at the onset of cracking

until it reached a strain value of approximately 3000 $\mu\epsilon$. Subsequently, the GFRP strain increased at a constant rate until it reached a strain value of 5510 $\mu\epsilon$ at a load value of 120 kN, where local slippage/debonding of the concerned GFRP rebar may have taken place. Specimen ND-NS-EB experienced a bi-linear CFRP strain response whereas specimen ND-NS-EB+MA featured a tri-linear strain response. After crack initiation, the rate of the CFRP strain in specimen ND-NS-EB and ND-NS-EB+MA was insignificantly different. For specimen ND-NS-EB, the CFRP strain increased at a constant rate until sudden delamination of the CFRP sheet took place at a strain value of 2592 $\mu\epsilon$. The CFRP strain in specimen ND-NS-EB+MA increased at a constant rate until it reached a strain value of 2256 $\mu\epsilon$ at a load level of 100 kN. Then, the CFRP strain increased at a higher rate due to development of new cracks and/or an increase in the width of existing cracks.

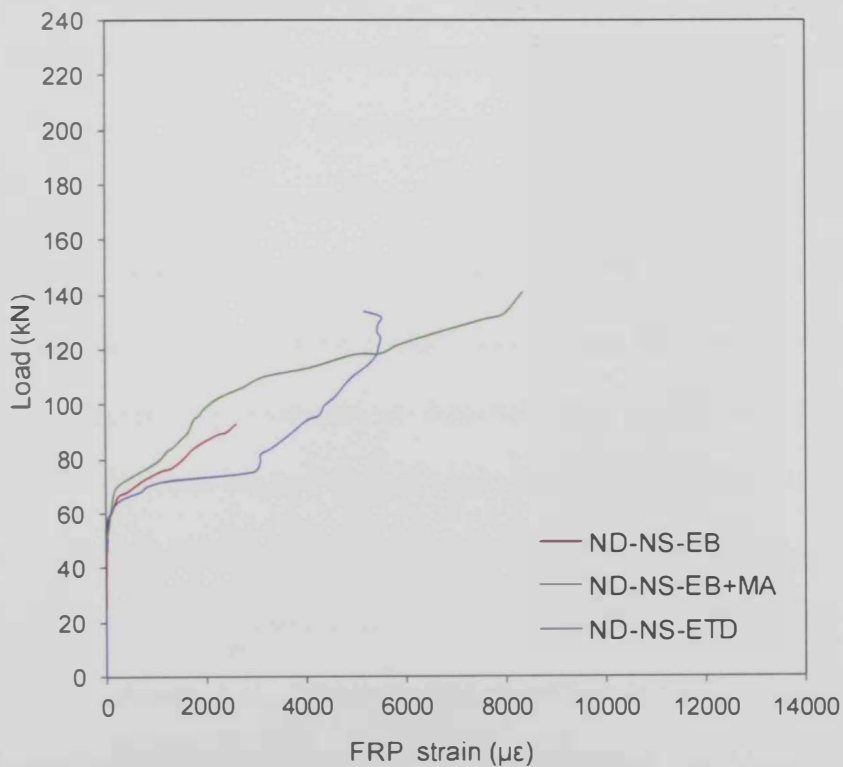


Figure 4.8: Load-FRP strain relationships for specimens of group [A]

This is consistent with the diagonal tensile displacement response of specimen ND-NS-EB+MA depicted in Figure 4.6. In the last stage, the CFRP strain continued to increase until the specimen reached its peak load at a CFRP strain value of 8334 $\mu\epsilon$. The inclusion of the MA in the CFRP system increased the effective CFRP strain by approximately three folds.

4.2.2 Group B

4.2.2.1 Specimens without initial shear damage

4.2.2.1.1 Failure mode

Typical modes of failure for specimens of group [B] that were not damaged prior to retrofitting and/or testing are shown in Figure 4.9 through Figure 4.12. Specimen ND-S1-NR experienced a classical shear mode of failure represented by formation of a band of diagonal shear cracks in the shear span as shown in Figure 4.9. Subsequently, yielding of stirrups occurred, followed by loss of the shear integrity. Specimen ND-S1-NR failed in a diagonal tension shear mode of failure. Specimen ND-S1-EB failed due to formation of diagonal shear cracks in the shear span followed by yielding of stirrups then sudden delamination of the CFRP sheets as shown in Figure 4.10. Specimen ND-S1-EB+MA failed by crushing of the diagonal concrete struts (web-crushing shear mode of failure). This was preceded by formation of diagonal shear cracks and yielding of stirrups. The specimen reached its peak load without delamination of the CFRP sheets. In the post-peak stage, pull-out of the MA system and peeling-off of the CFRP sheets took place. The crushed concrete was adhered to the CFRP sheets as shown in Figure 4.11. Specimen ND-S1-ETD exhibited diagonal shear cracks in the shear span followed by yielding of stirrups. The specimen failed by crushing of the concrete struts in a web-crushing shear mode of failure as

shown in Figure 4.12. Longitudinal splitting cracks running parallel to the compression steel reinforcement were observed at the peak load on the top surface of the flange in specimens ND-S1-EB+MA and ND-S1-ETD as shown in Figures 4.11 and 4.12, respectively. The longitudinal splitting cracks indicated that these two specimens were over-strengthened for shear.

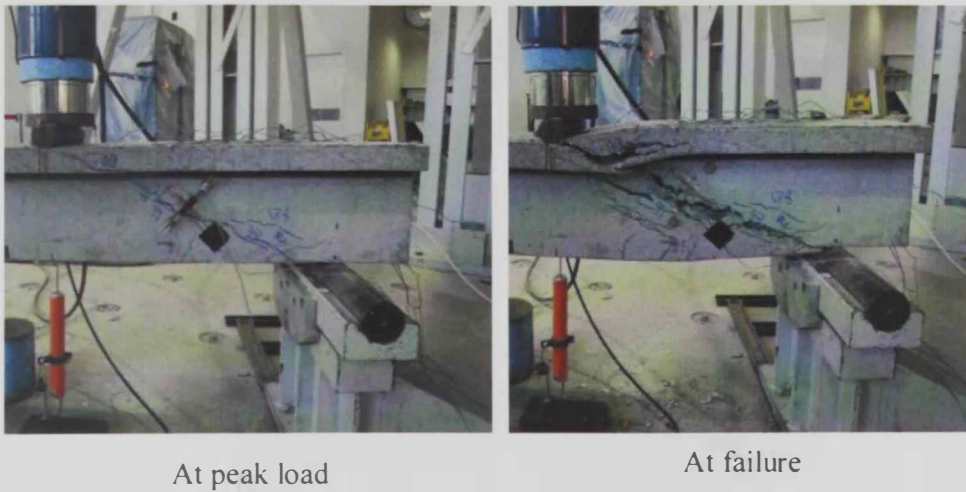


Figure 4.9: Failure mode of specimen ND-S1-NR

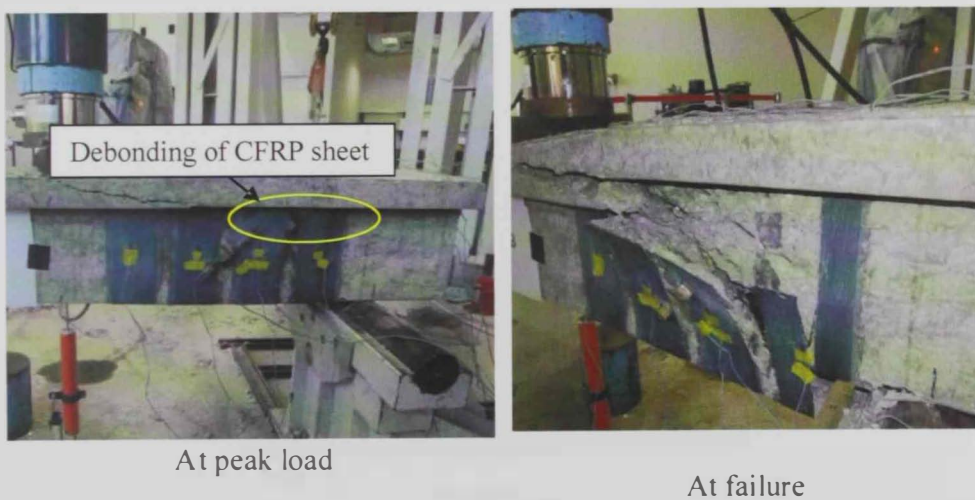


Figure 4.10: Failure mode of specimen ND-S1-EB



At peak load



At failure
(Side view)



At failure
(Top view)

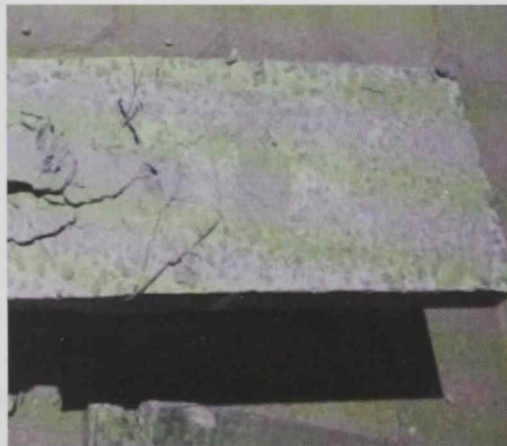
Figure 4.11: Failure mode of specimen ND-SI-EB+MA



At peak load



At failure
(Front view)



At failure
(Top view)

Figure 4.12: Failure mode of specimen ND-S1-ETD

4.2.2.1.2 Shear capacity

Results of specimens of group [B] that were not damaged prior to strengthening are given in Table 4.2. The unstrengthened control specimen ND-S1-NR recorded a peak load of 137 kN which corresponded to a shear resistance of 109.6 kN. The EB-CFRP shear strengthening system without the MA resulted in a 19% increase in the shear resistance. This reduced shear strength gain can be attributed to the premature debonding of the CFRP sheets. The integration of the MA in the EB-CFRP system prevented the premature delamination of CFRP and allowed the specimen to develop a higher shear resistance. The shear strength of specimen ND-S1-EB+MA was 36% higher than of the control specimen ND-S1-NR. The ETD-GFRP system resulted in a 40% gain in the shear resistance. The enhancement in the shear resistance provided by the ETD-GFRP system was comparable to that provided by the EB-CFRP system integrated with the MA.

Table 4.2: Test results for the non-damaged specimens of group [B].

Group	Specimen	Peak load P_{max} (kN)	Shear resistance ^a V_{max} (kN)	FRP shear resistance ^b $V_{f,exp}$ (kN)	Shear strength gain (%)	Effective FRP strain ϵ_{fe} ($\mu\epsilon$)
[B]	ND-S1-NR	137	109.6	-	-	-
	ND-S1-EB	163	130.4	20.8	19	2552
	ND-S1-EB+MA	186	148.8	39.2	36	7899
	ND-S1-ETD	192	153.6	44.0	40	13721

^a $V_{max} = 0.8P_{max}$

^b With respect to the control unstrengthened specimen ND-S1-NR

4.2.2.1.3 Deflection response

The load-deflection curves of the specimens of group [B] that were not damaged prior to strengthening and/or testing are illustrated in Figure 4.13.

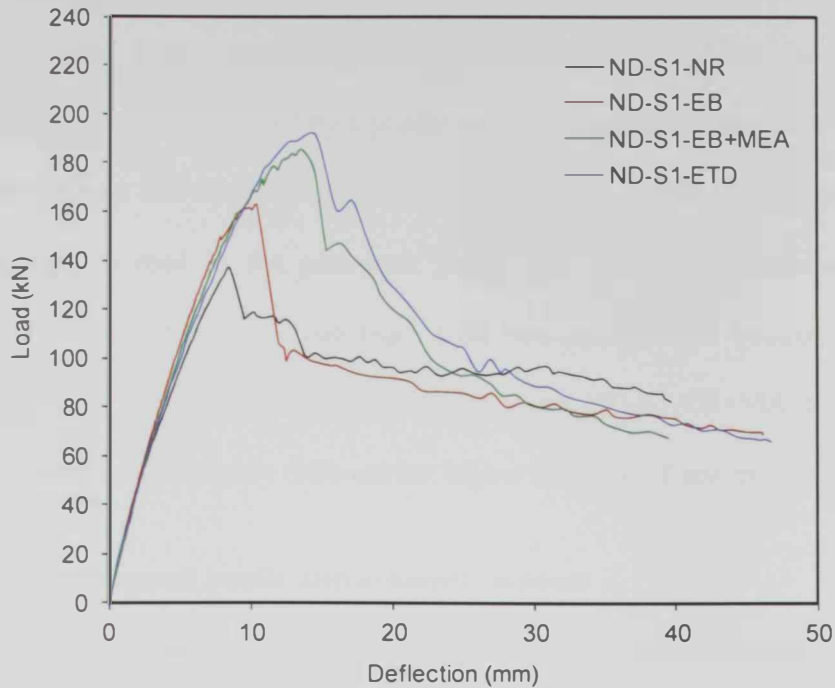


Figure 4.13: Load-deflection curves for the non-damaged specimens of group [B]

All specimens featured a linear deflection response up to initiation of shear cracks at approximately 60 kN followed by a quasi-linear load-deflection response till the peak-load. The strengthened specimens had higher stiffnesses compared to that of the non-strengthened control specimen ND-S1-NR. After crack initiation, a reduction in stiffness manifested by a higher rate of increase in the deflection was noticed for all specimens. The unstrengthened specimen ND-S1-NR reached its peak load at a deflection of 8.4 mm where a sudden drop in load took place, followed by a sudden increase in deflection, another drop in load, then a continuous increase in deflection without an increase in load. The strengthened specimens experienced a further reduction in stiffness after yielding of stirrups that took place at approximately 140 kN. The strengthened specimens ND-S1-EB, ND-NS-EB+MA, and ND-NS-ETD

reached their peak loads at deflection values of 10.3, 13.5 and 14.5, respectively. When specimen ND-S1-EB reached its peak load, a sudden drop in load took place followed by a plastic deflection response. Specimens ND-S1-EB+MA and ND-S1-ETD exhibited an increase in deflection with a gradual reduction in load in the post-peak stage. The strengthened specimens had higher energy absorption than that of the non-strengthened control specimen ND-S1-NR. The energy absorption of specimens ND-S1-EB+MA and ND-S1-ETD were insignificantly different but higher than that of specimen ND-S1-EB.

4.2.2.1.4 Diagonal tensile displacement response

Figure 4.14 shows the relationship between the load and diagonal tensile displacement for specimens of group [B] that were not damaged prior to strengthening and/or testing. The diagonal tensile displacement response of specimen ND-S1-ETD was not recorded due to malfunction of the clip gauge. All specimens exhibited no diagonal tensile displacement prior to initiation of shear cracks that took place at a load value of 60 kN, on average. Shear strengthening insignificantly increased the cracking load. In the post-cracking stage, the diagonal tensile displacement increased almost at a constant rate. Shear strengthening remarkably reduced the rate of increase of the diagonal displacement across cracks. Specimens ND-S1-EB and ND-S1-EB+MA exhibited almost similar rate of increase of the diagonal displacement across cracks. This indicated that although the MA system prevented the premature delamination of the CFRP sheets, and hence increased the shear strength gain, it had no effect on the rate of increase of the diagonal tensile displacement response in the post-cracking stage.

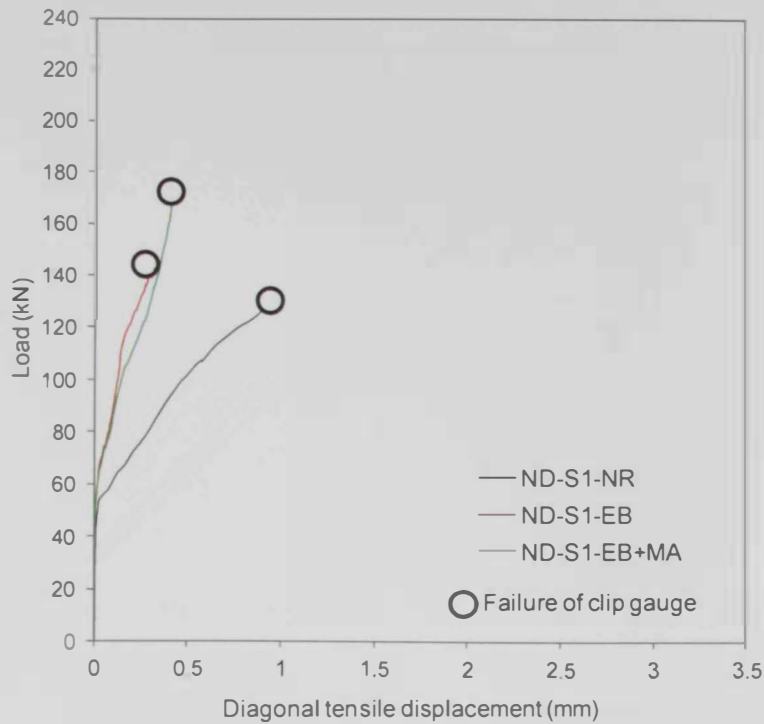


Figure 4.14: Load-diagonal tensile displacement curves for the non-damaged specimens of group [B].

4.2.2.1.5 Flexural steel strain response

The longitudinal tensile steel strain responses for specimens of group [B] that were not damaged prior to strengthening and/or testing are shown in Figure 4.15. The longitudinal tensile steel response for specimens ND-S1-EB+MA and ND-S1-ETD were not recorded due to malfunction of the strain gauges. The specimens experienced flexural cracks at approximately 15 kN. These cracks were not visible during testing. Following cracking, the longitudinal steel strain increased at a constant rate until the peak load was reached. The rate of the steel strain increase for the un-strengthened and strengthened specimens was insignificantly different. Specimens ND-S1-NR and ND-S1-EB reached their peak loads at longitudinal steel strain values of 1552 and 2200 $\mu\epsilon$, respectively. This confirmed that the specimens failed in a pure shear mode of failure without yielding of the tensile steel reinforcement.

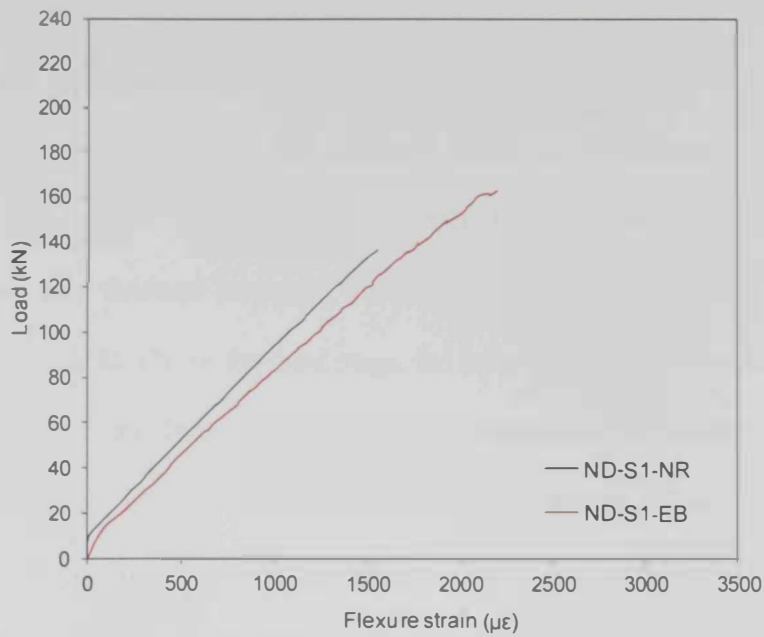


Figure 4.15: Load-flexural strain relationship for the non-damaged specimens of group [B]

4.2.2.1.6 Stirrups strain response

The stirrups strain responses for the specimens of group [B] that were not damaged prior to strengthening and/or testing are shown in Figure 4.16.

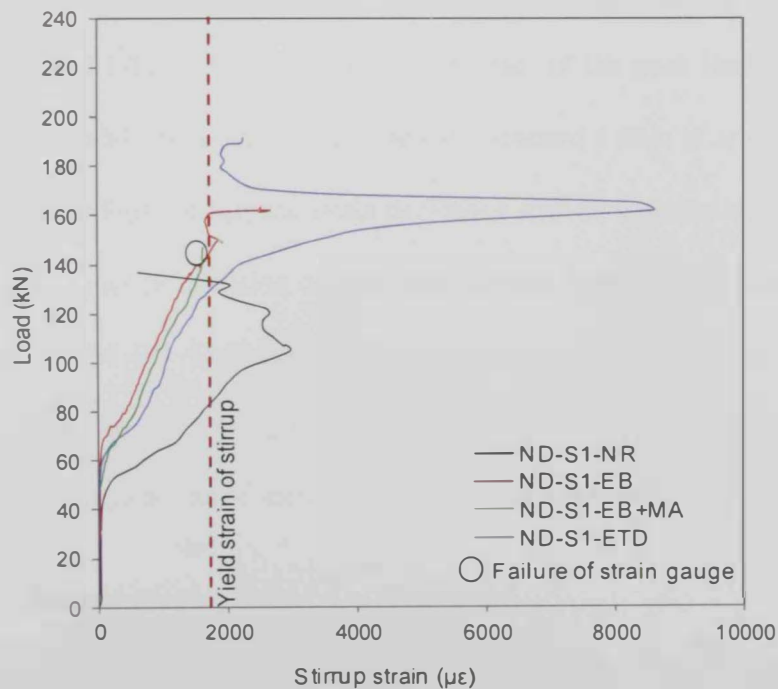


Figure 4.16: Load-stirrups strain curves for the non-damaged specimens of group [B]

The stirrups strain response featured three or four phases during loading. In the first stage, the stirrups were not strained prior to initiation of the shear cracks. For specimen ND-S1-NR, the stirrups started to contribute to the shear resistance at a load value of approximately 50 kN. Then, the stirrups strain increased at a constant rate until yielding of stirrups took place at a load of approximately 80 kN. In the third stage, the stirrups strain continued to increase but at a higher rate. In the fourth stage, the stirrups strain decreased as the load progressed possibly due to a local slippage/debonding of the stirrups. The stirrups in the strengthened specimens started to contribute to the shear resistance at 60 kN, on average. In the post-cracking stage, the stirrups strain increased at a much lower rate relative to that of specimen ND-S1-NR. The reduced rate of strain increase in the stirrups delayed their yielding and hence increased the shear resistance of the strengthened specimens. All strengthened specimens experienced similar stirrups strain response in the second stage till yielding of stirrups at 130 kN, on average. Following yielding of stirrups, specimen ND-S1-EB exhibited a plastic response till the peak load. Specimen ND-S1-ETD exhibited a plastic response till it reached a strain of approximately $8619 \mu\epsilon$. In the fourth stage, the strain decreased with an increase in load due to local slippage and/or initiation of new shear cracks at a different location. For specimen ND-S1-EB+MA, failure of strain gauge took place at the onset of yielding. Among the strengthened specimens, the specimen ND-S1-ETD exhibited the highest rate of increase in the stirrups strain after cracking.

4.2.2.1.7 FRP strain response

The FRP strain response for the specimens of group [B] that were not damaged prior to strengthening and/or testing are shown in Figure 4.17. The effective

FRP strain values are reported in Table 4.2. It should be noted that the maximum measured FRP strain is not necessarily the maximum absolute FRP strain experienced by the specimen.

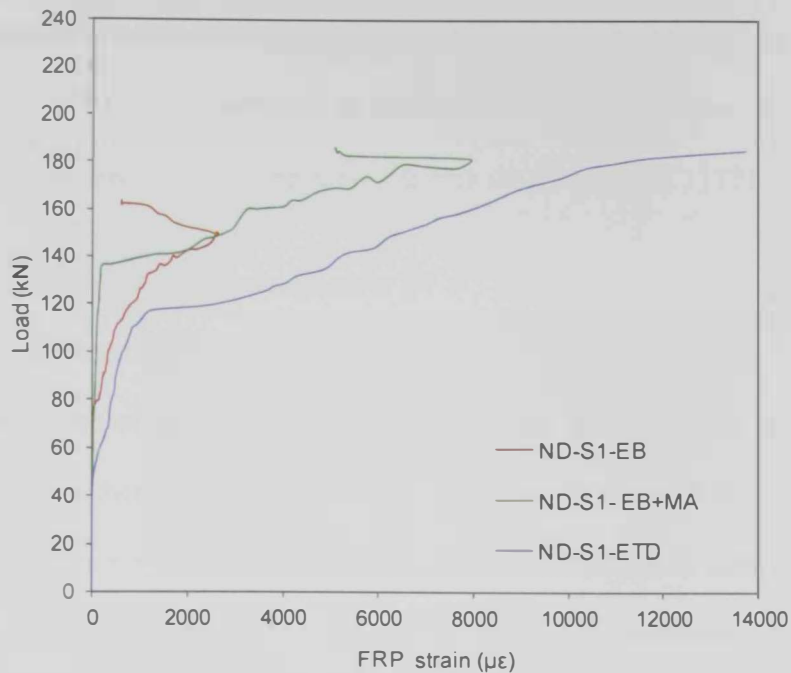


Figure 4.17: Load-FRP strain relationships for the non-damaged specimens of group [B]

The CFRP strain response for specimens ND-S1-EB and ND-S1-EB+MA featured four phases. The CFRP sheets were not strained prior to initiation of cracks. Following cracking, the CFRP strain increased at almost a constant rate till yielding of stirrups at approximately 140 kN. In the third stage, the CFRP strain increased at a higher rate until specimens ND-S1-EB and ND-S1-EB+MA reached effective CFRP strains of 2552 and 7899 $\mu\epsilon$, respectively. The MA adopted in specimen ND-S1-EB+MA resulted in a three-fold increase in the effective CFRP strain relative to that of specimen ND-S1-EB. This demonstrates the effectiveness of the MA system. In the fourth stage, the CFRP strain decreased as the load progressed which could be possibly due to local debonding of the CFRP sheets or development of new cracks at a different

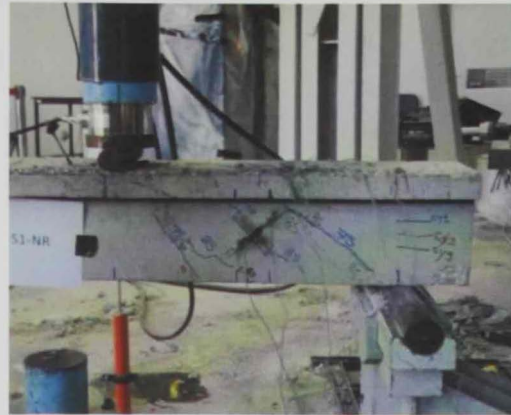
location. Specimen ND-S1-ETD featured a tri-linear GFRP strain response. In the first stage, the GFRP rebars remained unstrained till initiation of shear cracks at approximately 60 kN. In the second stage, the GFRP strain increased at a constant rate till yielding of stirrups at approximately 120 kN. In the third stage, the GFRP strain continued to increase but at a much higher rate until the specimen reached its peak load at an effective GFRP strain of 13721 $\mu\epsilon$.

4.2.2.2 Specimens with damage state D1

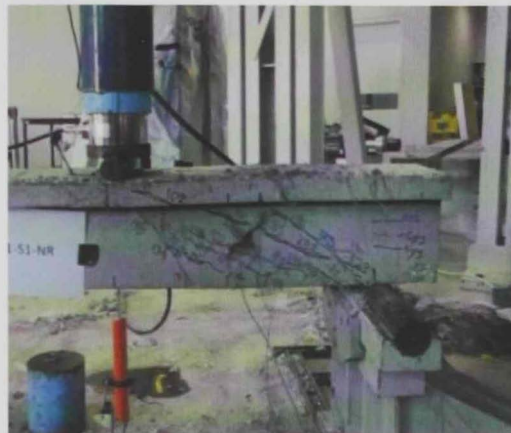
4.2.2.2.1 Failure mode

Typical modes of failure for specimens of group [B] that were pre-cracked prior to strengthening and/or testing are shown in Figure 4.18 through Figure 4.21. All specimens of this subgroup were pre-subjected to three cycles of loading then unloading. The initial cycles of loading-unloading resulted in formation of multiple shear cracks in the shear span. Specimen D1-S1-NR was retested to failure without retrofitting. The remaining pre-cracked specimens were retrofitted then retested to failure. Specimen ND-S1-NR failed in a diagonal tension shear mode of failure as shown in Figure 4.18. Specimen D1-S1-EB failed due to formation of diagonal shear cracks in the shear span succeeded by yielding of stirrups then an abrupt detachment of the CFRP sheets as shown in Figure 4.19. Specimen D1-S1-EB+MA failed due to crushing of the diagonal concrete struts followed by pull-out of the MA system and delamination of the CFRP sheets in the post-peak stage with crushed concrete adhered to them as shown in Figure 4.20. Crushing of the concrete struts in specimen D1-S1-EB+MA was preceded by formation of diagonal shear cracks and yielding of the stirrups. Specimen ND-S1-ETD exhibited diagonal shear cracks in the shear span followed by yielding of stirrups. The specimen failed

in a diagonal tension shear mode of failure as shown in Figure 4.21. In the post-peak load stage, significant parts of the concrete cover separated from the bottom soffit of the beam as shown in Figure 4.21. No rupture in the GFRP bars or in the CFRP sheets occurred in any of the strengthened specimens.



After initial shear damage D1



At peak load

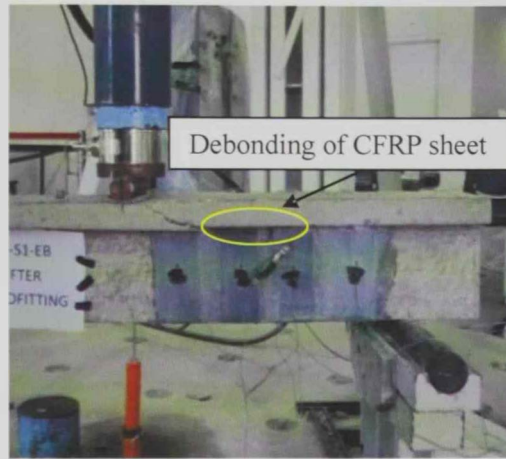


At failure

Figure 4.18: Failure mode of specimen D1-S1-NR



After initial shear damage D1



At peak load



At failure

Figure 4.19: Failure mode of specimen D1-S1-EB



After initial shear damage D1

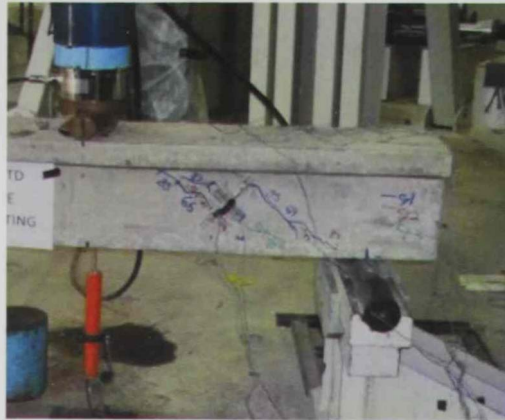


At peak load



At failure

Figure 4.20: Failure mode of specimen D1-S1-EB+MA



After initial shear damage D1



At peak load



At failure

Figure 4.21: Failure mode of specimen D1-S1-ETD

4.2.2.2.2 Shear capacity

Results of specimens of group [B] that were pre-cracked prior to strengthening and/or testing are shown in Table 4.3.

Table 4.3: Test results for specimens of group [B] with damage state D1

Group	Specimen	Peak load P_{max} (kN)	Shear resistance ^a V_{max} (kN)	FRP shear resistance ^b $V_{f,exp}$ (kN)	Shear strength gain (%)	Effective FRP strain ϵ_{fe} ($\mu\epsilon$)
[B]	D1-S1-NR	140	112.0	-	-	-
	D1-S1-EB	155	124.0	12.0	11	4312
	D1-S1-EB+MA	178	142.4	30.4	27	4808
	D1-S1-ETD	155	124.0	12.0	11	4818

^a $V_{max} = 0.8P_{max}$

^b With respect to the control unstrengthened specimen D1-S1-NR

Specimen D1-S1-NR recorded a peak load of 140 kN which corresponded to a shear resistance of 112 kN. The EB-CFRP shear strengthening system without the MA resulted in only 11% increase in the shear resistance. The integration of the MA in the EB-CFRP system prevented the early detachment of the CFRP and allowed the specimen to develop a higher shear resistance. The shear strength of specimen D1-S1-EB+MA was 27% higher than that of the control specimen D1-S1-NR. The ETD-GFRP system resulted in an 11% gain in the shear resistance.

4.2.2.2.3 Deflection response

The load-deflection curves for specimens of group [B] that were pre-cracked prior to strengthening and/or testing are illustrated in Figure 4.22. The initial three cycles of loading-unloading inducing cracking resulted in a permanent deflection of approximately 2.9 mm which shifted the entire load-deflection response. The non-strengthened pre-cracked specimen D1-S1-NR when loaded back to failure featured a quasi-linear deflection response up to yielding of stirrups at approximately 120 kN followed by a sudden increase in deflection.

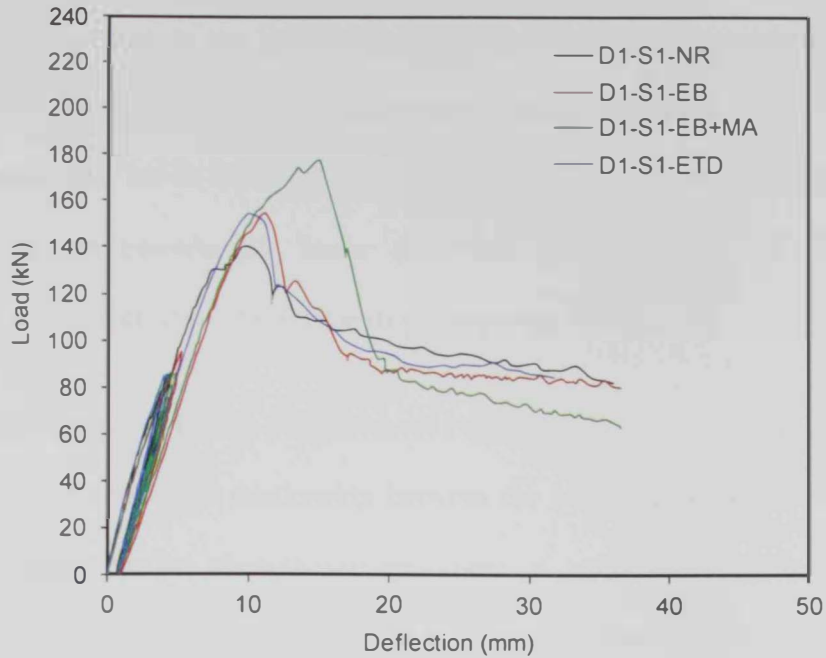


Figure 4.22: Load-deflection curves for specimens of group [B] with damage state D1.

As the load progressed, the deflection continued to increase until the specimen reached its peak load at a deflection of 9.61 mm. After retrofitting, specimens D1-S1-EB and D1-S1-ETD featured a quasi-linear deflection response until yielding of steel stirrups took place at a load value of approximately 120 kN. Then, the deflection increased at a slightly higher rate until the specimens reached their peak loads at deflection values of 11.2 and 9.7 mm for specimens D1-S1-EB and D1-S1-ETD, respectively. Following retrofitting, specimen D1-S1-EB+MA featured a quasi-linear deflection response up to yielding of stirrups at approximately 160 kN. Subsequently, the deflection increased at a higher rate till the peak load which took place at a deflection of 15 mm. The specimen D1-S1-EB+MA exhibited a sudden drop in the load when it reached its peak load followed by a plastic deflection response. Specimens D1-S1-NR,

D1-S1-EB and D1-S1-ETD exhibited an increase in deflection with a gradual reduction in load in the post-peak stage after reaching their ultimate shear strengths followed by a plastic load-deflection behavior. The energy absorption of specimens D1-S1-NR, D1-S1-EB and D1-S1-ETD was insignificantly different but considerably lower than that of specimen D1-S1-EB+MA strengthened with the EB-CFRP system integrated with the MA.

4.2.2.2.4 Diagonal tensile displacement response

Figure 4.23 shows the relationship between the load and the diagonal tensile displacement for the strengthened specimens of group [B] with the damage state D1 recorded during the final loading test to failure after the initial three cycles of loading-unloading. All specimens exhibited almost a bi-linear response started with a prompt increase in the diagonal deformation across cracks since all specimens were already cracked. Prior to yielding of stirrups, the diagonal displacement across cracks increased almost at a constant rate. After yielding of stirrups, all specimens exhibited a higher rate of increase in the diagonal displacement across cracks. Stirrups of specimens D1-S1-EB and D1-S1-ETD yielded at approximately 120 kN with a corresponding diagonal displacement across cracks of 0.44 mm. At the peak load, the diagonal displacements across cracks for specimens D1-S1-EB and D1-S1-ETD were 1 and 1.4 mm, respectively. The rate of increase of the diagonal displacement across cracks for both specimens was insignificantly different. Specimen D1-S1-EB+MA exhibited a lower rate of increase in the diagonal displacement across cracks compared to the rate of other retrofitted specimens with the damage state D1. The stirrups of specimen D1-S1-EB+MA strengthened with the EB-CFRP system integrated with the MA yielded at approximately 160 kN

with a corresponding diagonal displacement across cracks of 0.38 mm. At the peak load, this specimen reached a diagonal deformation across cracks of 0.84 mm. This demonstrates the importance of the MA in restricting and controlling shear deformation and crack propagation. The diagonal displacement across cracks for specimen D1-S1-NR was not recorded due to malfunction of the clip gauge.

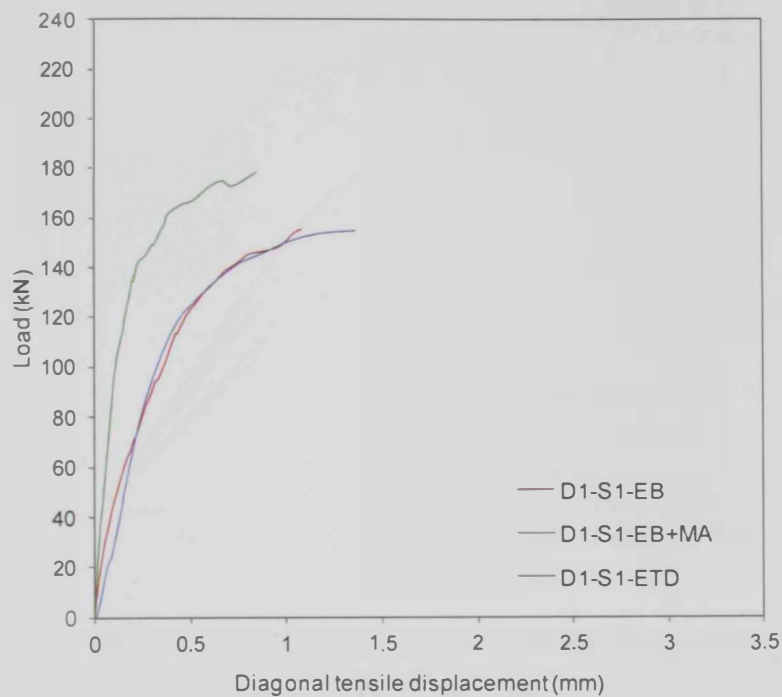


Figure 4.23: Load – diagonal tensile displacement response for specimens of group [B] with damage state D I

4.2.2.2.5 Flexural steel strain response

The longitudinal tensile steel strain responses for specimens of group [B] with damage state D I are shown in Figure 4.24. During the initial three cycles of loading-unloading, the specimens experienced flexural cracks at approximately 15 kN. These cracks were not visible during testing. In the final loading test to failure, the longitudinal steel strain increased at a constant rate till the peak

load. Specimens D1-S1-NR, D1-S1-EB and D1-S1-EB+MA reached their peak loads at strain values of 1529, 2385 and 2251 $\mu\epsilon$, respectively. This confirmed that the specimens failed in a pure shear mode of failure without yielding of the tensile steel reinforcement. The longitudinal tensile steel response for specimen D1-S1-ETD was not recorded due to malfunction of the strain gauge.

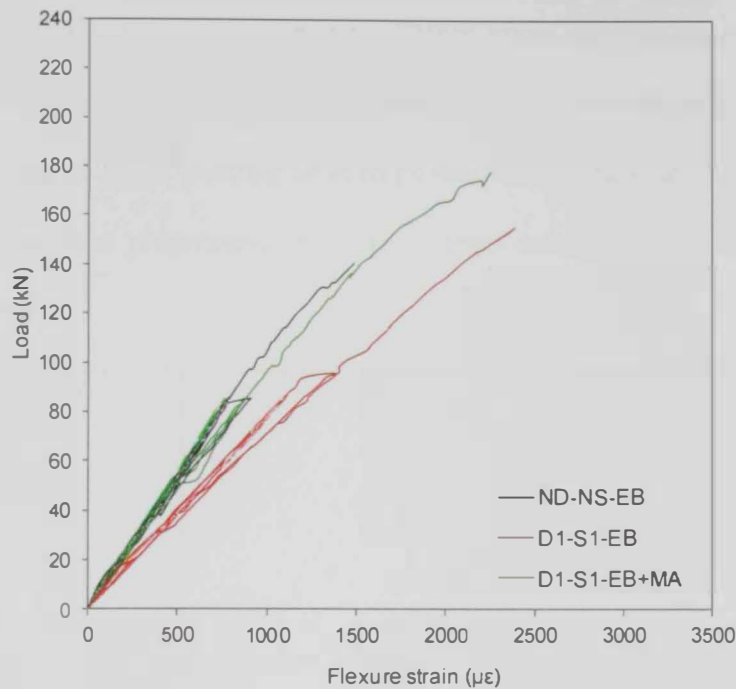


Figure 4.24: Load-flexural strain relationship for specimens group [B] with damage state D1

4.2.2.2.6 Stirrups strain response

The stirrups strain responses for the specimens of group [B] with the shear damage state D1 recorded in the final loading test to failure after the initial three cycles of loading-unloading are shown in Figure 4.25. The stirrups started to have prompt contribution to the shear resistance since the specimens were already cracked. The stirrups strain increased at a constant rate till yielding of stirrups. The EB-CFRP system reduced the rate of increase of the stirrups strain in the pre-yield stage relative to that of specimen D1-S1-NR. The ETD system

had no effect on the rate of increase of the stirrups strain compared to that of specimen D1-S1-NR. Specimens D1-S1-NR and D1-S1-ETD featured a linear stirrups strain response until yielding of stirrups that took place at load values of approximately 120 and 110 kN, respectively followed by a plastic strain response. Specimen D1-S1-EB featured a linear stirrups strain response until yielding of stirrups occurred, then no further strain increase was recorded due to malfunction of the strain gauge. Specimen D1-S1-EB+MA exhibited a linear strain response up to yielding of stirrups that took place at approximately 160 kN. As the load progressed, the stirrups strain continued to increase but at a higher rate.

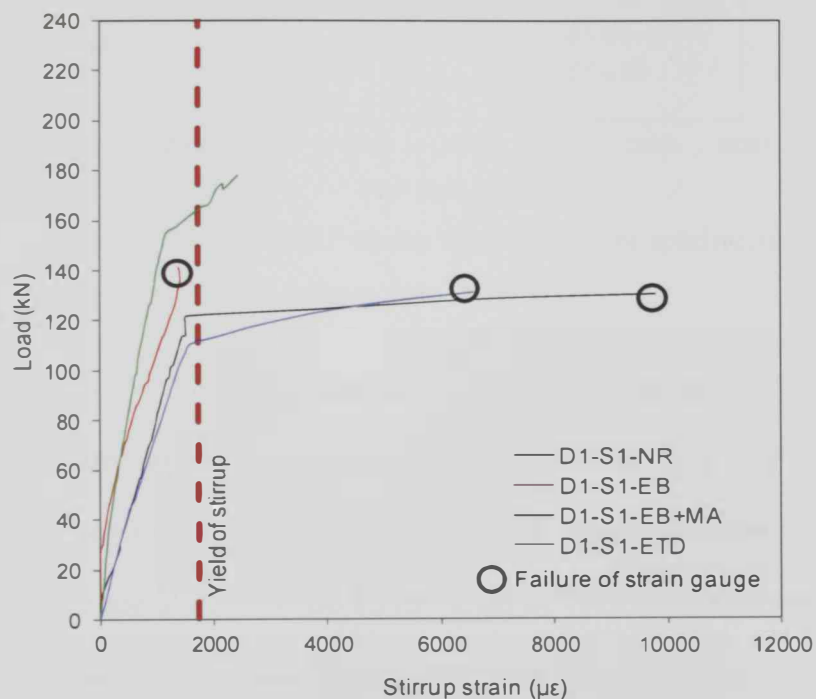


Figure 4.25: Load- stirrups strains curves for specimens of group [B] with damage state D1.

4.2.2.2.7 FRP strain response

The FRP strain responses for specimens of group [B] with the damage state D1 recorded in the final shear test to failure after retrofitting are shown in Figure

4.26. The effective FRP strain values are reported in Table 4.3. It should be noted that the maximum measured FRP strain is not necessarily the maximum absolute FRP strain experienced by the specimen.

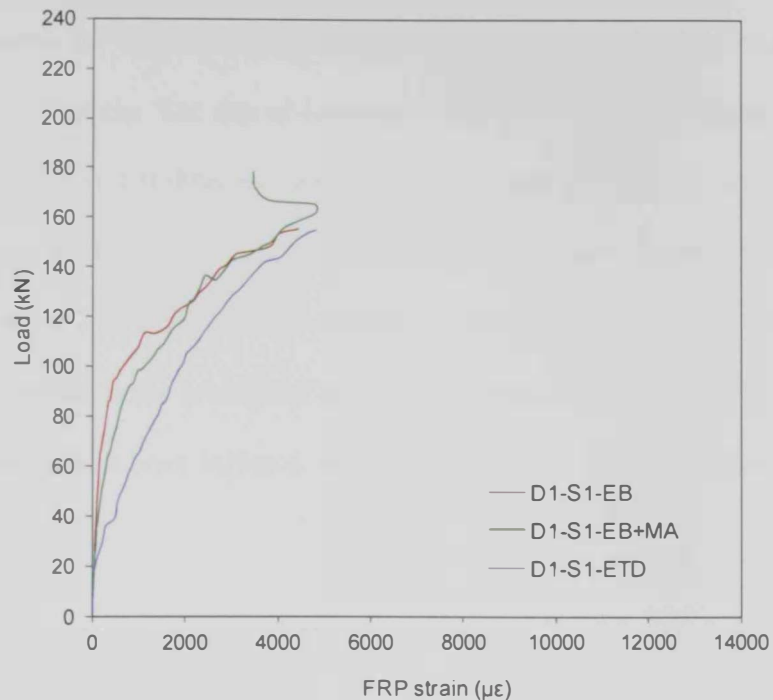


Figure 4.26: Load-FRP strains relationships for specimens of group [B] with damage state D1.

Specimen D1-S1-EB exhibited a gradual rate of increase in the CFRP strain till yielding of stirrups at approximately 120 kN followed by a higher rate of increase in the CFRP strain till it reached the peak load where debonding of the CFRP took place at an effective CFRP strain of 4312 $\mu\epsilon$. Specimen D1-S1-EB+MA experienced a quasi-linear CFRP strain response due to progressive development of multiple shear cracks till yielding of stirrups that took place at approximately 160 kN with a corresponding effective CFRP strain of 4808 $\mu\epsilon$. Following yielding of stirrups, the CFRP strain decreased as the load progressed due to possible local debonding or development of new cracks at a different location. Specimen D1-S1-ETD featured a gradual increase in the

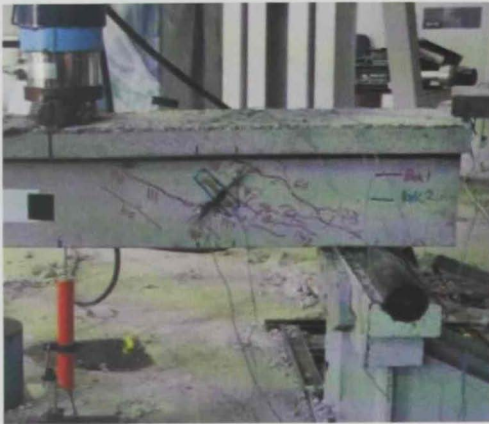
GFRP strain till yielding of stirrups at approximately 110 kN followed by a slightly higher rate of increase in the GFRP strain until the specimen reached its peak load at an effective GFRP strain of 4818 $\mu\epsilon$. Among the strengthened specimens, the specimen D1-S1-ETD experienced the highest rate of increase in the FRP strain. The rate of increase of the FRP strain for specimens D1-S1-EB and D1-S1-EB+MA was almost the same and significantly lower than that of specimen D1-S1-ETD. The higher rate of increase in the FRP strain for specimen D1-S1-ETD could be due to the reduced cross section at the locations of the vertical holes pre-drilled for the installation of the GFRP rebars. Drilling the holes could have initiated internal microcracks thus increasing the GFRP strains.

4.2.2.3 Specimens with the damage state D2

4.2.2.3.1 Failure mode

Typical modes of failure for specimens of group [B] that were pre-failed prior to retrofitting and/or testing are shown in Figure 4.27 through Figure 4.30. The control specimen D2-S1-NR was loaded up to its first peak load then unloaded. After that, the specimen was re-tested again for the second time up to failure. The other three specimens were loaded up to their first peak loads then unloaded. The specimens were then retrofitted with EB-CFRP system without the MA, EB-CFRP system integrated with the MA, and ETD-GFRP system. Specimen D2-S1-NR experienced a classical shear mode of failure represented by formation of a band of diagonal shear cracks in the shear span as shown in Figure 4.27. The specimen D2-S1-EB retrofitted with the EB-CFRP system without the MA failed by debonding of the CFRP sheets as shown in Figure 4.28, preceded by abrupt opening of existing diagonal shear cracks in the shear

span and yielding of stirrups. Specimen EB-CFRP+MA reached its peak load without debonding of the CFRP sheets. The specimen failed by crushing of the diagonal concrete struts (i.e. web-crushing shear mode of failure). This was preceded by opening of existing shear cracks and yielding of stirrups. In the post-peak stage, pull-out of the MA system and peeling-off of the CFRP sheets took place as shown in Figure 4.29. Specimen D2-S1-ETD failed in a diagonal tension shear mode of failure as shown in Figure 4.30. This was preceded by opening of existing diagonal shear cracks in the shear span and yielding of stirrups. No rupture of GFRP rebars or CFRP sheets occurred at failure in any of the retrofitted specimens.



At peak load (first shear test)

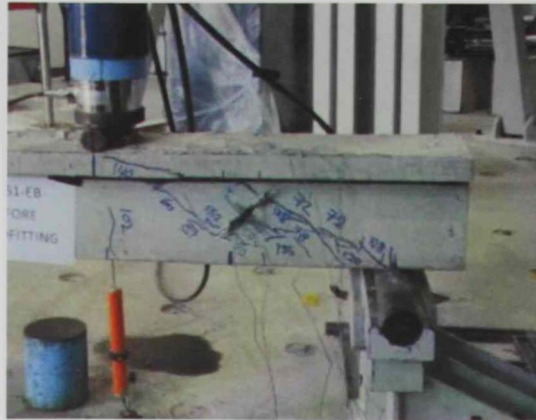


At peak load (second shear test)



At failure (second shear test)

Figure 4.27: Failure mode of specimen D2-S1-NR



At peak load
(first shear test)



At peak load
(second shear test)



At failure
(second shear test)

Figure 4.28: Failure mode of specimen D2-S1-EB



At peak load
(first shear test)

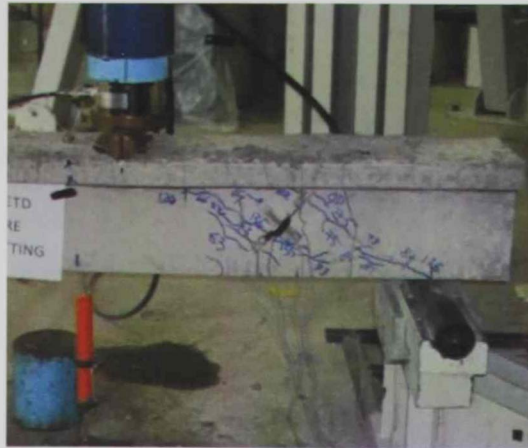


At peak load
(second shear test)

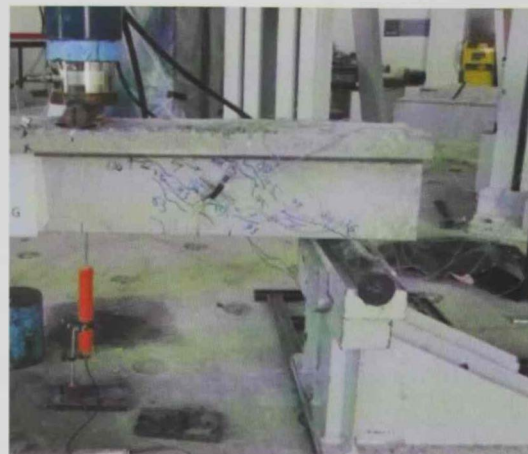


At failure
(second shear test)

Figure 4.29: Failure mode of specimen D2-S1-EB+MA



At peak load
(first shear test)



At peak load
(second shear test)



At peak load
(second shear test)

Figure 4.30: Failure mode of specimen D2-S1-ETD

4.2.2.3.2 Shear capacity

Results of specimens of group [B] that were pre-failed prior to retrofitting and/or testing are given in Table 4.4.

Table 4.4: Test results for specimens of group [B] with damage state D2

Group	Damage state	Specimen	First shear test (original loads)		Second shear test (new loads)		$V'_{f,exp}$ ^b (kN)	V'_{neu} / V'_{org}	Effective FRP strain ϵ_{fe} ($\mu\epsilon$)
			P_{org} (kN)	V'_{org} (kN) ^a	P_{neu} (kN)	V'_{neu} (kN) ^a			
[B]	D2	D2-S1-NR	144	115.2	130	104.0	-	0.90	-
		D2-S1-EB	137	109.6	107	85.6	0.0	0.78	1274
		D2-S1-EB+MA	118	94.4	165	132.0	47.0	1.40	5655
		D2-S1-ETD	137	109.6	133	106.4	7.8	0.97	8359

^a $V'_{org} = 0.8P_{org}$, $V'_{neu} = 0.8P_{neu}$

^b $V'_{f,exp} = V'_{neu} - 0.9V'_{org}$, residual shear strength prior to retrofitting = $0.9V'_{org}$ based on the results of specimen D2-S1-NR

The non-retrofitted control specimen D2-S1-NR reached a peak load of 144 kN which corresponded to a shear resistance of 115.2 kN in the first shear test. In the second shear test to failure, the specimen recorded a lower peak load of 130 kN that corresponded to a shear resistance of 104 kN. This means that the non-retrofitted specimen was able to restore 90% of its original shear strength recorded in the first shear test. Specimen D2-S1-EB reached a peak load of 137 kN which corresponded to a shear resistance of 109.6 kN in the first shear test. In the second shear test to failure, the retrofitted specimen could not restore its original shear capacity and recorded a lower peak load of 107 kN that corresponded to a shear resistance of 85.6 kN. The ratio V'_{neu}/V'_{org} for specimen D2-S1-EB was only 0.78 which indicates that the specimen restored only 78% of its original shear capacity due to the premature delamination of the CFRP sheets caused by opening of existing shear cracks. Specimen D2-S1-EB+MA reached a peak load of 118 kN which corresponded to a shear resistance of 94.4 kN in the first shear test. In the second shear test to failure, the retrofitted specimen recorded a higher peak load of 165 kN that corresponded to a shear

resistance of 132 kN. The ratio V_{new}/V_{org} for specimen D2-S1-EB+MA was 1.4 which indicates that the specimen was not only able to restore its original shear capacity but also upgraded its original shear capacity by 40%. This is because of the MA system that prevented the early detachment of the CFRP sheets and controlled opening of the pre-existing shear cracks. The specimen D2-S1-ETD recorded a peak load of 137 kN which corresponded to a shear resistance of 109.6 kN in the first shear test. In the second shear test to failure, the retrofitted specimen restored 97% of its original shear capacity.

4.2.2.3.3 Deflection response

The load-deflection curves for specimens of group [B] that were pre-failed prior to retrofitting and/or testing are illustrated in Figure 4.31 through Figure 4.34.

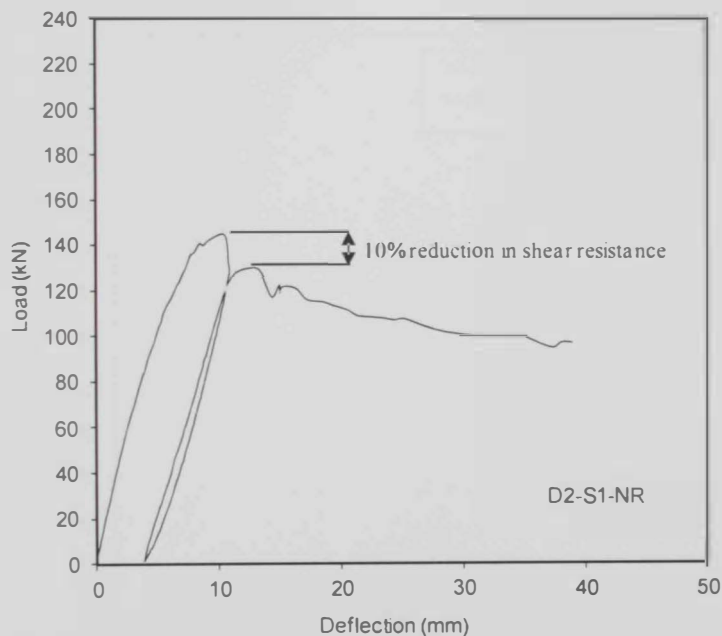


Figure 4.31: Load-deflection curves of specimen D2-S1-NR

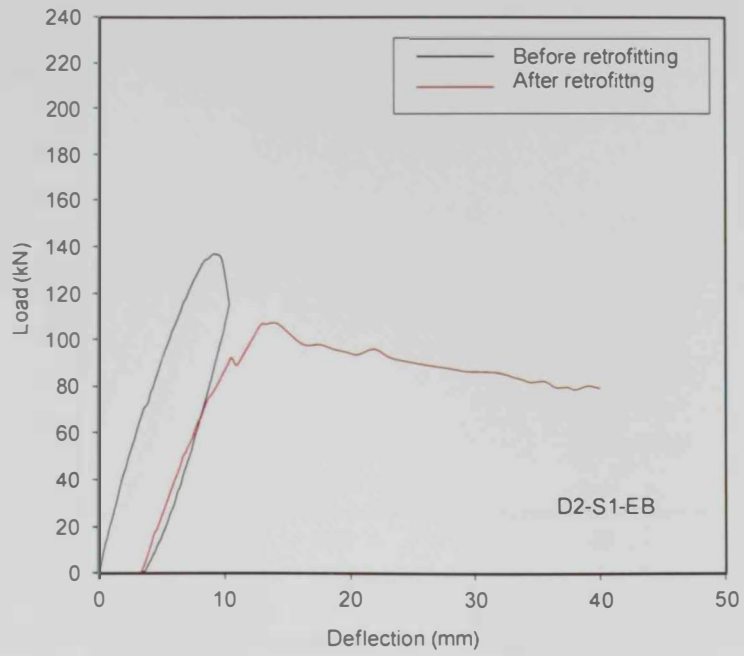


Figure 4.32: Load-deflection curves of specimen D2-S1-EB

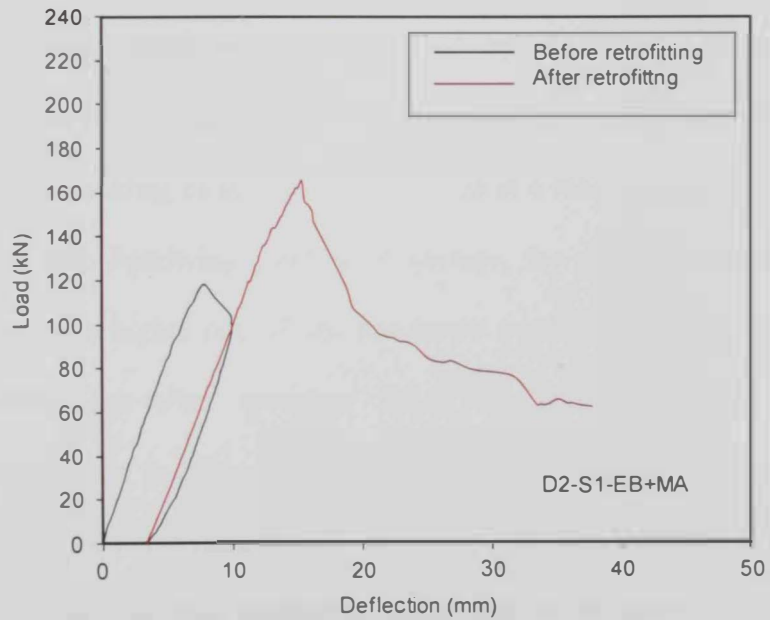


Figure 4.33: Load-deflection curves of specimen D2-S1-EB+MA

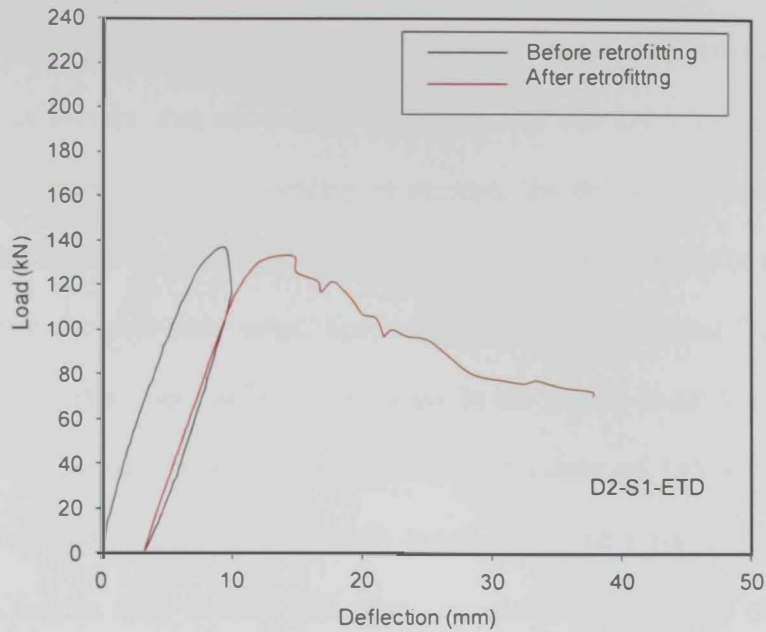


Figure 4.34: Load-deflection curves of specimen D2-S1-ETD

The initial cycle of loading to peak load-unloading resulted in a permanent deflection of 3.5 mm, on average, which shifted the load-deflection response recorded in the second shear test to failure. In the first shear test, all specimens exhibited almost a linear response up to crack initiation at a load value in the range of 50 to 60 kN. Then, the specimens exhibited a quasi-linear deflection response until yielding of stirrups that occurred at a load value in the range of 100 to 120 kN. Following yielding of stirrups, the deflection continued to increase but at a higher rate till the specimens reached their peak loads. The non-retrofitted pre-failed specimen D2-S1-NR featured almost a linear deflection response in the second shear test to failure till yielding of stirrups that took place at approximately 130 kN where a sudden increase in deflection took place. The specimen reached its peak load at the onset of yielding of stirrups. The specimen, then, exhibited a sudden drop in load, followed by a plastic deflection response. The initial shear damage D2 caused a 10% reduction in the shear resistance as shown in Figure 4.31. In the second shear

test to failure, the specimen D2-S1-EB exhibited almost a linear response till yielding of stirrups that occurred at approximately 100 kN where a decay in load took place. Following yielding of stirrups, the deflection increased at a higher rate till the peak load. The specimen featured almost a plastic deflection response in the post-peak stage. Specimens D2-S1-EB+MA and D2-S1-ETD featured almost a linear deflection response in the second shear test to failure till yielding of stirrups that took place at load values of 155 and 110 kN, respectively. Specimen D2-S1-EB+MA failed shortly after yielding of stirrups where a sudden drop in load took place. Specimen D2-S1-ETD exhibited a significant increase in deflection after yielding of stirrups. In the post-peak stage, both specimens D2-S1-EB+MA and D2-S1-ETD exhibited continuous increase in deflection with a gradual decrease in load.

4.2.2.3.4 Diagonal tensile displacement response

The relationships between the load and the diagonal displacement across cracks for the retrofitted specimens of group [B] with damage state D2 are shown in Figure 4.35 through Figure 4.37.

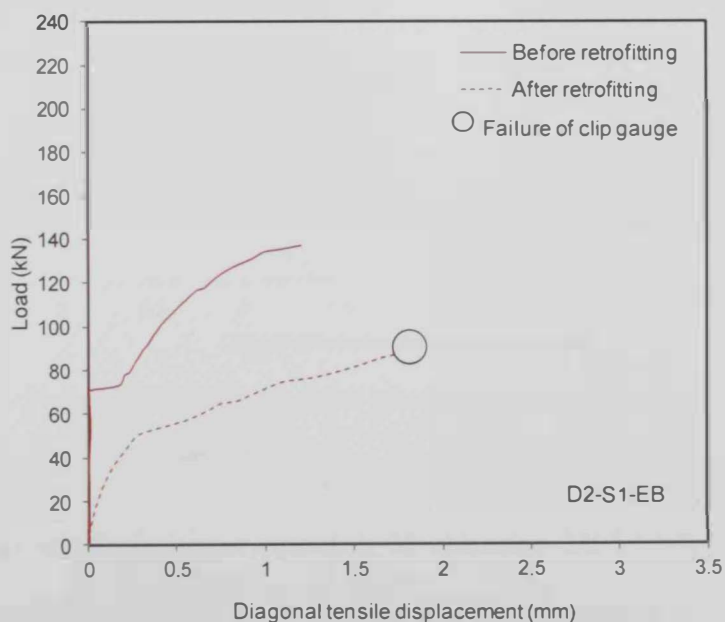


Figure 4.35: Load-diagonal tensile displacement curves for specimen D2-S1-EB

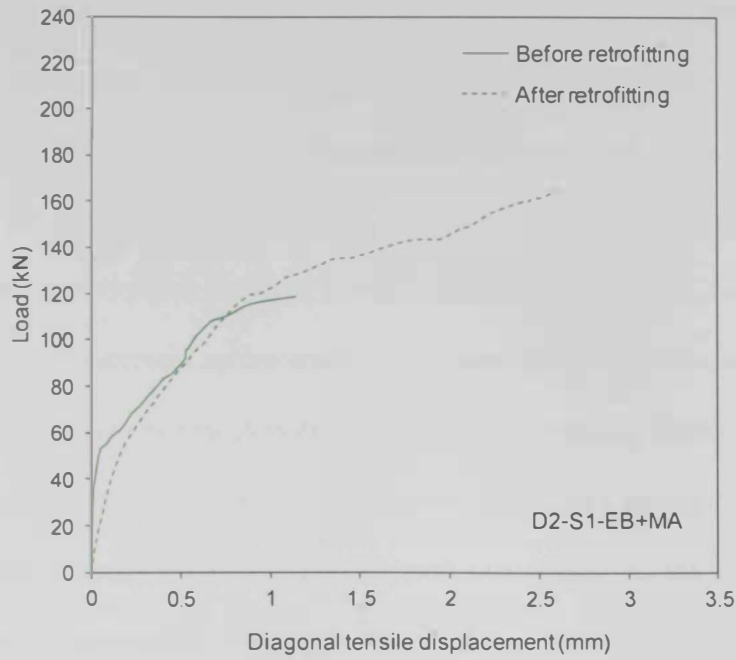


Figure 4.36: Load-diagonal tensile displacement curves for specimen D2-S1-EB+MA

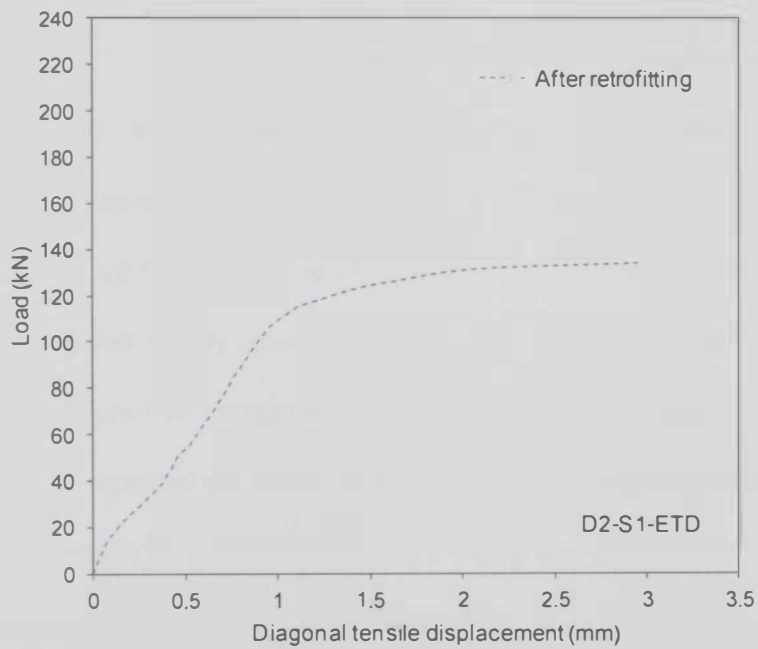


Figure 4.37: Load-diagonal tensile displacement curves for specimen D2-S1-ETD

The diagonal displacement response of specimen D2-S1-NR could not be recorded due to malfunction of the clip gauge. The response of specimen D2-

S1-EB featured three phases prior to retrofitting. In the first phase, no displacement was recorded till initiation of shear cracks at approximately 70 kN where a sudden increase in the diagonal displacement took place. In the second phase, the diagonal displacement across cracks increased at a higher rate until yielding of stirrup that occurred at approximately 100 kN with a corresponding diagonal displacement across cracks of 0.5 mm. In the third phase, the diagonal displacement across cracks continued to increase but at a higher rate until the specimen reached its peak load. After retrofitting, the diagonal displacement response of specimen D2-S1-EB featured two stages. In the first stage, the diagonal displacement across cracks increased from the beginning of the second shear test due to the pre-existence of internal cracks till it reached a load of 50 kN where opening of the pre-existing shear cracks and initial debonding of the CFRP sheets took place. In the second stage, the specimen experienced a higher rate of increase in the diagonal displacement across cracks due to progressive debonding of the CFRP sheets and widening of the pre-existing shear cracks until failure of the clip gauge took place at approximately 2 mm where no further results could be recorded. Specimen D2-S1-EB+MA featured three phases prior to retrofitting. In the first phase, no diagonal displacement values were recorded till initiation of shear cracks at approximately 55 kN. In the second stage, the specimen featured a higher rate of increase in the diagonal displacement across cracks until yielding of stirrups occurred at approximately 110 kN with a corresponding diagonal displacement across cracks of 0.75 mm. In the third stage, a plastic diagonal tensile displacement response took place. In the second shear test to failure (i.e. after retrofitting) the diagonal displacement across cracks in specimen D2-S1-EB+MA featured a quasi-linear

response till yielding of stirrups that took place at approximately 155 kN. The diagonal displacement across cracks continued to increase after yielding of stirrups till the specimen reached its peak load. The response of specimen D2-S1-ETD was not recorded prior to retrofitting due to malfunction of the clip gauge. After retrofitting, the diagonal displacement across cracks increased at almost a constant rate till yielding of stirrups that took place at approximately 110 kN with no pre-cracking stage. This rate of increase of the diagonal displacement across cracks for specimen D2-S1-ETD was higher than that of specimen D2-S1-EB+MA. Following yielding of stirrups, the specimen D2-S1-ETD experienced a plastic diagonal displacement response.

4.2.2.3.5 Flexural steel strain response

The longitudinal tensile steel strains for specimens of group [B] with the damage state D2 are shown in Figure 4.38 through Figure 4.40.

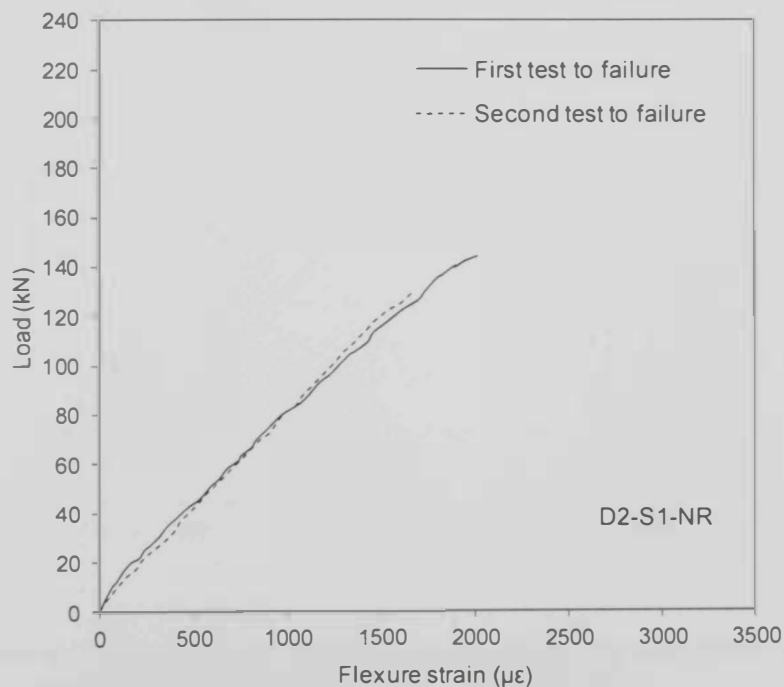


Figure 4.38: Load-flexural strain relationships for specimen D2-S1-NR

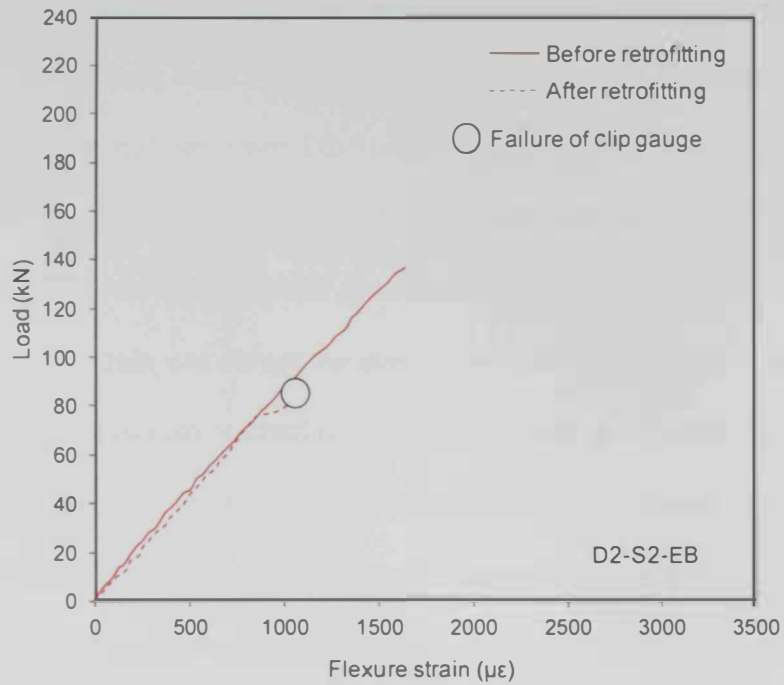


Figure 4.39: Load-flexural strain relationships for specimen D2-S1-EB

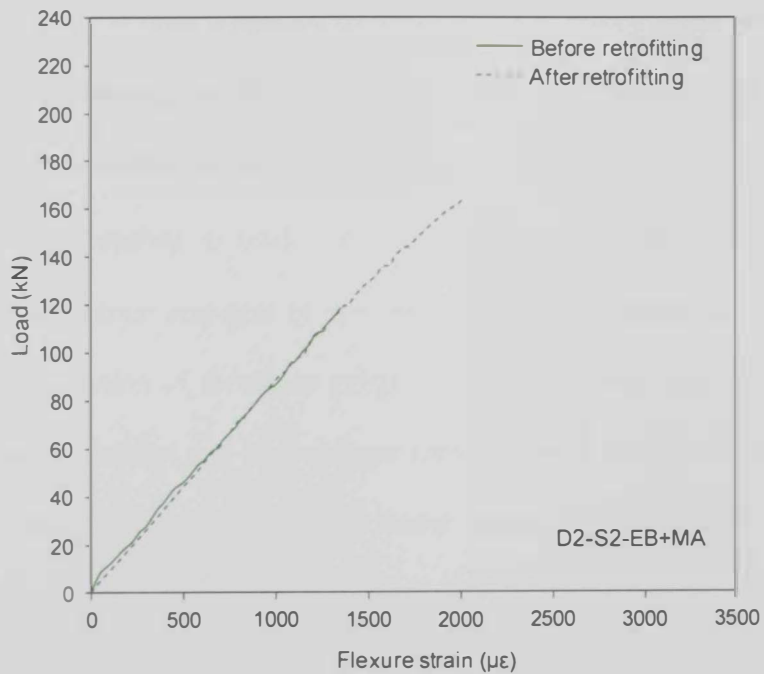


Figure 4.40: Load-flexural strain relationships for specimen D2-S1-EB+MA

In the first shear test, the specimens experienced flexural cracks at a load value

in the range of 10 to 20 kN followed by a continuous increase in the steel strains till the peak load. These flexural cracks were invisible during testing. In the first shear test, specimen D2-S1-NR featured a gradual rate of increase in the flexure steel strain until it reached its peak load at a flexure steel strain value of 1675 $\mu\epsilon$. In the second shear test to failure, the rate of increase of the flexure steel strain was almost the same as that recorded in the first shear test to failure. The specimen reached its second peak load at a flexure steel strain of 2020 $\mu\epsilon$. Specimen D2-S1-EB featured a steady rate of increase in flexure steel strain in the first shear test until it reached the peak load at a flexure steel strain value of 1639 $\mu\epsilon$. After retrofitting, the rate of the flexure steel strain increase was insignificantly different of that recorded in the first shear test. Specimen D2-S1-EB+MA featured a gradual rate of increase in the flexure steel strain in the first shear test until it reached its peak load at a flexure strain value of 1357 $\mu\epsilon$. After retrofitting, the rate of the flexure steel strain increase was almost the same as that recorded in the first shear test. In the second shear test to failure, the specimen reached its peak load at a flexure steel strain of 2039 $\mu\epsilon$. The flexural steel strain response of specimen D2-S1-ETD could not be recorded due to malfunction of the strain gauge. The flexural steel strain values at the peak loads in the first and second shear tests were well below the steel yielding strain. This confirms that all specimens failed in shear before and after retrofitting.

4.2.2.3.6 Stirrups strain response

The stirrups strain responses for specimens of group [B] with the damage state D2 are shown in Figure 4.41 through Figure 4.44.

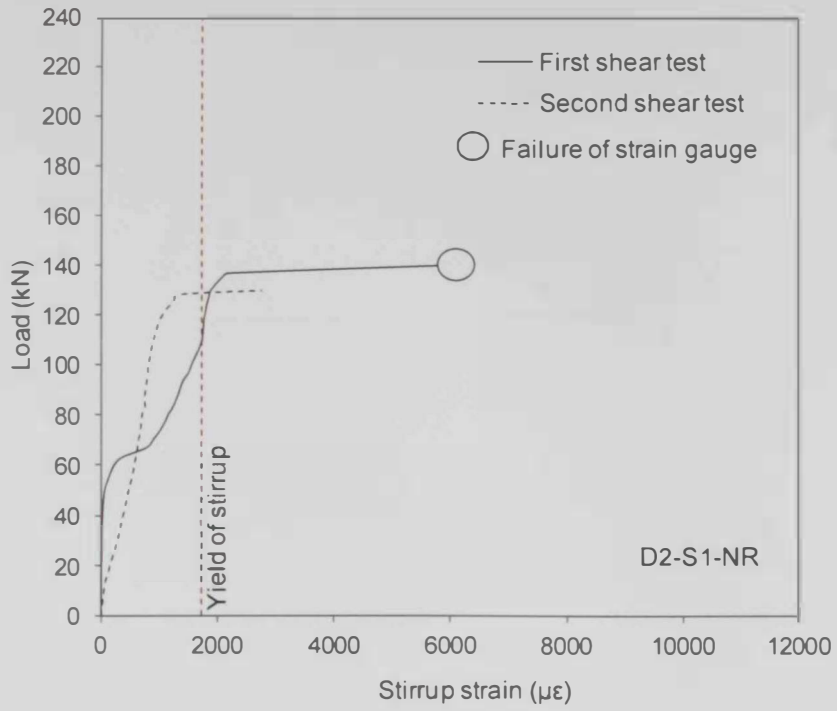


Figure 4.41: Load-stirrups strain response for specimen D2-S1-NR

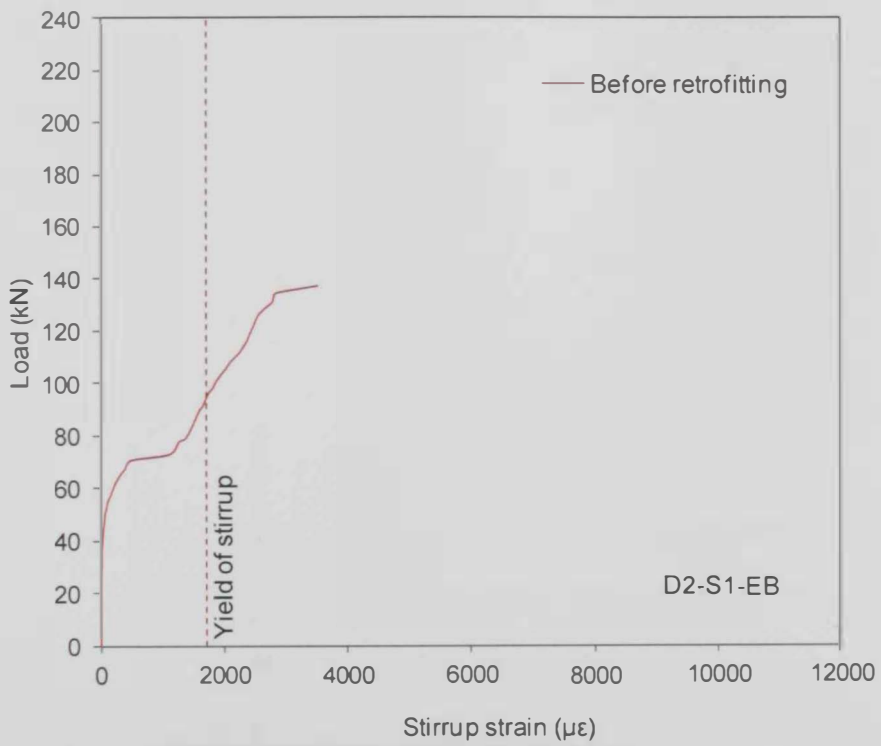


Figure 4.42: Load-stirrups strain response for specimen D2-S1-EB

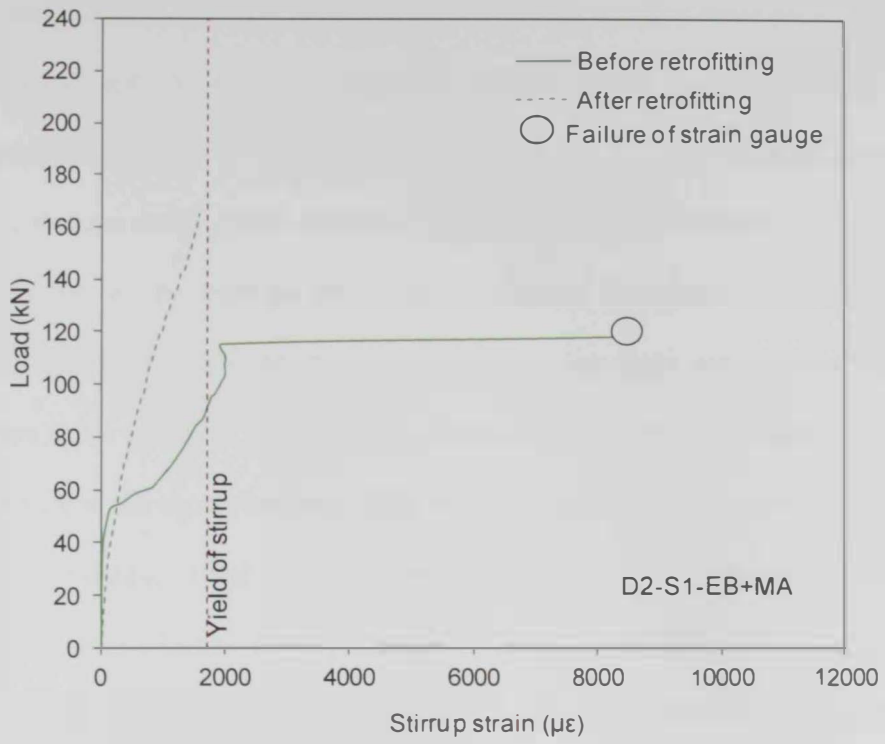


Figure 4.43: Load-stirrups strain response for specimen D2-S1-EB+MA

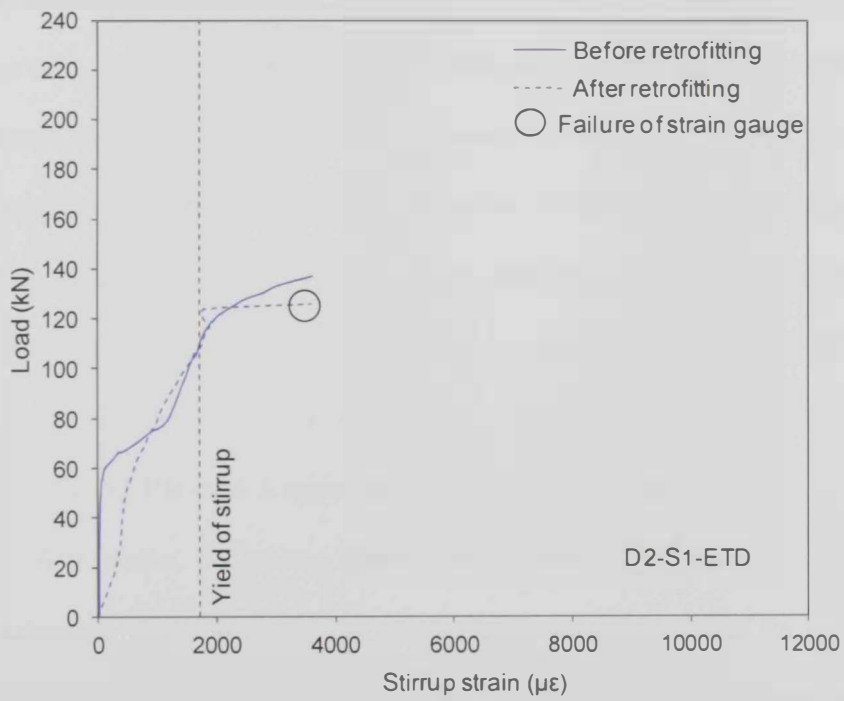


Figure 4.44: Load-stirrups strain response for specimen D2-S1-ETD

The stirrup strain response of specimen D2-S1-NR featured three phases in the first shear test. In the first stage, no stirrups strain was recorded up to approximately 50 kN where cracking took place followed by a sudden increase in the stirrups strain. In the second stage, the specimen exhibited a higher rate of increase in the stirrups strain up to yielding of stirrups that started at approximately 120 kN. In the third stage, the specimen exhibited a plastic stirrups strain response. In the second shear test to failure, the stirrups started to contribute to the shear resistance from the very beginning of the test because of the pre-existing shear cracks until yielding of stirrups occurred at approximately 130 kN. After yielding of stirrups, the specimen experienced a plastic stirrups strain response. The stirrups strain response for specimen D2-S1-EB demonstrated three phases prior to retrofitting. In the first phase, no stirrups strain was recorded up to a load value of approximately 65 kN where shear cracks developed followed by a sudden increase in the stirrups strain. In the second stage, the strain continued to increase as the load progressed up to yielding of stirrups that started at approximately 100 kN. In the third stage, the specimen exhibited a plastic strain response until it reached its peak load. The stirrups strain response after retrofitting was not recorded for specimen D2-S1-EB due to malfunction of the strain gauge. The stirrups strain response of specimen D2-S1-EB+MA featured three phases prior to retrofitting.

In the first phase, no stirrup strain was recorded up to a load value of approximately 55 kN where shear cracks initiated accompanied by a sudden increase in the stirrups strain. In the second phase, the strain increased as the load progressed until yielding of stirrups occurred at a load value of approximately 110 kN. After yielding of stirrups, a plastic stirrups strain

response took place. Subsequent to retrofitting, the specimen featured a quasi-linear stirrups strain response till yielding of stirrups at a load value of approximately 155 kN. The use of the EB-CFRP system integrated with the MA resulted in a significant reduction in the rate of increase of the stirrups strain. This in turn delayed yielding of stirrups and hence increased the specimen's shear resistance. The stirrups strain response of specimen D2-S1-ETD featured three phases prior to retrofitting.

In the first phase, no stirrups strain was recorded up to a load value of approximately 60 kN where shear cracks developed. After cracking, the strain continued to rise as the load progressed till yielding of stirrups at a load value of approximately 110 kN. In the last stage, the strain continued to increase in the stirrups but at a higher rate till the specimen reached its peak load. After retrofitting, the specimen exhibited a prompt contribution of stirrups from the beginning of the test. The rate of stirrups strain increase after retrofitting was almost the same as that recorded in the post-cracking stage during the first shear test, and hence the ETD-GFRP system did not result in an increase in the stirrups yielding load. This is possibly because of the presence of vertical holes that reduced the concrete section and also the presence of internal micro-cracks that could have been formed during drilling of the vertical holes for the installation of the GFRP rebars. This explains why the shear resistance of specimen D2-S1-ETD after retrofitting was almost the same as the original shear resistance recorded in the first shear test. In the last stage, the specimen experienced a plastic stirrups strain response.

4.2.2.3.7 FRP strain response

The FRP strain responses for the retrofitted specimens of group [B] with damage state D2 are shown in Figure 4.45. The effective FRP strain values are reported in Table 4.4. It should be noted that the maximum measured FRP strain is not necessarily the maximum absolute FRP strain experienced by the specimen.

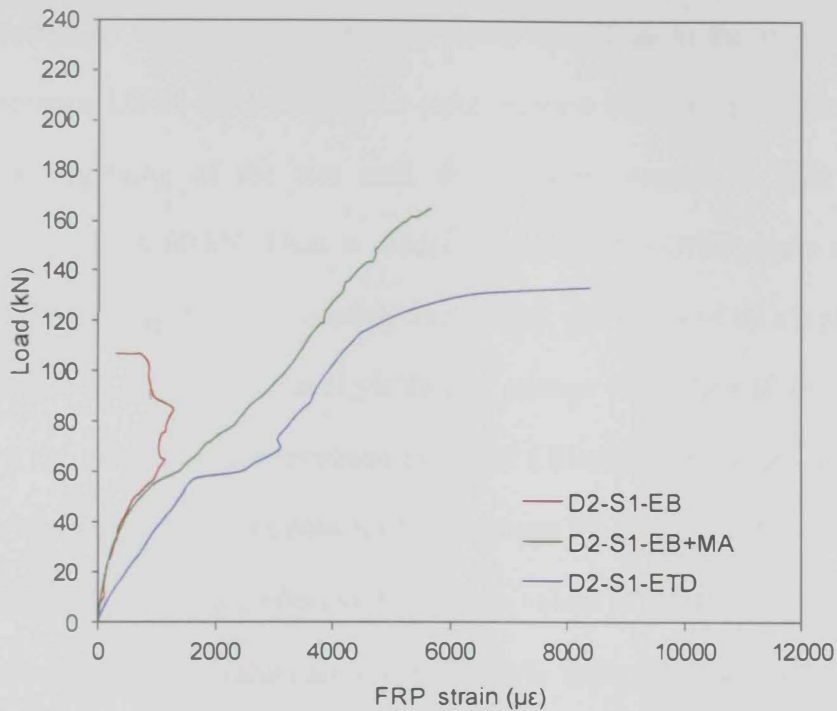


Figure 4.45: Load-FRP strains relationship for specimens of group [B] with damage state D2.

There was no pre-cracking stage in all specimens because the specimens were already cracked during the first shear test. Specimens D2-S1-EB and D2-S1-EB+MA exhibited similar FRP strain response till opening of the pre-existing cracks a load value of approximately 50 kN. Then, specimen D2-S1-EB exhibited initial/local debonding at a load value of approximately 65 kN followed by an insignificant increase in strain till the specimen reached a load value of approximately 85 kN where further debonding of the CFRP sheets

took place. This resulted in a reduction in the CFRP strain as the load progressed. After opening of the pre-existing cracks, specimen D2-S1-EB+MA showed a higher rate of increase in the CFRP strain till yielding of stirrups that took place at approximately 155 kN. Then, the specimen reached its peak load shortly after yielding of the stirrups. This means that the use of the CFRP system with the MA prevented debonding of the CFRP sheets, and hence allowed the CFRP reinforcement to further contribute to the shear resistance. Specimen D2-S1-ETD exhibited a rapid increase in the GFRP strain from the very beginning of the test until the specimen reached a load value of approximately 60 kN. Then, a sudden increase in the GFRP strain took place due to opening of the pre-existing cracks. This was followed by a higher rate of increase in GFRP strain until yielding of stirrups took place at approximately 110 kN. After that, the specimen exhibited a plastic GFRP strain response till the specimen reached its peak load. Specimens D2-S1-EB, D2-S1-EB+MA and D2-S1-ETD exhibited effective FRP strain values of 1274, 5655 and 8359 $\mu\epsilon$, respectively. These values are also reported in Table 4.4. The integration of the MA in the EB-CFRP system resulted in more than four-fold increase in the effective FRP strain.

4.2.3 Group C

4.2.3.1 Specimens without initial shear damage

4.2.3.1.1 Failure mode

Typical failure modes of specimens of group [C] that were not damaged prior to strengthening and/or testing are shown in Figure 4.46 through Figure 4.49.

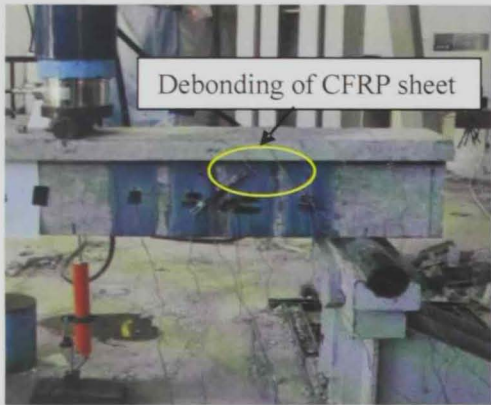


At peak load



At failure

Figure 4.46: Failure mode for specimen ND-S2-NR



At peak load



At failure

Figure 4.47: Failure mode of specimen ND-S2-EB



At peak load



At failure

Figure 4.48: Failure mode of specimen ND-S2-EB+MA

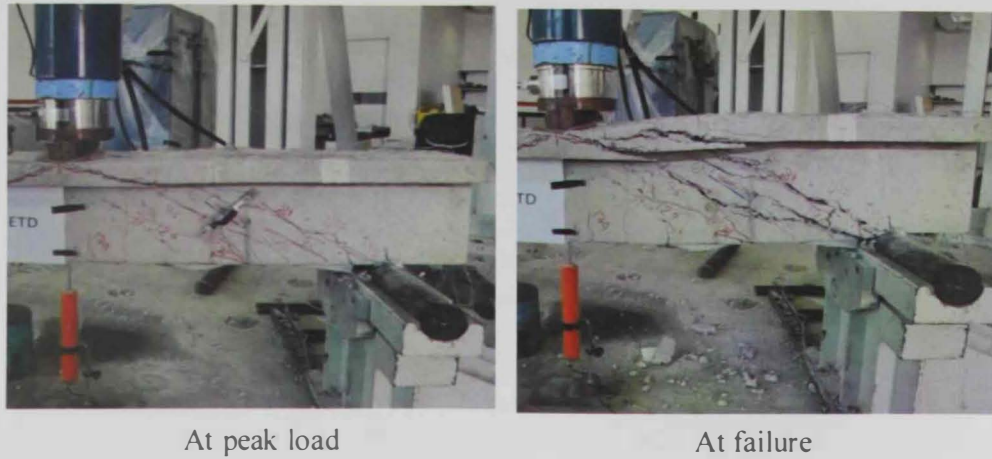


Figure 4.49: Failure mode of specimen ND-S2-ETD

The control specimen ND-S2-NR featured a classical diagonal tension shear mode of failure. The specimen failed due to formation of several inclined shear cracks in the shear span as shown in Figure 4.46 followed by yielding of stirrups then loss of shear integrity. This specimen exhibited a more wide spread shear cracking pattern compared with that exhibited by specimens ND-NS-NR and ND-S1-NR from groups [A] and [B], respectively. This is because of the higher amount of internal steel stirrups provided in this specimen. Specimen ND-S2-EB failed by debonding of the CFRP sheets preceded by formation of diagonal shear cracks in the shear span and yielding of stirrups as shown in Figure 4.47. Specimens ND-S2-EB+MA and ND-S2-ETD failed by crushing of the concrete struts in a web-crushing shear mode of failure as shown in Figure 4.48 and Figure 4.49, respectively. Specimen ND-S2-EB+MA reached its peak load without debonding of the CFRP sheets. In the post peak stage, pull-out of the MA system took place and peeling-off of the CFRP sheets occurred due to excessive widening of the shear cracks and excessive shear deformation.

4.2.3.1.2 Shear capacity

Results of specimens of group [C] that were not damaged prior to strengthening and/or testing are given in Table 4.5.

Table 4.5 : Test results for the non-damaged specimens of group [C].

Group	Specimen	Peak load P_{max} (kN)	Shear resistance ^a V_{max} (kN)	FRP shear resistance ^b V_{fexp} (kN)	Shear strength gain (%)	Effective FRP strain ϵ_{fe} ($\mu\epsilon$)
[C]	ND-S2-NR	151	120.8	-	-	-
	ND-S2-EB	171	136.8	16.0	13	3860
	ND-S2-EB+MA	200	160.0	39.2	32	4503
	ND-S2-ETD	196	156.8	36.0	30	10525

$$^a V_{max} = 0.8P_{max}$$

^b With respect to the control unstrengthened specimen ND-S2-NR

The non-strengthened control specimen ND-S2-NR reached a maximum load of 151 kN which corresponded to a shear resistance of 120.8 kN. The EB-CFRP shear strengthening system without the MA resulted in only 13% increase in the shear resistance. The inclusion of the MA in the EB-CFRP strengthening system increased the shear strength gain from 13% to 32% and allowed the specimen to develop its full shear capacity. The shear strength gain caused by the ETD-GFRP system, 30%, was almost the same as that provided by the EB-CFRP system integrated with the MA.

4.2.3.1.3 Deflection response

The load-deflection curves for specimens of group [C] that were not shear-damaged prior to strengthening and/or testing are illustrated in Figure 4.50. All specimens featured a linear deflection response until initiation of shear cracks at approximately 60 kN followed by a quasi-linear load-deflection response till yielding of stirrups. The deflection continued to increase after yielding of stirrups but at a higher rate till the specimens reached their peak loads. All

strengthened specimens were stiffer than the control specimen ND-S2-NR. Specimen ND-S2-EB reached its peak load at a deflection value of 10 mm. This value was almost the same as that of the control specimen ND-S2-NR. The stiffnesses of the strengthened specimens were insignificantly different. Among the strengthened specimens, specimen ND-S2-EB+MA exhibited the highest stiffness while specimen ND-S2-ETD exhibited the lowest stiffness. The reduced stiffness exhibited by specimen ND-S2-ETD can be attributed to the reduced cross section caused by the 20 mm diameter holes pre-drilled through the section depth at discrete location for the installation of the ETD-GFRP system.

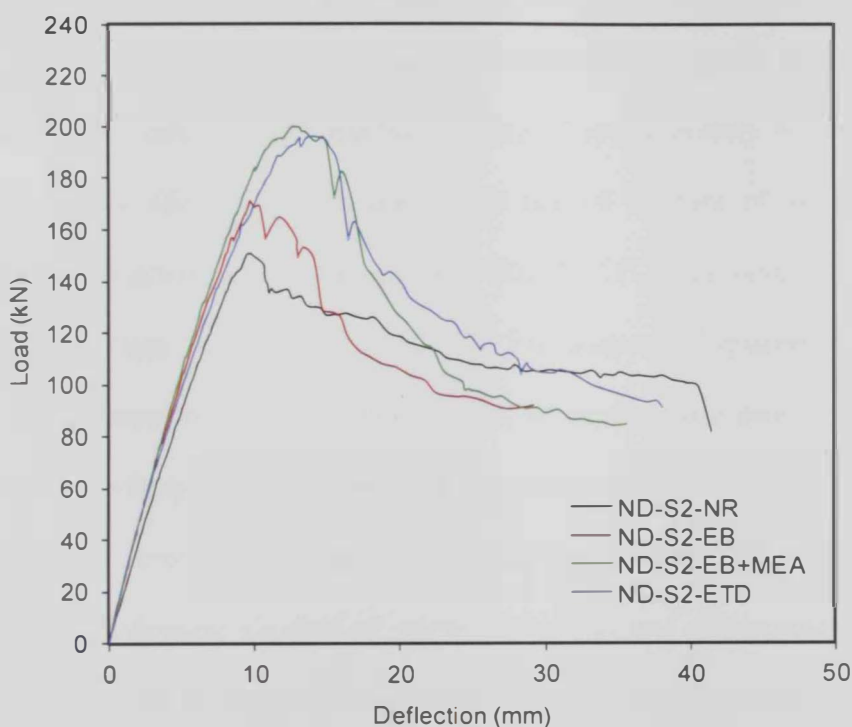


Figure 4.50: Load-deflection curves for the non-damaged specimens of group [C]

Specimens ND-S2-EB and ND-S2-EB+MA experienced several drops/increases in load in the post-peak stage possibly because of progressive

debonding of the CFRP sheets. Specimens ND-S2-EB+MA and ND-S2-ETD reached their peak loads at deflection values of 12.7 and 14.8 mm, respectively. The strengthened specimens exhibited higher energy absorption than that of the control specimen ND-S2-NR. The energy absorption of specimens ND-S2-EB+MA and ND-S2-ETD were higher than that of specimen ND-S2-EB.

4.2.3.1.4 Diagonal tensile displacement response

The load versus the diagonal tensile displacement relationships for the specimens of group [C] that were not damaged prior to strengthening and/or testing are shown in Figure 4.51. The specimens exhibited diagonal shear cracking at a load value in the range of 50 to 70 kN. After crack initiation, specimen ND-S2-NR showed a gradual increase in the diagonal displacement across cracks until the load reached a value of approximately 90 kN where failure of the clip gauge took place. The rate of increase of the diagonal displacement across cracks for specimen ND-S2-ETD was even higher than that of the control specimen ND-S2-NR. The diagonal displacement across cracks for specimen ND-S2-ETD continued to increase at a constant rate till yielding of stirrups that took place at approximately 150 kN. The diagonal tensile displacement at the onset of yielding for specimen ND-S2-ETD was 0.91 mm. Following yielding of stirrups, the diagonal displacement across cracks continued to increase but at a higher rate till the specimen reached its peak load. Both specimens ND-S2-EB and ND-S2-EB+MA exhibited similar rate of increase of the diagonal displacement across cracks. The diagonal displacement across cracks for specimens ND-S2-EB and ND-S2-EB+MA increased at a rate much lower than that of specimen ND-S2-ETD. For instance, at 100 kN, the diagonal displacement across cracks for specimen ND-

S2-ETD was 0.45 mm whereas for specimens ND-S2-EB and ND-S2-EB+MA, it was only 0.1 mm, on average. The higher rate of increase in the diagonal displacement across cracks for specimen ND-S2-ETD can be ascribed to the presence of vertical holes which reduced the cross sectional area of the concrete and could also have initiated micro-cracks during drilling.

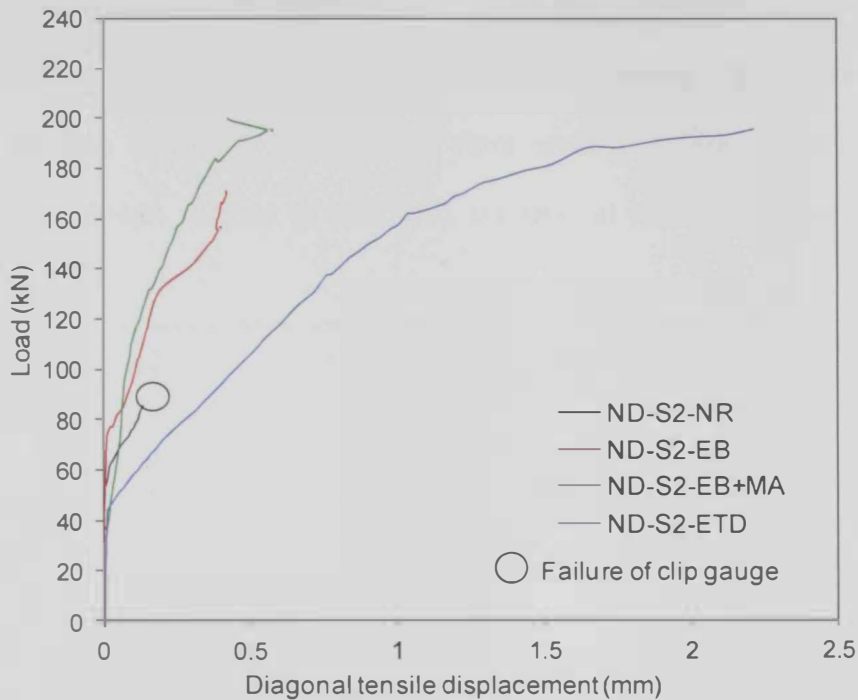


Figure 4.51: Load- diagonal tensile displacement curves for the non damaged specimens of group [C]

4.2.3.1.5 Flexural steel strain response

The flexure steel strain response for specimens of group [C] that were not damaged prior to strengthening and/or testing are shown in Figure 4.52. The flexural steel strain response of specimen ND-S2-ETD was not recorded due to malfunction of the strain gauge. All specimens exhibited a bi-linear flexural steel strain response. Initially, the flexural steel strain increased at a constant rate till initiation of flexural cracks at approximately 15 kN. Following initial

flexural cracks, the flexural steel strain continued to increase but at a higher rate till the specimens reached their peak loads. The rates of increase of the flexure steel strain for specimens ND-S2-EB and ND-S2-EB+MA were almost the same. Specimens ND-S2-NR, ND-S2-EB, and ND-S2-EB+MA reached their peak loads at flexural strain values of 1561, 2267, 2955 $\mu\epsilon$, respectively. This indicates that the specimens NS-S2-NR and ND-S2-EB failed in shear without yielding of the flexural tensile steel reinforcement. The specimen ND-S2-EB+MA failed in a web-crushing shear mode of failure. When specimen ND-S2-EB+MA reached its peak load, the flexural tensile steel was about to yield.

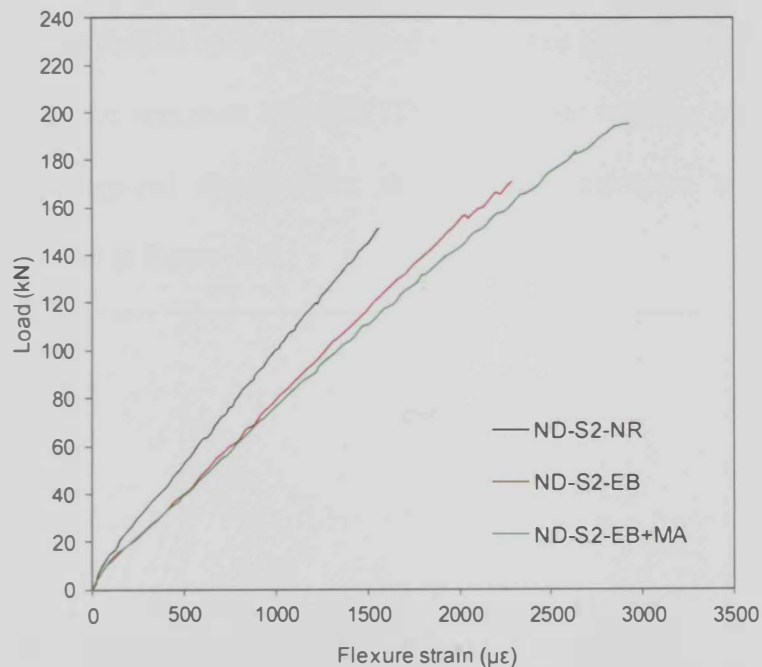


Figure 4.52: Load-flexural strain relationships for the non-damaged specimens of group [C]

4.2.3.1.6 Stirrups strain response

The stirrups strain response for specimens of group [C] that were not damaged prior to strengthening and/or testing are shown in Figure 4.53. The stirrups strain response featured a bi-linear relationship. The stirrups were not strained

prior to initiation of shear cracks. In the second stage, the stirrups strain increased at almost a constant rate up to the peak load that occurred shortly after the yielding of stirrups. The control specimen ND-S2-NR had the highest rate of increase of stirrups strain. The strengthened specimens, particularly ND-S2-EB and ND-S2-EB+MA exhibited a rate of increase of stirrups strain much lower than that of the control specimen ND-S2-NR. The reduced rate of stirrups strain increase exhibited by the strengthened specimens delayed yielding of stirrups and hence increased the shear capacity. Specimen ND-S2-ETD experienced a higher rate of increase of stirrups strain compared with that of specimens ND-S2-EB and ND-S2-EB+MA. This can be ascribed to the presence of the vertical holes as explained earlier. The higher rate of increase of stirrups strain for specimen ND-S2-ETD is consistent with the higher rate of increase of diagonal displacement across cracks exhibited by the same specimen shown in Figure 4.51.

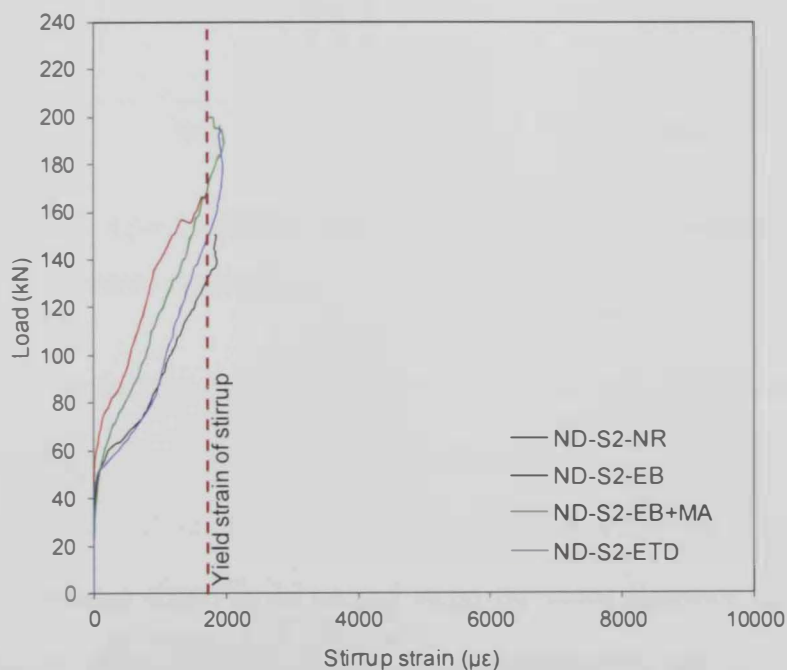


Figure 4.53: Load-stirrups strain response for the non-damaged specimens of group [C]

4.2.3.1.7 FRP strain response

The FRP strain responses for the strengthened specimens of group [C] that were not damaged prior to strengthening and/or testing are shown in Figure 4.54. The effective FRP strain values are reported in Table 4.5. It should be noted that the maximum measured FRP strain is not necessarily the maximum absolute FRP strain experienced by the specimen.

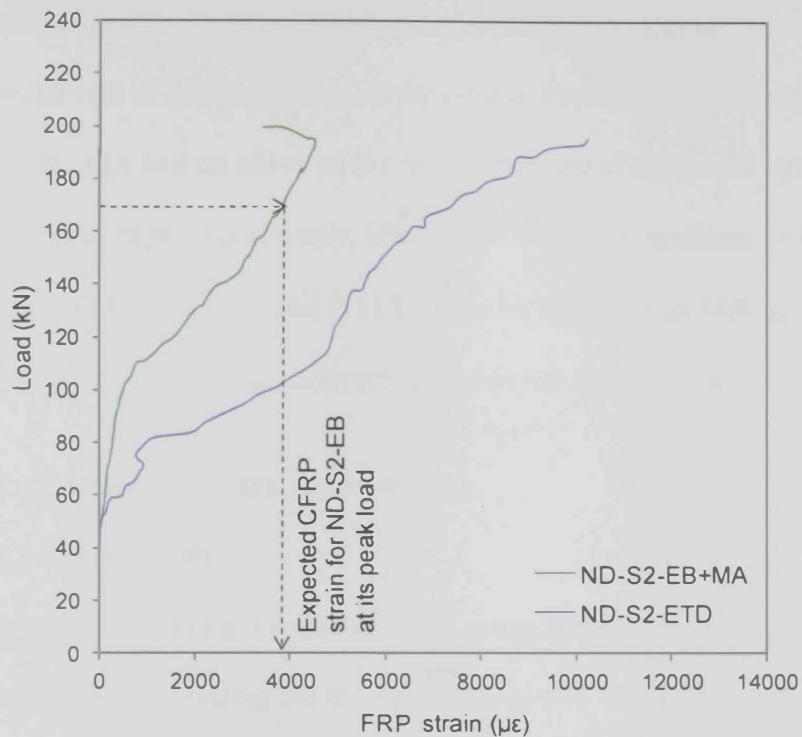


Figure 4.54: Load-FRP strain relationships for the non-damaged specimens of group [C]

The FRP strain response for specimen ND-S2-EB was not recorded due to malfunction of the strain gauges. The specimens featured a bi-linear FRP strain response. The FRP reinforcement did not contribute to the shear resistance in the pre-cracking stage. In the second stage, the strain increased gradually till yielding of stirrups which took place at approximately 160 kN. Following yielding of stirrups, the FRP strain continued to increase but at a higher rate.

The effective FRP strains in specimens ND-S2-EB+MA and ND-S2-ETD were 4503 and 10252 $\mu\epsilon$, respectively. Specimen ND-S2-ETD exhibited a higher rate of increase in the FRP strain compared with that of specimen ND-S2-EB+MA. This is consistent with the diagonal displacement response across cracks and the stirrups strain response exhibited by the same specimen shown in Figures 4.51 and 4.53, respectively. Specimens ND-S2-EB+MA and ND-S2-EB had similar rate of increase of the diagonal displacement across cracks and also similar rate of increase of the stirrups strain. Previous results demonstrated also that the MA had no effect on the rate of increase of the CFRP strain in the post-cracking stage. Accordingly, the CFRP strain of specimen ND-S2-EB without the MA at its peak load (171 kN) can be estimated as 3860 $\mu\epsilon$ from the FRP strain response of its counterpart specimen ND-S2-EB+MA.

4.2.3.2 Specimens with damage state (D2)

4.2.3.2.1 Failure mode

Typical modes of failure for specimens of group [C] that were pre-failed prior to retrofitting and/or testing are shown in Figure 4.55 through Figure 4.58. The non-retrofitted pre-failed control specimen D2-S2-NR was first loaded till it reached its peak load then unloaded. Subsequently, the specimen was tested again to failure for the second time. The other three specimens were first loaded till they reached their first peak loads then unloaded. After that, the specimens were retrofitted with EB-CFRP system without the MA, EB-CFRP system integrated with the MA, and ETD-GFRP system. Following retrofitting, the specimens were loaded back to failure. Specimen D2-S2-NR showed a classical shear mode of failure expressed by formation of a band of diagonal shear cracks in the shear span as shown in Figure 4.55. During the second shear test

to failure, specimen D2-S2-EB failed by sudden delamination of the CFRP sheets as shown in Figure 4.56. This was preceded by opening of the pre-existing cracks and yielding of stirrups. Specimen D2-S2-EB+MA failed by crushing of the diagonal concrete struts. This was also preceded by opening of the pre-existing diagonal shear cracks in the shear span and yielding of stirrups. The bottom concrete cover spalled-off at the onset of failure. In the post-peak stage, pull-out of the MA system and peeling-off of the CFRP sheets with a considerable amount of concrete adhered to them took place as shown in Figure 4.57. Specimen D2-S2-ETD failed by crushing of the diagonal concrete struts as shown in Figure 4.58. This was preceded by opening of existing cracks, development of new cracks, and yielding of stirrups.

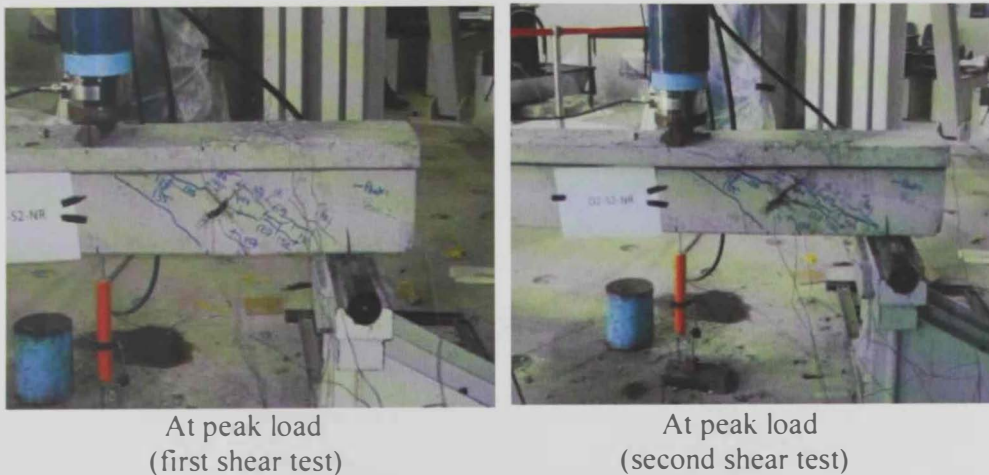


Figure 4.55: Failure mode of specimen D2-S2-NR



At peak load (first shear test)



At peak load (second shear test)



At failure (second shear test)

Figure 4.56: Failure mode of specimen D2-S2-EB



At peak load (first shear test)



At peak load (second shear test)



At failure (second shear test)

Figure 4.57: Failure mode of specimen D2-S2-EB+MA



At peak load (first shear test)



At peak load (second shear test)



At failure (second shear test)

Figure 4.58: Failure mode of specimen D2-S2-ETD

4.2.3.2.2 Shear capacity

Results of specimens of group [C] that were pre-failed prior to retrofitting are given in Table 4.6.

Table 4.6: Test results for specimens of group [C] with the damage state D2

Group	Damage state	Specimen	First shear test (original loads)		Second shear test (new loads)		$V_{f,exp}^b$ (kN)	V_{new}/V_{org}	Effective FRP strain ϵ_{fe} ($\mu\epsilon$)
			P_{org} (kN)	V_{org} (kN) ^a	P_{new} (kN)	V_{new} (kN) ^a			
[C]	D2	D2-S2-NR	157	125.6	146.0	116.8	-	0.93	-
		D2-S2-EB	151	120.8	136.0	108.8	-	0.90	2696
		D2-S2-EB+MA	148	118.4	164.0	131.2	21.1	1.11	3403
		D2-S2-ETD	154	123.2	186.0	148.8	34.2	1.21	10155

$$^a V_{org} = 0.8P_{org}, V_{new} = 0.8P_{new}$$

$$^b V_{f,exp} = V_{new} - 0.93V_{org}, \text{ residual shear strength prior to retrofitting} = 0.93V_{org} \text{ based on the results of specimen D2-S2-NR}$$

Specimen D2-S2-NR reached a peak load of 157 kN which corresponded to a shear resistance of 125.6 kN in the first shear test. In the second shear test to failure, the specimen recorded a lower peak load of 146 kN that corresponded to a shear resistance of 116.8 kN. This means that the non-retrofitted specimen was able to restore 93% of its original shear strength recorded in the first shear test. Prior to retrofitting, specimen D2-S2-EB reached a peak load of 151 kN which corresponded to a shear resistance of 120.8 kN. In the second shear test to failure (i.e. after retrofitting), the retrofitted specimen could not restore its original shear capacity and recorded a lower peak load of 136 kN that corresponded to a shear resistance 108.8 kN. The ratio V_{new}/V_{org} was only 0.90 which indicates that the specimen restored only 90% of its original shear capacity due to the early debonding of the CFRP sheets caused by opening of the pre-existing shear cracks. In the first shear test (i.e. prior to retrofitting), specimen D2-S2-EB+MA reached a peak load of 148 kN which corresponded

to a shear resistance of 118.4 kN. In the second shear test to failure (i.e. after retrofitting), the specimen recorded a higher peak load of 164 kN that corresponded to a higher shear resistance of 131.2 kN. The ratio V_{new}/V_{org} was 1.11 which indicates that the specimen was not only able to restore its original shear capacity, but also upgraded its original shear capacity by 11%. The specimen D2-S2-ETD recorded a peak load of 154 kN prior to retrofitting which corresponded to a shear resistance of 123.2 kN. In the second shear test to failure (i.e. after retrofitting), the specimen reached a peak load of 186 kN that corresponded to a shear resistance of 148.8 kN with a ratio of $V_{new}/V_{org} = 1.21$. This means that the specimen was able to fully restore its original capacity with an additional enhancement of 21%.

4.2.3.2.3 Deflection response

The load-deflection curves for specimens of group [C] that were pre-failed prior to retrofitting and/or testing are illustrated in Figure 4.60 through Figure 4.61. In the first shear test, all specimens exhibited almost a linear response up to initiation of shear cracks at a load value in the range of 50 to 60 kN. Then, the specimens exhibited a quasi-linear deflection response until yielding of stirrups which started at approximately 120 kN. Following yielding of stirrups, the deflection continued to increase but at a higher rate till the peak load. The non-retrofitted pre-failed specimen D2-S2-NR featured almost a linear deflection response in the second shear test to failure until yielding of stirrups that occurred at approximately 130 kN. The deflection then increased at a higher rate till the specimen reached its peak load shortly after yielding of stirrups. The initial shear damage D2 reduced the shear resistance by 7% as

shown in Figure 4.60. At the peak load, a slight drop in load took place. In the post-peak stage, the deflection increased accompanied by a gradual reduction in the load. Specimen D2-S2-EB exhibited almost a linear deflection response in the second shear test to failure till yielding of stirrups that occurred at approximately 130 kN. The specimen reached its peak load shortly after yielding of stirrups. Following yielding of stirrups, a sudden increase in deflection took place. In the post-peak stage, the specimen exhibited drop/increase in load followed by another drop in load possibly because of progressive debonding of the CFRP sheets. The specimen then exhibited a plastic load-deflection behavior. Specimen D2-S2-EB+MA featured almost a linear response in the second shear test to failure till yielding of stirrups which took place at approximately 150 kN. The deflection continued to increase after yielding of stirrups but at a higher rate until the specimen reached its peak load where a sudden drop in load took place followed by another increase/drop in load. Then, the specimen exhibited a plastic load-deflection behavior as shown in Figure 4.62. Specimen D2-S2-ETD exhibited almost a linear deflection response in the second shear test to failure till yielding of stirrups which took place at approximately 170 kN. Then, the deflection continued to increase but at a higher rate until the specimen reached its peak load. When the peak load was reached, a sudden drop in load took place followed by another increase/drop in load. Then, the specimen exhibited a plastic deflection response as shown in Figure 4.61.

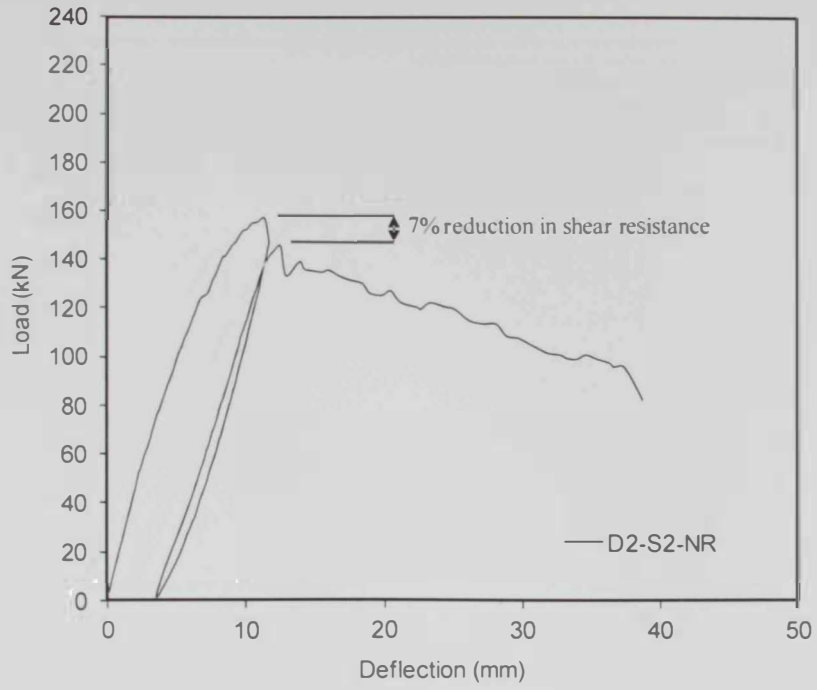


Figure 4.60: Load-deflection curves of specimen D2-S2-NR

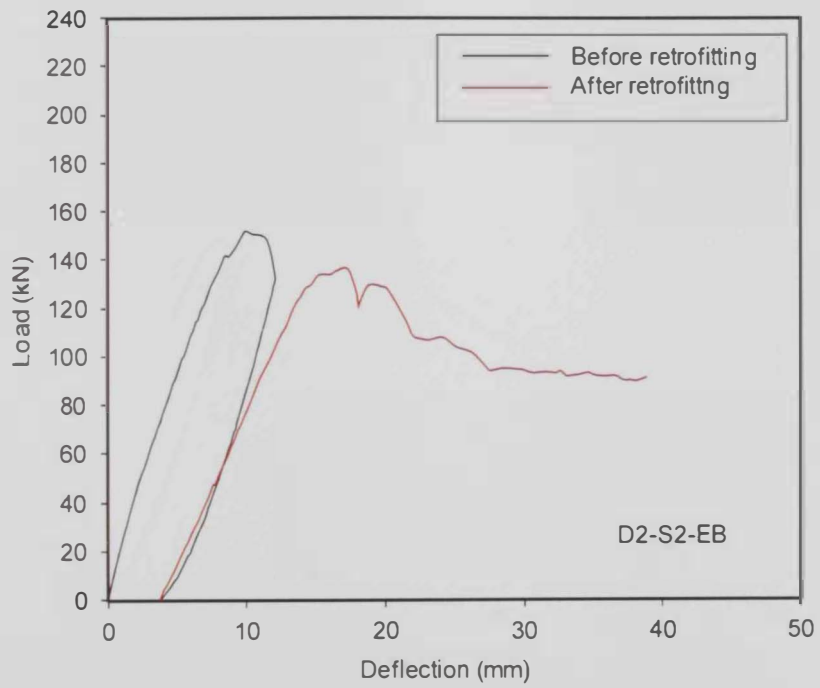


Figure 4.59: Load-deflection curves of specimen D2-S2-EB

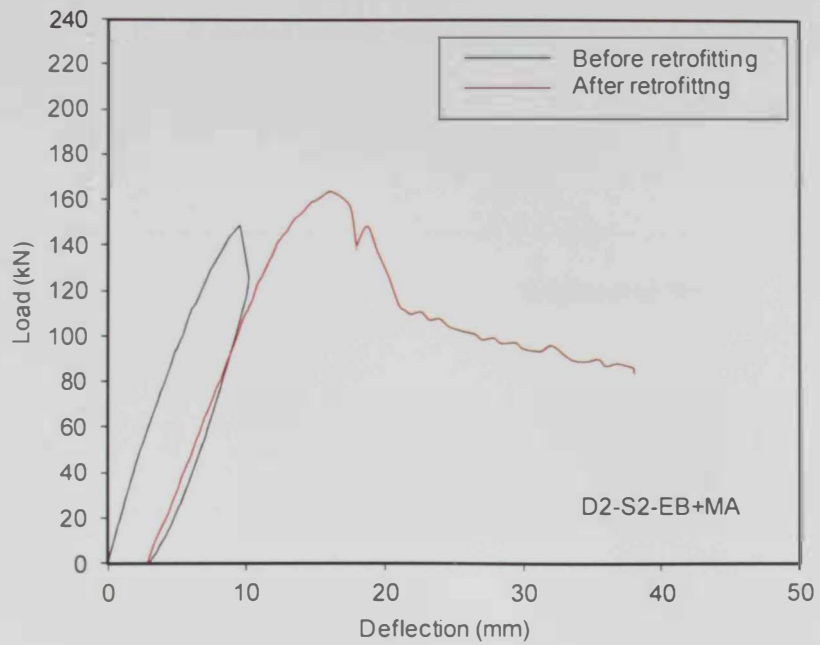


Figure 4.62: Load-deflection curves of specimen D2-S2-EB+MA

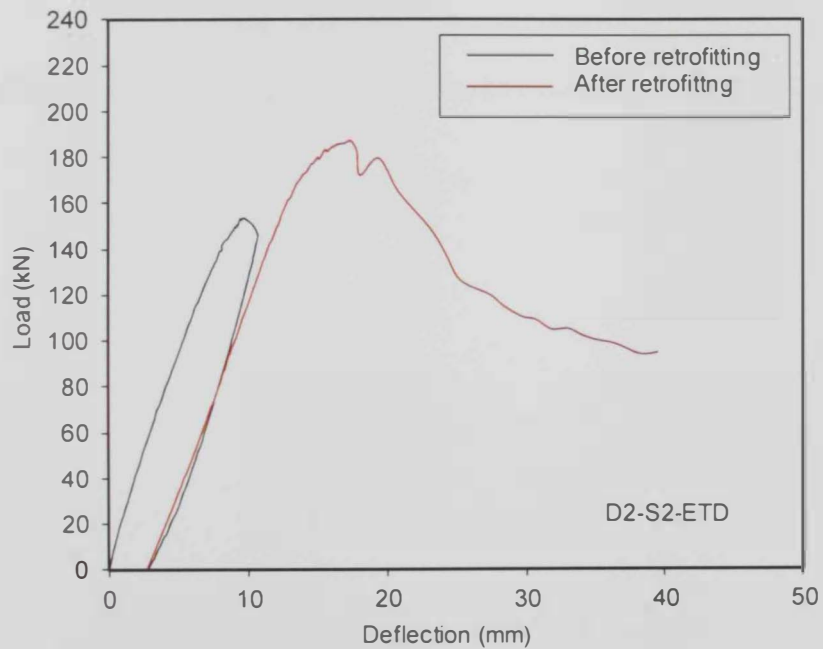


Figure 4.61: Load-deflection curves of specimen D2-S2-ETD

4.2.3.2.4 Diagonal tensile displacement response

The load versus the diagonal tensile displacement curves for specimens of group [C] with the damage state D2 are shown in Figure 4.63 through Figure 4.66.

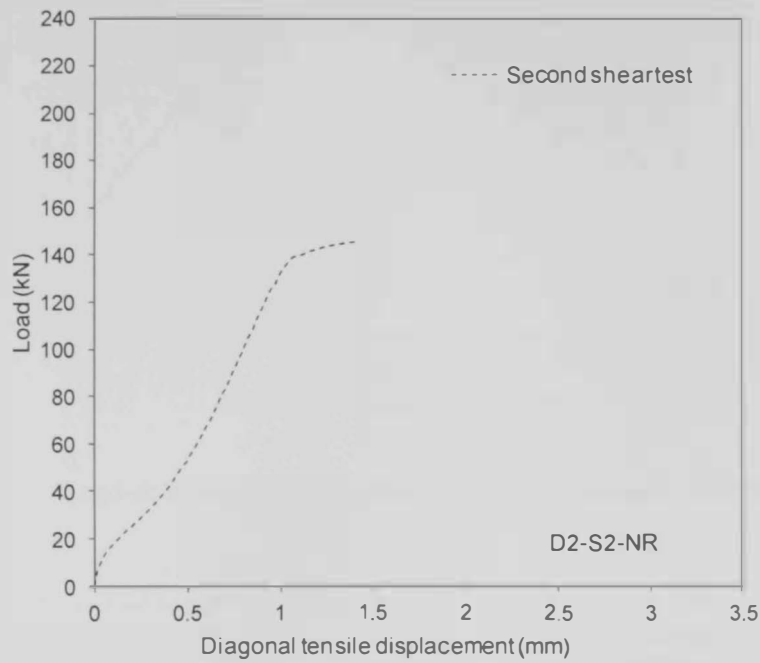


Figure 4.63: Load-diagonal tensile displacement for specimen D2-S2-NR

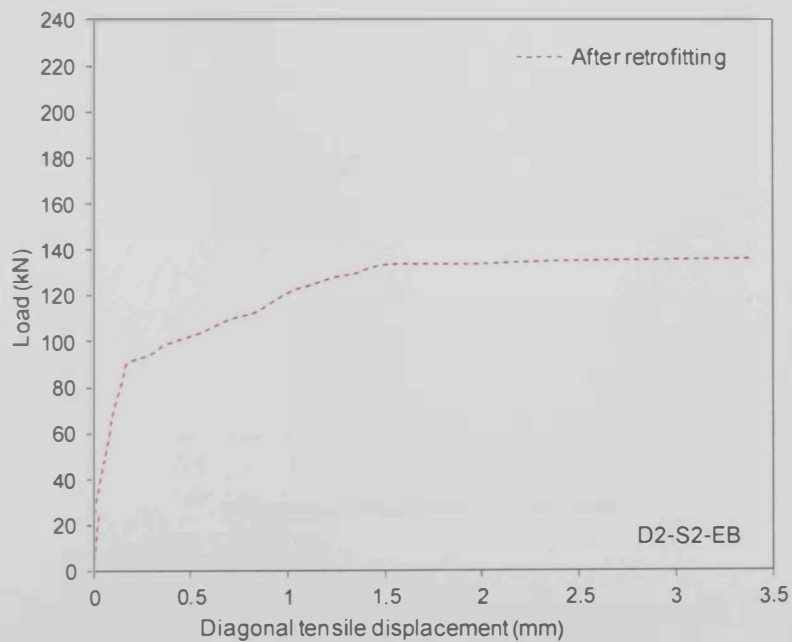


Figure 4.64: Load-diagonal tensile displacement for specimen D2-S2-EB

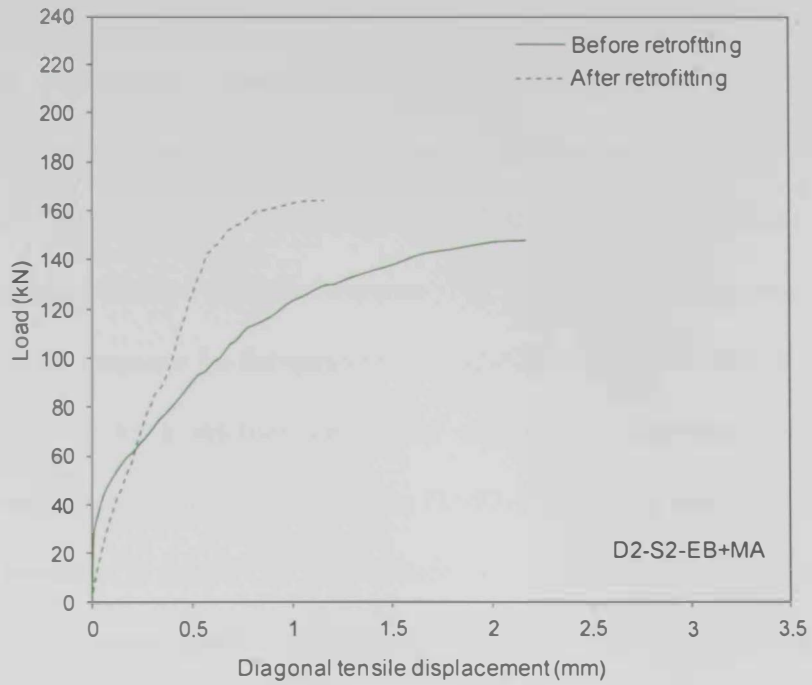


Figure 4.65: Load-diagonal tensile displacement for specimen D2-S2-EB+MA

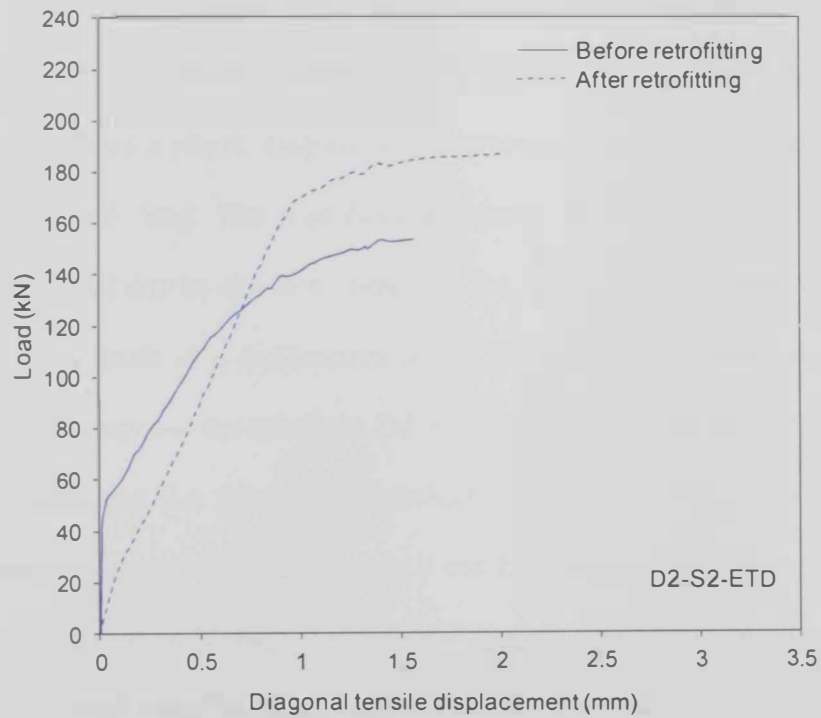


Figure 4.66: Load-diagonal tensile displacement for specimen D2-S2-ETD

There was no pre-cracking stage during the second shear test to failure. The diagonal displacement across cracks for specimen D2-S2-NR increased gradually in the second shear test until yielding of stirrups started at approximately 120 kN. After yielding of stirrups, the diagonal tensile displacement exhibited a plastic response. The load versus the diagonal tensile displacement response for the specimen D2-S2-NR was not recorded in the first shear test due to a malfunction of the clip gauge. The diagonal tensile displacement across cracks for specimen D2-S2-EB featured three stages in the second shear test to failure (i.e. after retrofitting). In the first stage, the diagonal tensile displacement across cracks increased linearly until the load reached a value of approximately 90 kN where initial/local debonding of the CFRP sheets and opening of the pre-existing cracks took place. In the second stage, the diagonal displacement across cracks increased at a higher rate until yielding of stirrups which took place at approximately 130 kN. In the third stage, the specimen featured a plastic diagonal displacement response until the specimen reached its peak load. The load-diagonal tensile displacement response for specimen D2-S2-EB in the first shear test (i.e. prior to retrofitting) was not recorded as a result of a malfunction of the clip gauge. The diagonal tensile displacement response for specimen D2-S2-EB+MA exhibited three phases in the first shear test (i.e. prior to retrofitting). In the first phase, no diagonal displacement values were recorded until the load reached a value of 35 kN followed by a slight increase in the diagonal displacement till initiation of shear cracks that took place at approximately 50 kN. In the second phase, the diagonal displacement increased at a constant rate as the load progressed till yielding of stirrups which started at approximately 120 kN. In the last phase,

the diagonal displacement continued to increase but at a higher rate until the specimen reached its peak load. After retrofitting (i.e. in the second shear test to failure), the diagonal displacement across cracks increased from the beginning of the test as the load progressed till yielding of stirrups which took place at approximately 150 kN. Then, a plastic diagonal displacement response took place until the specimen reached its peak load. The diagonal tensile displacement response for specimen D2-S2-ETD featured three stages in the first shear test (i.e. prior to retrofitting). In the first stage, the specimen did not show any signs of diagonal displacement till initiation of shear cracks at approximately 50 kN. In the second stage, the diagonal displacement increased at a constant rate as the load progressed till yielding of stirrups which started at approximately 120 kN. In the last stage, the diagonal tensile displacement across cracks continued to increase but at a higher rate till the specimen reached its peak load. After retrofitting, during the second shear test to failure, the diagonal displacement across cracks increased from the very beginning of the test as the load progressed till yielding of stirrups at approximately 170 kN. Following yielding of stirrups, the diagonal tensile displacement across cracks continued to increase with insignificant increase in load till the specimen reached its peak load.

4.2.3.2.5 Flexural steel strain response

The longitudinal tensile steel strains for the specimens of group [C] with the damage state D2 are shown in Figure 4.67 through Figure 4.70. In the first shear test, the specimens experienced flexural cracks at a load value in the range of 10 to 15 kN. These cracks were invisible during testing. After initiation of flexural cracks, the flexural tensile steel strain increased at a

constant rate till the peak load was reached. In the second shear test to failure, the flexural steel strain increased at a rate similar to that recorded in the first shear test.

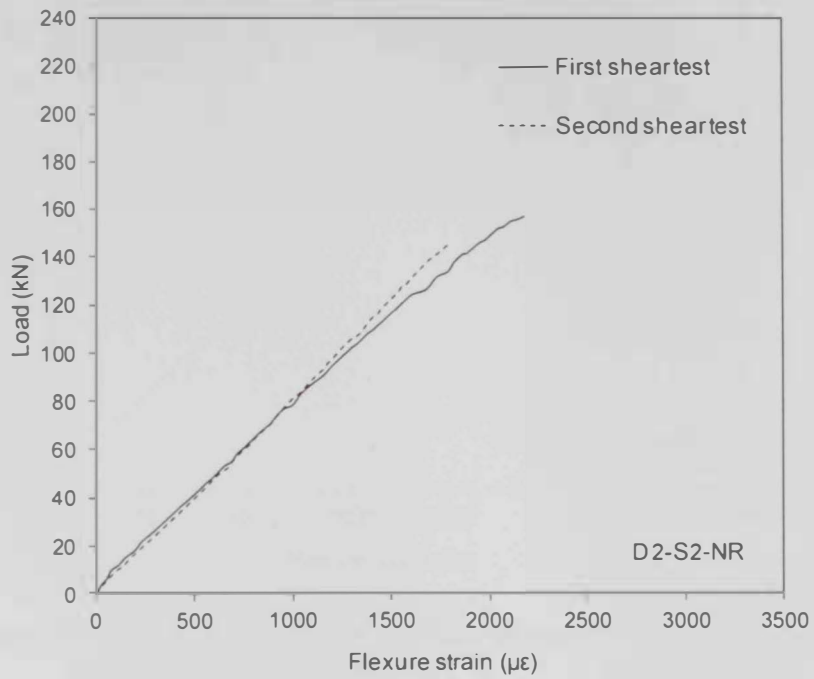


Figure 4.67: Load-flexural strain relationship for specimen D2-S2-NR

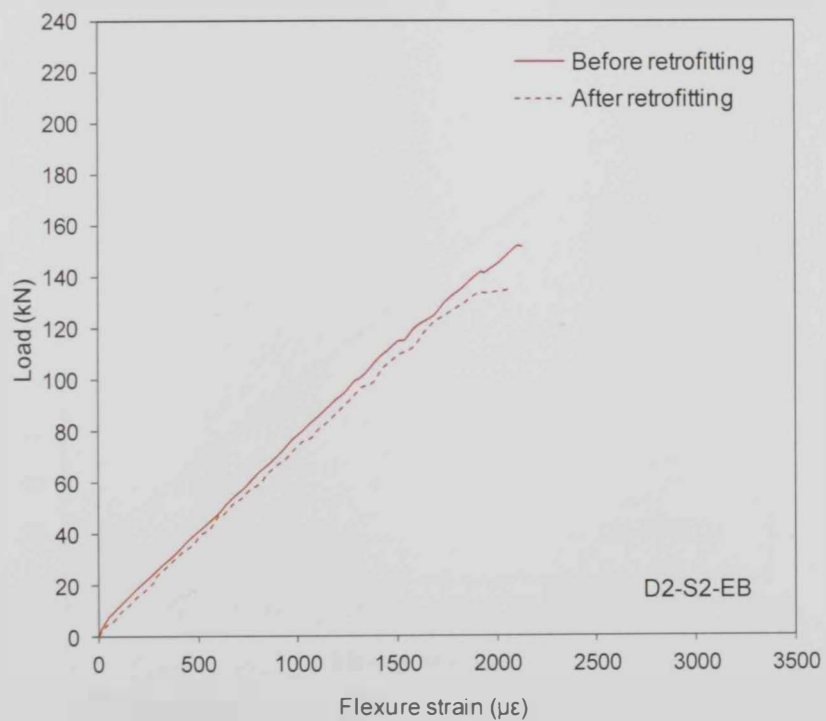


Figure 4.68: Load-flexural strain relationship for specimen D2-S2-EB

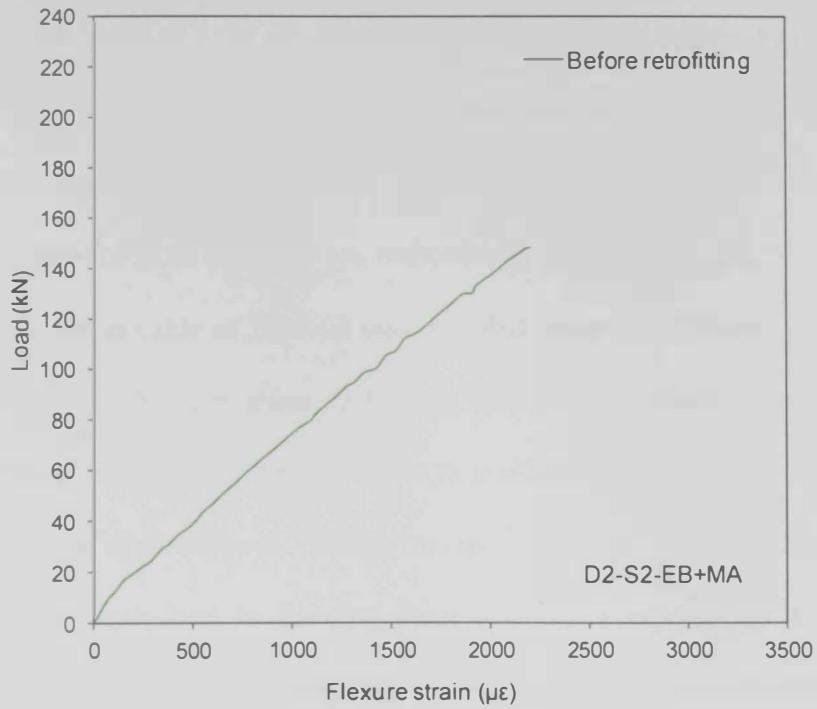


Figure 4.69: Load-flexural strain relationship for specimen D2-S2-EB+MA

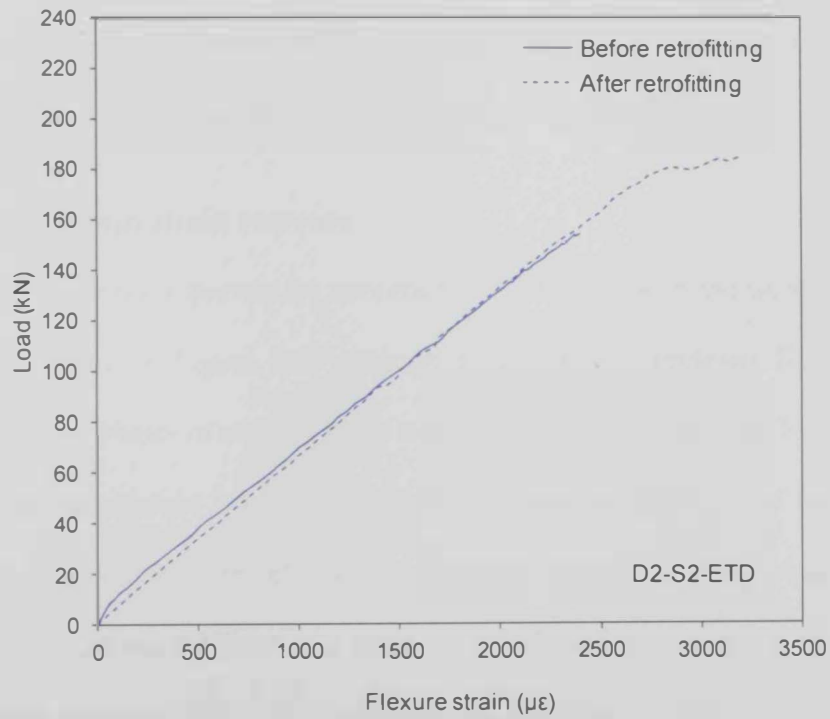


Figure 4.70: Load-flexural strain relationship for specimen D2-S2-ETD

Specimen D2-S2-NR reached its peak load in the first shear test at a tensile steel strain value of 2178 $\mu\epsilon$. In the second shear test to failure, the specimen reached its peak load at a flexural tensile steel strain of 1806 $\mu\epsilon$. Specimen D2-S2-EB reached its peak loads in the first and second shear tests at flexural steel strain values of 2130 and 2077 $\mu\epsilon$, respectively. For specimen D2-S2-EB+MA, a flexure strain value of 2205 $\mu\epsilon$ was recorded when the specimen reached its peak load in the first shear test. The flexural steel strain response after retrofitting could not be recorded due to malfunction of the strain gauge. A flexural steel strain value of 2380 $\mu\epsilon$ was recorded when specimen D2-S2-ETD reached its peak load in the first shear test. After retrofitting, the rate of increase of the flexure steel strain was almost the same as that recorded prior to retrofitting but the specimen reached its peak load at a higher flexural steel strain of 3205 $\mu\epsilon$. This indicates that crushing of the diagonal concrete struts occurred in the second shear test (i.e. after retrofitting) almost at the same time where the tensile steel reinforcement started to yield.

4.2.3.2.6 Stirrups strain response

The stirrups strain responses for specimens of group [C] with the damage state D2 are shown in Figure 4.71 through Figure 4.74. Specimen D2-S1-NR featured three phases of stirrups strain response in the first shear test. In the first stage, no strain values were recorded until initiation of shear cracks that took place at approximately 60 kN, where a sudden increase in the stirrups strain occurred. In the second phase, the strain increased at a higher rate until yielding of stirrups which started at approximately 120 kN. After yielding of stirrups, a plastic strain response took place.

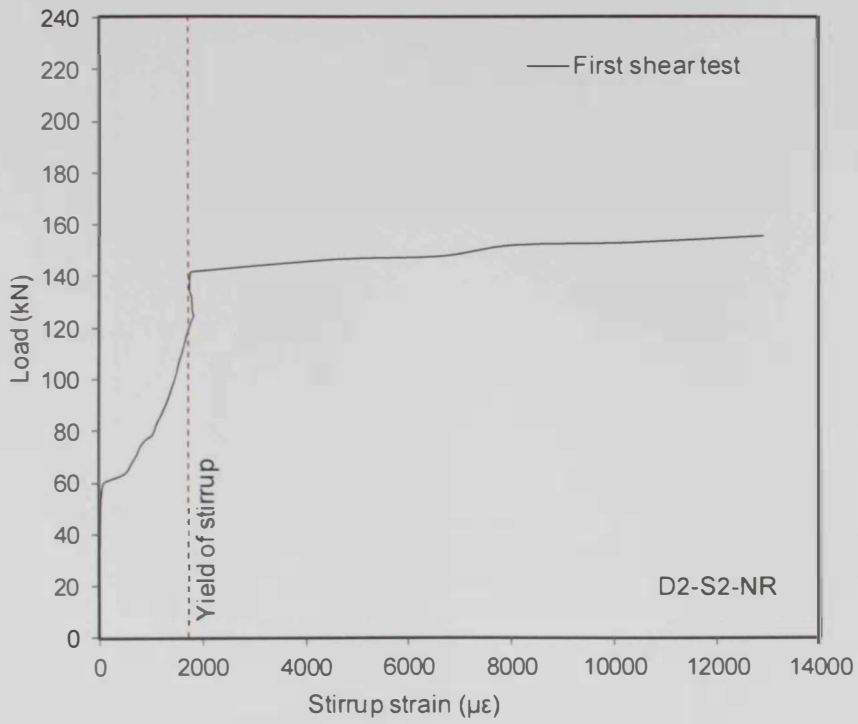


Figure 4.71: Stirrup's strain response of specimen D2-S2-NR

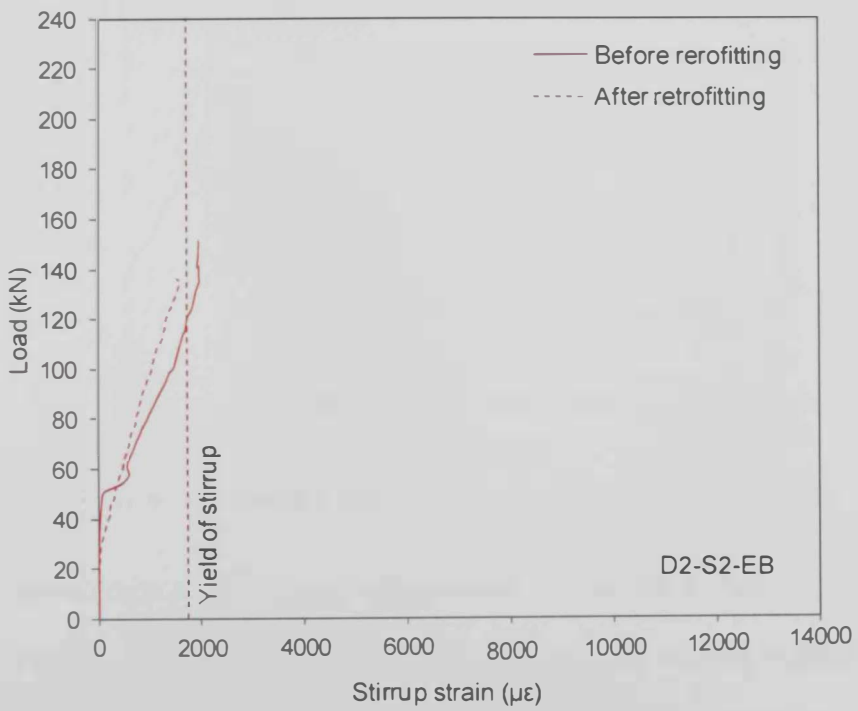


Figure 4.72: Stirrup's strain response of specimen D2-S2-EB

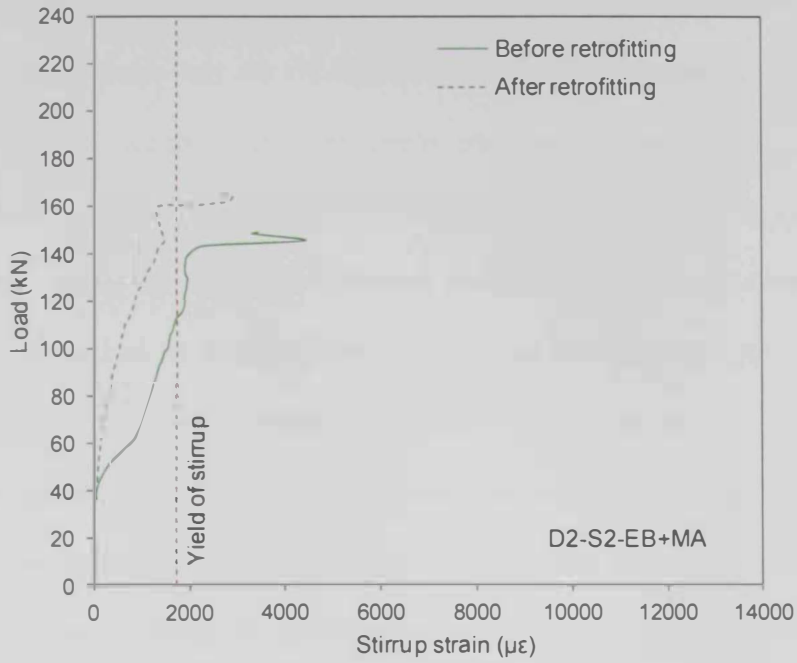


Figure 4.73: Stirrup's strain response of specimen D2-S2-EB+MA

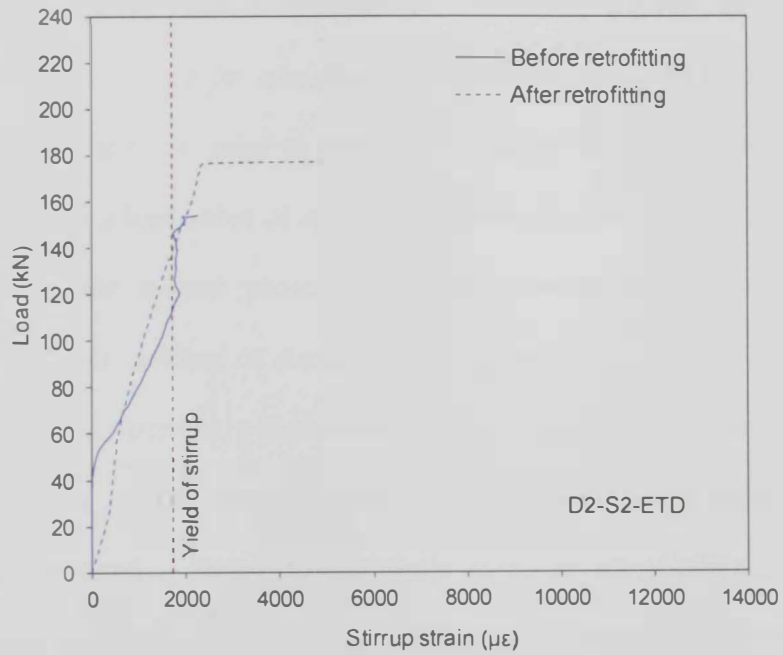


Figure 4.74: Stirrup's strain response of specimen D2-S2-ETD

The load-stirrups strain response of specimen D2-S2-NR in the second shear test to failure was not recorded due to malfunction of the strain gauge. The stirrups strain response of specimen D2-S2-EB featured three stages prior to

retrofitting. In the first phase, no strain was recorded until initiation of shear cracks at approximately 60 kN followed by a sudden increase in the stirrups strain. In the second stage, the strain continued to increase as the load progressed until yielding of stirrups which started at approximately 120 kN. In the third stage, the specimen exhibited no further increase in strain till the specimen reached its peak load possibly because of slippage of stirrups. After retrofitting, the strain increased from the beginning of the test in a linear fashion till yielding of stirrups which took place at approximately 130 kN. The specimen reached its peak load, 136 kN, shortly after yielding of stirrups. The rate of increase of stirrups strain before and after retrofitting was almost the same. This explains why the EB-CFRP system without the MA was not able to restore the shear resistance of the specimen recorded in the first shear test. The stirrups strain response for specimen D2-S2-EB+MA featured three phases in the first shear test (i.e. prior to retrofitting). In the first phase, no strain was recorded up to a load value of approximately 40 kN, where shear cracks were initiated. In the second phase, the strain increased linearly as the load progressed until yielding of stirrups which started at approximately 120 kN. After yielding of stirrups, a plastic stirrups strain response took place followed by a reduction in strain for a short fourth stage. Subsequent to retrofitting, the specimen featured a linear stirrups strain response till yielding of stirrups occurred at approximately 150 kN followed by no increase in the stirrups strain until the load reached a value of 160 kN where a plastic strain response took place. The stirrups strain response for specimen D2-S2-ETD featured three stages prior to retrofitting. In the first stage, no strain was recorded till initiation of shear cracks at approximately 50 kN. After shear cracking, the strain

continued to rise as the load progressed till yielding of stirrups which started at approximately 120 kN. In the last phase, no further increase in the strain was found possibly because of slippage of stirrups. After retrofitting, in the second shear test to failure, the specimen exhibited a prompt stirrups contribution from the beginning of the test. The stirrups strain increased almost at a constant rate till yielding of stirrups which occurred at approximately 170 kN. This was followed by a plastic stirrups strain response.

4.2.3.2.7 FRP strain response

The FRP strain responses for the retrofitted specimens of group [B] with the damage state D2 are shown in Figure 4.75. The effective FRP strain values are reported in Table 4.6. It should be noted that the maximum measured FRP strain is not necessarily the maximum absolute FRP strain experienced by the specimen. There was no pre-cracking stage in all specimens because the specimens were already cracked in the first shear test. The FRP reinforcement started to contribute to the shear resistance from the beginning of the test. For specimen D2-S2-EB, the CFRP strain increased gradually until the specimen reached a load value of 60 kN, where opening of pre-existing shear cracks and initial debonding of the CFRP sheets took place. Then, the load continued to increase with insignificant increase in the CFRP strain until the specimen reached a load value of approximately 90 kN at a corresponding effective FRP strain of 2696 $\mu\epsilon$. Then, the FRP strain decreased as the load progressed due to progressive debonding of the CFRP sheets. The FRP strain in specimen D2-S2-EB+MA increased gently until the specimen reached a load value of 60 kN where opening of pre-existing shear cracks took place. The FRP strain continued, however, to increase since the MA system prevented the early

debonding of the CFRP sheets. At a load value of approximately 110 kN, the FRP strain started to decrease as the load progressed possibly due to local debonding of the CFRP sheets until the specimen reached a load value of 160 kN where the CFRP started to increase again. The specimen reached its peak load at an effective CFRP strain of 3403 $\mu\epsilon$. Specimen D2-S2-ETD featured the highest rate of FRP strain increase among the retrofitted specimens. The FRP strain increased gradually in specimen D2-S2-ETD until it reached a load value of approximately 40 kN where opening of pre-existing cracks took place. Then, the FRP strain continued to increase at almost a constant rate until yielding of stirrups which took place at approximately 170 kN. Following yielding of stirrups, the FRP strain increased rapidly at a higher rate until the specimen reached its peak load, 185 kN, at a corresponding effective GFRP strain of 10155 $\mu\epsilon$.

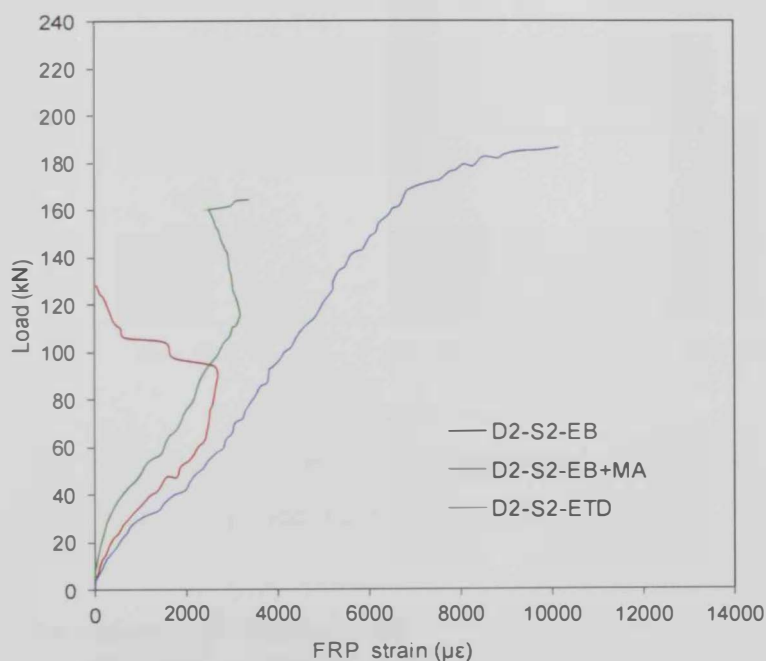


Figure 4.75: Load-FRP strain relationships for specimens of group [C] with damage state D2

4.3 Analysis of test results and discussion

In this section, the effects of varying the strengthening/retrofitting system, amount of internal stirrups, and shear damage state prior to retrofitting on the shear strength gain are analyzed and discussed.

4.3.1 Performance evaluation of the non-damaged specimens

For the specimens that were not damaged prior to strengthening, the shear strength gain was dependent of the strengthening system used in strengthening and presence/amount of internal steel stirrups. The interaction between the strengthening system, amount of internal steel stirrups and shear strength gain is demonstrated in Figure 4.76.

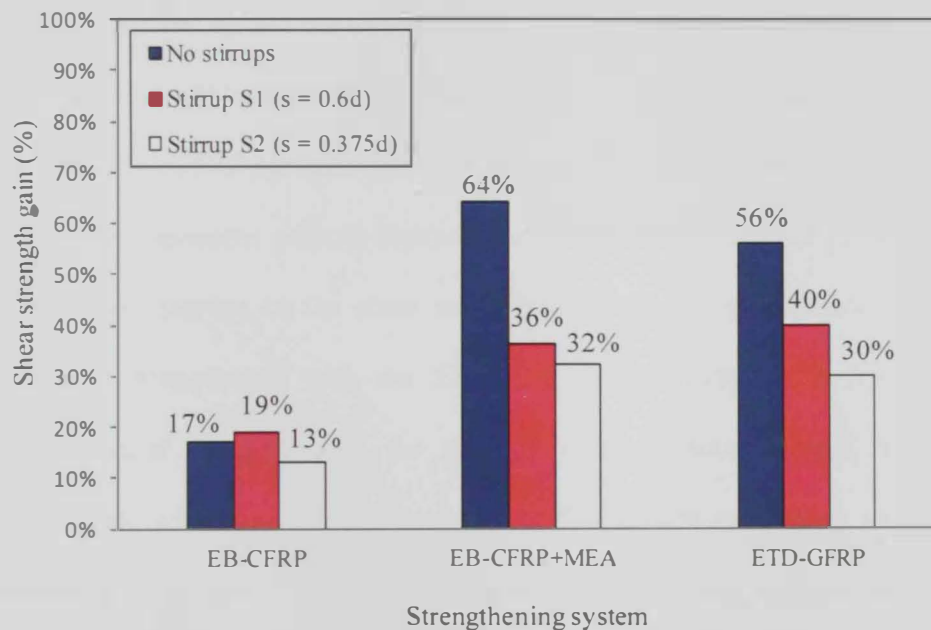


Figure 4.76: Interaction between strengthening system, amount of internal steel stirrups and shear strength gain

4.3.1.1 Effect of strengthening system

Figure 4.76 demonstrates that the EB-CFRP system without the MA was less effective in improving the shear resistance than the EB-CFRP system with the

MA and the ETD-GFRP system. In the absence of steel stirrups, the integration of the MA in the EB-CFRP system increased the shear strength gain from 17% to 64% (i.e. the inclusion of the MA resulted in a 3.8-fold increase in the shear strength gain). For the specimens with the internal steel stirrups, the inclusion of the MA in the EB-CFRP system resulted in approximately a two-fold increase in the shear resistance. The shear strength gain caused by the ETD-GFRP system was comparable to that caused by the EB-CFRP system integrated with the MA.

4.3.1.2 Effect of amount of internal stirrups

Generally, the shear strength gain decreased as the amount of internal steel stirrups increased as demonstrated in Figure 4.76. The shear strength gains of the specimens with internal steel stirrups strengthened with the EB-CFRP+MA and the ETD-GFRP systems were on average 42% lower than those of their counterpart specimens without internal steel stirrups. The effect of presence of internal steel stirrups on the shear strength gain was less pronounced for the specimens strengthened with the EB-CFRP system without the MA. The reduced shear strength gain for the specimen without internal stirrups strengthened with the EB-CFRP without the MA can be ascribed to the early debonding of the CFRP sheets caused by the rapid widening and growth of the developed shear cracks in the absence of any internal steel stirrups.

The shear strength gain decreased as the amount of the internal steel stirrups increased. For the specimens strengthened with the EB-CFRP system without the MA, decreasing the stirrups spacing from $s_1 = 0.6d$ to $s_2 = 0.375d$ resulted in approximately a 30% reduction in the shear strength gain. For the specimens strengthened with the EB-CFRP+MA and the ETD-GFRP systems, decreasing

the spacing between stirrups decreased the shear strength gain by 11 and 25%, respectively.

4.3.2 Performance evaluation of the pre-damaged specimens

For the specimens that were shear-damaged prior to retrofitting, the shear strength gain was dependent of the initial shear damage state and the retrofitting system used to upgrade the shear capacity.

4.3.2.1 Effect of initial shear damage

4.3.2.1.1 Specimens with the lower amount of stirrups

The effect of the initial shear damage on the shear strength gain of the specimens with the lower amount of stirrups is demonstrated in Figure 4.77. The initial shear damage D1 (i.e. pre-cracking) reduced the shear strength gain in all specimens. The reduction in shear strength gain was dependent of the retrofitting system. The reduction in the shear strength gain caused by the pre-cracking was a maximum for the specimen retrofitted with the ETD-GFRP system, 72.5%, and a minimum, 25%, for the specimen retrofitted with the EB-CFRP+MA. The pre-cracking reduced the shear strength gain of the specimen retrofitted with the EB-CFRP without the MA by approximately 42%.

The shear strength gain further reduced as the severity of the initial shear damage increased to shear damage D2 (pre-failure) for the specimens retrofitted with the EB-CFRP system without the MA and the specimen retrofitted with the ETD-GFRP system. No shear strength gain was recorded for the pre-failed specimen retrofitted with the EB-CFRP system without the MA. A negligible shear strength gain of 8% was recorded for the pre-failed specimen retrofitted with the ETD-GFRP system. There is one anomaly result

for the specimen with the damage state D2 retrofitted with the EB-CFRP+MA, which had a shear strength gain higher than that of their counterpart specimens with no damage or damage state D1. This anomaly result can be ascribed to the reduced shear resistance of this particular specimen recorded in the first shear test prior to retrofitting, 94.4 kN, that was below the average value, 112 kN, of its counterparts (refer to Table 4.4—specimen D2-S1-EB+MA). The shear strength gain typically increases as the initial shear resistance prior to retrofitting decreases.

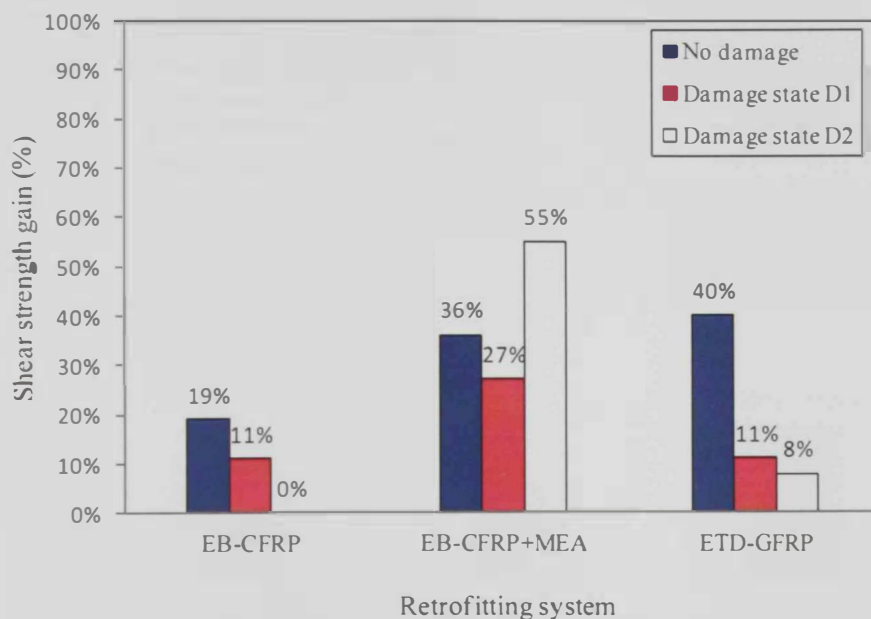


Figure 4.77: Effect of initial shear damage on shear strength gain of the specimens with the lower amount of stirrups

Based on the results presented in Figure 4.77, it is not recommended to use neither the EB-CFRP system without the MA nor the ETD-GFRP system to retrofit pre-damaged T-girders containing low amount of internal steel stirrups. The presence of initial shear damage prompted early debonding of the CFRP and hence no or minimal shear strength gain was recorded for the specimens retrofitted with the EB-CFRP system without the MA. It seems also that

drilling of holes in the pre-cracked/pre-failed specimens for the ETD-GFRP system aggravated the initial shear damage, and hence no appreciable shear strength gain was recorded. The EB-CFRP system integrated with the MA was the only retrofitting solution that was successful in upgrading the shear resistance of these specimens, with a noticeable shear strength gain.

4.3.2.1.2 Specimens with the higher amount of stirrups

The effect of the initial shear damage D2 on the shear strength gain of the specimens with the higher amount of stirrups is demonstrated in Figure 4.78.

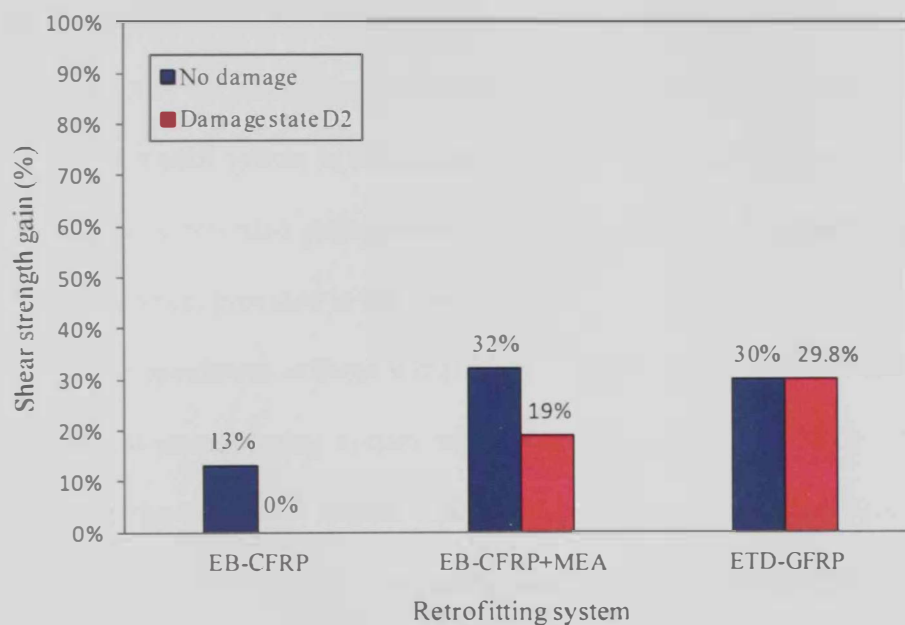


Figure 4.78: Effect of shear damage D2 on shear strength gain of the specimens with the higher amount of stirrups

The EB-CFRP system without the MA was not successful in retrofitting the pre-failed specimen (i.e. with the initial shear damage D2), since no shear strength gain was recorded. This is obviously because of the early debonding of the EB-CFRP sheets. For the specimen retrofitted with the EB-CFRP system integrated with the MA, the initial shear damage D2 resulted in approximately

41% reduction in the shear strength gain. Nevertheless, the EB-CFRP system integrated with the MA was able to increase the shear resistance of the pre-failed specimen by 19%. The shear strength gain provided by the ETD-GFRP system was not affected by the initial shear damage D2. This indicates that in the presence of high amount of internal stirrups, the ETD-GFRP system still can result in a considerable increase in the shear resistance of the pre-damaged T-girders.

4.4 Efficiency of the strengthening/retrofitting systems

Table 4.7 compares the efficiencies of the composite-based systems adopted in the present study for strengthening/retrofitting of test specimens. The efficiency factor (EF) for each system is defined as the ratio of the contribution of FRP to shear resistance recorded experimentally, $V_{f,exp}$, to the tensile strength of all FRP reinforcement provided in the shear span.

For the specimens without initial shear damage, the ETD-GFRP was the most efficient strengthening system with EF in the range of 12.7% to 15.6% followed by the EB-CFRP system with MA having EF in the range 10.4% to 11.7%. The EB-CFRP without MA was the least efficient system with EF in the range of 3.2% to 5.5%.

For the pre-cracked and pre-failed specimens with limited amount of stirrups, the EB-CFRP with MA was the most efficient system with EF in the range of 8.1% to 12.5%. The EFs of the ETD-GFRP system when used in retrofitting pre-cracked and pre-failed specimens with limited amount of stirrups were 4.2% and 2.8%, respectively. The EB-CFRP system without MA was not effective in retrofitting pre-cracked or pre-failed specimens regardless of the amount of internal steel stirrups.

For the pre-failed specimens with considerable amount of stirrups, the ETD-GFRP system was the most efficient retrofitting solution with EF of 12.1% compared to EF of 5.6% for the EB-CFRP with MA. The EB-CFRP system without MA was not successful in retrofitting pre-failed specimens, even in the presence of considerable amount of internal stirrups.

Table 4.7: Efficiency of the strengthening systems

Damage state prior to retrofitting	Specimen Designation	Total cross section area of FRP in shear span N^*A_f (mm ²)	Tensile strength of FRP reinforcement in shear span (TS) (kN)	$V_{f,exp}$ (kN)	Efficiency Factor (EF) ^a (%)
No damage	ND-NS-EB	108.8	375.4	12	3.2
	ND-NS-EB+MA	108.8	375.4	44	11.7
	ND-NS-ETD	314.2	282.7	38.4	13.6
	ND-S1-EB	108.8	375.4	20.8	5.5
	ND-S1-EB+MA	108.8	375.4	39.2	10.4
	ND-S1-ETD	314.2	282.7	44	15.6
	ND-S2-EB	108.8	375.4	16	4.3
	ND-S2-EB+MA	108.8	375.4	39.2	10.4
	ND-S2-ETD	314.2	282.7	36	12.7
Pre-cracked	D1-S1-EB	108.8	375.4	12	3.2
	D1-S1-EB+MA	108.8	375.4	30.4	8.1
	D1-S1-ETD	314.2	282.7	12	4.2
Pre-failed	D2-S1-EB	108.8	375.4	0	0.0
	D2-S1-EB+MA	108.8	375.4	4.7	12.5
	D2-S1-ETD	314.2	282.7	7.8	2.8
	D2-S2-EB	108.8	375.4	0	0.0
	D2-S2-EB+MA	108.8	375.4	21.1	5.6
	D2-S2-ETD	314.2	282.7	34.2	12.1

CHAPTER 5: ANALYTICAL INVESTIGATION

5.1 Introduction

This chapter presents a summary of design equations adopted by existing international guidelines/standards for prediction of the contribution of EB-CFRP reinforcement to shear resistance. Analytical models published recently in the literature that take into account the interaction between internal steel stirrups and external EB-CFRP reinforcement are also presented and reviewed in this chapter. The contribution of the ETD-GFRP system to shear resistance has been calculated based on analytical procedure published recently in the literature. The accuracy and validity of the analytical approaches published in the literature and/or recommended by international guidelines/standards have been examined.

5.2 Shear resistance of the EB-CFRP system

5.2.1 International guidelines/ standards for EB-CFRP resistance

The analytical models recommended by five different international guidelines/standards namely; the American ACI 440.2R (2008), European fib TG 9.3 (2001), Italian CNR-DT200 (2004), Australian HB 305 (2008), and the Japanese JSCE (2001), to calculate the design shear resistance of the EB-CRP reinforcement, V_{fd} are reviewed in this section. The fib TG 9.3 (2001) analytical approach is mainly based on the analytical model introduced previously by Triantafillou and Antonopoulos (2000). The HB 305 analytical approach is based on the analytical model developed by Chen and Teng (2003).

The nominal shear resistance of the EB-CFRP reinforcement, V_{fn} , predicted by these international guidelines/standards has also been calculated by considering all safety factors (i.e. strength reduction factors and materials factors) equal to 1. For the EB-CFRP without MA, the equations specified for the U-wrap configurations have been adopted. The equations specified for the full-wrapping configurations have been used to calculate the shear resistance of the EB-CFRP reinforcement with MA. It should be noted that analytical approach specified by the Canadian Standards Association CSA S806-02 is not valid for EB-CFRP reinforcement with a debonding mode of failure, and hence can not be used to predict the contribution of CFRP to shear resistance of test specimens without MA. For RC beams retrofitted with U-shaped CFRP wraps having sufficient bond length and/or anchorage, the CSA S806-02 specifies a value of 0.004 for the effective CFRP strain, ϵ_{fe} , which is the same value specified by the ACI 440.2R (2008) for the full-wraps configuration (adopted in this study for the specimens with MA). As such, the nominal CFRP shear resistance predicted by the CSA S806-02 for test specimens retrofitted by EB-CFRP with MA would be a replicate of that predicted by the ACI 440.2R (2008).

5.2.1.1 ACI 440.2R (2008)

The ACI 440.2R-08 (2008) adopted Equation 5.1 to calculate the design shear resistance of the EB-CFRP, V_{fd} , as follows :

$$V_{fd} = \phi \Psi \frac{A_f E_f \epsilon_{fe} d_f (\sin \alpha + \cos \alpha)}{s_f} \quad (5.1)$$

$$\phi = 0.75$$

For U-wraps

$$\Psi = 0.85$$

$$\varepsilon_{fe} = \kappa_v \varepsilon_{fu} \leq 0.004 \quad (5.2)$$

$$\kappa_v = \frac{\kappa_1 \kappa_2 L_e}{11900 \varepsilon_{fu}} \leq 0.75 \quad (5.3)$$

$$L_e = \frac{23300}{(t_f E_f)^{0.58}} \leq d_f \quad (5.4)$$

$$\kappa_1 = \left(\frac{f'_c}{27} \right)^{0.67} \quad (5.5)$$

$$\kappa_2 = \left(\frac{d_f - L_e}{d_f} \right) \quad (5.6)$$

For full-wrapping

$$\Psi = 0.95$$

$$\varepsilon_{fe} = 0.004 \leq 0.75 \varepsilon_{fu} \quad (5.7)$$

5.2.1.2 *fib* TG 9.3 (2001)

The *fib* TG 9.3 (2001) adopted Equation 5.8 to calculate the design shear resistance of the EB-CFRP, V_{fd} , as follows :

$$V_{fd} = 0.9 \frac{\kappa \varepsilon_{fe}}{\gamma_f} E_f \rho_f b_w d (\cot \theta + \cot \alpha) \sin \alpha \quad (5.8)$$

$$\rho_f = \frac{A_f}{b_w s_f} \quad (5.9)$$

For U-shaped wraps:

$$\varepsilon_{fe} = \min \left\{ \begin{array}{l} 0.17 \left(\frac{f'_c}{E_f \times 10^{-3} \rho_f} \right)^{0.67} \varepsilon_{fu} \\ 0.65 \left(\frac{f'_c}{E_f \times 10^{-3} \rho_f} \right)^{0.56} \times 10^{-3} \end{array} \right. \quad (5.10)$$

$$\varepsilon_{fe} \leq 0.006$$

$$\gamma_f = 1.3$$

For full-wrapping/properly anchored CFRP

$$\varepsilon_{fe} = 0.17 \left(\frac{f_c^{2/3}}{E_f \times 10^{-3} \rho_f} \right)^{0.67} \varepsilon_{fu} \quad (5.11)$$

$$\varepsilon_{fe} \leq 0.006$$

$$\gamma_f = 1.2$$

5.2.1.3 CNR-DT200 (2004)

The CNR-DT200 (2004) adopted Equation 5.12 to calculate the design shear resistance of the EB-CFRP, V_{fd} , as follows :

$$V_{fd} = \frac{0.9}{\gamma_{Rd}} \frac{A_f f_{fed} d (\cot\theta + \cot\alpha)}{s'_f} \quad (5.12)$$

$$\gamma_{Rd} = 1.2$$

For U-wraps

$$f_{fed} = f_{fdd} \left(1 - \frac{1}{3} \frac{L_e \sin\alpha}{\min\{0.9d; h_w\}} \right) \quad (5.13)$$

$$L_e = \sqrt{\frac{E_f t_f}{2 f_{ctm}}} ; \quad f_{fdd} = \frac{0.8}{\gamma_{fd}} \sqrt{\frac{2 E_f G_{fk}}{t_f}} \quad (5.14)$$

$$\gamma_{fd} = 1.2$$

$$G_{fk} = 0.03 \kappa_b \sqrt{f'_c f_{ctm}} ; \quad \kappa_b = \sqrt{\frac{2 - \frac{w_f}{s_f \sin\alpha}}{1 + \frac{w_f}{400}}} \geq 1 ; \quad \frac{w_f}{s_f \sin\alpha} \geq 0.33 \quad (5.15)$$

$$f_{ctm} = 0.3 (f'_c)^{2/3} \quad (5.16)$$

For full-wrapping:

$$f_{fed} = f_{fdd} \left(1 - \frac{1}{6} \frac{L_e \sin \alpha}{\min \{0.9d; h_w\}} \right) + \frac{1}{2} \left(\Phi_R f_{fd} - f_{fdd} \right) \left(1 - \frac{L_e \sin \alpha}{\min \{0.9d; h_w\}} \right) \quad (5.17)$$

$$f_{fd} = f_{fu} / \gamma_f \quad (5.18)$$

$$\Phi_R = 0.2 + 1.6 \frac{r_w}{b_w} ; \quad 0 \leq \frac{r_w}{b_w} \leq 0.5 \quad (5.19)$$

$$\gamma_f = 1.1$$

5.2.1.4 HB 305 (2008)

The HB 305 (2008) adopted Equation 5.20 to calculate the design shear resistance of the EB-CFRP, V_{fd} , as follows :

$$V_{fd} = \frac{\phi A_f f_{fe} h_{fe} (\sin \alpha + \cos \alpha)}{s_f} \quad (5.20)$$

$$h_{fe} = z_b - z_t ; \quad z_b = 0.9d - d_{fb} ; \quad z_t = d_{ft}$$

$$f_{fe} = D_f \sigma_{f,max} \quad (5.21)$$

$$\phi = 0.7$$

For U- wraps:

$$D_f = \begin{cases} \frac{2}{\pi \lambda} \frac{1 - \cos(\frac{\pi \lambda}{2})}{\sin(\frac{\pi \lambda}{2})} & \lambda \leq 1 \\ 1 - \frac{\pi - 2}{\pi \lambda} & \lambda > 1 \end{cases} \quad (5.22)$$

$$\lambda = \frac{L_{max}}{L_e} ; \quad L_{max} = \frac{h_{fe}}{\sin \alpha} ; \quad L_e = \sqrt{\frac{E_f t_f}{\sqrt{f'_c}}} \quad (5.23)$$

$$\sigma_{f,max} = \min \left\{ \begin{array}{l} 0.8 f_{fu} \\ 0.315 \beta_w \sqrt{\frac{E_f \sqrt{f'_c}}{t_f}} \end{array} \right. \quad (5.24)$$

$$\beta_w = \sqrt{\frac{2 - \frac{w_f}{s_f \sin \alpha}}{1 + \frac{w_f}{s_f \sin \alpha}}} \quad (5.25)$$

For full wrapping:

$$D_f = 0.5 \left[1 + \left(\frac{z_t}{z_b} \right) \right] \quad (5.26)$$

$$\sigma_{f,max} = \min \left\{ \begin{array}{ll} 0.8 f_{fu}, & \varepsilon_{fu} \leq \varepsilon_{max} \\ 0.8 E_f \varepsilon_{max}, & \varepsilon_{fu} > \varepsilon_{max} \end{array} \right. \quad (5.27)$$

$$\varepsilon_{max} = 1.5\%$$

5.3.1.5 JSCE (2001)

The JSCE (2001) adopted Equation 5.28 to calculate the design shear resistance of the EB-CFRP, V_{fd} , as follows :

$$V_{fd} = K \left[\frac{A_f f_{fud} (\sin \alpha + \cos \alpha)}{s_f} \right] \left(\frac{z}{\gamma_b} \right) \quad (5.28)$$

$$z = d/1.15$$

$$0.4 \leq K = 1.68 - 0.67R \leq 0.8$$

$$\gamma_b = 1.25$$

$$R = \left(\rho_f E_f \times 10^{-3} \right)^{1/4} \left[\frac{f_{fud}}{E_f \times 10^{-3}} \right]^{2/3} \left[\frac{1}{f'_{cd}} \right]^{1/3} \quad (5.29)$$

$$f_{fud} = f_{fu} / \gamma_m \quad (5.30)$$

$$\gamma_m = 1.2 - 1.3 \text{ (taken as 1.25)}$$

$$0.5 \leq R \leq 2.0$$

$$\rho_f = \frac{A_f}{b_w s_f} \quad (5.31)$$

$$f'_{cd} = \frac{f'_c}{\gamma_c} \quad (5.32)$$

$$\gamma_c = \begin{cases} 1.3 & f'_c < 50 \text{ MPa} \\ 1.5 & f'_c \geq 50 \text{ MPa} \end{cases}$$

The JSCE (2001) equations are valid only for fully wrapped/properly anchored FRP laminates.

5.3.2 Recent analytical models for EB-CFRP shear resistance

The analytical approach adopted by existing guidelines/standards do not take into consideration the interaction between the internal steel stirrups and EB-CRP shear reinforcement. This section reviews two analytical models published recently in the literature that can predict the nominal shear resistance of the EB-CRP system, V_{fn} , considering the effect of internal steel stirrups.

5.3.2.1 Mofidi and Chaallal (2011) analytical model

The contribution of the EB-CFRP to shear, V_{fn} , is calculated using the following equations. The model takes into consideration the effects of internal steel stirrups and strip width-to-spacing ratio on the CFRP shear resistance through the factors β_c and k_f , respectively. The model is, however, not valid for RC members strengthened with a full-wrap configuration.

$$V_{fn} = \frac{2 t_f w_f \varepsilon_{fe} E_f d_f (\cot \theta + \cot \alpha) \cdot \sin \alpha}{s_f} (k_f) \quad (5.33)$$

$$\varepsilon_{fe} = 0.31 \beta_c \beta_l \beta_w \sqrt{\frac{f'_c}{t_f E_f}} \leq \varepsilon_{fu} \quad (5.34)$$

$$\beta_c = \frac{0.6}{\sqrt{\rho_f E_f + \rho_s E_s}} \quad (5.35)$$

$$\beta_L = \begin{cases} 1 & \text{if } \lambda \geq 1 \\ (2-\lambda).\lambda & \text{if } \lambda < 1 \end{cases}$$

$$\beta_w = \sqrt{\frac{2 - \frac{w_f}{s_f}}{1 + \frac{w_f}{s_f}}} ; \quad \lambda = \frac{L_{max}}{L_e} \quad (5.36)$$

$$L_e = \sqrt{\frac{E_f t_f}{2f_{ct}}} \quad (mm); \quad f_{ct} = 0.53 \sqrt{f'_c} \quad (5.37)$$

Where E_f and E_s are in GPa.

$$k_f = \frac{1 + \left(\frac{w_f}{s_f} - \frac{1}{2}\right)^2}{1 - \left(\frac{w_f}{s_f} - \frac{1}{2}\right)^2} \quad (5.38)$$

5.3.2.2 Chen et al. (2013) analytical model

This model takes into consideration the interaction between the internal steel shear reinforcement (stirrups) and the external FRP shear reinforcement through a shear interaction factor “ K ”. The general expression of V_{fn} is given as:

$$V_{fn} = 2f_{f,e} t_f w_f \frac{h_{f,e}(\cot \theta + \cot \alpha) \sin \alpha}{s_f} (K) \quad (5.39)$$

$$f_{f,e} = \sigma_{f,max} D_{frp} \quad (5.40)$$

$$\sigma_{f,max} = \min \left\{ \begin{array}{l} f_{fu} \\ \sigma_{db,max} \end{array} \right.$$

$$\sigma_{db,max} = \begin{cases} \sqrt{\frac{2 E_f G_f}{t_f}} & L_{max} \geq L_e \\ \sin\left(\frac{\pi}{2} \cdot \frac{L_{max}}{L_e}\right) \sqrt{\frac{2 E_f G_f}{t_f}} & L_{max} < L_e \end{cases} \quad (5.41)$$

For U strips

$$L_{max} = \frac{L_v}{\sin \beta} \quad (5.42)$$

$$D_{frp} = 1 - \left(1 - \frac{\pi}{4}\right) \cdot \frac{h_{df}}{h_{f,e}} \quad (5.43)$$

$$h_{df} = 2\delta_f \cdot \frac{h_{f,e}}{w_{e,p} \sin(\theta + \alpha)} \quad (5.44)$$

$$w_{e,p} = \delta_f \cdot \frac{1 + \frac{\pi}{2} \left(\frac{h_{f,e}}{L_e \sin \alpha} - 1\right)}{\sin(\theta + \alpha)} \quad (5.45)$$

$$L_e = \frac{\pi}{2} \sqrt{\frac{E_f t_f \delta_f}{\tau_f}} \quad (5.46)$$

$$\delta_f = \frac{2G_f}{\tau_f} \quad (5.47)$$

$$G_f = 0.308 \beta_w^2 \sqrt{f_t} \quad (5.48)$$

$$\tau_f = 1.5 \beta_w f_t \quad (5.49)$$

$$\beta_w = \sqrt{\frac{2 - w_f / (s_f \sin \beta)}{1 + w_f / (s_f \sin \beta)}} \quad (5.50)$$

$$f_t = 0.395 f_{cu}^{0.55} \quad (5.51)$$

$$f_{cu} = f'_c / 0.8 \quad (5.52)$$

The factor "K" is given by:

$$K = 1 - \mu \cdot (1 - K_s) \quad (5.53)$$

$$\mu = \frac{f_y A_{sv}}{f_{f,e} A_{frp}} \quad (5.54)$$

$$K_s = \frac{w_{e,p}^{1.4}}{z + w_{e,p}^{1.4}} \quad (5.55)$$

$$z = A / (\cos \theta)^{1.4} \quad (5.56)$$

$$A = \frac{1.48 [\ln(h_{fe}) - 4.52] (f_y - 173) (\phi_s + 0.935)}{10000} \quad (5.57)$$

ϕ_s = diameter of stirrup

5.3 Shear resistance of the ETD-GFRP system

5.3.1 Mofidi et al. (2012) analytical model

Mofidi et.al (2012) introduced an analytical model to calculate the nominal shear resistance of the ETD-FRP system. The contribution of ETD-GFRP rebars to shear capacity can be calculated using the following equations:

$$V_{fn} = k_L \cdot k_s \frac{A_f E_f \varepsilon_{frp} d_f (\sin \alpha + \cos \alpha)}{s_f} \quad (5.58)$$

$$k_L = \begin{pmatrix} 1 & \frac{d_f}{2} \geq L_{eff}(s_m) \\ \frac{d_f}{\sqrt{\frac{E_f D_{frp}}{2} \cdot \frac{s_m}{\tau_m} \cdot \frac{1 + \alpha'}{(1 - \alpha')^2}}} & \frac{d_f}{2} < L_{eff}(s_m) \end{pmatrix} \quad (5.59)$$

$$d_f = \text{greater of } \begin{cases} 0.72 h \\ 0.9 d \end{cases}$$

$$L_{eff}(s_m) = \frac{f(s_m) \cdot D_{frp}}{4 \tau_m} \cdot \frac{1 + \alpha'}{1 - \alpha'} \quad (5.60)$$

$$f(s_m) = \sqrt{\frac{8 E_f \tau_m \cdot s_m}{D_{frp} \cdot (1 + \alpha')}} \quad (5.61)$$

$$\varepsilon_{frp} = \frac{8}{D_{frp} \cdot E_f} \left(\frac{\tau_m \cdot s_m}{1 + \alpha'} \right) \leq 0.004 \quad (5.62)$$

k_s is set to 0.6 if the stirrups spacing is less than $2d/3$, and is set to 1 if there are no stirrups or stirrups are spaced greater than or equal to $2d/3$. In the previous equations, τ_m = maximum bond stress between ETD-GFRP rod and concrete, s_m = slip of the ETD-GFRP rod at maximum bond stress, α' = bond-slip curve

fitting parameter. The bond parameters τ_m , s_m , and α' for the ETD-GFRP rebars are not currently available. In the present study, the bond parameters of $\tau_m = 8.4$ MPa, $s_m = 0.08$ mm, and $\alpha' = 0.09$ derived by Mofidi et al. (2012) for sand-coated ETD-CFRP rebars and also the parameters of $\tau_m = 9.5$ MPa, $s_m = 0.2$ mm, and $\alpha' = 0.3$ derived by De Lorenzis (2004) for NSM-GFRP rebars have been adopted and examined.

5.4 Maximum shear resistance

The code provisions limit the shear resistance of RC beams to a maximum value representing crushing of web struts. The equations adopted by the ACI 318-08 (2008), Eurocode 2- 2004, CNR-DT200 (2004), AS 3600 (2001), and JSCE (2007) for calculation of the maximum design shear strength of RC beams, $V_{d,max}$ are reviewed in this section. The maximum design shear resistance provided by CFRP, $V_{fd,max}$, is given by:

$$V_{fd,max} = V_{d,max} - V_{cd} - V_{sd} \quad (5.63)$$

Where $V_{d,max}$ = maximum design shear strength of the concrete member

V_{cd} = design shear resistance of concrete

V_{sd} = design shear resistance of stirrups

ACI 318-08 (2008)

$$V_{d,max} = \frac{5}{6} \sqrt{f'_c} b_w d \phi \quad (5.64)$$

$$V_{cd} = \frac{1}{6} \sqrt{f'_c} b_w d \phi \quad (5.65)$$

$$V_{sd} = \frac{A_v f_y d}{s} \phi \quad (5.66)$$

$$\phi = 0.75$$

Eurocode 2-2004

$$V_{d,max} = \frac{v_l f_c'}{\gamma_c} \frac{b_w (0.9)d}{(\cot\theta + \tan\theta)} \quad (5.67)$$

$$V_{cd} = \frac{[0.18 \kappa (100\rho f_c')^{1.3}] b_w d}{\gamma_c} \quad (5.68)$$

$$V_{sd} = \frac{A_v f_y (0.9d)}{(\gamma_s) s} \quad (5.69)$$

$$v_l = 0.6 \left[1 - \frac{f_c'}{250} \right] ; \kappa = 1 + \sqrt{\frac{200}{d}} \leq 2 ; \rho = \frac{A_s}{b_w d} \leq 0.02$$

$$\gamma_c = 1.5 ; \gamma_s = 1.15$$

CNR-DT200 (2004)

$$V_{d,max} = 0.3 f_{cd} b_w d \quad (5.70)$$

$$V_{cd} = 0.6 f_{ctd} b_w d \quad (5.71)$$

$$V_{sd} = \frac{A_v f_y (0.9d)}{(\gamma_s) s} \quad (5.72)$$

$$f_{cd} = \frac{f_c'}{\gamma_c} ; f_{ctd} = 0.7 \frac{f_{ctm}}{\gamma_c} ; f_{ctm} = 0.3 (f_c')^{\frac{2}{3}} \quad (5.73)$$

$$\gamma_c = 1.6 ; \gamma_s = 1.15$$

AS 3600 (2001)

$$V_{d,max} = 0.2 f_c' b_w d \phi \quad (5.74)$$

$$V_{cd} = \beta_I b_w d \left(\frac{A_s f_c'}{b_w d} \right)^{\frac{1}{3}} \phi \quad (5.75)$$

$$V_{sd} = \frac{A_v f_y d \cot\theta}{s} \phi \quad (5.76)$$

$$\phi = 0.7$$

$$\beta_1 = 1.1 \left[1.6 - \frac{d}{1000} \right] \geq 1.1 \quad (5.77)$$

JSCE (2007)

$$V_{d,max} = \frac{f_{wcd} b_w d}{\gamma_b} \quad (5.78)$$

$$V_{cd} = \frac{\beta_p \beta_d f_{wcd} b_w d}{\gamma_b} \quad (5.79)$$

$$V_{sd} = \frac{A_v \frac{f_y}{\gamma_s} \left(\frac{z}{s} \right)}{\gamma_{bs}} \quad (5.80)$$

$$f_{wcd} = 1.25 \sqrt{f'_{cd}} \leq 7.8 ; f'_{cd} = \frac{f'_c}{\gamma_c} ; \beta_p = (100\rho)^{\frac{1}{3}} ; \beta_d = \left(\frac{1000}{d} \right)^{\frac{1}{4}} \leq 1.5$$

$$f_{vcd} = 0.2 \left(\frac{f'_c}{\gamma_c} \right)^{\frac{1}{3}} \leq 0.72 ; z = \frac{d}{1.15}$$

$$\gamma_c = 1.3 ; \quad \gamma_b = 1.3 ; \quad \gamma_{bs} = 1.1 , \gamma_s = 1.05$$

The summary of $V_{fd,max}$ and $V_{fn,max}$ values for the previously discussed guidelines/standards are shown in Tables 5.1 and 5.2, respectively. The nominal maximum FRP shear resistance is calculated by setting all safety factors (i.e. materials factors or strength reduction factors) equal to 1.

Table 5.1: The values of $V_{fd,max}$ based on the guidelines/standards

Standards/guidelines	$V_{fd,max}$ (kN)		
	Specimens with no stirrups	Specimens with stirrups spacing $s_1 = 0.6d$	Specimens with stirrups spacing $s_2 = 0.375d$
ACI 318-08 (2008)	68.9	45.4	31.3
Eurocode 2-2004	96.6	72.0	57.3
CNR-DT200 (2004)	123.3	98.8	84.0
AS 3600 (2001)	73.3	51.4	38.2
JSCE (2007)	86.2	62.6	48.4

Table 5.2: The values of $V_{fn,max}$ based on the guidelines/standards

Standards/guidelines	$V_{fn,max}$ (kN)		
	Specimens with no stirrups	Specimens with stirrups spacing $s_1 = 0.6d$	Specimens with stirrups spacing $s_2 = 0.375d$
ACI 318-08 (2008)	91.9	60.5	41.7
Eurocode 2-2004	144.9	116.6	99.7
CNR-DT200 (2004)	197.3	169.1	152.1
AS 3600 (2001)	104.7	73.4	54.5
JSCE (2007)	129.7	102.4	86.0

5.5. Comparative analysis for specimen's strengthened with EB-CFRP system

A comparative analysis between the analytical and experimental results concerning the contribution of the EB-CFRP reinforcement to shear resistance is presented and discussed in this section.

5.5.1. Accuracy of international guidelines/standards

Predictions of international guidelines/standards for the contribution of the EB-CFRP reinforcement to shear resistance are given in Table 5.3. The ratios of predicted to experimental EB-CFRP shear resistance are given in Table 5.4. The analytical predictions are also plotted versus the experimental values of the non-damaged, pre-cracked, and pre-failed specimens in Figures 5.1, 5.2, and 5.3, respectively.

Table 5.3: Guidelines/predictions or EB-CFRP shear resistance

Damage state prior to retrofitting	Specimen	Exp.	Analytical Results (V_{fn}) kN ^a					Analytical Results (V_{fd}) kN ^b				
			$V_{f,exp}$	ACI 440	fib TG 9.3	CNR-DT200	HB 305	JSCE 2001	ACI 440	fib TG 9.3	CNR-DT200	HB 305
No Damage	ND-NS-EB	12.0	23.9	35.6	24.9	17.3	-	15.2	21.9	17.3	12.1	-
	ND-S1-EB	20.8	23.9	35.6	24.9	17.3	-	15.2	21.9	17.3	12.1	-
	ND-S2-EB	16.0	23.9	35.6	24.9	17.3	-	15.2	21.9	17.3	12.1	-
	ND-NS-EB+MA	44.0	31.3	56.3	34.1	52.0	85.8	22.3	37.5	24.7	36.4	60.3
	ND-S1-EB+MA	39.2	31.3	56.3	34.1	52.0	85.8	22.3	37.5	24.7	36.4	60.3
	ND-S2-EB+MA	39.2	31.3	56.3	34.1	52.0	85.8	22.3	37.5	24.7	36.4	48.4
Pre-cracked	D1-S1-EB	12.0	23.9	35.6	24.9	17.3	-	15.2	21.9	17.3	12.1	-
	D1-S1-EB+MA	30.4	31.3	56.3	34.1	52.0	85.8	22.3	37.5	24.7	36.4	60.3
Pre-failed	D2-S1-EB	0.0	23.9	35.6	24.9	17.3	-	15.2	21.9	17.3	12.1	-
	D2-S2-EB	0.0	23.9	35.6	24.9	17.3	-	15.2	21.9	17.3	12.1	-
	D2-S1-EB+MA	47.0	31.3	56.3	34.1	52.0	85.8	22.3	37.5	24.7	36.4	60.3
	D2-S2-EB+MA	21.1	31.3	56.3	34.1	52.0	85.8	22.3	37.5	24.7	36.4	48.4*

^a V_{fn} = nominal FRP shear resistance (without reduction/safety factors)

^b V_{fd} = design FRP shear resistance (with reduction/safety factors)

* $V_{fd,max}$ was adopted

Table 5.4: Comparison between the experimental values and guidelines/standards predictions (EB-CFRP system)

Damage state prior to retrofitting	Specimen	Ratio ($V_m / V_{f,exp}$)					Ratio ($V_{fd} / V_{f,exp}$)				
		<i>ACI 440</i>	<i>fib TG 9.3</i>	<i>CNR-DT200</i>	<i>HB 305</i>	<i>JSCF 2001</i>	<i>ACI 440</i>	<i>fib TG 9.3</i>	<i>CNR-DT200</i>	<i>HB 305</i>	<i>JSCF 2001</i>
No Damage	ND-NS-EB	1.99	2.97	2.08	1.44	-	1.27	1.83	1.44	1.01	-
	ND-S1-EB	1.15	1.71	1.20	0.83	-	0.73	1.05	0.83	0.58	-
	ND-S2-EB	1.49	2.23	1.56	1.08	-	0.95	1.37	1.08	0.76	-
	ND-NS-EB+MA	0.71	1.28	0.78	1.18	1.95	0.51	0.85	0.56	0.83	1.37
	ND-S1-EB+MA	0.80	1.44	0.87	1.33	2.19	0.57	0.96	0.63	0.93	1.54
	ND-S2-EB+MA	0.80	1.44	0.87	1.33	2.19	0.57	0.96	0.63	0.93	1.24
Pre-cracked	D1-S1-EB	1.99	2.97	2.08	1.44	-	1.27	1.83	1.44	1.01	-
	D1-S1-EB+MA	1.03	1.85	1.12	1.71	2.82	0.73	1.23	0.81	1.20	1.98
Pre-failed	D2-S1-EB	N.A	N.A	N.A	N.A	N.A	N.A	N.A	N.A	N.A	N.A
	D2-S2-EB	N.A	N.A	N.A	N.A	N.A	N.A	N.A	N.A	N.A	N.A
	D2-S1-EB+MA	0.67	1.20	0.73	1.11	1.83	0.47	0.80	0.52	0.77	1.28
	D2-S2-EB+MA	1.48	2.67	1.62	2.46	4.07	1.06	1.78	1.17	1.72	2.29

^a V_m = nominal FRP shear resistance (without reduction/safety factors)

^b V_{fd} = design FRP shear resistance (with reduction/safety factors)

5.5.1.1 Non-damaged specimens

Specimens strengthened by EB-CFRP without MEA

In the absence of stirrups, all international guidelines/standards, except HB 305, provided non-conservative predictions for the nominal and design EB-CFRP shear resistances when the EB-CFRP system was used without MEA. This is possibly because of the rapid propagation and widening of shear cracks which promoted early debonding of the EB-CFRP. This indicates that a limited amount of internal steel stirrups is needed to restrict widening and extension of shear cracks so that the EB-CFRP system can contribute to the shear resistance. The HB 305 overestimated the nominal shear resistance of specimen ND-NS-EB but provided accurate prediction for its design shear resistance. In the presence of stirrups, all international guidelines/standards, except HB 305, overestimated the nominal shear resistance of the EB-CFRP without MEA. The error in predicting V_{fn} increased as the amount of the internal stirrups increased. When safety factors were adopted to calculate the design shear resistance, V_{fd} , all guidelines/standards except, *fib* TG 9.3, provided a conservative/reasonable prediction for the design shear strength.

Specimens strengthened by EB-CFRP with MEA:

Predictions of the ACI 440 and CNR-DT 200 for the nominal EB-CFRP shear resistance, V_{fn} , of the non-damaged specimens strengthened by the EB-CFRP with MEA were conservative whereas the *fib* TG 9.3 and the HB 305 overestimated the nominal EB-CFRP shear resistance. All international guidelines/standards, except JSCE, provided conservative predictions for the EB-CFRP design shear resistance, V_{fd} , of the non-damaged specimens strengthened by the EB-CFRP with MEA. The *fib* TG 9.3 and the HB 305

tended to provide more accurate predictions for V_{fd} compared with predictions of the ACI 440 and CNR-DT 200.

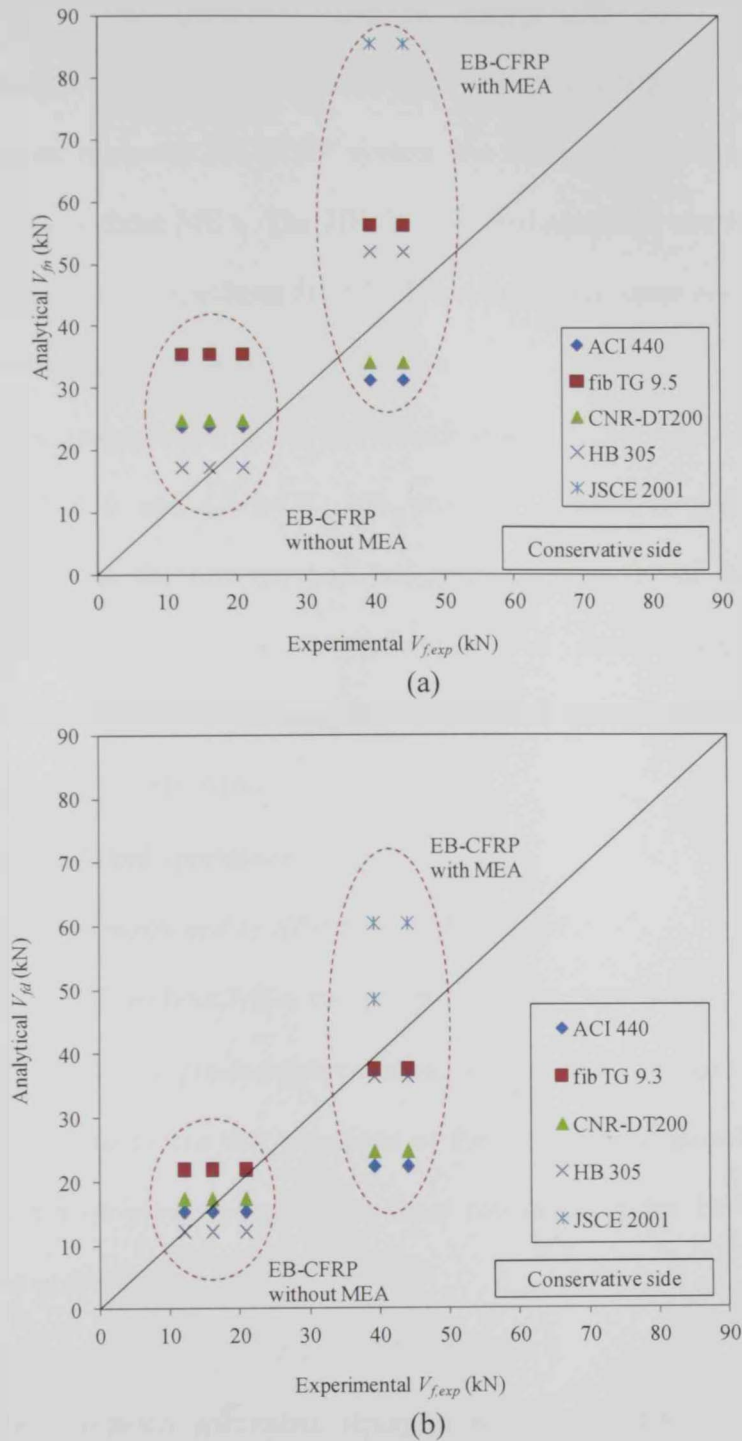


Figure 5.1: Comparison between experimental results of the non-damaged specimens and predictions of international guidelines/standards for EB-CRP system; (a) V_{fm} vs. $V_{f,exp}$, (b) V_{fd} vs. $V_{f,exp}$

5.5.1.2 Pre-cracked specimens

Specimens strengthened by EB-CFRP without MEA:

All international guidelines/standards, except HB 305, provided non-conservative predictions for both nominal and design EB-CFRP shear resistances when the EB-CFRP system was used in retrofitting pre-cracked specimens without MEA. The HB 305 overestimated the nominal EB-CFRP shear resistance of specimen D1-SI-EB but the design shear resistance V_{fd} was almost identical to the experimental value.

Specimens strengthened by EB-CFRP with MEA:

The ACI 440 and CNR-DT 200 provided reasonable and conservative predictions for the nominal and design shear strengths of the pre-cracked specimen D1-SI-EB+MA, respectively. All other guidelines/standards overestimated both the nominal and design shear strengths of the pre-cracked specimen D1-SI-EB+MA.

5.5.1.3 Pre-failed specimens

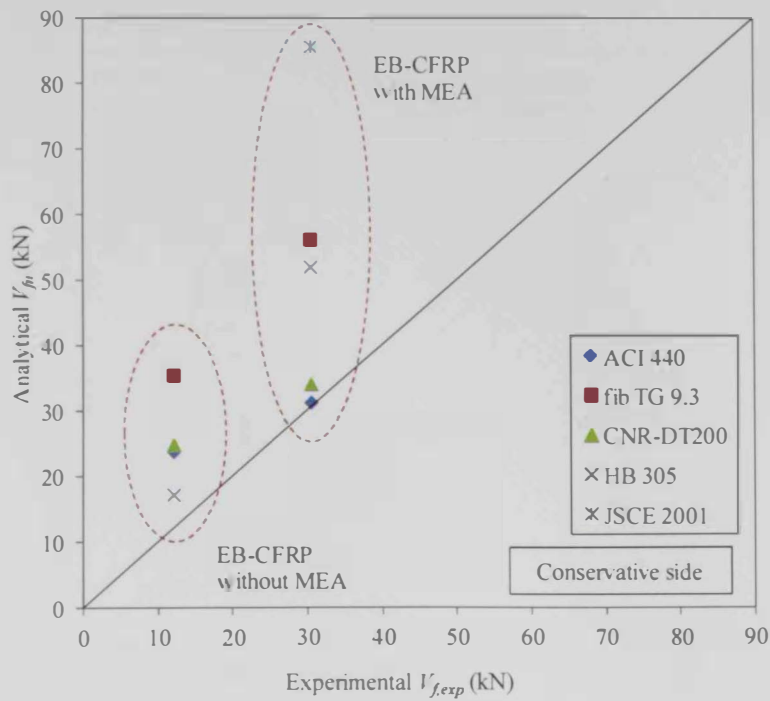
Specimens strengthened by EB-CFRP without MEA:

The EB-CFRP without MEA did not provide any extra shear resistance when used in retrofitting pre-failed specimens, and hence all design equations were not valid. This means that equations of the international guidelines/standards should not be used to predict the shear resistance of the EB-CFRP system without proper end anchors.

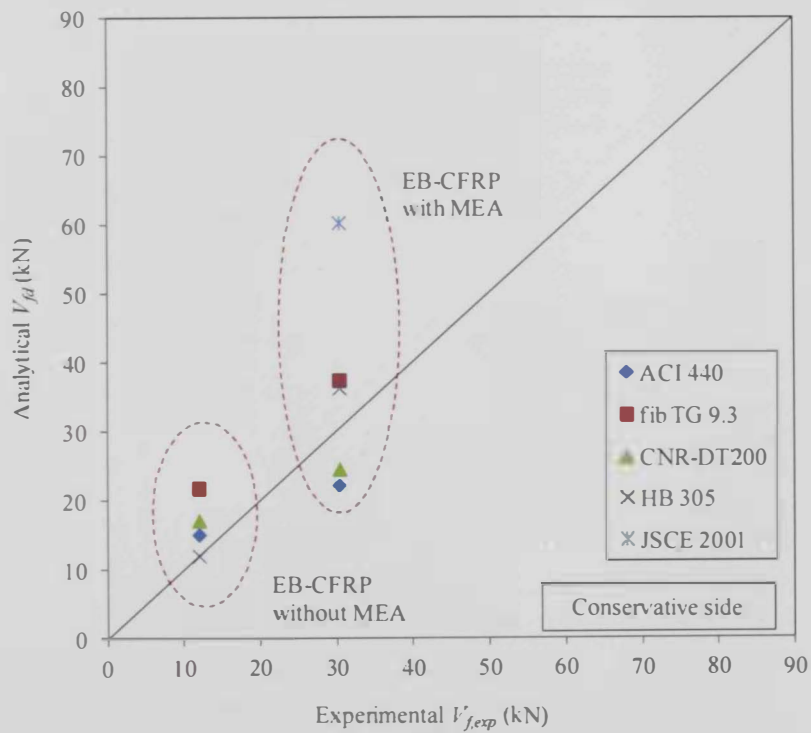
Specimens strengthened by EB-CFRP with MEA:

For the pre-failed specimens strengthened by EB-CFRP with MEA, the accuracy of the international guidelines/standards was dependent of the amount of internal stirrups. For specimen D2-SI-EB+MA with limited amount of

internal stirrups: the ACI 440 and CNR-DT 200 provided a conservative prediction for the nominal shear resistance, the *fib* TG 9.3 and CNR-DT 200 slightly overestimated the nominal shear resistance by 20 and 11%, respectively, and the JSCE significantly overestimated the shear resistance by 83%. All guidelines/standards, except JSCE, provided a conservative prediction for the design shear strength of specimen D2-S1-EB+MA. The JSCE overestimated the design shear strength of specimen D2-S1-EB+MA by 28%. For specimen D2-S2-EB+MA with a considerable amount of stirrups, all international guidelines/standards overestimated the nominal and also the design shear resistance. Nevertheless, the design shear resistance of specimen D2-S2-EB+MA predicted by the ACI 440 was only 6% higher than the experimental value.

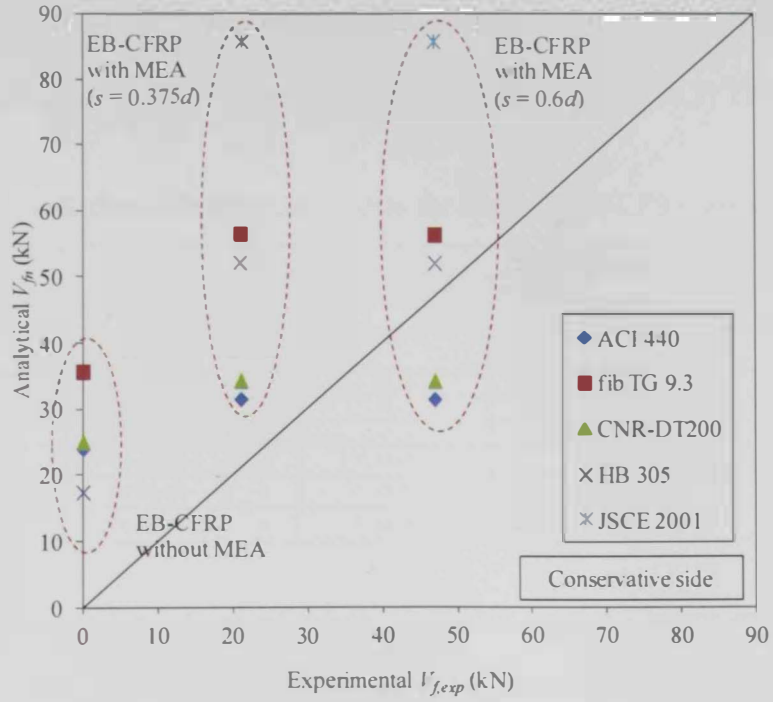


(a)

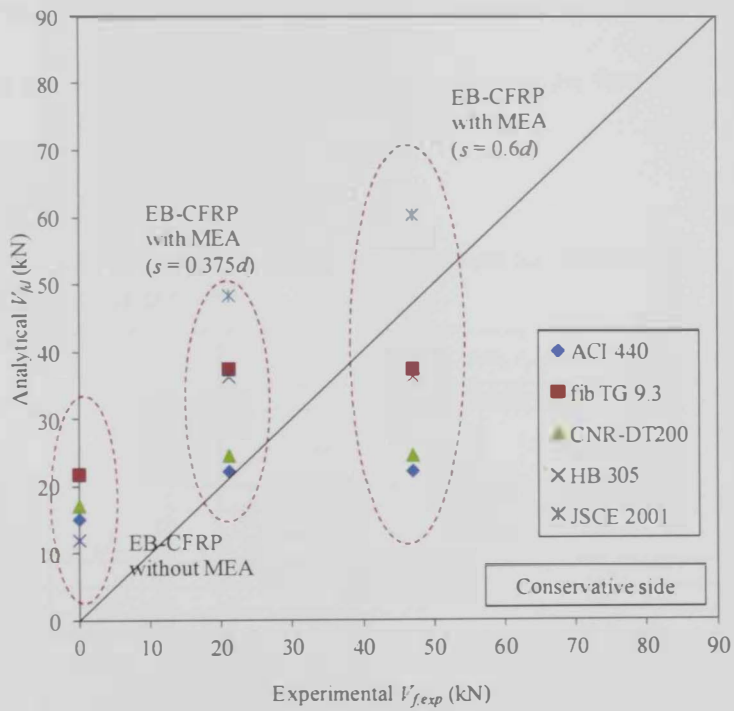


(b)

Figure 5.2: Comparison between experimental results of the pre-cracked specimens and predictions of international guidelines/standards for EB-CFRP system; (a) V_{fm} vs. $V_{f,exp}$, (b) V_{fd} vs. $V_{f,exp}$



(a)



(b)

Figure 5.3: Comparison between experimental results of the pre-failed specimens and predictions of international guidelines/standards for EB-CFRP system; (a) V_{fn} vs. $V_{f,exp}$, (b) V_{fd} vs. $V_{f,exp}$

5.5.2 Accuracy of recent analytical models published in the literature

The nominal EB-CFRP shear resistance, V_{fn} , predicted by models introduced by Mofidi and Chaallal (2011) and Chen and Teng (2013) are given in Table 5.5.

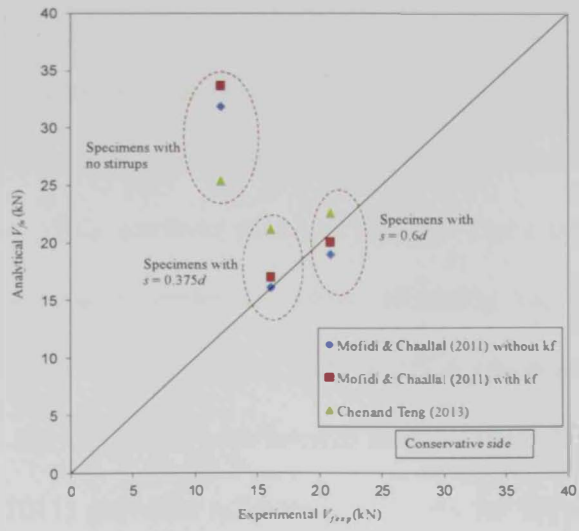
Table 5.5: Predictions of analytical models for nominal EB-CFRP shear resistance

Damage state prior to retrofitting	Specimen	Exp.	Analytical results, V_{fn} (kN)		
		V_{fexp}	Mofidi and Chaallal (2011)		Chen and Teng (2013)
			Without K_f	With K_f	
No Damage	ND-NS-EB	12	31.90	33.7	25.42
	ND-S1-EB	20.8	19.03	20.1	22.62
	ND-S2-EB	16	16.16	17.1	21.22
Pre-cracked	D1-S1-EB	12	19.03	20.12	22.62
Pre-failed	D2-S1-EB	0	19.03	20.12	22.62
	D2-S2-EB	0	16.16	17.09	21.22

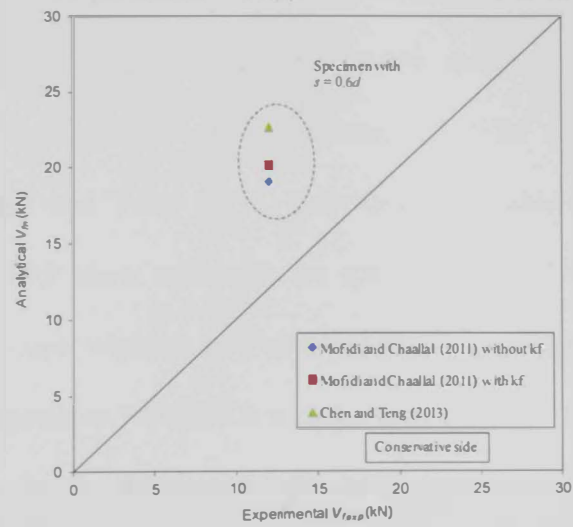
The ratios of predicted to experimental EB-CFRP shear resistance are given in Table 5.6. The analytical predictions are also plotted versus the experimental values of the non-damaged, pre-cracked, and pre-failed specimens in Figure 5.4 (a), (b), and (c), respectively. It should be noted that these two models are valid only for U-wraps configurations.

Table 5.6: Comparison between experimental values and predictions of analytical models (EB-CFRP)

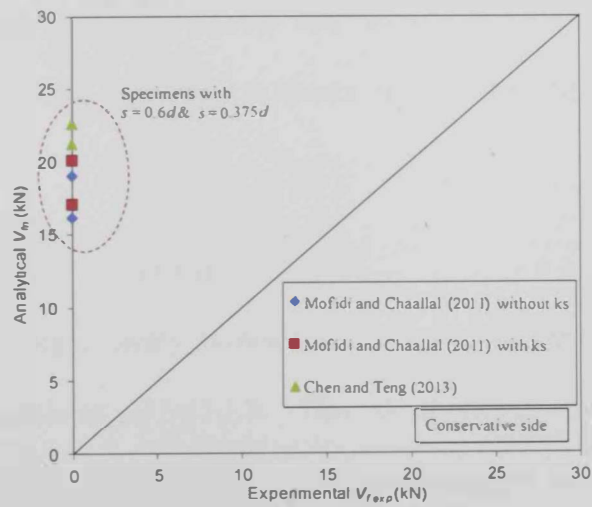
Damage state prior to retrofitting	Specimen	Ratio V_{fn}/V_{fexp} (kN)		
		Mofidi and Chaallal (2011)		Chen and Teng (2013)
		Without K_f	With K_f	
No Damage	ND-NS-EB	2.66	2.81	2.12
	ND-S1-EB	0.92	0.97	1.09
	ND-S2-EB	1.01	1.07	1.33
Pre-cracked	D1-S1-EB	1.59	1.68	1.89
Pre-failed	D2-S1-EB	N.A	N.A	N.A
	D2-S2-EB	N.A	N.A	N.A



(a)



(b)



(c)

Figure 5.4: Analytical models predictions of V_{fn} vs. $V_{fn,exp}$ for EB-CFRP system; (a) non damaged, (b) pre-cracked, (c) pre-failed specimens

5.5.2.1 Non-damaged specimens

In the absence of stirrups, the two models overestimated the nominal EB-CFRP shear resistance. This confirms previous findings that a minimum amount of internal steel stirrups is needed to restrict widening and extension of shear cracks so that the EB-CFRP system without MEA can contribute to the shear resistance. For the specimens with internal steel stirrups, the model by Mofidi and Chaallal (2011) provided accurate predictions for the nominal EB-CFRP shear resistance. The predicted results were within 8% error band. Considering the effect of strip-width-spacing ratio in the analysis represented by the coefficient k_f slightly increased the predicted EB-CFRP shear resistance. The model by Chen and Teng (2013) provided reasonable prediction for the nominal EB-CFRP shear resistance for specimen ND-S1-EB with the lower amount of stirrups whereas it overestimated the nominal EB-CFRP shear resistance for specimen ND-S2-EB with the higher amount of stirrups. It should be noted that for the specimens with internal stirrups, predictions of both models indicated that the contribution of the EB-CFRP to shear resistance decreased as the amount of internal steel stirrups increased. This trend is in good agreement with experimental results of specimens ND-S1-EB and ND-S2-EB.

5.5.2.2 Pre-cracked specimens

The two models significantly overestimated the nominal shear resistance of the pre-cracked specimen D1-S1-EB. This demonstrates that the available analytical models for the U-wraps configurations are not valid for pre-cracked specimens.

5.5.2.3 Pre-failed specimens

Experimental results demonstrated that the EB-CFRP system without MEA did not provide any extra shear resistance when used in retrofitting pre-failed specimens. This indicates that the available analytical models are not valid for pre-failed specimens strengthened with the U-wraps configurations without MEA.

5.6 Comparative analysis for specimens strengthened with ETD-GFRP system

A comparison between the predicted and experimental contribution of the ETD-GFRP reinforcement to shear resistance is demonstrated in Table 5.7. In this model, two sets of bond parameters were adopted. A set of bond parameters is based on results of Mofidi et al. (2012) for ETD-CFRP rebars (sand-coated) and the other set is based on results of De Lorenzis (2004) for NSM-GFRP rebars. The effect of inclusion the factor $k_s = 0.6$ in the analysis for the specimens containing internal steel stirrups as suggested by Mofidi et al. (2012) has been investigated.

5.6.1 Accuracy of Mofidi et al. (2012) analytical model

The model's predictions were very sensitive to the bond parameters implemented in the analysis. Predictions of the model considering the bond parameters by De Lorenzis (2004) were two times the model's predictions when the bond parameters by Mofidi et al. (2012) were adopted. More discussion on the accuracy and validity of the model is given herein.

5.6.1.1 Non-damaged specimens

The model gave conservative predictions for the nominal ETD-GFRP shear

resistance of the non-damaged specimens even when the factor k_s was not considered in the analysis, and regardless of the bond parameters used. The inclusion of the factor $k_s = 0.6$ in the analysis significantly underestimated the contribution of the ETD-GFRP to shear resistance. When the bond parameters by De Lorenzis (2004) were adopted without considering the factor k_s , better correlation between the predicted and experimental results was recorded.

5.6.1.2 Pre-cracked specimens

The model significantly overestimated the contribution of the ETD-GFRP to shear resistance of the pre-cracked specimen D1-S1-ETD. When the bond parameters by Mofidi et al. (2012) were adopted considering the factor $k_s = 0.6$, a better correlation between the predicted and experimental results was recorded. This means that to obtain a reasonable prediction for the nominal EDT-GFRP shear resistance in a pre-cracked specimen, it is recommended to adopt the conservative bond parameters by Mofidi et al. (2012) and include the safety factor of $k_s = 0.6$ in the analysis.

5.6.1.3 Pre-failed specimens

The model significantly overestimated the nominal ETD-GFRP shear resistance of the pre-failed specimen D2-S1-ETD with the lower amount of stirrups regardless of the bond parameters adopted in the analysis. Nevertheless, the model provided conservative or reasonable prediction for the nominal ETD-GFRP shear resistance of the pre-failed specimen D2-S2-ETD with the higher amount of stirrups. For this specimen, the model tended to provide more reasonable predictions for the nominal ETD-GFRP shear resistance when the bond parameters by De Lorenzis (2004) were adopted. Adopting the bond

parameters by Mofidi et al. (2012) resulted in very conservative predictions for the nominal shear resistance of specimen D2-S2-ETD with the higher amount of stirrups.

Table 5.7: Analytical and experimental values of ETD-GFRP shear resistance

		ETD-GFRP shear resistance						Ratio			
Damage state prior to retrofitting	Specimen	Experimental $V_{f,exp}$ (kN)	Bond parameters by Mofidi et al. (2012) V_{fn} (kN)		Bond parameters by De Lorenzis (2004) V_{fn} (kN)		Bond parameters by Mofidi et al. (2012) $V_{fn}/V_{f,exp}$		Bond parameters by De Lorenzis (2004) $V_{fn}/V_{f,exp}$		
			Parameters : $t_m = 8.4$, $s_m = 0.08$, $\alpha = 0.09$		Parameters : $t_m = 9.5$, $s_m = 0.2$, $\alpha = 0.3$		without k_s	with k_s	without k_s	with k_s	
			without k_s	with k_s	without k_s	with k_s	without k_s	with k_s	without k_s	with k_s	
No Damage	ND-NS-ETD	38.4	19.2	19.2	37.3	37.3	0.50	0.50	0.97	0.97	
	ND-S1-ETD	44.0	19.2	11.5	37.3	22.4	0.44	0.26	0.85	0.51	
	ND-S2-ETD	36.0	19.2	11.5	37.3	22.4	0.53	0.32	1.04	0.62	
Pre-cracked	D1-S1-ETD	12.0	19.2	11.5	37.3	22.4	1.60	0.96	3.11	1.87	
Pre-failed	D2-S1-ETD	7.8	19.2	11.5	37.3	22.4	2.47	1.48	4.78	2.87	
	D2-S2-ETD	34.2	19.2	11.5	37.3	22.4	0.56	0.34	1.09	0.65	

CHAPTER 6: CONCLUSIONS AND RECOMMENDATIONS

6.1 General

The viability of using composites in retrofitting shear-deficient RC T-girders with different amounts of internal steel stirrups has been investigated in this research work. The beams were retrofitted using either EB-CFRP system, with or without a MA, or ETD-GFRP system. Prior to retrofitting, the beams were undamaged, pre-cracked, or pre-failed. The study comprised experimental testing and analytical investigations. The main conclusions of the work along with recommendations for practical applications and future studies are summarized herein.

6.2. Conclusions

6.2.1. Conclusions of the experimental work

Based on the experimental results, the following conclusions are drawn:

- In the absence of internal stirrups, the EB-CFRP system without MA increased the shear resistance of the non-damaged specimen by 17% only. The inclusion of MA in the EB-CFRP system increased the shear strength gain to 64%. The shear strength gain provided by the ETD-GFRP system, 56%, was comparable to that provided by the EB-CFRP system with MA.
- For the non-damaged specimens with lower amount of stirrups, $s_I = 0.6d$, shear strengths gains of 19, 36, and 40% were recorded for the specimens strengthened with EB-CFRP solely, EB-CFRP with MA, and ETD-GFRP systems, respectively.
- The shear strength gain for the non-damaged specimens decreased as the amount of stirrups increased. For the specimens strengthened using EB-

CFRP without MA, EB-CFRP with MA, and ETD-GFRP systems, decreasing the stirrups spacing from $0.6d$ to $0.375d$ resulted in approximately 32, 11, and 25% reductions in the shear strength gain.

- The presence of shear damage prior to retrofitting significantly reduced the strengthening effectiveness. For the pre-cracked specimens with the lower amount of stirrups, only 11, 27, 11% shear strength gains were recorded after retrofitting with the EB-CFRP solely, EB-CFRP with MA, and ETD-GFRP systems, respectively.
- The EB-CFRP system without MA was not successful in restoring the shear resistance of the pre-failed specimens where no shear strength gain was recorded regardless of the amount of stirrups. The EB-CFRP system with MA and the ETD-GFRP system were capable of restoring the shear resistance of the pre-failed specimens. The shear resistances of the pre-failed specimens with the lower and higher amounts of stirrups retrofitted by the EB-CFRP system with MA were even 40 and 11%, higher than the original shear strengths recorded prior to retrofitting, respectively.
- The ETD-GFRP system restored 97% of the original shear resistance of the pre-failed specimen with the lower amount of stirrups. For the pre-failed specimen with the higher amount of stirrups the ETD-GFRP system fully restored and also upgraded the original shear resistance by approximately 11%.

6.2.2. Conclusions of the analytical investigation

Based on the analytical investigation, the following conclusions are drawn:

- For the non-damaged specimens, all international guidelines/standards tended to provide non-conservative predictions for the nominal EB-CFRP

shear resistance when the EB-CFRP system was used without MA. A limited amount of internal steel stirrups is needed to restrict widening and extension of shear cracks so that the EB-CFRP system without MA can contribute to the shear resistance. The error in predicting V_{fn} increased as the amount of the internal stirrups increased. When safety factors were adopted to calculate the design shear resistance, V_{fd} , all guidelines/standards except, *fib* TG 9.3, provided a conservative/reasonable prediction for the design shear strength of the EB-CFRP system without MA. For the non-damaged specimens strengthened by the EB-CFRP with MA, all international guidelines/standards, except JSCE, provided conservative predictions for the EB-CFRP design shear resistance, V_{fd} . The ACI 440 and CNR-DT 200 tended to provide a more conservative prediction for V_{fd} than the *fib* TG 9.3 and the HB 305.

- For the pre-cracked specimens strengthened by the EB-CFRP without MA, the international guidelines/standards equations tended to overestimate both the nominal and design EB-CFRP shear resistances. For the pre-cracked specimens strengthened by EB-CFRP with MA, the ACI 440 and CNR-DT 200 provided reasonable/conservative predictions for the nominal and design shear strengths. All other guidelines/standards overestimated the nominal and design shear strengths of the pre-cracked specimen even in the presence of the MA.
- The EB-CFRP without MA did not provide any extra shear resistance when used in retrofitting pre-failed specimens, and hence all design equations were not valid.

- For the pre-failed specimen with the lower amount of stirrups strengthened by EB-CFRP with MA, the ACI 440 and CNR-DT 200 provided a conservative prediction for the nominal shear resistance, the *fib* TG 9.3 and CNR-DT 200 slightly overestimated the nominal shear resistance by 20 and 11%, respectively, and the JSCE significantly overestimated the shear resistance by 83%. All guidelines/standards, except JSCE, provided a conservative prediction for the design shear strength of the pre-failed specimen with the lower amount of stirrups strengthened by EB-CFRP with MA.
- For the pre-failed specimen with the higher amount of stirrups strengthened by EB-CFRP with MA, all international guidelines/standards overestimated the nominal and also the design shear resistance.
- In the absence of stirrups, the two models by Mofidi and Chaallal (2011) and Chen and Teng (2013) overestimated the nominal EB-CFRP shear resistance of the non-damaged specimens. For the specimens with internal steel stirrups, the model by Mofidi and Chaallal (2011) provided accurate predictions for the nominal EB-CFRP shear resistance. The predicted results were within 8% error band. The model by Chen and Teng (2013) provided a reasonable prediction for the nominal EB-CFRP shear resistance in the presence of a limited amount of stirrups but overestimated the nominal EB-CFRP shear resistance in the presence of a considerable amount of stirrups. The two models significantly overestimated the nominal shear resistance of the pre-cracked specimen. These analytical models were not valid for pre-failed specimens strengthened with the U-wraps configurations without MA.

- The model by Mofidi et al. (2012) for prediction of the nominal EDT-GFRP shear resistance is very sensitive to the bond parameters implemented in the analysis. Predictions of the model considering the bond parameters by De Lorenzis (2004) were two times the model's predictions when the bond parameters by Mofidi et al. (2012) were adopted. The model gave conservative predictions for the nominal EDT-GFRP shear resistance of the non-damaged specimens regardless of the bond parameters used.
- For the pre-cracked specimen, model by Mofidi et al. (2012) tended to overestimate the nominal EDT-GFRP shear resistance. To obtain a reasonable prediction for the nominal EDT-GFRP shear resistance in a pre-cracked specimen, it is recommended to adopt the conservative bond parameters by Mofidi et al. (2012) and include the safety factor of $k_s = 0.6$ in the analysis.
- The model by Mofidi et al. (2012) significantly overestimated the nominal EDT-GFRP shear resistance of the pre-failed specimen with the limited amount of stirrups regardless of the bond parameters adopted in the analysis. In the presence of a considerable amount of stirrups, the model provided, however, a conservative or reasonable prediction for the nominal EDT-GFRP shear resistance of the pre-failed specimen.

6.3. Recommendations for practical applications

Based on results of the present research, the following recommendations can be made for successful applications of composites in retrofitting shear-deficient RC T-girders.

- For RC T-girders without initial shear damage, the ETD-GFRP is considered the most efficient strengthening system followed by the EB-CFRP system with MA then the EB-CFRP without MA. The EB-CFRP system without MA provides a marginal increase in shear resistance.
- For pre-cracked and pre-failed RC T-girders with a limited amount of stirrups, the EB-CFRP with MA is considered the most efficient system followed by the ETD-GFRP system. It is not recommended to use the EB-CFRP system without MA in retrofitting pre-cracked or pre-failed RC T-girders regardless of the amount of internal steel stirrups because no shear strength gain will be obtained.
- For pre-failed RC T-girders with considerable amount of stirrups, the ETD-GFRP system is considered the most efficient retrofitting solution followed by the EB-CFRP with MA. The EB-CFRP system without MA is not recommended for retrofitting pre-failed RC T-girders, even in the presence of a considerable amount of internal stirrups.
- The ETD-GFRP system should be used with caution to ensure that steel reinforcement will not be damaged during drilling of holes for the installation of the ETD-GFRP rebars. For pre-cracked and pre-failed RC T-girders, particularly those with a limited amount of stirrups, installation of the ETD-GFRP system could aggravate the existing concrete damage. In such cases, it is recommended to repair existing shear cracks using epoxy-injection technique prior to installation of the ETD-GFRP system.

6.4. Recommendations for future studies

Findings of this research work provided insights into the effectiveness of using EB-CFRP and ETD-GFRP systems in retrofitting shear-deficient RC T-girders. More research is needed to enrich the literature and support development of design guidelines and standards on the subject. The following are recommendations for future studies in this field:

- Study the effect of fire and elevated temperatures on shear response of RC T-girders strengthened with composites.
- Study the shear response of pre-damaged then strengthened RC girders when epoxy-injection is used for repair of shear cracks, rather than surface crack sealing, prior to installation of the composite system.
- Study the bond behavior of ETD-FRP rebars in concrete.
- Study the effect of concrete section size and amount/type of ETD-FRP reinforcement on shear response on RC girders.
- Develop finite element (FE) models for the RC girders tested in the present study. The FE models, when verified, can be used as a numerical platform for performance prediction of RC girders strengthened with composite-based systems.

REFERENCES

- ACI Committee, American Concrete Institute, & International Organization for Standardization. (2008). Building Code Requirements for Structural Concrete (ACI 318-08) and Commentary. American Concrete Institute.
- ACI, A. (2002). 440.2 R-02: Guide for the design and construction of externally bonded FRP systems for strengthening concrete structures. American Concrete Institute, Farmington Hills, USA.
- <http://www.acmanet.org/the-industry/history>
- Alrousan, R., Issa, M. (2009), "Size Effect of Reinforced Concrete Beams on Shear Contribution of CFRP Composites," Proceedings, 9th International RILEM Symposium on Non-Metallic (FRP) Reinforcement for Concrete Structures (FRPRCS-9), Sidney, Australia, 4 pp.
- Angst, U. (2011), "Chloride induced reinforcement corrosion in concrete: Concept of critical chloride content—methods and mechanisms".
- Australia, S. (2001). Australian Standard for Concrete Structures AS 3600-2001. Australia, Jun.
- Belarbi, A., Bae, A. and Brancaccio, S. (2009), "Behavior Of RC T-Beams Strengthened in Shear With Externally Bonded FRP Sheets." Proceedings, 9 146th International Symp. On Fiber-Reinforced Polymer Reinforcement for Concrete Structures (FRPRCS-9), ICE,
- Bousselham, A., & Chaallal, O. (2006). "Behavior of Reinforced Concrete T-Beams Strengthened in Shear with Carbon Fiber-Reinforced Polymer" An Experimental Study. ACI structural journal, 103(3).
- Bousselham, A., & Chaallal, O. (2008). "Mechanisms of shear resistance of

- concrete beams strengthened in shear with externally bonded FRP". *Journal of Composites for Construction*, 12(5), 499-512. Melbourne, Australia
- Carolin, A., & Täljsten, B. (2005). "Theoretical study of strengthening for increased shear bearing capacity". *Journal of Composites for Construction*, 9(6), 497-506.
- Castro, P. F., & Carino, N. J. (1998). "Tensile and nondestructive testing of FRP bars". *Journal of composites for construction*, 2(1), 17-27.
- Ceroni, F., Pecce, M., Matthys, S., & Taerwe, L. (2008). "Debonding strength and anchorage devices for reinforced concrete elements strengthened with FRP sheets". *Composites Part B: Engineering*, 39(3), 429-441.
- Chaallal, O., Mofidi, A., Benmokrane, B., & Neale, K. (2012). "Embedded through-section FRP rod method for shear strengthening of RC beams: Performance and comparison with existing techniques". *Journal of Composites for Construction*, 15(3), 374-383.
- Chen, G. M., Teng, J. G., & Chen, J. F. (2012). "Shear strength model for FRP-strengthened RC beams with adverse FRP-steel interaction". *Journal of Composites for Construction*, 17(1), 50-66.
- Chen, J. F., & Teng, J. G. (2003). "Shear capacity of FRP-strengthened RC beams: FRP debonding". *Construction and Building Materials*, 17(1), 27-41.
- CNR, D. (2004). 200/2004. Guide for the Design and Construction of Externally Bonded FRP Systems for Strengthening Existing Structures.
- Comitee, A. C. I. 318.(2005). Building code requirements for structural concrete ACI, 318-05.
- Concrete Committee. JSCE (2007). Standard Specifications for Concrete Structures.

- CSA-S806-02 (2002). "Design and construction of building components with fibre-reinforced polymers". Mississauga,(Ont., Canada): Canadian Standards Association.
- De Lorenzis, L. (2004). "Anchorage Length of Near-Surface Mounted Fiber-Reinforced Polymer Rods for Concrete Strengthening Analytical Modeling". *ACI Structural Journal*, 101(3).
- Deifalla, A., & Ghojarah, A. (2010). "Strengthening RC T-beams subjected to combined torsion and shear using FRP fabrics: Experimental study". *Journal of Composites for Construction*, 14(3), 301-311.
- Dirar, S., Lees, J. M., & Morley, C. T. (2012). "Precracked Reinforced Concrete T-Beams Repaired in Shear with Prestressed Carbon Fiber-Reinforced Polymer Straps". *ACI Structural Journal*, 110(5).
- El-Maaddawy, T., & Chekfeh, Y. (2012). "Retrofitting of severely shear-damaged concrete t-beams using externally bonded composites and mechanical end anchorage". *Journal of Composites for Construction*, 16(6), 693-704.
- El-Maaddawy, T., & Chekfeh, Y. (2013). "Shear Strengthening of T-Beams with Corroded Stirrups Using Composites". *ACI Structural Journal*, 110(5).
- El-Maaddawy, T., & El-Ariss, B. (2012). "Behavior of concrete beams with short shear span and web opening strengthened in shear with CFRP composites". *Journal of Composites for Construction*, 16(1), 47-59.
- EN, B. (2004). 1-2: 2004 Eurocode 2: Design of concrete structures-Part 1-2: General rules-Structural fire design. European Standards, London.
- Eshwar, N., Nanni, A., & Ibell, T. J. (2008). "Performance of two anchor systems of externally bonded fiber-reinforced polymer laminates". *ACI Materials Journal*, 105(1).

fib-TG 9.3 (2001), "Externally Bonded FRP Reinforcement for RC Structures."

International Federation for Structural Concrete, Lausanne, Switzerland,
pp. 139.

Gamino, A., Sousa, J., and Bittencourt, T. (2009), "Application of Carbon Fiber Reinforced Polymer in Strengthening to Shear R/C T Beams," Proceedings, 9th International RILEM Symp. Non-Metallic (FRP) Reinforcement for Concrete Structures (FRPRCS-9), Sidney, Australia, 4 pp.

Godat, A., L'hady, A., Chaallal, O., & Neale, K. W. (2012). "Bond Behavior of the ETS FRP Bar Shear-Strengthening Method". *Journal of Composites for Construction*, 16(5), 529-539.

Godat, A., Qu, Z., Lu, X. Z., Labossiere, P., Ye, L. P., & Neale, K. W. (2010). "Size effects for reinforced concrete beams strengthened in shear with CFRP strips". *Journal of Composites for Construction*, 14(3), 260-271.

Grande, E., Imbimbo, M., & Rasulo, A. (2009). "Effect of transverse steel on the response of RC beams strengthened in shear by FRP: Experimental study". *Journal of Composites for Construction*, 13(5), 405-414.

Grelle, S. V., & Sneed, L. H. (2013). "Review of anchorage systems for externally bonded FRP laminates". *International Journal of Concrete Structures and Materials*, 7(1), 17-33.

Haddad, R. H., Al-Rousan, R. Z., & Al-Sedyiri, B. K. (2013). "Repair of shear-deficient and sulfate-damaged reinforced concrete beams using FRP composites". *Engineering Structures*, 56, 228-238.

HB 305-2008 (2008), "Design Handbook for RC Structures Retrofitted with FRP

- and Metal Plates: Beams and Slabs." Standards Australia, Sydney, NSW
2001, Australia, 76 pp.
- Higgins, C., Williams, G. T., Mitchell, M. M., Dawson, M. R., & Howell, D.
(2012). "Shear Strength of Reinforced Concrete Girders with Carbon
Fiber-Reinforced Polymer: Experimental Results". *ACI Structural Journal*,
109(6).
- Hoult, N. A., and Lees, J. M. (2009). "Efficient CFRP strap configurations for the
shear strengthening of reinforced concrete T-beams." *J. Compos. Constr.*,
13(1), 45–52.
- Hussein, M., Afefy, H. M. E. D., & Khalil, A. H. A. K. (2013). "Innovative
Repair Technique for RC Beams Predamaged in Shear". *Journal of
Composites for Construction*, 17(6).
- ISIS Canada Educational Module No. 4 (2004). An Introduction to FRP
Strengthening of concrete structures. ISIS Canada. Section 2S. 5.
- ISIS Canada Educational Module No. 2 (2006). An Introduction to FRP
composites for construction. ISIS Canada. Section 2.
- Ivan, E., Solis, R. G., & Lopez-Salazar, L. R. (2005). "Carbonation Induced
Corrosion in Urban Concrete Structures". *CORROSION* 2005.
- JSCE, 2001, Recommendation for Upgrading of Concrete Structures with use of
Continuous Fiber Sheets, Concrete Engineering Series 41, Japan Society
of Civil Engineers, Tokyo, Japan.
- Kalfat, R., Al-Mahaidi, R., & Smith, S. T. (2013). "Anchorage devices used to
improve the performance of reinforced concrete beams retrofitted with
FRP composites: State-of-the-art review". *Journal of Composites for
Construction*, 17(1), 14-33.

- Kesse, G., & Lees, J. M. (2007). "Experimental behavior of reinforced concrete beams strengthened with prestressed CFRP shear straps". *Journal of composites for construction*, 11(4), 375-383.
- Khalifa, A., Alkhrdaji, T., Nanni, A., & Lansburg, S. (1999). "Anchorage of surface mounted FRP reinforcement". *CONCRETE INTERNATIONAL-DETROIT-*, 21, 49-54.
- Kim, Y., Quinn, K. T., Satrom, C. N., Ghannoum, W. M., & Jirsa, J. O. (2011). "Shear strengthening RC T-beams using CFRP laminates and anchors". *ACI Special Publication*, 275.
- Koutas, L., & Triantafillou, T. C. (2012). "Use of anchors in shear strengthening of reinforced concrete T-beams with FRP". *Journal of Composites for Construction*, 17(1), 101-107.
- Mofidi, A., & Chaallal, O. (2011). "Shear strengthening of RC beams with externally bonded FRP composites: Effect of strip-width-to-strip-spacing ratio". *Journal of Composites for Construction*, 15(5), 732-742.
- Mofidi, A., & Chaallal, O. (2010). "Shear strengthening of RC beams with EB FRP: Influencing factors and conceptual debonding model". *Journal of Composites for Construction*, 15(1), 62-74.
- Mofidi, A., Chaallal, O., Benmokrane, B., & Neale, K. (2012). "Experimental tests and design model for RC beams strengthened in shear using the embedded through-section FRP method". *Journal of Composites for Construction*, 16(5), 540-550.
- Mofidi, A., Chaallal, O., Benmokrane, B., & Neale, K. (2012). "Performance of end-anchorage systems for RC beams strengthened in shear with epoxy-bonded FRP". *Journal of Composites for Construction*, 16(3), 322-331.

- Mofidi, A., & Chaallal, O. (2014). "Effect of Steel Stirrups on Shear Resistance Gain Due to Externally Bonded Fiber-Reinforced Polymer Strips and Sheets". *ACI Structural Journal*, 111(1-6).
- Nikopour, H., & Nehdi, M. (2011). "Shear repair of RC beams using epoxy injection and hybrid external FRP". *Materials and structures*, 44(10), 1865-1877.
- Nogueira, C. G., Venturini, W. S., & Coda, H. B. (2013). "Material and geometric nonlinear analysis of reinforced concrete frame structures considering the influence of shear strength complementary mechanisms". *Latin American Journal of Solids and Structures*, 10(5), 953-980.
- Ortega, C. A., Belarbi, A., & Bae, S. W. (2009). "End anchorage of externally bonded FRP sheets for the case of shear strengthening of concrete girders". In *Ninth International Symposium on Fiber Reinforced Polymer Reinforcement for Concrete Structures, FRPRCS (Vol. 9)*.
- Panda, K. C., Bhattacharyya, S. K., & Barai, S. V. (2012). "Effect of transverse steel on the performance of RC T-beams strengthened in shear zone with GFRP sheet". *Construction and Building Materials*, 41, 79-90.
- Panigrahi, A. K., Biswal, K. C., & Barik, M. R. (2014). "Strengthening of shear deficient RC T-beams with externally bonded GFRP sheets". *Construction and Building Materials*, 57, 81-91.
- Pellegrino, C., & Modena, C. (2006). "Fiber-reinforced polymer shear strengthening of reinforced concrete beams: Experimental study and analytical modeling". *ACI Structural Journal*, 103(5).
- Rizkalla, S., Hassan, T., & Hassan, N. (2003). "Design recommendations for the

- use of FRP for reinforcement and strengthening of concrete structures".
Progress in Structural Engineering and Materials, 5(1), 16-28.
- SAFSTRIP[®] (2008). Fiber reinforced strengthening strip, Strongwell,
www.strongwell.com.
- Tanarslan, H. M., Ertutar, Y., & Altin, S. (2008). "The effects of CFRP strips for
improving shear capacity of RC beams. Journal of Reinforced Plastics and
Composites, 27(12), 1287-1308.
- Teng, J. G., Chen, G. M., Chen, J. F., Rosenboom, O. A., & Lam, L. (2009).
"Behavior of RC beams shear strengthened with bonded or unbonded FRP
wraps". Journal of Composites for Construction, 13(5), 394-404.
- Triantafillou, T. C., & Antonopoulos, C. P. (2000). "Design of concrete flexural
members strengthened in shear with FRP". Journal of Composites for
Construction, 4(4), 198-205.
- Wight, J. K., Richart, F. E., and MacGregor, J. G. (2012). "Reinforced Concrete:
Mechanics and Design, Pearson".
- Yousef Mohammed Bachar Chekfeh (2012), "Strengthening of Reinforced
Concrete Beams Pre-damaged in Shear." MS thesis. United Arab Emirates
University. Print.
- Zhang, Z., & Hsu, C. T. T. (2005). "Shear strengthening of reinforced concrete
beams using carbon-fiber-reinforced polymer laminates". Journal of
composites for construction, 9(2), 158-169.

APPENDIX A: STRAIN RESPONSE OF FRP

Plots of the load versus FRP strain relationships are provided in this appendix. Each CFRP sheet or GFRP rebar was instrumented by a strain gauge. The symbol (S.G 1) refers to the strain gauge nearest to the support point whereas (S.G 2) refers to the strain gauge nearest to the load point.

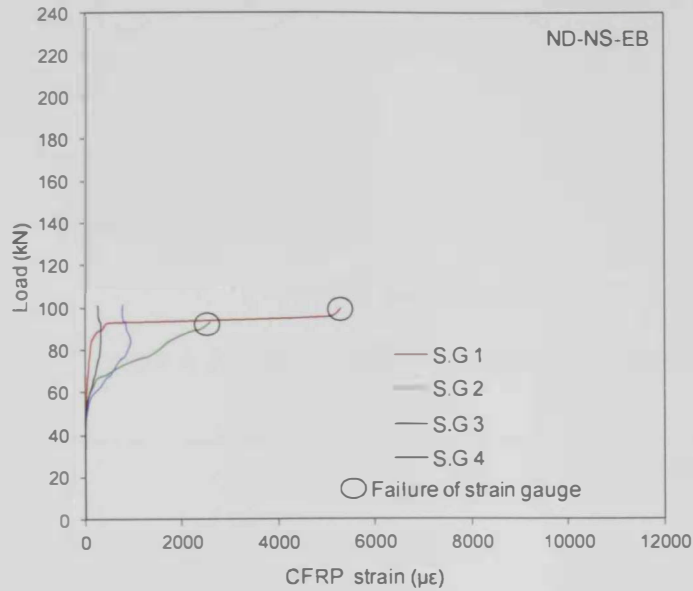


Figure A.1: Load vs. CFRP strain for ND-NS-EB

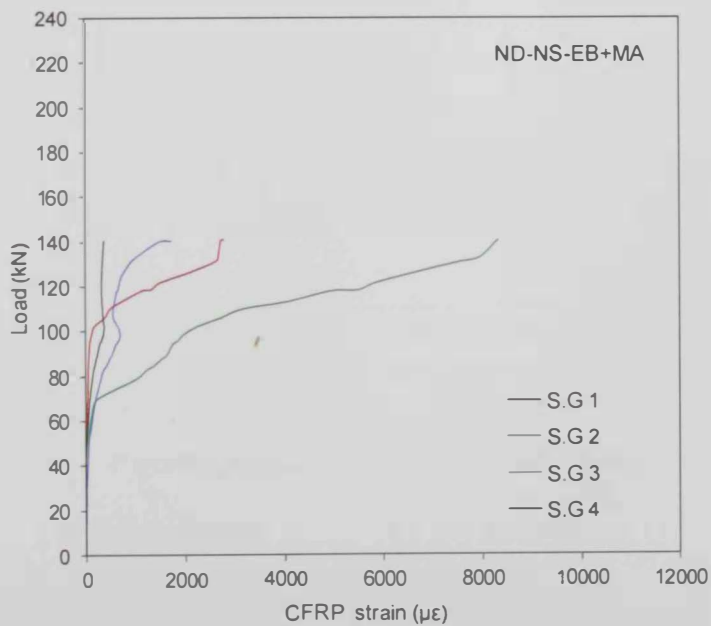


Figure A.2: Load vs. CFRP strain for ND-NS-EB+MA

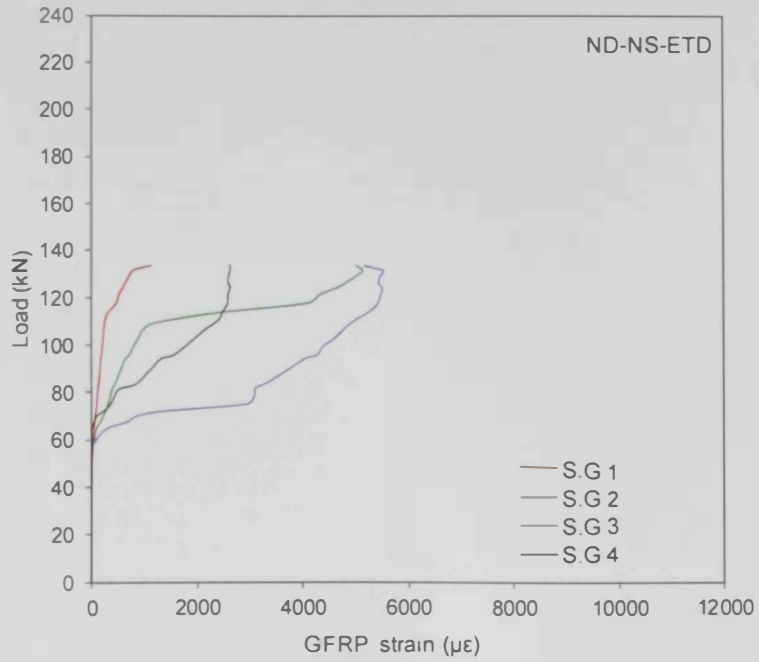


Figure A.3: Load vs. GFRP strain for ND-NS-ETD

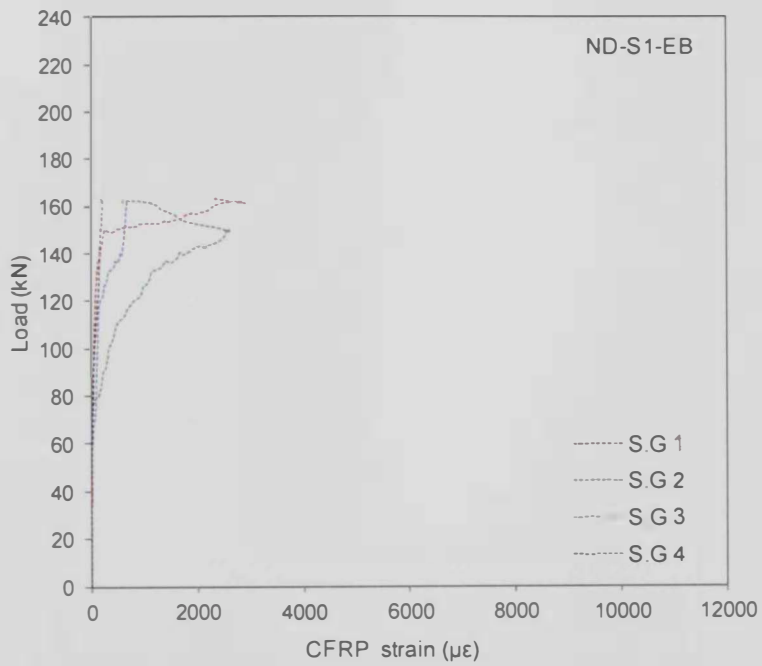


Figure A.4: Load vs. FRP strain for ND-S1-EB

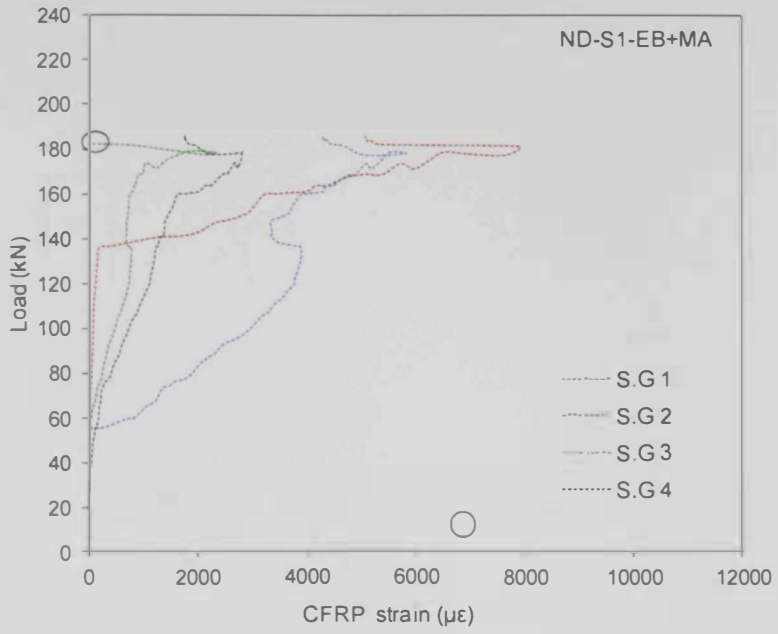


Figure A.5: Load vs. FRP strain for ND-S1-EB+MA

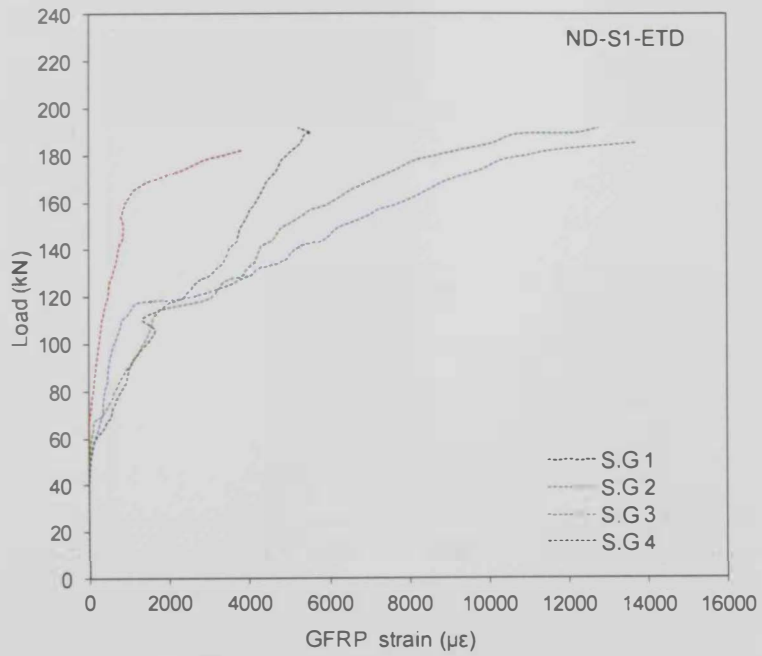


Figure A.6: Load vs. FRP strain for ND-S1-ETD

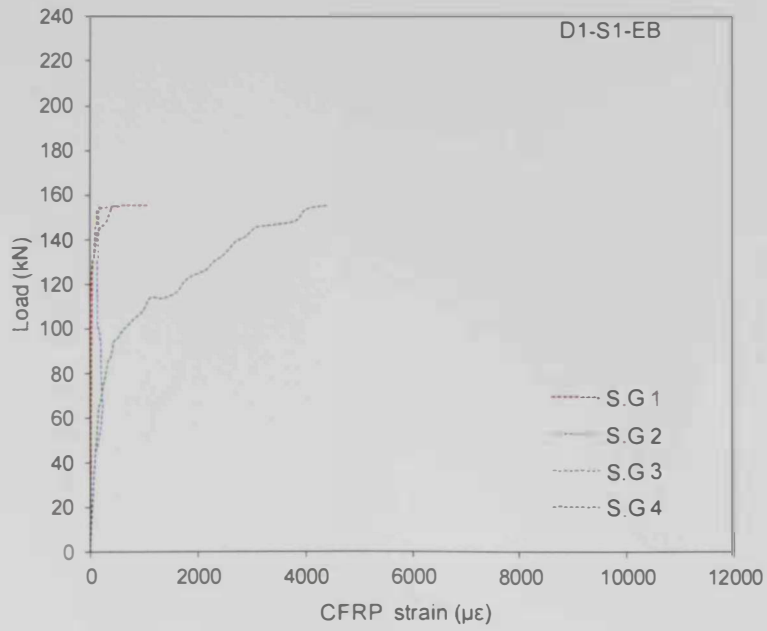


Figure A.7: Load vs. FRP strain for D1-S1-EB

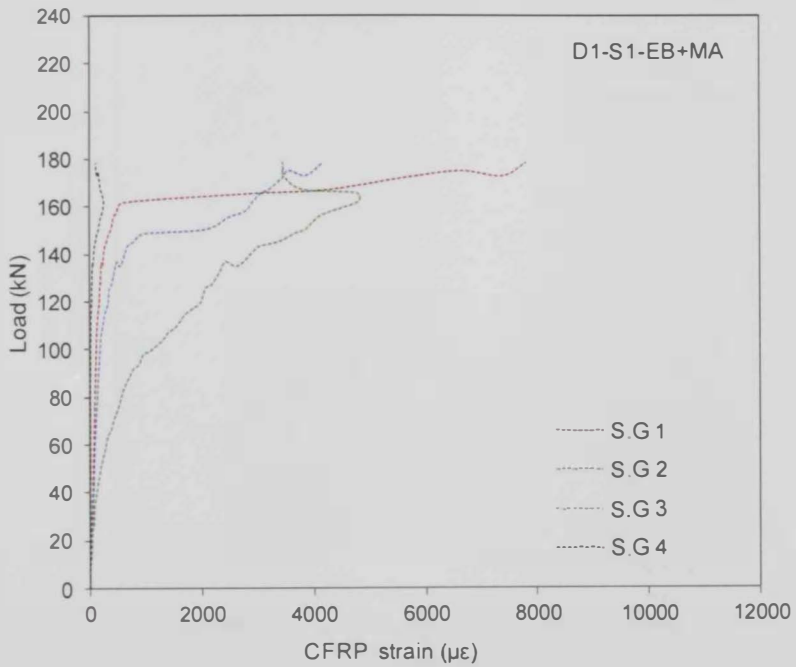


Figure A.8: Load vs. FRP strain for D1-S1-EB+MA

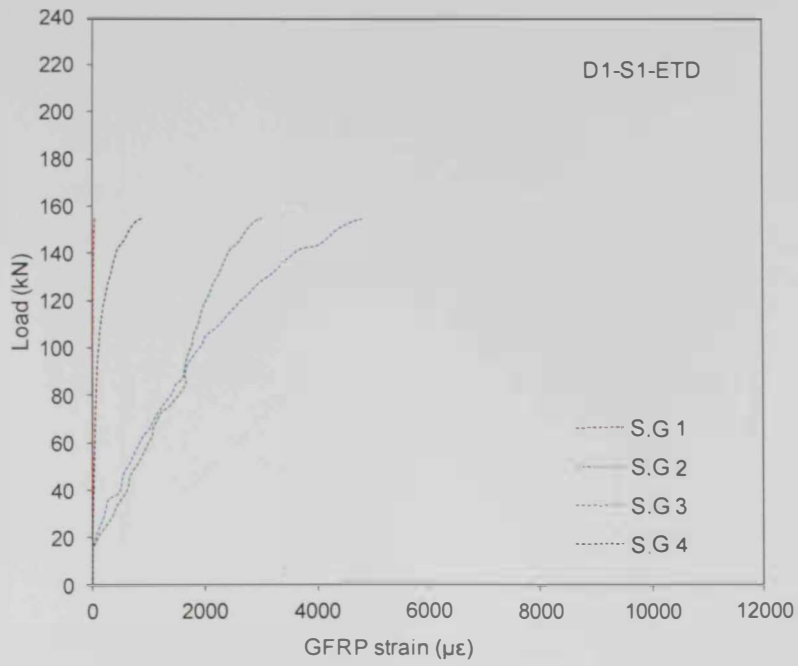


Figure A.9: Load vs. FRP strain for D1-S1-ETD

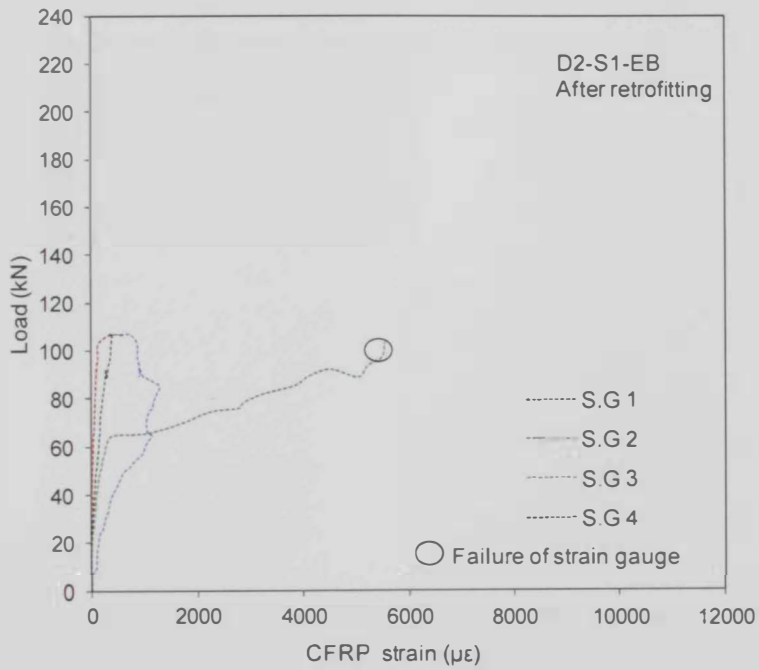


Figure A.10: Load vs. FRP strain for D2-S1-EB

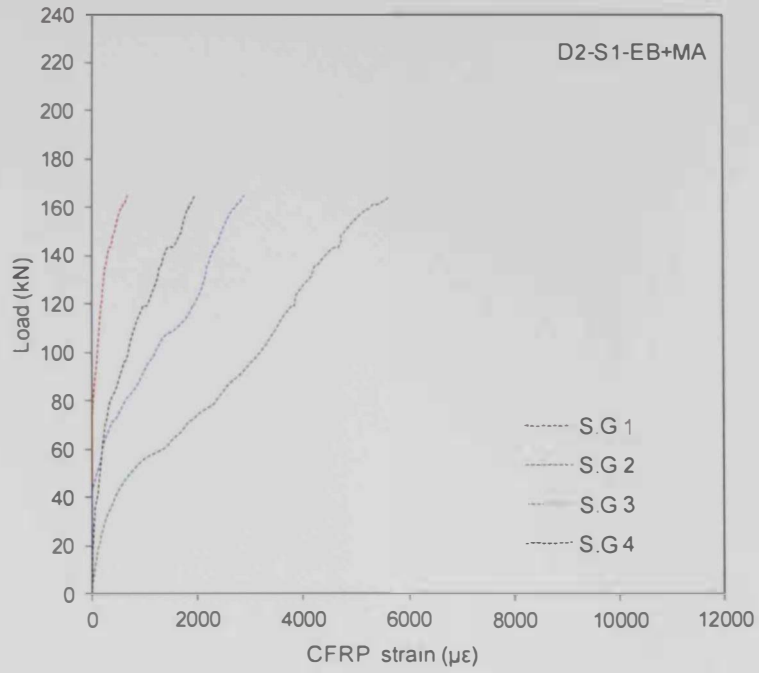


Figure A.11: Load vs. FRP strain for D2-S1-EB+MA

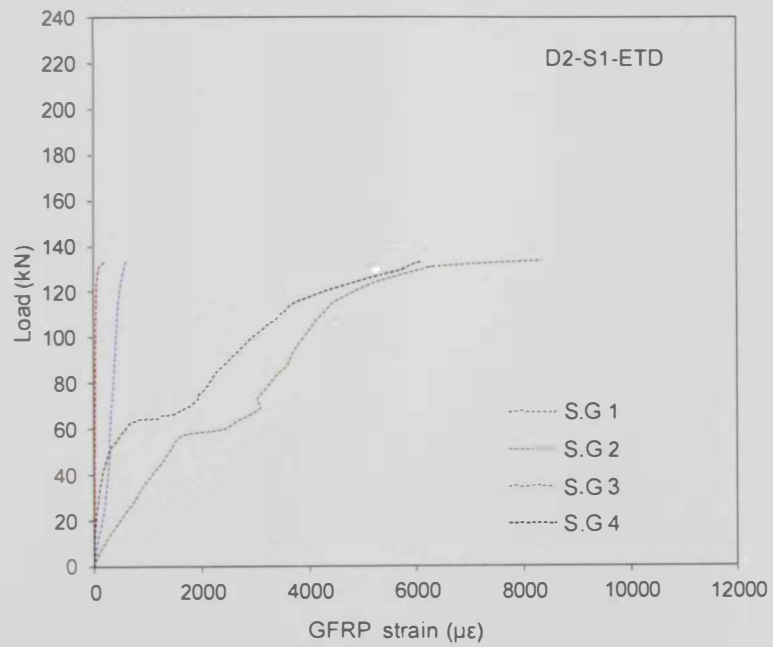


Figure A.12: Load vs. FRP strain for D2-S1-ETD

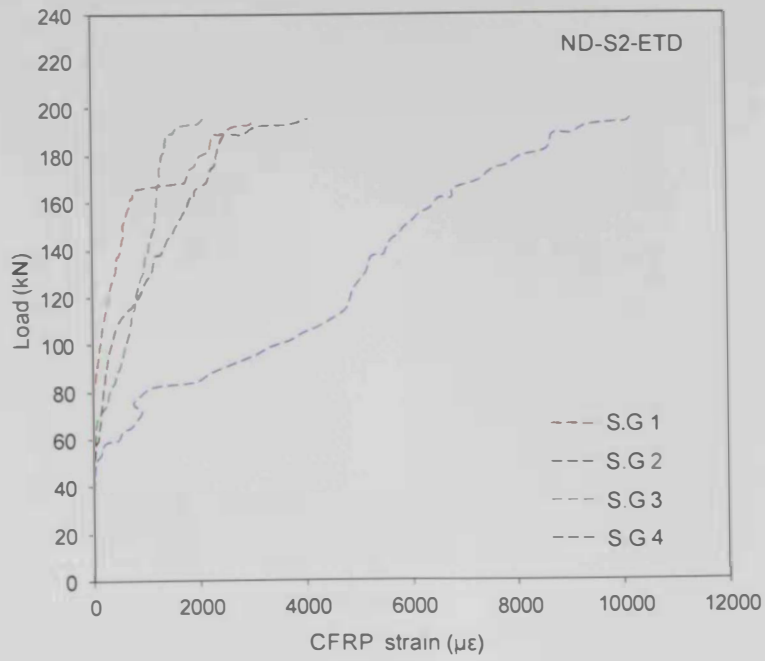


Figure A.13: Load vs. CFRP strain for ND-S2-ETD

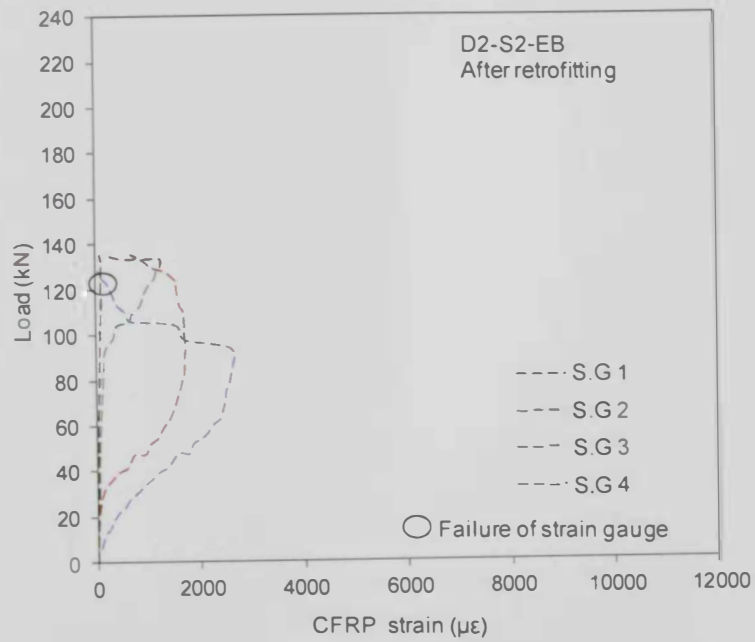


Figure A.14: Load vs. CFRP strain for D2-S2-EB

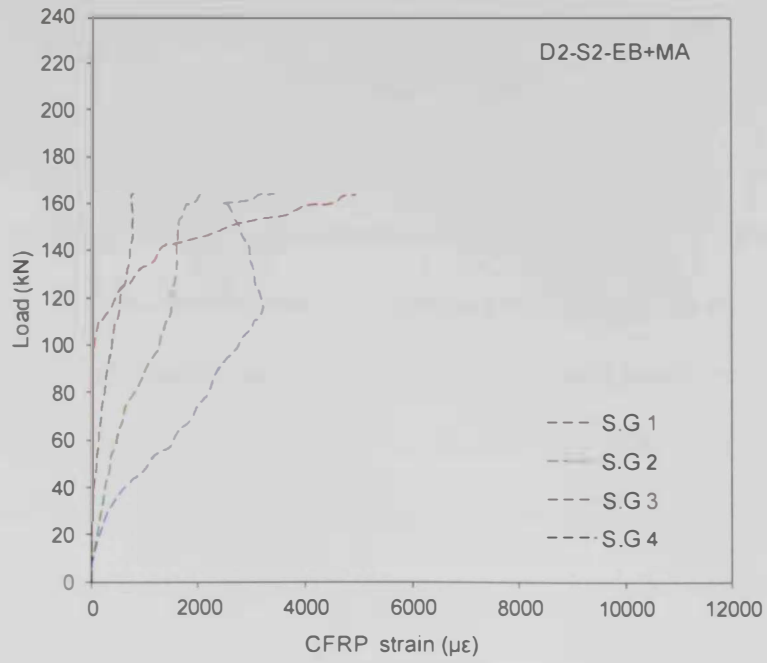


Figure A.15: Load vs. CFRP strain for D2-S2-EB+MA

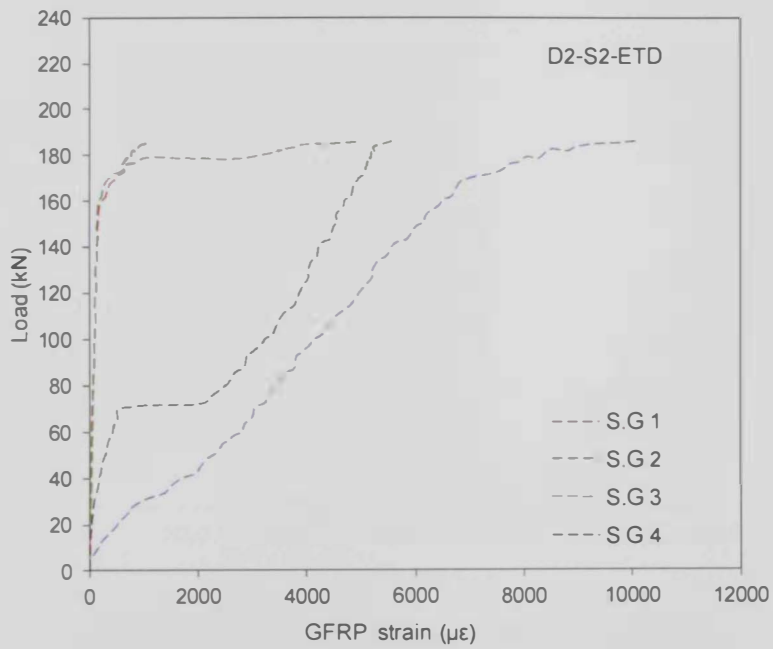


Figure A.16: Load vs. GFRP strain for D2-S2-ETD

APPENDIX B: STRAIN RESPONSE OF STIRRUPS

Plots of the load versus stirrup strain relationships are provided in this appendix. For the specimens with the lower amount of stirrups, the middle three stirrups in the shear span were instrumented by strain gauges. The symbols (S.G 1) and (S.G 3) refer to the strain gauge nearest to the support and load points, respectively. For the specimens with the higher amount of stirrups, the middle four stirrups in the shear span were instrumented by strain gauges. The symbols (S.G 1) and (S.G 4) refer to the strain gauge nearest to the support and load points, respectively.

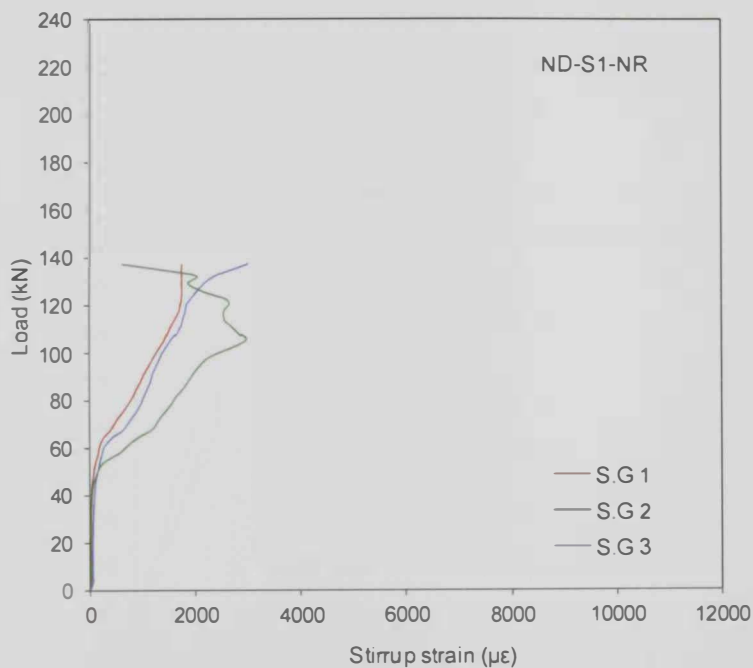


Figure B.1: Load vs. stirrup strain for ND-S1-NR

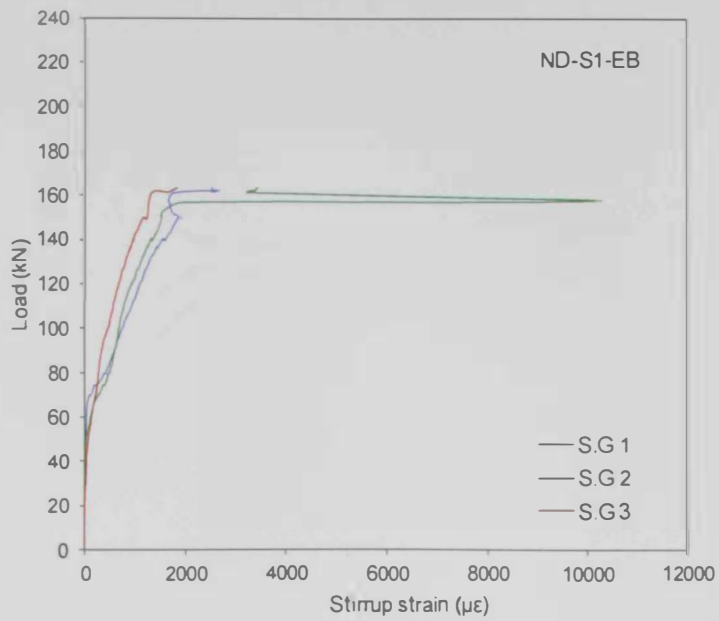


Figure B.2: Load vs. stirrup strain for ND-S1-EB

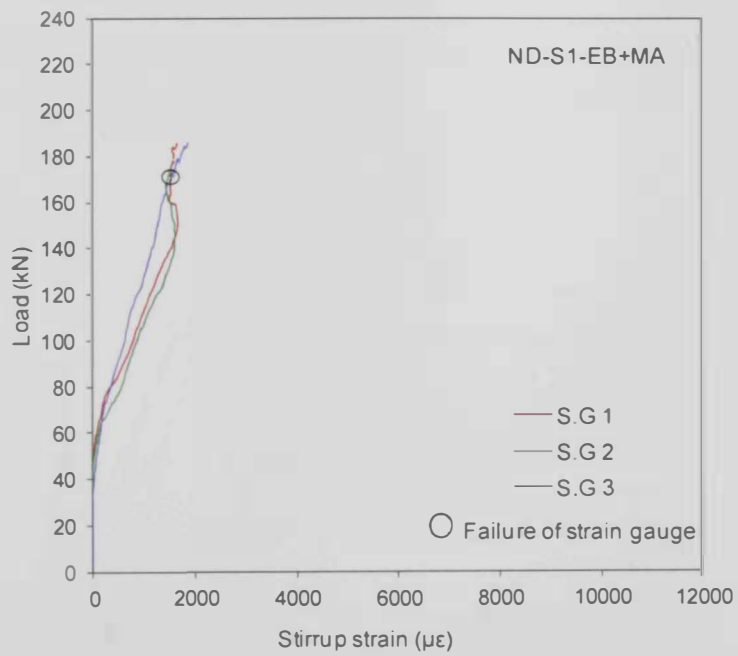


Figure B.3: Load vs. stirrup strain for ND-S1-EB+MA

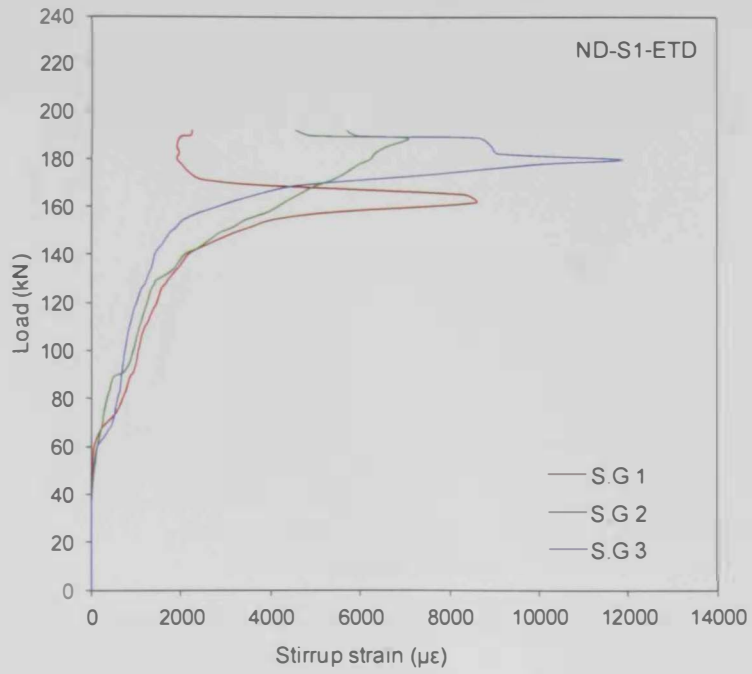


Figure B.4: Load vs. stirrup strain for ND-S1-ETD

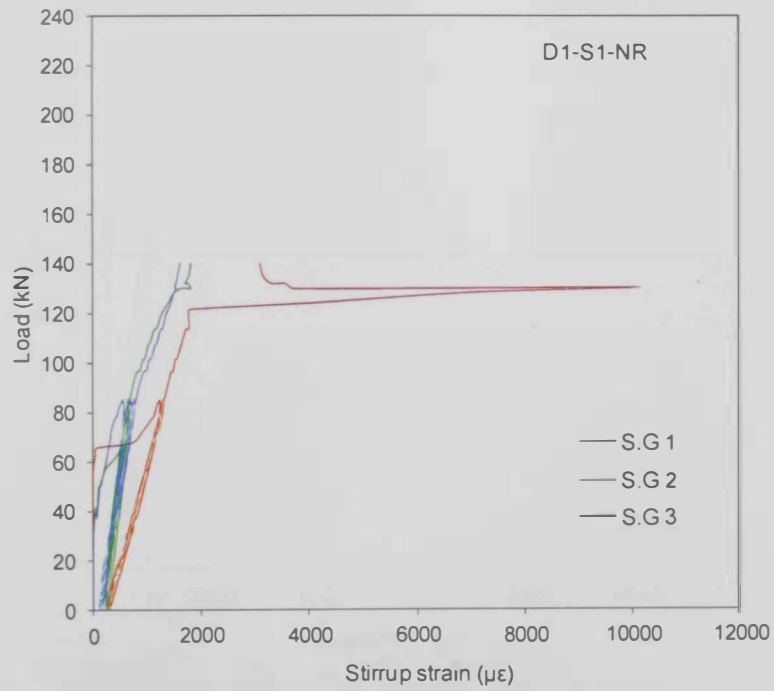


Figure B.5: Load vs. stirrup strain for D1-S1-NR

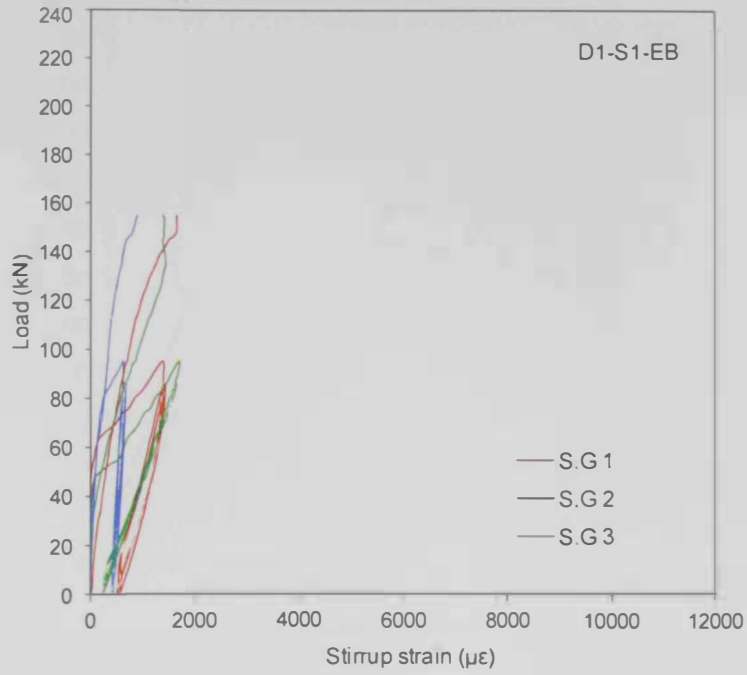


Figure B.6: Load vs. stirrup strain for D1-S1-EB

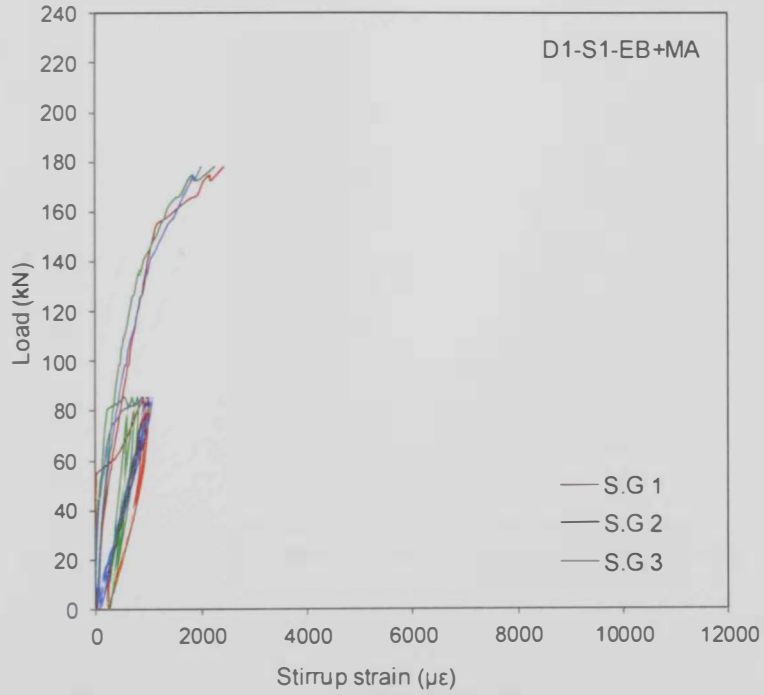


Figure B.7: Load vs. stirrup strain for D1-S1-EB+MA

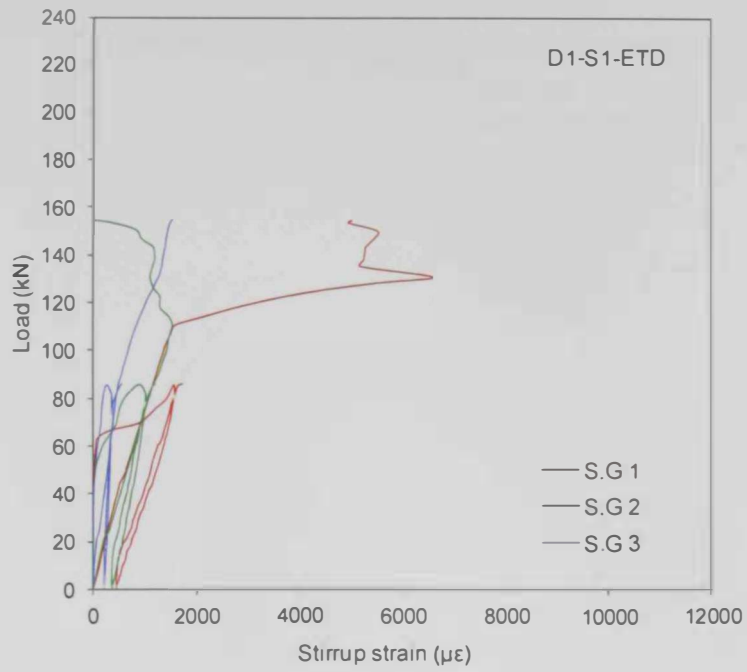


Figure B.8: Load vs. stirrup strain for D1-S1- ETD

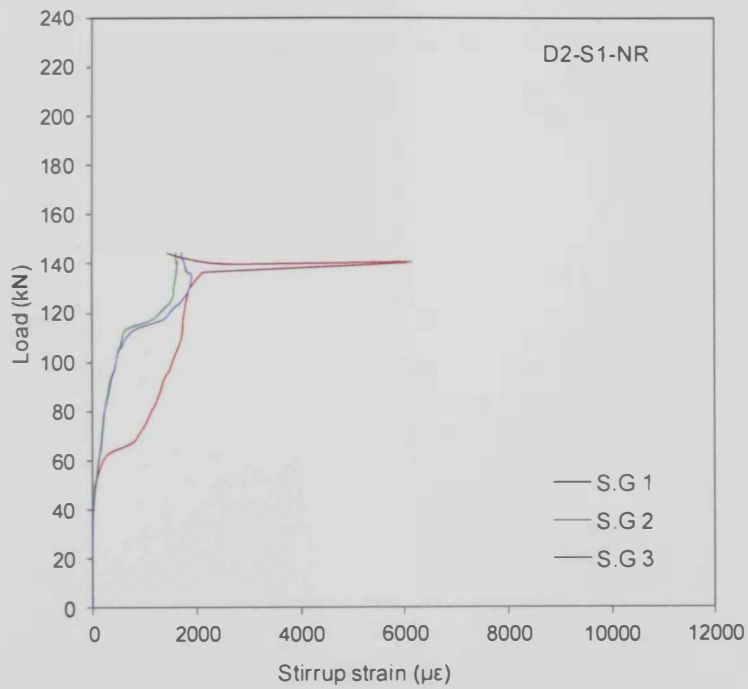


Figure B.9: Load vs. stirrup strain for D2-S1-NR

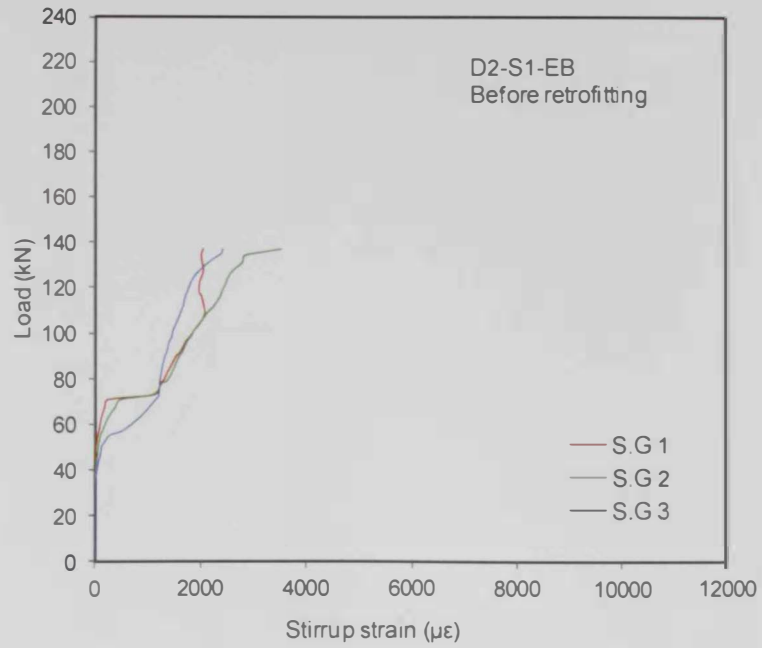


Figure B.10: Load vs. stirrup strain for D2-S1-EB before retrofitting

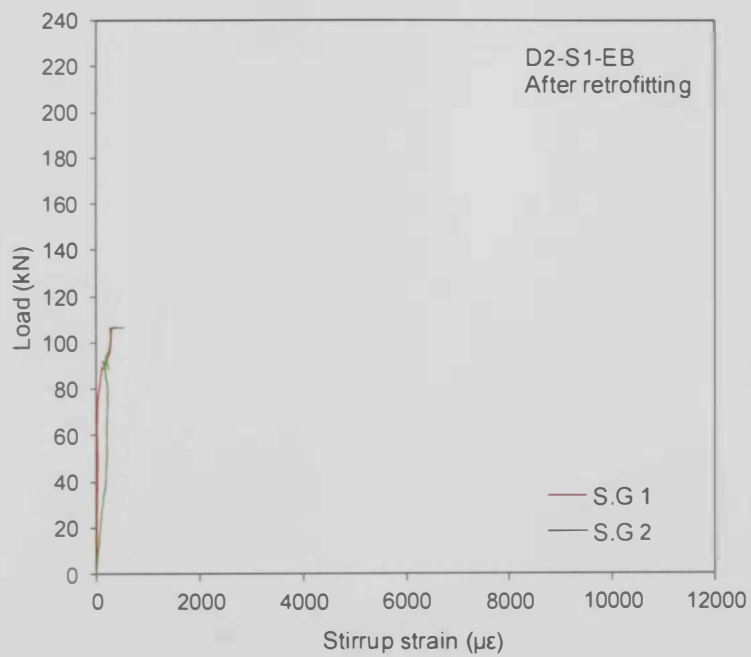


Figure B.11: Load vs. stirrup strain for D2-S1-EB after retrofitting

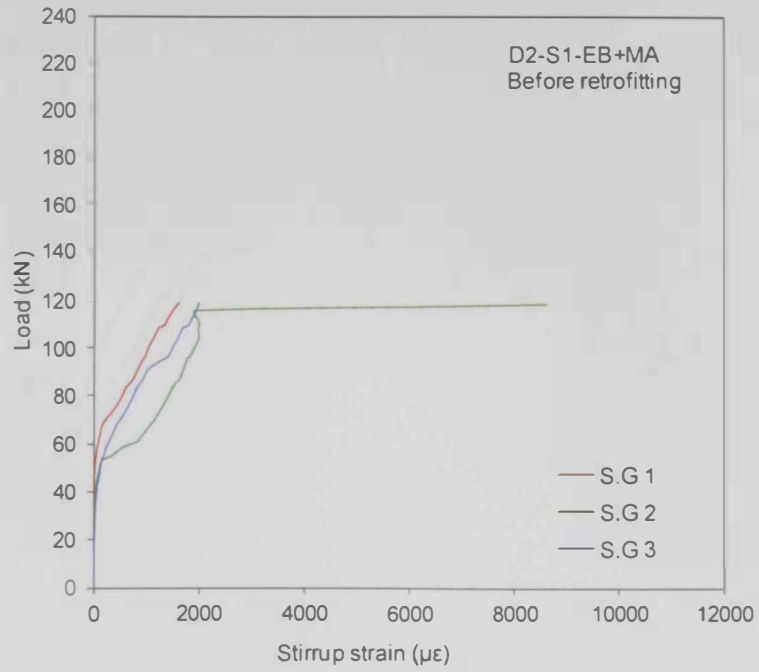


Figure B.12: Load vs. stirrup strain for D2-S1-EB+MA before retrofitting

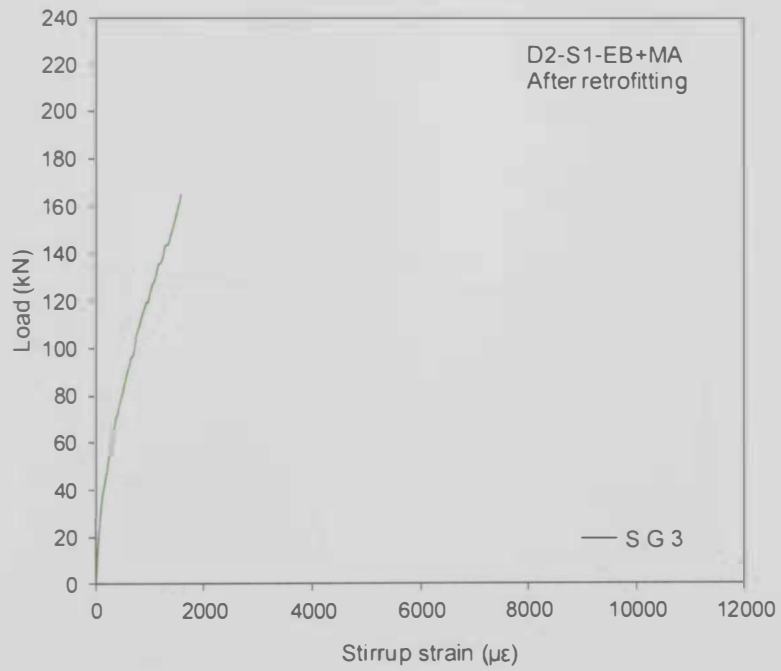


Figure B.13: Load vs. stirrup strain for D2-S1-EB+MA after retrofitting

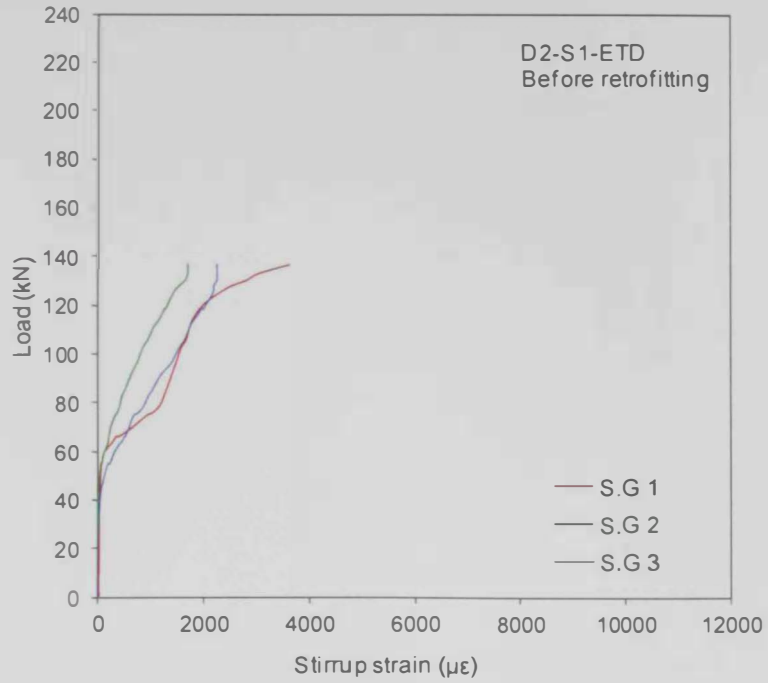


Figure B.14: Load vs. stirrup strain for D2-S1-ETD before retrofitting

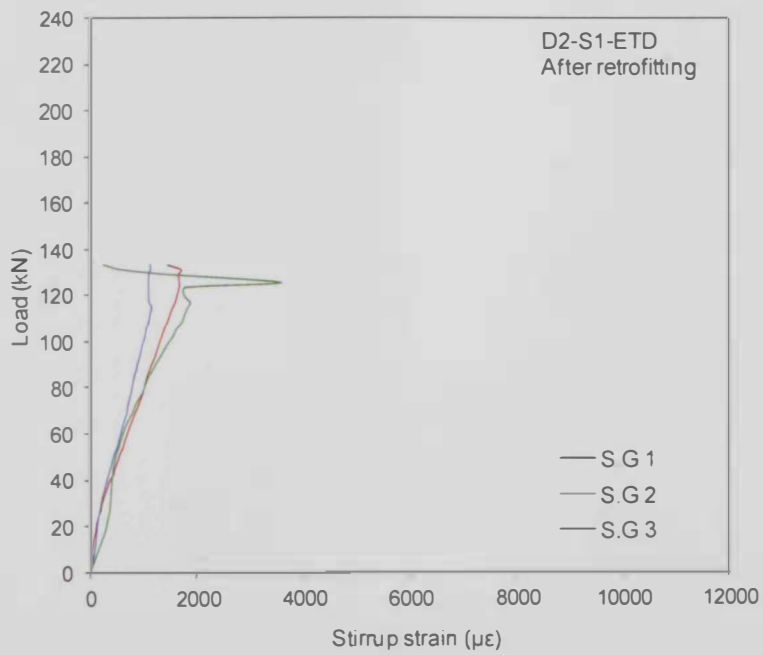


Figure B.15: Load vs. stirrup strain for D2-S1-ETD after retrofitting

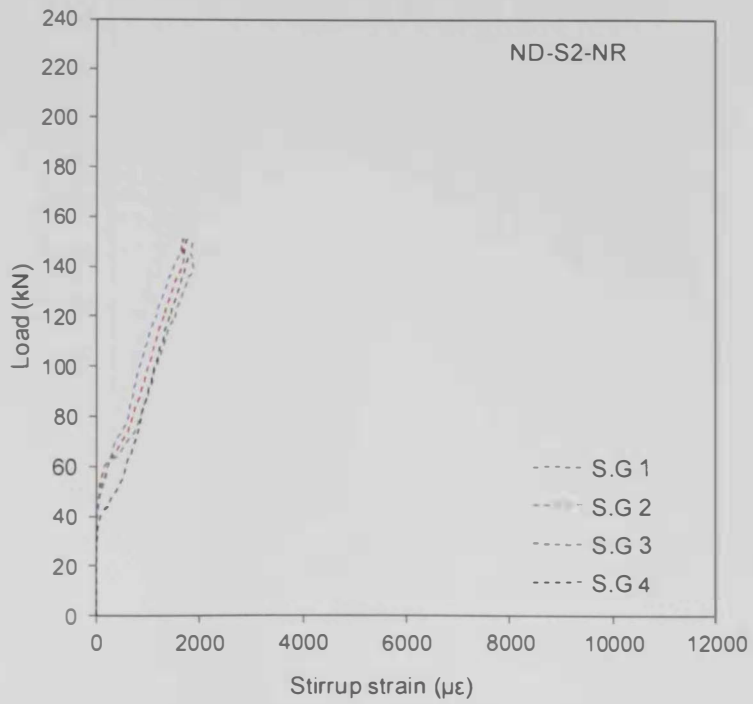


Figure B.16: Load vs. stirrup strain for ND-S2-NR

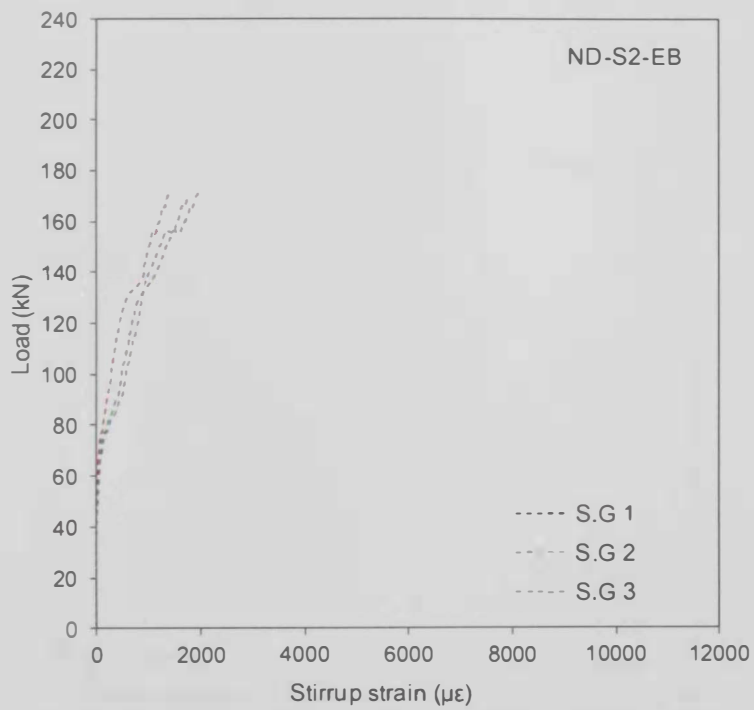


Figure B.17: Load vs. stirrup strain for ND-S2-NR

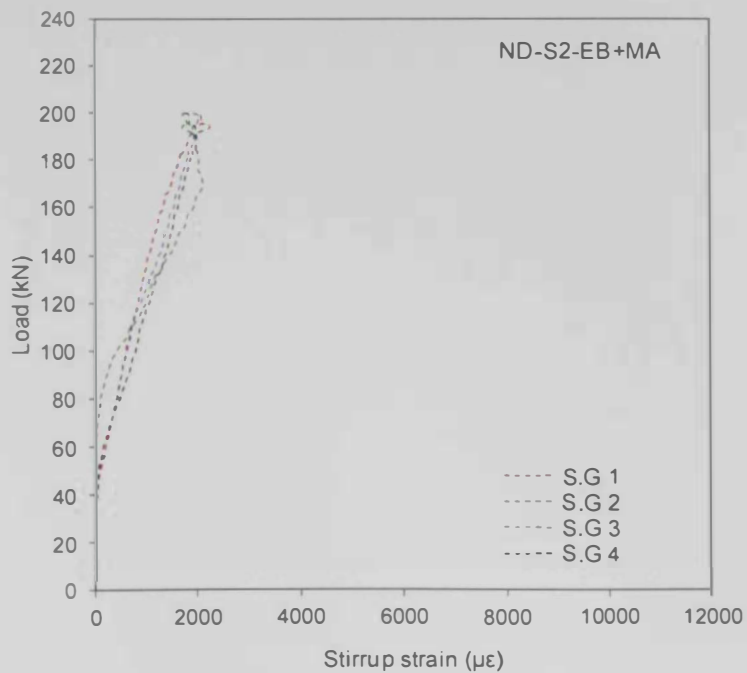


Figure B.18: Load vs. stirrup strain for ND-S2-EB+MA

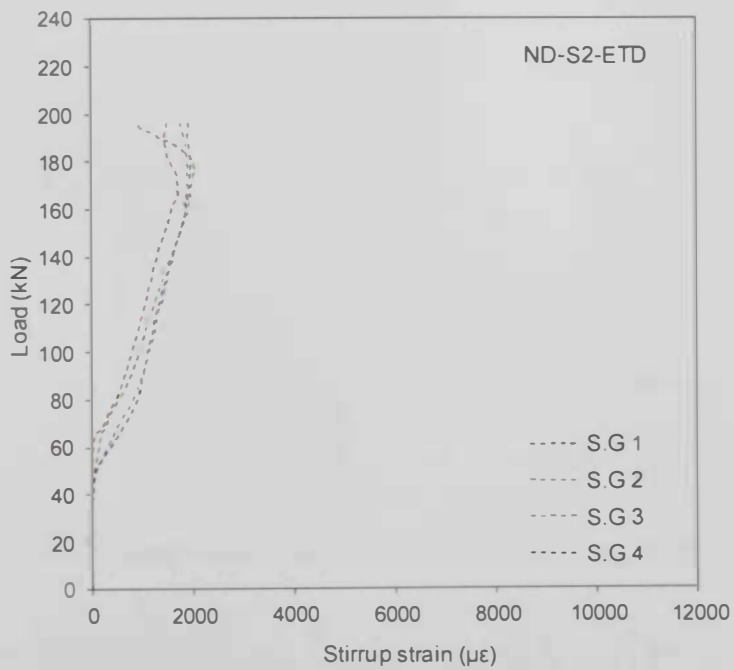


Figure B.19: Load vs. stirrup strain for ND-S2-ETD

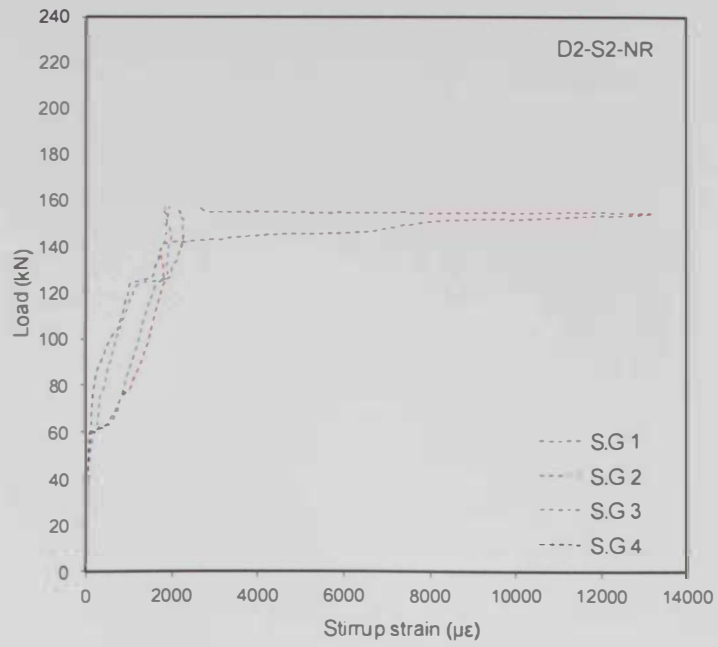


Figure B.20: Load vs. stirrup strain for D2-S2-NR

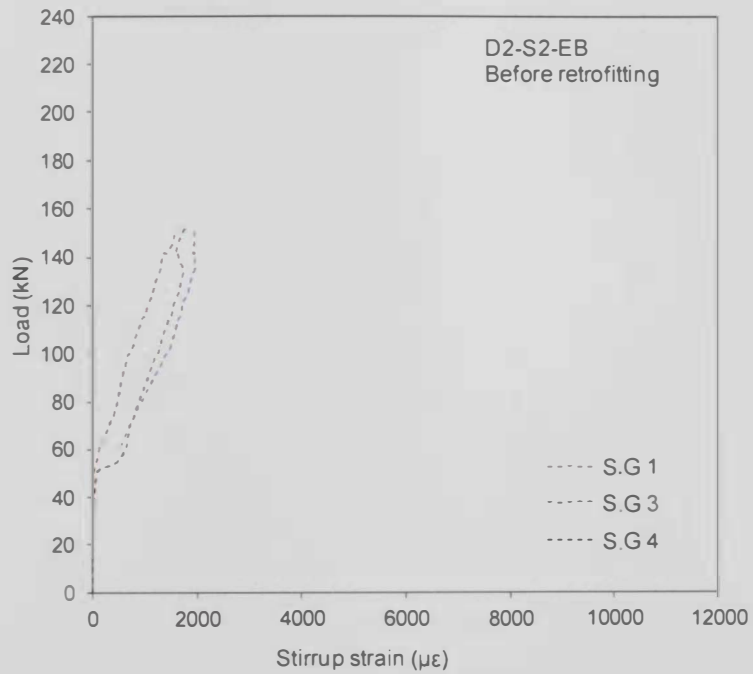


Figure B.21: Load vs. stirrup strain for D2-S2-EB before retrofitting

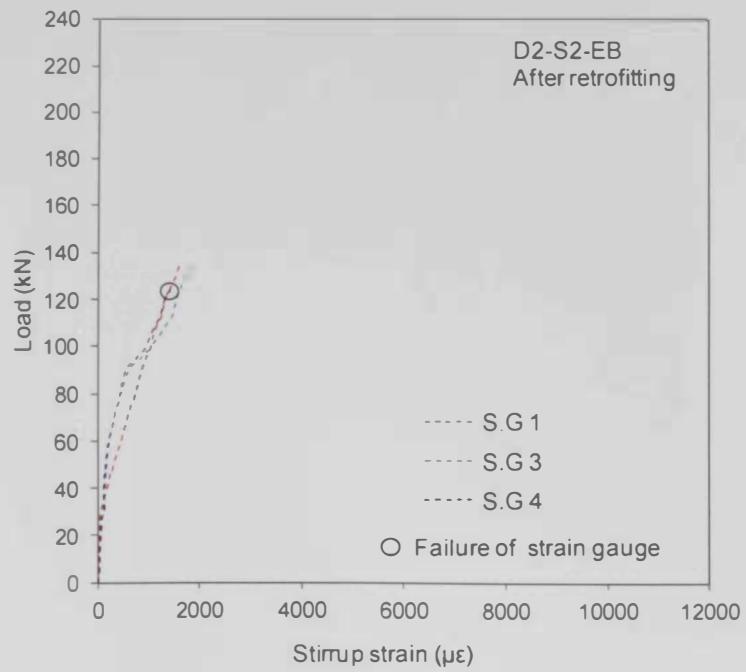


Figure B.22: Load vs. stirrup strain for D2-S2-EB after retrofitting

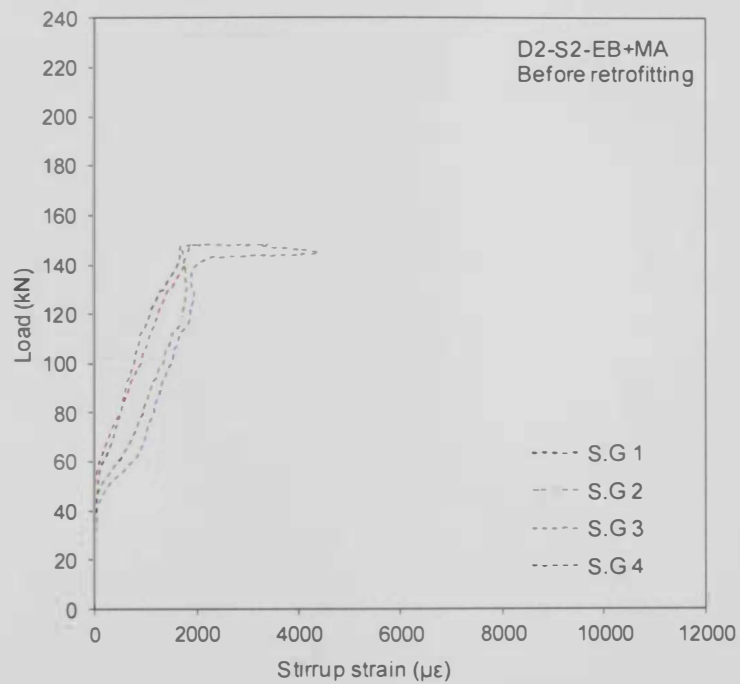


Figure B.23: Load vs. stirrup strain for D2-S2-EB+MA before retrofitting

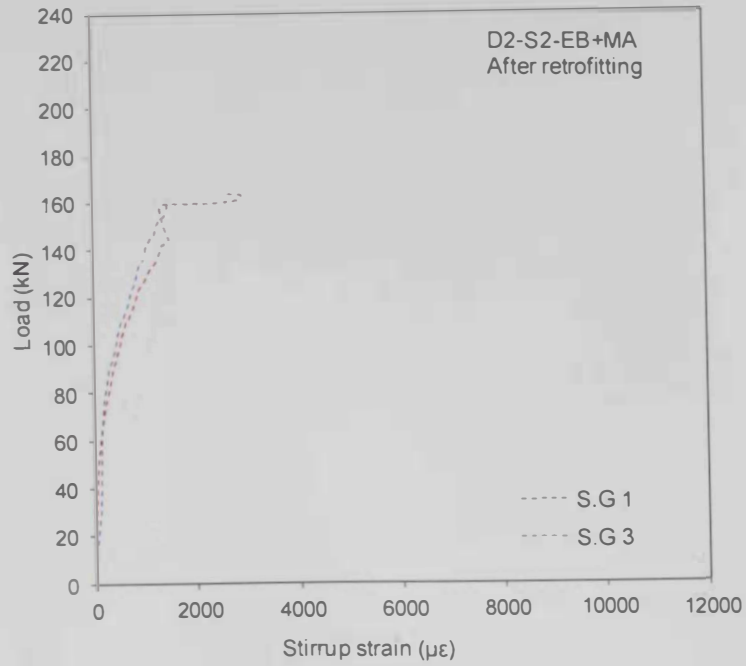


Figure B.24: Load vs. stirrup strain for D2-S2-EB+MA after retrofitting

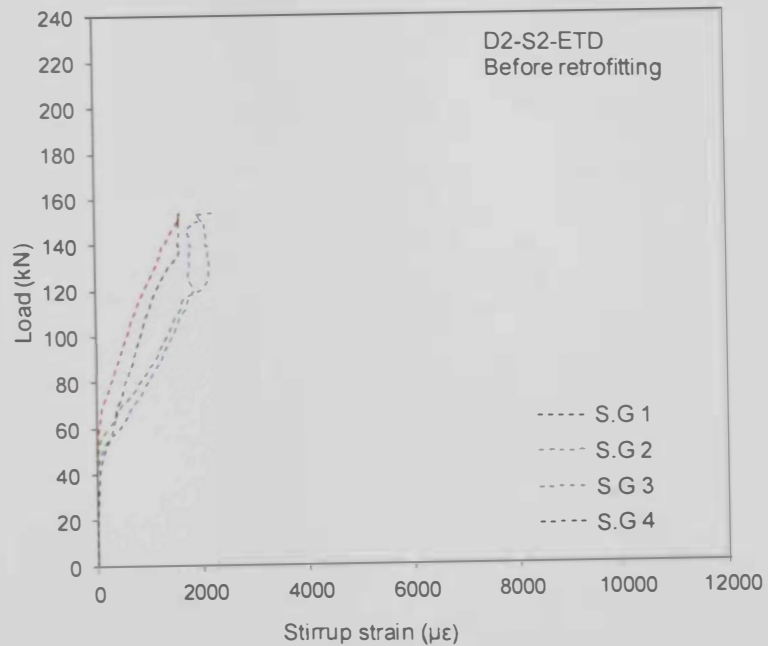


Figure B.25: Load vs. stirrup strain for D2-S2-ETD before retrofitting

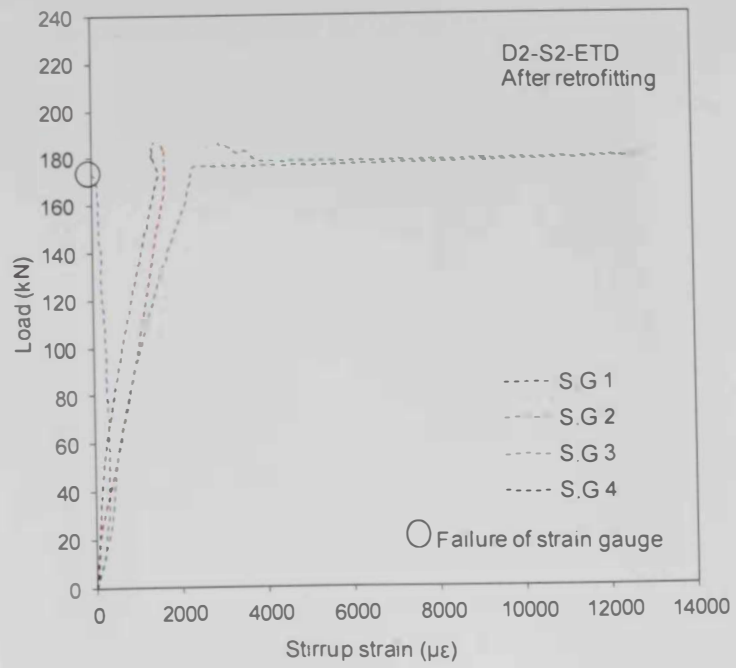


Figure B.26: Load vs. stirrup strain for D2-S2-ETD after retrofitting

كانت حديد التسليح، زادت مقاومة القص المكمّبة نتيجة التقوية بنسبة 11% للعينات التي تم ترميمها بواسطة ألياف الكربون المصقّفة خارجياً (EB-CFRP)، و 27% للعينات التي تم ترميمها بواسطة ألياف الكربون المصقّفة خارجياً (EB-CFRP) المثبتة ميكانيكياً باستخدام المسامير على الأطراف الخارجية (MA)، و 11% للعينات التي تم ترميمها بألياف الزجاج المدرجة خلال عمق العينة (ETD-GFRP). تم إثبات عدم فاعلية استخدام نظام ألياف الكربون المصقّفة خارجياً (EB-CFRP) في ترميم المنشآت المسبقة الإنهيار بسبب أحمال القص حيث لم يتم ملاحظة أي زيادة في مقاومة القص بعد التقوية في حين أن استخدام نظام ألياف الكربون المصقّفة خارجياً (EB-CFRP) المثبت بواسطة المسامير على الأطراف الخارجية (MA) أو استخدام نظام ألياف الزجاج المدرجة خلال عمق العينة (ETD-GFRP) في ترميم المنشآت المسبقة الإنهيار بسبب أحمال القص قد أثبت فاعليته في استعادة مقاومة القص الأصلية للعينة. و كانت مقاومة القص للعينات مسبقة الإنهيار بسبب أحمال القص بعد ترميمها باستخدام نظام ألياف الكربون المصقّفة خارجياً (EB-CFRP) المثبت بواسطة المسامير على الأطراف الخارجية (MA) في حدود 1.1 إلى 1.4 ضعف مقاومة القص الأصلية للعينة قبل الإنهيار والتقوية، في حين أنها كانت في حدود 1 إلى 1.1 ضعف مقاومة القص الأصلية للعينة عند ترميمها بواسطة ألياف الزجاج المدرجة خلال عمق العينة (ETD-GFRP).

و في الدراسة التحليلية، تم تقييم النتائج بواسطة خمس معايير وقوانين دولية بالإضافة إلى دراستين تحليليتين حديثتي النشر للنتيجة بمقدار مساهمه نظام التقوية باستخدام نظام ألياف الكربون المصقّفة خارجياً (EB-CFRP) في قدرة الجسور على مقاومة أحمال القص. إضافة إلى ذلك، فقد تم الاستعانة بدراسة تحليلية حديثة النشر للنتيجة بمقدار مساهمه نظام ألياف الزجاج المدرجة خلال عمق العينة (ETD-GFRP) في قدرة الجسور على مقاومة أحمال القص.

الكلمات المفتاحية : خرسانة، مواد مركبة، قص، ترميم، تثبيت

مخلص الرسالة

يهدف البحث إلى دراسة إمكانية استخدام المواد المركبة بألياف مختلفة لرفع مستوى مقاومة القص للجسور الخرسانية المعرضة لأضرار ناجمة عن أحمال القص. متغيرات البحث التي تم دراستها تتضمن آلية التدعيم: باستخدام ألياف الكربون المصقفة خارجياً (EB-CFRP) سواءً مع أو بدون التثبيت الميكانيكي باستخدام المسامير على الأطراف الخارجية (MA)، أو استخدام ألياف الزجاج المدرجة خلال عمق العينة (ETD-GFRP)؛ تواجد/توزيع كانات حديد التسليح في منطقة الاختبار بكميات محدودة ($s_1 = 0.6d$) أو بكميات كبيرة ($s_2 = 0.375d$)؛ و حالة المنشأ سواءً إن كانت غير مسبقة الأضرار، مسبقة التشقق، أو مسبقة الانهيار. يتضمن البحث مقارنة بين نتائج الاختبارات التجريبية و الدراسة التحليلية.

أظهرت الاختبارات التجريبية نقص مقاومة القص المكتسبة الناتجة عن التقوية بالنسبة للعينات الغير مسبقة الأضرار نتيجة القص كلما زادت كمية كانات حديد التسليح في منطقة الاختبار. إن استخدام ألياف الكربون المصقفة خارجياً (EB-CFRP) دون تثبيتها ميكانيكياً باستخدام المسامير على الأطراف الخارجية أدى إلى زيادة مقاومة القص المكتسبة الناتجة عن التقوية بمقدار 17% للعينات التي لم تحتوي على كانات حديد التسليح، و 19% للعينات التي تحتوي على كميات محدودة من كانات حديد التسليح، و 13% للعينات التي تحتوي على كميات كبيرة من كانات حديد التسليح. في حين أن إضافة التثبيت الميكانيكي باستخدام المسامير على الأطراف الخارجية (MA) إلى العينات المقواة بواسطة ألياف الكربون المصقفة خارجياً (EB-CFRP) أدى إلى زيادة مقاومة القص المكتسبة الناتجة عن التقوية بمقدار 64% للعينات التي لم تحتوي على كانات حديد التسليح في منطقة الاختبار، و 36% للعينات التي تحتوي على كميات محدودة من كانات حديد التسليح، و 32% للعينات التي تحتوي على كميات كبيرة من كانات حديد التسليح. أما بالنسبة العينات المقواة بألياف الزجاج المدرجة خلال عمق العينة (ETD-GFRP)، فقد كانت نتائجها مماثلة لنظيراتها المقواة بواسطة ألياف الكربون المصقفة خارجياً (EB-CFRP) المثبتة ميكانيكياً باستخدام المسامير على الأطراف الخارجية (MA).

و أظهرت الدراسة أن وجود أضرار ناجمة عن أحمال القص في الجسور الخرسانية قد قلل من فاعلية آلية التدعيم المستخدمة بشكل ملحوظ. ففي العينات مسبقة التشقق والتي تحتوي على كميات محدودة من

جامعة الإمارات العربية المتحدة
كلية الهندسة
قسم الهندسة المدنية والبيئية

إعادة تأهيل الجسور الخرسانية المسلحة الضعيفة في تحمل قوى القص بواسطة
المواد المركبة

علاء أحمد عطا معالي

تم تقديم هذه الرسالة لتلبية متطلبات الحصول على ماجستير في الهندسة المدنية والبيئية

تحت إشراف

د. تامر المعداوي

أستاذ مشارك

قسم الهندسة المدنية والبيئية

جامعة الإمارات العربية المتحدة

يونيو 2014